การวิเคราะห์และออปติไมซ์เซชันของกระบวนการร่วมระหว่างแก๊สซิฟิเคชันชีวมวลและฟิชเชอร์
โทรปสำหรับการผลิตเชื้อเพลิงสังเคราะห์

นางสาวคริษฐา อิ่มเอิบ

วิทยานิพนธ์นี้เป็นส่วนหนึ่งของการศึกษาตามหลักสูตรปริญญาวิศวกรรมศาสตรดุษฎีบัณฑิต
สาขาวิชาวิศวกรรมเคมี ภาควิชาวิศวกรรมเคมี
คณะวิศวกรรมศาสตร์ จุฬาลงกรณ์มหาวิทยาลัย
ปีการศึกษา 2558
ลิขสิทธิ์ของจุฬาลงกรณ์มหาวิทยาลัย

ANALYSIS AND OPTIMIZATION OF A BIOMASS GASIFICATION AND
FISCHER-TROPSCH INTEGRATED PROCESS FOR SYNTHESIS FUEL
PRODUCTION

Miss Karittha Im-orb

A Dissertation Submitted in Partial Fulfillment of the Requirements
for the Degree of Doctor of Engineering Program in Chemical Engineering
Department of Chemical Engineering
Faculty of Engineering
Chulalongkorn University
Academic Year 2015

Thesis Title	ANALYSIS AND OPTIMIZATION OF A BIOMASS GASIFICATION AND FISCHER-TROPSCH INTEGRATED PROCESS FOR SYNTHESIS FUEL PRODUCTION
By	Miss Karittha Im-orb
Field of Study	Chemical Engineering
Thesis Advisor	Assistant Professor Amornchai Arpornwichanop, D.Eng.

Accepted by the Faculty of Engineering, Chulalongkorn University in Partial Fulfillment of the Requirements for the Doctoral Degree

.... Dean of the Faculty of Engineering
(Associate Professor Supot Teachavorasinskun, D.Eng.)

THESIS COMMITTEE

.... Chairman
(Associate Professor Sarawut Rimdusit, Ph.D.)
.... Thesis Advisor
(Assistant Professor Amornchai Arpornwichanop, D.Eng.)
.... Examiner
(Assistant Professor Apinan Soottitantawat, D.Eng.)
.... Examiner
(Associate Professor Kasidit Nootong, Ph.D.)
.... External Examiner
(Wisitsree Wiyarat, Ph.D.)

iv

คริษฐา อิ่มเอิบ : การวิเคราะห์และออปติไมซ์เซชันของกระบวนการร่วมระหว่างแก๊สซิฟิเคชันชีวมวลและฟิชเชอร์โทรปสำหรับการผลิตเชื้อเพลิงสังเคราะห์ (ANALYSIS AND OPTIMIZATION OF A BIOMASS GASIFICATION AND FISCHER-TROPSCH INTEGRATED PROCESS FOR SYNTHESIS FUEL PRODUCTION) อ.ที่ปรึกษาวิทยานิพนธ์หลัก: ผศ. ดร.อมรชัย อาภรณ์วิชานพ, 191 หน้า.

งานวิจัยนี้ได้นำเสนอการวิเคราะห์สมรรถนะของกระบวนการร่วมระหว่างแก๊สซิฟิเคชันชีวมวลและฟิชเชอร์โทรปที่ใช้ฟางข้าวเป็นวัตถุดิบ เริ่มต้นจากการวิเคราะห์เชิงตัวแปรของกระบวนการแก๊สซิฟิเคชันที่ใช้แก๊สซิไฟอิ้งเอเจนท์ต่างชนิดกัน ได้แก่ กระบวนการที่ใช้ไอน้ำและอากาศ และกระบวนการที่ใช้ไอน้ำและก๊าซคาร์บอนไดออกไซด์ เพื่อศึกษาความเป็นไปได้ของการผลิตแก๊สสังเคราะห์ที่มีอัตราส่วนระหว่างไฮโดรเจนต่อคาร์บอนมอนอกไซด์ตามต้องการจากแก๊สซิไฟเออร์ที่ดำเนินการภายใต้สภาวะพึ่งพาตัวเองได้ทางความร้อน โดยศึกษาผลของการเปลี่ยนแปลงอัตราส่วนป้อนของแก๊สซิไฟอิ้งเอเจนท์ที่มีต่อปริมาณแก๊สสังเคราะห์ที่ผลิตได้ อัตราส่วนระหว่างไฮโดรเจนและคาร์บอนมอนนอกไซด์ ปริมาณการใช้พลังงานรวมของระบบ และประสิทธิภาพการผลิตแก๊สสังเคราะห์ ณ อุณหภูมิดำเนินการของแก๊สซิไฟเออร์ต่างๆ พบว่าปริมาณแก๊สสังเคราะห์ที่ได้มีแนวโน้มเพิ่มขึ้นอย่างมีนัยสำคัญที่อุณหภูมิต่ำ และเริ่มคงที่ที่อุณหภูมิสูงกว่า 700 องศาเซลเซียส และกระบวนการที่ใช้ไอน้ำและก๊าซคาร์บอนไดออกไซด์จะให้ปริมาณแก๊สสังเคราะห์สูงกว่า และให้อัตราส่วนระหว่างไฮโดรเจนต่อคาร์บอนมอนนอกไซด์ต่ำกว่า แต่ไม่สามารถดำเนินการได้ที่สภาวะพึ่งพาตัวเองได้ทางความร้อน จากนั้นได้ศึกษาสรรถนะของระบบร่วมระหว่างแก๊สซิฟิเคชันชีวมวลและฟิชเชอร์โทรปที่แก๊สซิไฟเออร์ที่ดำเนินการภายใต้สภาวะพึ่งพาตัวเองได้ทางความร้อน ในเชิงเทคนิค เศรษฐศาสตร์ และสิ่งแวดล้อม โดยเริ่มจากการประเมินความเป็นไปได้ของการรีไซเคิลก๊าซเชื้อเพลิงที่ได้จากกระบวนการฟิชเชอร์โทรปกลับไปยังกระบวนการแก๊สซิฟิเคชัน ซึ่งการวิเคราะห์ทางด้านเทคนิคได้อธิบายผลการเปลี่ยนแปลงสัดส่วนรีไซเคิลก๊าซเชื้อเพลิงจากกระบวนการร่วมที่มีขนาดของเครื่องปฏิกรณ์ฟิชเชอร์โทรปแตกต่างกันที่มีต่อสมรรถนะของระบบการผลิตแก๊สสังเคราะห์ กระบวนการฟิชเชอร์โทรป และประสิทธิภาพทางพลังงานของกระบวนการร่วม พบว่าสามารถเพิ่มอัตราการผลิตแก๊สสังเคราะห์ ดีเซล ก๊าซเชื้อเพลิง และกระแสไฟฟ้า จากกระบวนการร่วมดังกล่าวได้โดยการปรับสัดส่วนรีไซเคิลก๊าซเชื้อเพลิงและการเลือกขนาดเครื่องปฏิกรณ์ฟิชเชอร์โทรปที่เหมาะสม ส่วนผลการวิเคราะห์ทางเศรษฐศาสตร์ที่ใช้การคำนวณมูลค่าปัจจุบันสุทธิส่วนเพิ่มเป็นดัชนีชี้วัด พบว่าการรีไซเคิลก๊าซเชื้อเพลิงที่ได้จากกระบวนการร่วมโดยไม่มีการติดตั้งอุปกรณ์อื่นเพิ่มเติมมีความคุ้มค่าทางเศรษฐศาสตร์ต่ำกว่าเทียบกับกระบวนการที่ไม่มีการรีไซเคิล นอกจากนี้ได้มีการเปรียบเทียบสมรรถนะของกระบวนการร่วมแบบที่ไม่มีการติดตั้งหน่วยกำจัดทาร์ และที่ติดตั้งหน่วยกำจัดทาร์ชนิดรีฟอร์มมิ่งด้วยไอน้ำ และชนิดออโตเทอร์มอล ในเชิงของปริมาณดีเซลและกระแสไฟฟ้าที่ผลิตได้ พลังงานที่ใช้ ศักยภาพในการก่อให้เกิดผลกระทบต่อสิ่งแวดล้อม และดัชนีชี้ผลร่วมระหว่างอัตราการผลิตดีเซลกับศักยภาพในการก่อให้เกิดผลกระทบต่อสิ่งแวดล้อม พบว่ากระบวนการร่วมที่ติดตั้งหน่วยกำจัดทาร์ชนิดออโตเทอร์มอล เป็นกระบวนการที่มีความเป็นไปได้มากที่สุด และการนำเสนอกระบวนการร่วมที่มีการออกแบบระบบแลกเปลี่ยนความร้อนที่ให้ประสิทธิภาพในการใช้พลังงานสูงที่สุด จากนั้นทำการอ๊อปติไมซ์ระบบดังกล่าวเพื่อหาสภาวะการผลิตที่เหมาะสมที่ทำให้มูลค่าปัจจุบันสุทธิมีค่าสูงที่สุด และมีการศึกษาผลของอุณหภูมิดำเนินการของแก๊สซิไฟเออร์ อุณหภูมิและความดันของเครื่องปฏิกรณ์ฟิชเชอร์โทรป ที่มีต่ออัตราการผลิตดีเซลและศักยภาพในการก่อให้เกิดผลกระทบต่อสิ่งแวดล้อม สุดท้ายได้ประเมินสมรรถนะของกระบวนการร่วมดังกล่าวในเชิงเศรษฐศาสตร์ร่วมกับสิ่งแวดล้อม และนำเสนอสภาวะการผลิตที่ให้สมรรถนะสูงที่สุด

ภาควิชา	วิศวกรรมเคมี	ลายมือชื่อนิสิต	_____
สาขาวิชา	วิศวกรรมเคมี	ลายมือชื่อ อ.ที่ปรึกษาหลัก	_____
ปีการศึกษา	2558		

5571451921 : MAJOR CHEMICAL ENGINEERING

KEYWORDS: BIOMASS GASIFICATION / FISCHER-TROPSCH / RICE STRAW / PROCESS ANALYSIS

KARITTHA IM-ORB: ANALYSIS AND OPTIMIZATION OF A BIOMASS GASIFICATION AND FISCHER-TROPSCH INTEGRATED PROCESS FOR SYNTHESIS FUEL PRODUCTION. ADVISOR: ASST. PROF. AMORNCHAI ARPORNWICHANOP, D.Eng., 191 pp.

The performance analysis of the biomass gasification and Fischer-Tropsch integrated (BG-FT) process of rice straw feedstock are presented in this research. A parametric analysis of the gasification processes utilizing different types of gasifying agent i.e., steam-air and steam-CO2, is firstly performed to investigate the possibility of syngas production with desired H2/CO ratio from a thermal self-sufficient gasifier. The effects of changes in the ratio of gasifying agent on the syngas yield, H2/CO ratio, total energy consumption and cold gas efficiency of the system at different gasifying temperatures are investigated. The syngas yield of both gasification processes significantly increases at low temperature until it reaches a maximum value and is stable at temperatures higher than 700 °C, However the steam-CO2 system offers higher syngas productivity and lower H2/CO ratio; however, the thermal self-sufficient condition is not achieved. The technical, economic and environmental studies of the BG-FT process which gasifier is operated under thermal self-sufficient condition are further performed. The feasibility of FT-offgas recycle to the gasifier is firstly investigated. Regarding to technical aspect, the influence of changing an off-gas recycle fraction at different values of the FT reactor volume on the performance of the syngas processor, the FT synthesis and the energy efficiency is discussed. The production rate of syngas, diesel product and FT off-gas, as well as electricity from the BG-FT process, can be maximized via suitable adjustment of the recycle fraction and selection of the FT reactor volume. The economic analysis using an incremental NPV as an economic indicator implies that the use of the recycle concept in the BG-FT process without the installation of any secondary equipment is less feasible than the once-through concept from an economic point of view. The performance of BG-FT processes with and without tar removal unit based on steam reforming and autothermal reforming (ATR) are compared in term of the produced diesel and electricity, energy consumption, the overall potential environmental impact (PEI) and the combined effect of diesel production rate and PEI. And the BG-FT process with ATR is found to be the most practical configuration, and the process offering maximum internal heat recovery and minimum external utility requirements is proposed. The optimization of the new designed BG-FT process based on the economic objective is performed to determine the optimum operating condition offering the maximum net present value (NPV). The influence of gasifying temperature, FT operating temperature and FT pressure on the diesel production rate and the PEI is investigated. The combined evaluation in term of economic and environmental point of view is further performed using the AHP index, calculated based on the multi-criteria decision analysis (MCDA) method using AHP analysis, as an indicator. The suitable condition offers the best performance from both economic and environmental point of view is finally proposed.

Department:	Chemical Engineering	Student's Signature _____
Field of Study:	Chemical Engineering	Advisor's Signature _____
Academic Year:	2015	

ACKNOWLEDGEMENTS

CONTENTS

LIST OF TABLES

LIST OF FIGURES

CHAPTER I
INTRODUCTION

1.1 Inspiration of the thesis

Nowadays, the world consumption rate of fossil fuel extremely increases, especially in developed countries, such as China and India, where the energy demand is driving by a strong economic growth. In the year 2015, the total world energy consumption was 12,928.4 Mtoe which increase 0.9 % higher than that in year 2014 (BP, 2015). Although, the new globally reserved fossil fuel i.e., shale gas and tight oil, has been continuously invented especially in the US which has become the world largest oil and natural gas producer since year 2014. However, Thailand is still the fuel-imported country. Moreover, emission gases released from combustion engines result in air pollution, public health and global worming issues. All industrialized and some developing countries legislate the stringent environmental law to limit the emission level of pollutant gases. In year 2015, the Paris Climate Change Conference (COP21) was organized and several countries agreed to limit the rise in global temperature below 2 ^{o}C compared to that at the industrial revolution period by year 2035 (UNFCCC, 2015). The solutions to maintain this target such as the improvement of carbon capture storage (CCS) technology, the increase of process energy efficiency and the reduction of fossil fuel utilization in energy production process by replacing with the alternative resources i.e., wind, solar and biomass, are increasingly interest. However, the latter practice using biomass as an energy source seems to be a suitable practice for Thailand, predominantly an agricultural-based country.

The transportation sector is one which not only consumes a high amount of energy (liquid transportation fossil fuel, i.e., gasoline and diesel) but is also responsible for a large part of CO_2 emissions. In Thailand, this sector is the second most consumed energy next to an industrial sector; the transportation sector represented approximately 35.4% of the overall energy consumption in year 2014. As the liquid transportation fuel plays an importance role in human daily life, replacing of energy derived-fossil fuel required in this sector with the one derived from

renewable resource such as biomass in order to relieve the impact of the emitted gas and to increase the in-house energy production has been received considerable attention. The Ministry of Energy mandates a target for the use of renewable energy of 25% of total energy consumption by 2021, by which time diesel can be replaced by the new energy by approximately 25 million liters per day (DEDE, 2012). One of the promising technologies used to produce green liquid fuels is the combination of biomass gasification and Fischer-Tropsch synthesis process (BG-FT), which is also known as a biomass to liquid (BTL) process (Omer, 2008).

Biomass is nowadays given closer attention due to its CO_2 neutral and environmental friendliness. Moreover, the utilization of biomass as a feedstock for fuel production is substantially supported by current energy policy. Thailand is one of the agricultural countries which produce a wide variety of agricultural products such as sugarcane, rice, soybean, corn, palm oil and cassava. In the year 2010, rice was the second favorite agricultural product next to sugarcane, but it provides the highest amount of biomass residue, which is called rice straw. Based on its production of 31.5 million tons, the 25.6 million tons of rice straw was approximately produced (DEDE, 2012). Rice straw is the stalk of the rice plant that is left over as waste products on the field upon harvesting of the rice grain. In Thailand, around 90% of rice straw collected during the peak harvesting season between November and December are burned in the open fields. This practice leads to air pollution and public health issues. Rice straw is grouped into a lignocellulosic biomass. Unlike carbohydrate or starch, it is not easily digestible by humans; therefore, its use for biogas or bio-oil productions does not threaten the world food supply (Lim et al., 2012). Rice straw mainly contains carbon, hydrogen and oxygen which have a potential to be converted to energy. The conversion of rice straw to energy has many advantages, including the reduction of agricultural waste generated from rice industry, the reduction of environmental impact and the acquisition of new alternative energy resource for in-house energy production which reduces the import of fossil energy. Based on the rice straw lower heating value (LHV) of 3.09 kcal/kg, the 79,088 MMkcal of energy can be achieved if all of produced rice straw is converted, which corresponds to 159,687 barrel/day of diesel when diesel heating value of 10.08 kcal/kg is considered (DEDE, 2012).

Presently, several technologies could be employed to convert solid biomass into a usable gas, such as gasification, pyrolysis, fermentation, liquefaction and hydrolysis. Among the existing technologies, gasification is recognized as the most effective technology, offering the ability to handle a wide range of feedstock including biomass residuals. In the gasification process, solid biomass reacts with controlled oxidizing agents, such as steam, oxygen or air, to form mixed gases, char, tar and heavy hydrocarbon. A typical gasification process generally follows the sequence of steps (i.e., drying, pyrolysis, oxidation and gasification). The main reactions of biomass gasification in the gasifier reported by Shen et al. (2008) consist of the water gas, Boudouard, water gas shift, methanation and methane steam reforming reactions. The gasification provides a large amount of produced gas and its energy efficiency could be achieved via the design of an effective heat integration system due to its high temperature operation. The produced gas can be used in various manners, for example, used to drive the gas turbine system for electricity generation, used as a fuel gas for the internal combustion engine and used as substitute for fuel oil in direct heat of industrial furnace (Rajvanshi, 1986).

The tar formation is one of the biggest problems during gasification; it condenses under reduced temperature which causes fouling of downstream equipment and piping system and the reduction of heat transfer rate would be found afterward. The attempts of minimizing tar formation, such as selecting the suitable operating condition, using catalyst and installation of secondary equipment in order to remove the tar from the produced gas are still the topic of interest (Pereira et al., 2012). Li et al. (2004) reported that sawdust tar and cornstalks tar showed aromatic character, while cornstalks tar contained more aliphatic compounds than sawdust tar. They also found that the tar yield decreased exponentially when temperature increased. Vivanpatarakij and Assabumrungrat (2013) proposed the combined unit of biomass gasifier and tar steam reformer in order to remove tar and increased hydrogen production simultaneously. Josuinkas et al. (2014) found that that benzene (the tar model compound) and methane were completely converted to H_2 and CO via the steam reforming reaction over a Ni-based catalyst at the operating condition of 780 ˚C and 1 atm.

In general, the produced gas can be converted to synthesis gas which mainly consists of hydrogen and carbon monoxide via gas cleaning units where the impurities are removed. It may go through a water gas shift reactor where carbon dioxide is converted to carbon monoxide via the water gas shift reaction. The derived synthesis gas is used as not only a fuel gas for combustion units, but also a raw material for chemical plants, such as methanol, olefins, dimethyl ether and liquid fuel (Hamelinck and Faaij, 2006; Swain et al., 2011). The different properties of synthesis gas are required for different desired chemical production. For example, the synthesis gas with the H_2/CO ratio around one is required for the oxo-synthesis process in the aldehyde and alcohol production, whereas the H_2/CO ratio close to two is required for the production of Fischer-Tropsch (FT) fuels and methanol production (X. Song and Guo, 2006).

Several works have been studied on the gasification process relying on both experiment and simulation. Many experimental studies were done in order to study the influence of operating conditions, such as gasifying temperature and pressure, feed material temperature, equivalent ratio and steam-to-biomass ratio on produced gas composition, heating value and biomass conversion efficiency (Li et al., 2004). Some experiments were carried out to investigate the kinetics of the gasification reactions (Kojima et al., 1993). Modeling of the gasification process based on either the kinetic or thermodynamic approaches has also been the topic of interest. Although the kinetic model provides essential data on kinetic mechanism to describe the conversion of biomass in the gasification process, but it requires a lot of kinetic parameters. For preliminary, basic design of gasification process, a thermodynamic model is sometime preferable as only the feed elemental composition and chemical reactions data are needed. Regarding the thermodynamic approach, an equilibrium reaction is assumed, the deviation of produced gas compositions obtained from the model and actual data are generally observed and the tar formation could not well be predicted. To improve the model accuracy, the tar formation and reaction kinetics of char gasification should be taken into account. The previous studies mostly performed a parametric analysis of the gasification process in terms of the producer gas composition and heating value and the biomass conversion efficiency. (Loha et al.,

2011; Mitta et al., 2006; Nikoo and Mahinpey, 2008; Zainal et al., 2001). However, a design of the gasification process to produce the synthesis gas having the desired fraction of hydrogen and carbon monoxide, which is suitable for specific applications, is less extensively studied.

The transportation of fuel gas to the area far away from the fuel source is still has a limitation. The fuel gas must be compressed to the liquid phase in order to be convenient to transport and this practice is prone to be exploded. Thus, the FT process which is a catalytic process become attractive technology as it can be used to convert the synthesis gas to liquid fuel. The fuel products are diversified, such as lube oil, wax, naphtha, sulphur-free diesel and jet fuel, and has higher amount of valued portion compared to the one derived from crude distillation. The synthesis liquid fuels are the ultraclean product which can also apply to the existing infrastructure and car technology very well. When the product yield patterns of the synthesized fuel are adjusted to achieve the user requirements, the profit ability of the oil producer increases (Fatih Demirbas, 2009; Wood et al., 2012).

Presently, many experimental studies on the FT process have been performed. The improvement of catalyst performance to meet the maximum yield of desired products is one of the key successes for FT process. The effect of various metal loading on performance of Iron and Cobalt based catalysts was investigated and the factors that influence on the catalyst deactivation were also reported (Hu et al., 2012). The influence of operating conditions, such as feed gas composition, operating temperature and pressure on the yield patterns of synthesized fuel, heating value and carbon conversion efficiency were investigated in the previous study (Choosri et al., 2012). Moreover, some experiments were done to evaluate the kinetic expression of the FT reaction over various catalysts (Anfray et al., 2007). In addition to the experimental works, a development of the model explaining the FT process has been interest. The developed models are widely used to investigate the catalyst-fluid behavior inside the FT reactor and the influence of operating conditions on the yield patterns of synthesized fuel. The energy analysis of the FT process was also investigated. S. Wang et al. (2013) developed the one-dimensional heterogeneous model of fixed bed reactor which developed based on the kinetic data and the fact that

catalysts pores were filled with liquid wax under realistic condition and used it to investigate the effect of process parameters on the reaction behavior of the system with recycle operation. The model of bubble column slurry reactor was developed by de Swart and Krishna (2002) to investigate the mixing behavior of liquid and catalyst particle phase inside the commercial scale reactor.

The success of liquid fuel production via the FT process is currently limited to the fossil (natural gas and coal) feedstock. There are several commercial scale FT plants existing in the world today, i.e., three coal-based plants in South Africa (150,000 bpd, Sasol), one natural gas-based in South Africa (23,000 bpd, PetroSA) and one natural gas-based plant in Malaysia (15,000 bpd, Shell) (A.P. Steynberg and Dry, 2004) . The use of biomass feedstock via the BG-FT process is still in the research and development phase and its synthesized liquid fuel price still not completes with the one derived from crude distillation due to the higher operating cost is the concern issue for commercial scale implementation, therefore, the study of this process in several aspects such as technical, economic and environmental, in order to improve its performance have continuously raised today attentions. Hamelinck et al. (2004) reported that the price of green diesel derived from BG-FT process is four time higher than that of the low sulphur fossil diesel due to the large required capital investment. Avella et al. (2016) performed economic analysis and found that cost of electricity and synthesized liquid fuel strongly depended on the plant configurations. Hunpinyo et al. (2013) reported that the investment cost per plant capacity decreased when the size of the production plant increased. Even though, the technical and economic of BG-FT process are not currently proven, the benefit in term of environmental friendliness is obviously revealed. As a result, the continuous improvement of this technology in order to competitive with liquid fossil fuel is the topic of interest. Previous works mostly focused on the process performance evaluation and the economic feasibility of the BG-FT process; however, the evaluation of an environmental impact, such as greenhouse gas emission and potential environmental impact (PEI), is less extensively presented.

This research will focus on the study of BG-FT process. Rice straw, mostly found biomass in Thailand, is considered feedstock for the gasification unit. Due to

the simplicity, inexpensive and low tar content in product gas, the biomass gasification process with a downdraft configuration is selected in this study. Firstly, the performance of gasification process utilizing different types of gasifying agents (i.e., air-steam and CO_2-steam) is investigated to determine the suitable condition offering the high production rate of syngas with desired H_2/CO ratio. The suitable gas conditioning technique consisting of gas cleaning and water gas shift units and the FT synthesis are studied. Then, the technical, economic and environmental studies of the BG-FT processes with different configurations i.e., a once-through process, the process included recycle and the one equipped with different tar removal units based on steam reforming and autothermal reforming (ATR), are performed to determine whether process is the most practical which offers the best performance. In technical aspect, the parametric analysis is performed to investigate the effect of operating parameters such as gasifying temperature, FT operating temperature and pressure on the overall process performance. The optimal structure of heat exchanger network is designed based on the pinch design method for the most practical BG-FT process. The optimization with respected to the economic objective, aiming at the NPV maximization is then performed using FEASOPT optimizer embedded in Aspen Custom Modeller (ACM) to determine the optimum condition. In economic evaluation, the net present value (NPV) and the incremental NPV are used as economic indicators. The potential environmental impact (PEI) calculated based on the waste reduction (WAR) algorithm is used as an environmental indicator. Moreover, the multi-criteria decision analysis (MCDA) using analysis hierarchy process (AHP), which the economic and environmental performances are integrated into one AHP index, is also performed to determine the suitable condition offers the best performance in economic and environmental point of view.

1.2 Objective of research

To analysis, optimize and evaluate the performance of the BG-FT process of rice straw feedstock for synthesis fuel production in term of technical, economic and environmental point of view.

1.3 Scope of research

The scope of this research is summarized in Figure 1.1. Firstly the influence of changing the operating parameters on the gasification performance is investigated. Then, the technical, economic and environmental studies of the BG-FT process with different configurations, the heat exchanger network design and the process optimization are performed.

1.3.1 To investigate the production of syngas with desired H_2/CO ratio via gasification process utilizing different types of gasifying agent (i.e., steam-air and steam-CO_2) at various gasifying temperature. The feasibility of thermal self-sufficient operation at gasifier is also investigated.

1.3.2 To perform techno-economic analysis of the BG-FT process with different configurations (i.e., once-through and with recirculation concepts). The influence of changing an FT off-gas recycle fraction at various FT reactor volumes on the performance of the syngas processor, the FT synthesis and the overall energy efficiency of BG-FT process is investigated and justified which configuration offers the best performance in both technical and economic points of view.

1.3.3 To analyze the performance of the BG-FT processes with and without tar removal unit based on steam reforming and ATR in technical and environmental aspects as well as the utility demand and justify which type of BG-FT process is the most practical one.

1.3.4 To design the heat exchanger network offering the optimal heat integration for BG-FT process based on the pinch design method. Then, the new designed BG-FT process is optimized to determine the optimum conditions offering the maximum NPV.

1.3.5 To investigate the influence of changing an gasifying temperature, FT operating temperature and FT pressure on the diesel production rate, the PEI and the combination thereof and justify which operating condition offers the best performance in economic and environmental points of view.

9
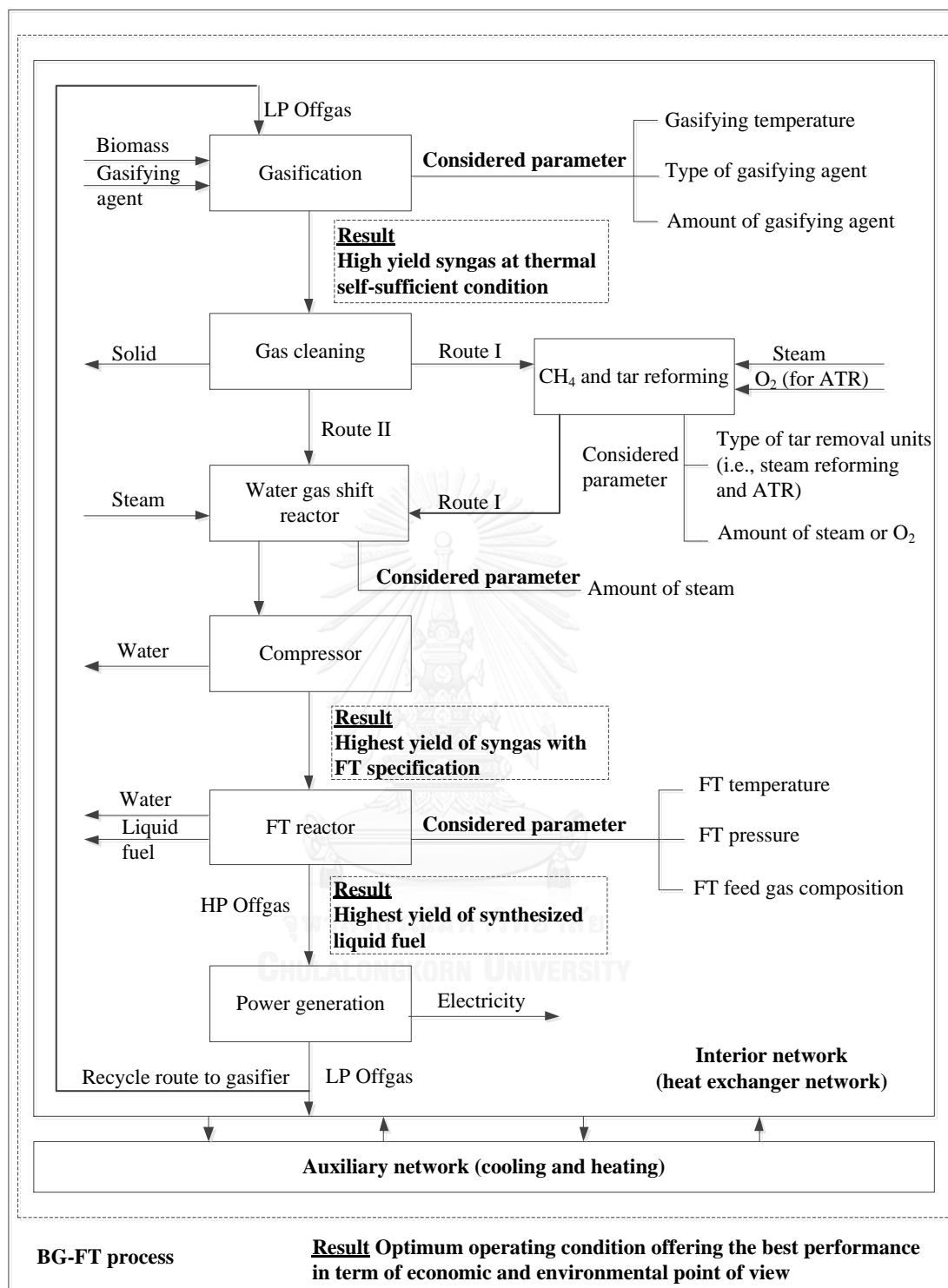
Figure 1.1 Overall scope of this research

1.4 Research methodology

For this work, the research methodology consists of several steps as given below.

1.4.1 Study the potential of biomass in Thailand for energy production and the basic principle of the BG-FT process for green fuel production.

1.4.2 Develop the equilibrium model of gasification process to preliminary study two gasification systems utilizing different types of gasifying agent (i.e., steam-air and steam-CO_2). The influence of changes in the ratio of gasifying agents on the syngas yield, H_2/CO ratio, total energy consumption and cold gas efficiency (CGE) at different gasifying temperatures are investigated.

1.4.3 Improve the accuracy of the gasification model by including tar formation and reaction kinetic of char gasification.

1.4.4 Integrate the gasification model with the model of downstream units including syngas cleaning and conditioning, FT synthesis and power generation units to develop the complete BG-FT model.

1.4.5 Perform the techno-economic analysis using the developed BG-FT model to investigate the feasibility of FT off-gas recycle compares with the once-through process. The influence of changing an FT off-gas recycle fraction at different FT reactor volumes on the performance of the syngas processor, the FT synthesis and the overall energy efficiency of BG-FT process is investigated.

1.4.6 Perform the techno-environmental analysis using the developed BG-FT model to analyze and compare the performances of the BG-FT process with and without tar removal unit based on steam reforming and ATR whether process is the most practical one. The diesel and electricity production rate, the PEI and the demand of utility are used as performance indicators.

1.4.7 Design the heat exchanger network offering the optimal heat integration for BG-FT process based on the pinch design method and performs the optimization to determine the optimum operating condition offers the maximum NPV.

1.4.8 Investigate the influence of gasifying temperature, FT operating temperature and FT operating pressure on the diesel production rate and PEI.

1.4.9 Perform the multi-criteria decision analysis (MCDA) using analysis hierarchy process (AHP), which the economic and environmental performances are integrated into one AHP index, to determine the suitable condition offers the best performance in economic and environmental point of view.

1.4.10 Discuss the results and make the conclusions

1.4.11 Write up the thesis

1.5 Dissertation overview

This dissertation is divided in nine chapters and their briefly information are given below.

Chapter I describes the background and the inspiration of this research. The objectives, scope of work and research methodology are also presented.

Chapter II summarizes the basic principles and theory related to this research which consists of the biomass characteristic, gasification technology including the main reactions, gasifying agents and type of gasifier, synthesis gas cleaning, tar removal technology and FT technology including related reactions, FT catalysts and types of FT reactors. Moreover, the calculation methodology of energy efficiency, pinch analysis, economic analysis as well as environmental impact evaluation applied in this study is also discussed.

Chapter III presents the literature reviews which gather and summarized the related works reported in the previous literatures. The reviewed topic of gasification process consists of the potential of biomass in Thailand, the biomass gasification including the influence of feedstock characteristic, the parametric analysis, the design of plant configuration and the tar formation and removal. For the FT synthesis process, the FT catalyst improvement, the parametric analysis, the correlations of chain growth probability proposed and the studies of integrated of the BG-FT process are also presented.

Chapter IV presents the developing of biomass gasification model and the BG-FT model which the tar formation and reaction kinetic of char gasification are taken into account at gasification. The correlations, parameters and the model assumptions are presented.

Chapter V presents the study of the effects of changes in the ratio of gasifying agent on the syngas yield, H_2/CO ratio, total energy consumption and CGE of the gasification systems utilizing different types of gasifying agent (i.e., air-steam and CO_2-steam) at different gasifying temperatures.

Chapter VI presents the technical and economic studies of the BG-FT process with different configurations (i.e., once-through and with recirculation concepts). The influence of changing an FT off-gas recycle fraction at different FT reactor volumes on the performance of the syngas processor, the FT synthesis and the overall energy efficiency of BG-FT process is discussed.

Chapter VII presents the technical and environmental studies of the BG-FT process with and without tar removal unit based on steam reforming and ATR. The most practical BG-FT process including the optimum structure of heat exchanger which designed based on the pinch design method is proposed. The optimization respected to economic objective, aiming at NPV maximization is also discussed.

Chapter VIII presents the parametric analysis of the new designed BG-FT process derived from chapter VII. The effect of changing a gasifying temperature, FT operating temperature and FT pressure on the diesel production rate, the PEI and the combination thereof is discussed. The suitable condition offers the best performance in economic and environmental point of view is proposed.

Chapter IX summarized all the results found in this research.

CHAPTER II
THEORY

In this chapter, the basic principles and theory related to this research are summarized. The interesting theory consists of the biomass characteristic, gasification technology including the main reactions, gasifying agents and type of gasifier, synthesis gas cleaning, tar removal technology, FT technology, FT catalysts and types of FT reactors. Moreover, the calculation methodology of energy efficiency, pinch analysis, economic analysis as well as environmental impact evaluation applied in this study is also discussed.

2.1 Biomass

2.1.1 Meaning of biomass

Biomass is the organic materials that are derived from plants or animal, it includes only living and recently dead biological species that can be used as fuel or feedstock in chemical production. It does not include organic materials that over many millions of years have been transformed by geological processes into substances such as coal or petroleum. Biomass comes from botanical (plant species) or biological (animal waste or carcass) sources, or from a combination of these. Common sources of biomass are:

- Agricultural: food gain, bagasse, corn stalks, straw, seed hulls, nutshells and manure from cattle.
- Forest: trees, wood waste, wood or bark, sawdust, timber slash, and mill scrap.
- Municipal: sewage sludge, food waste and waste paper.
- Energy: poplars, willows, alfalfa, corn, and soybean and other plant oils. Biological: animal waste, aquatic species, biological waste.

2.1.2 Biomass formation

Botanical biomass is formed through conversion of carbon dioxide (CO_2) in the atmosphere into carbohydrate by the solar energy in the presence of chlorophyll and water. Biological species grow by consuming botanical or other biological species. The process is shown in Eq.(2.1).

$$\text{Living plant} + CO_2 + H_2O + \text{sunlight} \rightarrow CH_mO_n + O_2 - 480 \text{kJ/mol} \qquad (2.1)$$

The chemical energy stored in plants is then passed to the animals and human those take the plants as food. Animal and human waste also contributes to biomass.

2.1.3 Types of Biomass

Biomass could be classified into two major groups as shown in Table 2.1. Virgin biomass comes directly from plants or animals. Waste comes from biomass-derived products.

Table 2.1 Two major groups of biomass and their sub classifications (Basu, 2010a)

Virgin	Terrestrial biomass	Forest biomass, grasses, energy crops, cultivated crops
	Aquatic biomass	Algae, Water plant
Waste	Municipal waste	Municipal solid waste, bio-solid, sewage, landfill gas
	Agricultural solid waste	Livestock and manures, agricultural crop residue
	Forestry residues	Bark, leaves, floor residues
	Industrial wastes	Demolition wood, sawdust, waste oil or fat

2.2 Gasification technology

Gasification is the controlled partial oxidation of a carbonaceous material which proceeds at temperatures ranging between 600 and 1500 $^{\circ}$C, and it is achieved by supplying less oxygen than the stoichiometric requirement for complete combustion. This process is an intermediate process between combustion (thermal degradation with excess oxygen) and pyrolysis (thermal degradation in the absence of oxygen). Depending upon the process type and operating conditions, producer gas

with different heating value (which is a combination of combustible and non-combustible gases) is produced.

Gasification technology has been widely used to produce commercial fuels and chemicals. The use of gasification facilities to produce synthesis gas in the chemical manufacturing and petroleum refinery industries has been widely developed. An advantage of this technology is its ability to produce a reliable, high-quality syngas product that can be used for energy production or as a building block for chemical manufacturing processes. In addition, it can handle with a wide variety of gaseous, liquid, and solid feedstocks. Conventional fuels such as coal and oil, as well as low- or negative-value materials and wastes such as petroleum coke, heavy refinery residuals, secondary oil-bearing refinery materials, municipal sewage sludge, and chlorinated hydrocarbon byproducts have all been used successfully in gasification operations. Biomass and crop residues also have been gasified successfully.

2.2.1 Mechanism of biomass gasification

Biomass gasification involves a complex series of chemical reactions, as shown in Figure 2.1. In a typical gasification process, several reaction stages e.g., drying, pyrolysis, char and tar gasification, are usually take place.
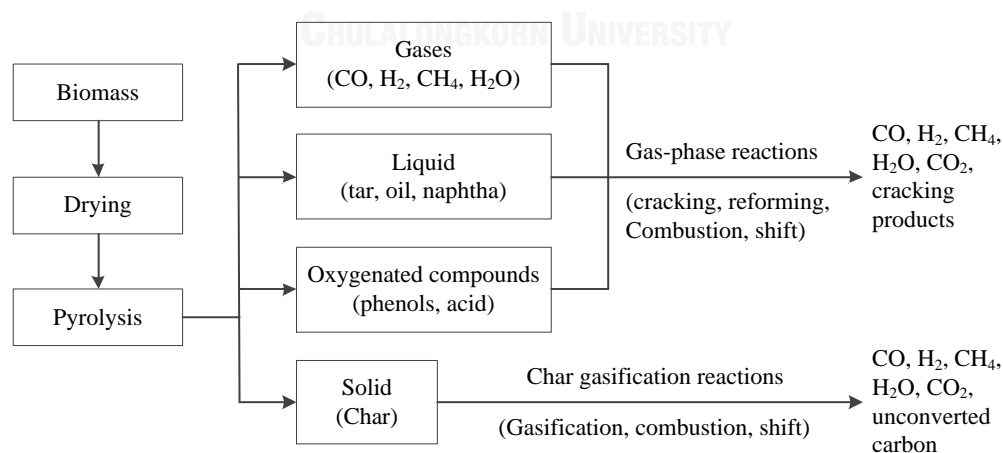
Figure 2.1 Basic chemistry of biomass gasification process (Yang and Chen, 2015).

The detailed reactions that occur during gasification are summarized in Table 2.2. Biomass materials are preheated and dried at 100-200 ^{o}C, before entering the pyrolysis stage. As the initial stage of gasification, pyrolysis which takes place at relatively low temperatures in the range of 200-700 ^{o}C without the use of a gasifying agent, partially removes carbon from the feed but does not add hydrogen. During pyrolysis, a portion of biomass is transformed into condensable hydrocarbon tars, gases, and solid char (R1). Thereafter, a series of reactions occur in the gasifier, including a homogeneous gas-phase reaction and a heterogeneous gas-solid char gasification reaction shown as reactions (R2-R14). Partial (R2) and complete combustion (R3) of char, as well as water gas reaction (R5) and hydrogasification (R6), which involves adding hydrogen to carbon to produce fuel with a higher hydrogen-to-carbon (H/C) ratio. Among all reactions, the complete combustion of char releases highest amount of energy. In gas phase gasification reactions, oxidation (R7-R9), steam reforming (R13), and cracking (R14) reactions of volatiles take place. The water gas shift (WGS) reaction (R10) plays a significant role in generating hydrogen. The methanation reaction (R11) always proceeds in the absence of any catalyst. Both water gas shift and methanation reactions are reversible reaction; therefore it can proceed in either direction depending on the specific temperature, pressure, and concentration of the reacting species. As a result of the above reactions, the product gas from gasification is a mixture mainly consists of H_2, CO_2, CO, CH_4 and water vapor.

Table 2.2 Main chemical reactions of biomass gasification (Yang and Chen, 2015).

Reactions	ΔH_{298}, kJ/mol	Reaction number	Eqs.
Pyrolysis			
Biomass $\rightarrow$ char + tar + H_2O+light gas ($CO+H_2+CO_2+CH_4+C_2+...$)	Endothermic	R1	(2.2)
Char combustion			
$C+0.5O_2 \rightarrow CO$	-111	R2	(2.3)
$C+O_2 \rightarrow CO_2$	-394	R3	(2.4)
Char gasification			
$C+CO_2 \rightarrow 2CO$	172	R4	(2.5)
$C+H_2O \rightarrow CO+H_2$	131	R5	(2.6)
$C+2H_2 \rightarrow CH_4$	-75	R6	(2.7)
Homogeneous volatile oxidation			
$CO+0.5O_2 \rightarrow CO_2$	-254	R7	(2.8)
$H_2+0.5O_2 \rightarrow H_2O$	-242	R8	(2.9)
$CH_4+2O_2 \rightarrow CO_2+2H_2O$	-283	R9	(2.10)
$CO+H_2O \rightarrow CO_2+H_2$	-41	R10	(2.11)
$CO+3H_2 \rightarrow CH_4+H_2O$	-88	R11	(2.12)
Tar reactions			
$C_nH_m+(n/2)O_2 \rightarrow nCO+(m/2)H_2$	Endothermic	R12	(2.13)
$C_nH_m+nH_2O \rightarrow nCO+(m/2+n)H_2$		R13	(2.14)
$C_nH_m \rightarrow (m/4)CH_4 + (n-m/4)C$		R14	(2.15)
$C_nH_m+(2n-m)H_2 \rightarrow nCH_4$		R15	(2.16)

2.2.2 Gasifying agents

The gasifying agents react with carbonaceous materials to convert them into light gases such as CO and H_2. The use of different gasifying agents resulted in different heating value of product gas. The commonly used gasifying agents are air, oxygen and steam.

2.2.2.1 Air gasification

The air gasification is the simplest gasification process. Excess char derived from the pyrolysis process is burned with a restricted supply of air (usually at an equivalence ratio of 0.25). The product is a low-energy gas containing primarily hydrogen and carbon monoxide diluted with the nitrogen from the air. The heating value of the produced gas is in the range of 3.5-7.8 MJ/Nm^3, which makes it suitable for boiler and engine applications. The reactor temperature depends on the air and also biomass feed rates. The bed temperature decreases as the air feed rate decreases, as a result, the yield of gas decreases while that of tar increases.

2.2.2.2 Steam gasification

The external heat source is required for steam gasification due to the endothermic steam reforming reactions. Using a mixture of steam and air as a gasifying agent is therefore has been studied by several researchers. The combustion of biomass, which is the highly exothermic reaction, can provide the required heat. At the elevated temperature, various gases are produced in the biomass devolatilization process. Steam reacts with carbon monoxide to produce hydrogen and carbon dioxide. Compared to air gasification, steam gasification produces a higher energy producer gas. The produced gas, which is rich in hydrogen, had been found to have a heating value ranging in the range of 10-18 MJ/Nm^3.

2.2.2.3 Oxygen gasification

If the amount of nitrogen supplied to the gasification process is limited, the oxygen is selected as a gasifying agent. Normally, the product gas derived from oxygen gasification has a heating value ranging in the range of 12-28 MJ/Nm^3. A produced gas is economically distributed in pipeline network systems; therefore, it is conveniently used as fuel for combustion unit or possibly as raw material for chemical production process. However, in this case, an oxygen plant or a nearby source of oxygen is required, which may elevate the capital cost necessary for the plant installation.

2.2.3 Biomass gasifiers

A gasifier is the device in which biomass gasification takes place. The gasifier can be categorized into three types (Figure 2.2) i.g., updraft, downdraft, and fluidized beds. All of these types have the same four reaction zones: drying, pyrolysis, combustion, and reduction. However, the zones are distributed differently in each type. In a typical updraft gasifier (Figure 2.2(a)), the preheated gasifying agent enters the reactor from the bottom and flows upward, and the producer gas leaves from the top of the reactor where incoming biomass is added. This type of gasifier can be used with a wide range of moisture contained fuel, as the heat transfer is enhanced with the counter flow arrangement. The disadvantage of the updraft gasifier is the high tar yield because the tar formed during pyrolysis is partly taken away by producer gas. In a downdraft gasifier (Figure 2.2(b)), the reaction zones differ from those of updraft gasifiers. Compared with the updraft gasifier, some large molecular tars can be decomposed by thermal cracking in the downdraft type; the produced gas contains less concentrations of tar. For this reason, the downdraft gasifier has the widest applications, especially for small-scale engines and heating supply. In a fluidized bed gasifier, oxygen or steam enters at the bottom of the reactor, carrying biomass, which has been reduced to a fine particle size, upward through a bed of heated silica particles. The biomass is decomposed in the hot bed, forming char and gaseous product. Fluidized bed gasifiers can be further classified into bubbling fluidized bed and circulating fluidized bed (Figure 2.2(c)). Fluidized beds typically operate in the temperature range of 800-1000 ^{o}C, in order to avoid the ash agglomeration and sintering, allowing the safe operation of fuel with high ash content. Additionally, the large thermal inertia and vigorous mixing benefit the flexibility of various biomass feed rates and compositions.
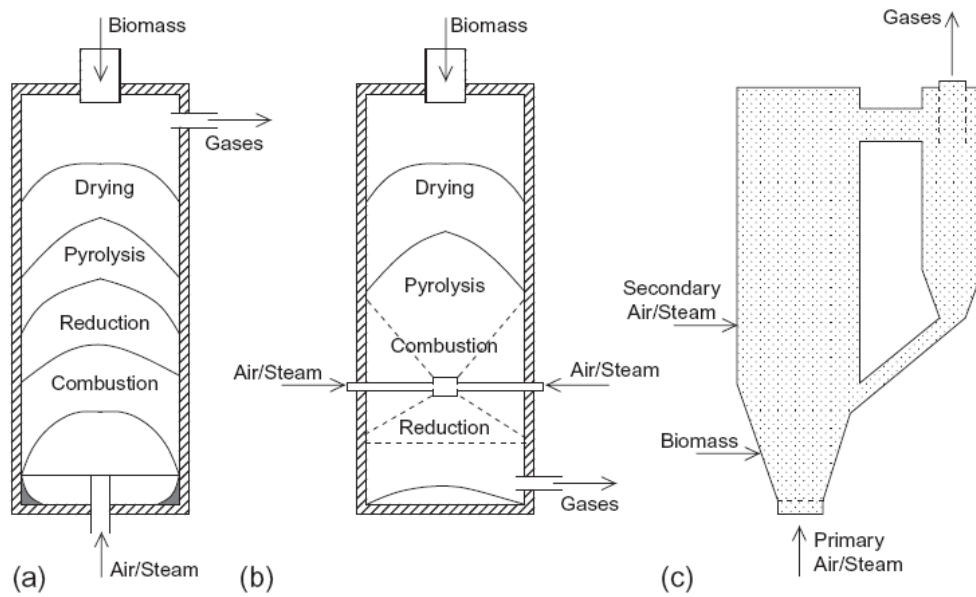
Figure 2.2 Schematic structure of different gasifiers: (a) updraft, (b) downdraft, and (c) fluidized bed (Yang and Chen, 2015).

As the gasifier plays a crucial role in a gasification plant, and it is responsible for keeping syngas production as steady as possible, the selection of suitable gasifier which depends on feedstock properties, the reaction conditions, the desired end use, and the quantity of the producer gas, is therefore required. The advantages and disadvantages of different types of gasifier are summarized in Table 2.3.

Table 2.3 Properties of biomass gasifier (Yang and Chen, 2015).

Advantages	Disadvantages
Fixed/ moving bed, updraft	
- Simple and reliable design	- Large tar production
- High carbon conversion efficiency	- Potential channeling, bridging, clinkering
- Low dust levels in gas	- Small feed size
- High thermal efficiency	- Low-output
Fixed/moving bed, downdraft	
- Simple, inexpensive process	- Minimum feed size
- Low tar content in product gas	- Limited ash content allowable in feed
	- Limits to scale up capacity
	- Potential for bridging and clinkering
Fluidized bed	
- Short residence time	- Low char conversion rate
- High ash fuels acceptable	- The efficiency is not high
- Excellent heat and mass exchange	- High product gas temperature
- Flexible feed rate and composition	- High tar and fines content in gas
- Uniform temperature distribution in gasifier	- Possibility of high carbon content in fly ash
- High CH_4 in product gas	- Complicated operation
- High volumetric capacity	
- Able to pressurize	

2.3 Synthesis gas cleaning

The gas produced by gasification contains impurities; typical are the organic impurities tars, the inorganic impurities NH_3, HCN, H_2S, COS, HCl and furthermore volatile metals, dust and soot. The raw syngas maybe further treated to clean syngas prior transfers to the chemical plants in order to meet the process feed gas specifications. Figure 2.3 showed the well-known and commercially available cleaning technologies of raw syngas. In general practice, hot raw syngas is cooled down when directly contact with water in quench tower then the solid particles and the volatile alkaline metals are removed. NH_3 and halides (HCl, HBr, and HF) are removed together in a water washer and H_2S is removed either by absorption or conversion to elementary sulphur. Due to lower price of sulphur, the absorption is preferred when relatively small amounts of H_2S are presented. For COS and HCN which are difficulty removed impurities could be captured in active carbon filters which are also applied as downstream guard beds.
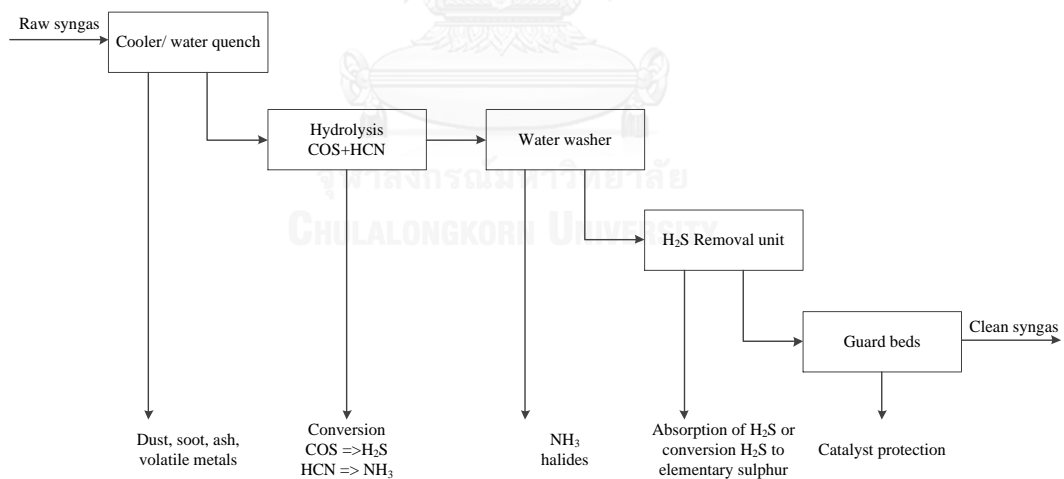
Figure 2.3 Schematic of the well-known and commercially available cleaning technologies of raw syngas (Boerrigter et al., 2004).

2.4 Tar destruction

Tars are condensable organic compounds with boiling points between 80-350 ^oC. Tars start to condense when the system temperature decreases below 350 ^oC. The condensed tar causes fouling of downstream equipment and ultimately in failure of the system. There are three well-known methods of tar destruction i.e. thermal cracking, catalytic cracking and scrubbing. At temperature above 1000-1200 ^oC, tars are destroyed without a catalyst, usually by addition of steam and oxygen which acts as selective oxidant. The disadvantages of this practice are high production of soot and low thermal efficiency and the high thermal resistance material is required due to its high operating temperature. The mentioned problems are eliminated when the catalytic cracking using dolomite or Ni-based catalyst is applied. However, the technology is still not fully proven as the catalyst consumption and costs are the concern issues. Tar can also be removed at low temperature by advance scrubbing with an oil based medium which the tar is subsequently stripped from the oil and returns to the gasifier. In the combined syngas and chemical production process, the conversion of tar to syngas is widely paid attention because it can increase the amount of syngas and also downstream products. The advantages and disadvantages of different syngas production technologies are summarized in Table 2.4.

Table 2.4 Syngas production technologies (Bengtsson, 2011; Stemmler and Müller, 2011).

Technology	Advantages	Disadvantages
Steam reforming (SMR)	- Most extensive industrial experience - Oxygen is not required - Lowest process temperature - Best H_2/CO ratio for H_2 production application	- H_2/CO ratio often higher than required when CO also is to be produced - Highest air emissions

Table 2.4 Syngas production technologies (Cont.)

Technology	Advantages	Disadvantages
Heat exchanger reforming	- Compact overall size and "footprint" - Application flexibility offers additional options for providing incremental capacity	- Limited commercial experience - In some configurations, must be used in tandem with another syngas generation technology
Two-step reforming	- Size of SMR is reduced - Low CH_4 slip favors high purity syngas applications - CH_4 content can be tailored by adjusting secondary reformer outlet temperature	- Increase process complexity - Higher process temperature than SMR - Usually requires oxygen
Autothermal reforming (ATR)	- H_2/CO often is favorable - Lower process temperature requirement than POX - Low CH_4 content can be tailored by adjusting reformer outlet temperature	- Limited commercial experience - Usually requires oxygen
Partial oxidation (POX)	- Feedstock desulfurization is not required - Absence of catalyst permits carbon formation and therefore, operation without steam, significantly lowering syngas CO_2 content - Low methane slip - Low natural H_2/CO ratio is an advantage for applications requiring ratio < 2.0	- Low H_2/CO is a disadvantage for applications requiring ratio 2 - Very high process operating temperatures - Usually requires oxygen - Complicated heat integration is required - CH_4 content in syngas is low and not easily modified to meet downstream processing requirements

2.5 Fischer-Tropsch technology

The Fischer-Tropsch (FT) process is recognized as a process used to produce long-chain hydrocarbons from synthesis gas which mainly consists of H_2 and CO. This process is a highly exothermic polymerization reaction over Cobalt or Iron based catalysts which CO is hydrogenated to form $-CH_2-$ intermediate which then grows to form different hydrocarbons of variable lengths, the reaction is shown in Eq.(2.18).

$$nCO+2nH_2 \rightarrow (-CH_2-)_n +nH_2O \tag{2.18}$$

The other possible reactions are shown in Eqs.(2.19)-(2.22).

$$2CO+H_2 \rightarrow (-CH_2-)_n +CO_2 \tag{2.19}$$

$$3CO+H_2 \rightarrow (-CH_2-)_n +2CO_2 \tag{2.20}$$

$$CO_2+H_2 \rightarrow (-CH_2-)_n +H_2O \tag{2.21}$$

$$CO+H_2O \rightarrow H_2+CO_2 \tag{2.22}$$

Eqs.(2.23)-(2.27) show the desired products (alkanes, alkenes, and alcohols) and undesired products (aldehydes, ketones, esters, acids, carbon) formed during FT synthesis.

Alkanes: $\quad nCO+(2n+1)H_2 \rightarrow C_nH_{2n+2}+nH_2O \tag{2.23}$

Alkenes: $\quad nCO+2nH_2 \rightarrow C_nH_{2n} +nH_2O \tag{2.24}$

Alcohols: $\quad nCO+2nH_2 \rightarrow C_nH_{2n+2}O+(n-1)H_2O \tag{2.25}$

Aldehydes; ketones: $\quad nCO+(2n-1)H_2 \rightarrow C_nH_{2n}O+(n-1)H_2O \tag{2.26}$

Carboxylic acids: $\quad nCO+(2n-2)H_2 \rightarrow C_nH_{2n}O_2 +(n-2)H_2O \tag{2.27}$
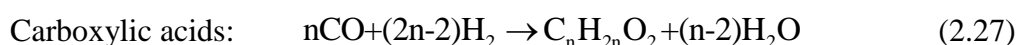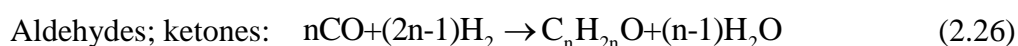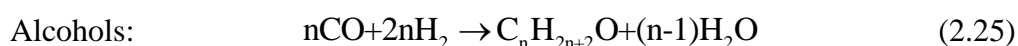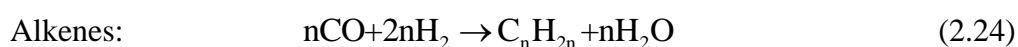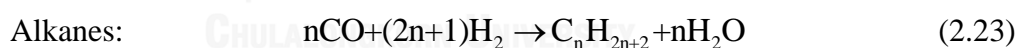
2.5.1 Fischer-Tropsch reactor

Since the FT reactions are highly exothermic, therefore it is important to rapidly remove the heat of reaction from the catalyst particles in order to avoid overheating of the catalyst which would otherwise result in an increased rate of

deactivation due to sintering and fouling and also in the undesirable high production of methane. High rates of heat exchange are achieved by forcing the syngas at high linear velocities through long narrow tubes packed with catalyst particles to achieve turbulent flow, or better, by operating in fluidized catalyst bed reactor. The commercial available types of FT reactor e.g., multitubular fixed bed and fluidized bed reactors, are explained as follow:

2.5.1.1 Multitubular fixed-bed FT reactor

This reactor equipped with large amount of tubes packed with catalyst which the high linear velocity syngas is forced through. The steam which is supplied on the shell side is used as a coolant for heat removal (Figure 2.4). The reactor temperature is controlled by setting the pressure at which the steam raised and released. The multitubular fixed-bed FT reactor has an advantage in term of robustness and provides high productivity; however, it is difficult to design and scale-up, poor heat transfer and needs high investment cost due to its complex structure. Regarding to the complex structure, the pressure drop inside the reactor is found to be high; as a result, the small size of catalyst is required. Moreover, the catalyst deactivation caused from the fouling of heavy wax at the pore entrance is another encountered problem, which the periodical replacement of catalyst is necessary.
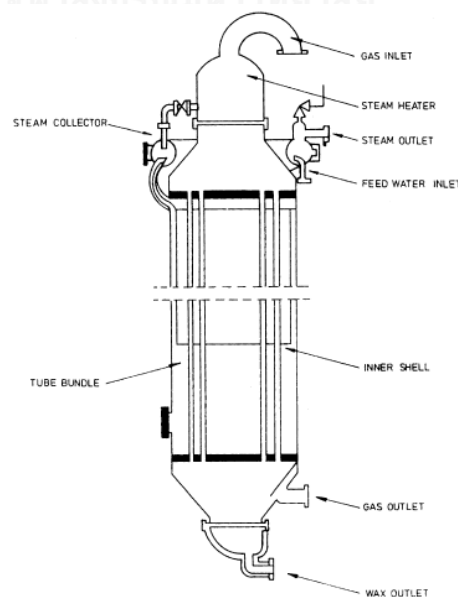
Figure 2.4 Multitubular fixed bed FT reactor (Dry, 2002).

2.5.1.2 Fluidized-Bed Reactor

There are two classes of fluidized-bed reactor e.g., two-phase reactors which only solid catalyst and gas are presented (Figures 2.5(a) and (b)) and three-phase slurry reactors which the finely catalyst is suspended in liquid wax with gas bubbling through Figure 2.5(c).
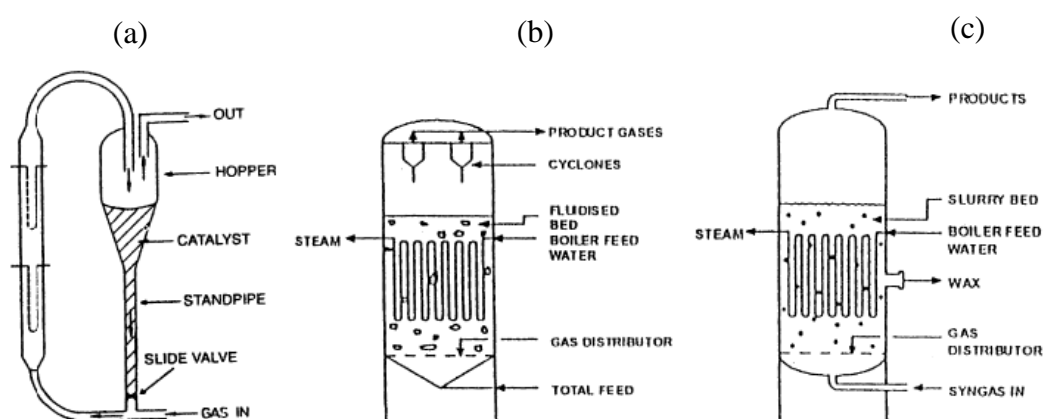
Figure 2.5 Fluidized bed FT reactors; (a) CFB reactor; (b) FFB reactor and (c) slurry phase bubbling bed reactor (Dry, 2002).

1) Two-phase reactor

There are two types of two-phase reactor: circulating fluidized-bed (CFB) and fixed fluidized-bed (FFB) as shown in Figures 2.5(a) and (b), respectively. The operation of CFB is similar to that of catalytic crackers, with fluidized catalyst moving down the standpipe in dense phase mode and then being transported at high gas velocities by the incoming syngas up the reaction zone side in lean phase mode. The FFB operated as a dense phase turbulent bed reactor. The advantages of a fluidized-bed reactor compare with a fixed-bed reactor are the good temperature control during highly exothermic FT reactions, higher gas and solid catalyst contact efficiency due to the fluidization, easy replacement of the catalyst in a shorter time and the possibility of loading fresh catalyst during the normal operation and high production capacity due to higher gas throughput. However, the fluidized-bed reactor

has some limitations that it needs special equipment such as cyclones for catalyst separation which can have an effect on the cost efficiency. Also while using small catalyst particles, the deposition of heavy product on the catalyst causing agglomeration and blockage of the fluidization.

2) Three-phase reactor (Slurry phase bubbling bed reactor)

The slurry phase bubbling bed reactor Figure 2.5(c) is a cylindrical vessel in which gaseous reactants (i.e. synthesis gas) is sparged into slurry of liquid products (liquid wax) and finely dispersed catalyst particles. The catalyst particles are transported in the slurry by rising of gas bubbles and it promotes the chemical reaction that converts the synthesis gas to the variable lengths of hydrocarbon products which can be further upgraded to valuable products such as gasoline, diesel or jet fuel. Compared to the multitubular fixed-bed reactor, the slurry reactor is much easier to design and more economically attractive. It also has the advantages in term of fast heat removal and good temperature control due to the well mixing.

2.5.2 Fischer-Tropsch catalyst

Figure 2.6 shows that Iron, Nickel, Cobalt and Ruthenium are the only metals that have the FT activity required for commercial applications. If the price of Iron is 1.0, the price of Nickel is 250, the price of Cobalt is 1000 and that of Ruthenium is 50000. As Nickel has high selectivity to CH_4 and the price of Ruthenium is far too high and furthermore the availability of this metal is too low for large scale application, therefore, the Iron and Cobalt are the only feasible metals for FT synthesis. Cobalt is used in the low-temperature FT process, because at high temperature the selectivity of this catalyst to CH_4 is high. Price of Cobalt is more expensive than that of Iron; therefore, the dispersion of Cobalt on high surface area stable supports such as Al_2O_3, SiO_2 or TiO_2 is applied, typically by impregnating the supports with aqueous solutions of Cobalt salt. The main deactivation reasons for Cobalt and Iron based FT catalysts are reoxidation of the active phase by water and poisoning by sulphur. Water has stronger effect on Iron based catalysts, whereas Cobalt is more sensitive to sulphur compounds.

Active Metals	Cost	Activity
Ni	1	Methane formation
Fe	250	WGS activity
Co	1000	Very active; linear, high C_n, low temp
Ru	50,000	Very active; very expensive!
Rh	∞	Impossible to use on industrial scale

Figure 2.6 Comparison of catalytic activity of each metal (Dry, 2002)

2.5.3 H_2/CO usage ratio

Over a Cobalt based catalyst, approximately 2.1 molecules of H_2 react with 1 molecule of CO to form 1 molecule of hydrocarbon unit (-CH_2-) and 1 molecule of H_2O, therefore, the H_2/CO usage ratio equal to 2.1 is required. For Iron based catalyst, the water gas shift reaction takes place simultaneously in the reactor; hence lowering the usage ratio less than 2.1 makes it possible to feed in the FT reactor. Such the syngas derived from coal or biomass gasification contains low concentration of H_2 which cause H_2/CO ratio less than 2.1. In case of low temperature FT process over Cobalt based catalyst the water gas shift reaction is slow and does not often reach equilibrium. The adjustment of H_2/CO ratio in external water gas shift unit is required in order to correct the H_2/CO ratio of the syngas before supplying to the FT reactor.

2.5.4 Fischer-Tropsch reaction conditions

There are currently two FT reactor operating conditions e.g., high temperature (HTFT) and low temperature (LTFT) FT synthesis. Typically, the FT operating pressure is in the range of 20-60 bar. The comparison of operation characteristic for HTFT and LTFT processes as well as the reactor types which are used in each case is summarized in Table 2.5.

2.5.4.1 High-temperature FT (HTFT)

The reactions take place in the range of temperature around 300-350 ^{o}C over the Iron based catalysts. The mainly derived products are gasoline and linear low molecular weight olefins. Significant amount of oxygenates are also produced. Diesel may be further produced by oligomerisation of the olefins.

2.5.4.2 Low-temperature FT (LTFT)

The reactions take place in the range of temperature around 200-250 ^{o}C over either the Iron or Cobalt based catalysts. The mainly derived product contains high amounts of paraffin and linear chain hydrocarbon, the selectivity to high molecular weight linear waxes is very high. The primary diesel cut and the hydrocracking of the waxes give high yield of diesel fuels. The primary gasoline cut needs further treatment to obtain a high octane number.

Table 2.5 Operation characteristics for LTFT and HTFT processes (Dry, 2002).

	LTFT	HTFT
Reactor Types	Multitubular, fixed bed Three-phase	Two-phase
Temperature	220-250 ^{o}C	300-350 ^{o}C
Catalysts	Iron or Cobalt	Iron
Products	Diesel and Waxes	Olefins and Gasoline

2.5.5 Fischer-Tropsch product distribution

The FT product consists of the straight chain saturated hydrocarbons from CH_4 up to heavy waxes, olefins and oxygenates compound which are derived from polymerization process of $-CH_2-$ monomer. Due to the step-wise growth mechanism, the hydrocarbon products can be described by the ASF (Anderson, Schulz, Flory) distribution which can be shown in its molar (M_n) or mass (W_n) distribution variants as shown in Eqs.(2.28) and (2.29), respectively.

$$M_n = \alpha^{n-1}(1-\alpha) \tag{2.28}$$

$$W_n = \alpha^{n-1}(1-\alpha)^2 n \tag{2.29}$$

The example of ASF distributions are shown in Figure 2.7. The chain growth probability *(α)* is recognized as a parameter used to characterize a FT product distribution. High value of α means that the product contains more long chain hydrocarbons while less CH_4. The selectivity of a catalyst to long-chain hydrocarbons is often given as the selectivity to C_5^+. The higher value of α occurs at the higher pressure, lower temperature and also lower inlet H_2/CO ratio. The value of α is also dependent on the characteristics of the catalyst such as pellet size, pore size, degree of reduction of the active metal and promoters. In order to derive the highest yield of diesel, the highest amount of wax is firstly produced then hydrocracked it into the diesel fraction (C_9-C_{25}). Hence, the world-wide FT research is today focused on how to prepare catalysts that give high value of α. A typical value of α today is around 0.9 for a wax-producing FT process.
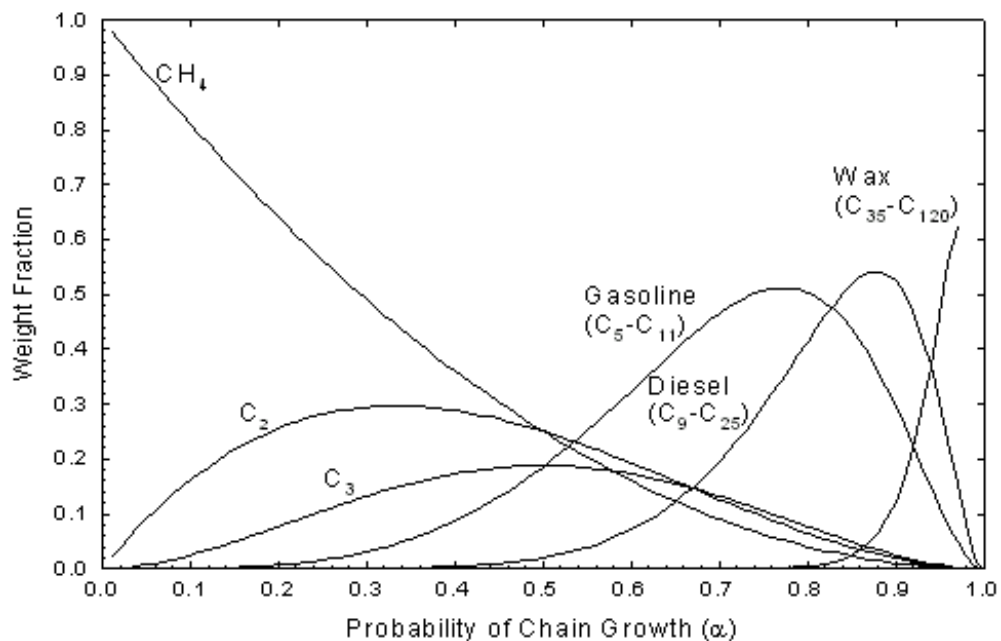
Figure 2.7 Schematic showed the ASF distribution (A. P. Steynberg et al., 2004)

The synthesized FT liquid fuel is ultraclean product due to its sulphur free characteristic and has higher amount of valued portion compared to the one derived from crude distillation. Figure 2.8 shows a comparison of the products derived from crude distillation and the typical FT process.

Figure 2.8 Products derived from FT and from crude distillation (Wood et al., 2012)

2.6 Energy analysis

2.6.1 Energy efficiency

The energy analysis is performed to investigate whether the biomass is efficiently converted to the required product. In the analysis, the energy efficiency is defined as the ratio of the enthalpy of valuable products and that of biomass (Vaezi et al., 2008) as shown in Eq.2.28.

$$\text{energy efficiency} = \frac{\text{heating value of valuable products}}{\text{heating value of biomass}} \tag{2.28}$$

33

2.6.2 Thermal pinch analysis

The thermal pinch analysis is the methodology used in whole plant energy management by determining the optimal structure of the heat exchanger which offers the maximum internal heat recovery and minimum external utilities requirement.

2.6.2.1 Composite curves

The fundamental concept in pinch analysis is composite curves which visualize the flow of heat between the hot and cold process streams selected for heat integration. A composite curve is obtained by plotting the cumulative enthalpy of streams, cold or hot, against temperature. The relative position of the composite curves depends on the minimum temperature difference (ΔT_{min}) between cold and hot streams. This sets the pinch position as the place where the heat transfer between the hot and cold streams is the most constrained. The composite curves allow determining the minimum energy requirement (MER) from stream data without ever designing the heat exchangers. These MER are the minimum hot (Q_h) and cold (Q_c) utilities required for driving the heat exchanger network (HEN), with a minimum driving force of ΔT_{min} at pinch. The pinch principle states that any design where heat is transferred across the pinch will require more energy than minimum requirements; therefore, a heat recovery problem is divided into two sub-systems e.g., above and below pinch.

The composite curve construction is explained in the following example. Table 2.6 presents the stream data chosen to illustrate the construction of the composite curves. The necessary information consists of stream or segment temperatures (e.g. supply (T_s) and target (T_t)) and heat capacity of each stream or segment which defined in Eq.(2.29).

$$CP = \Delta H / \Delta T \tag{2.29}$$

where ΔH is the enthalpy variation over the temperature interval ΔT. Conversely, the enthalpy change of a stream segment is calculated from Eq.(2.30).

$$\Delta H = CP \times (T_t - T_s) \tag{2.30}$$

where, $CP = F \times C_P$ $\tag{2.31}$

F and C_P shown in Eq.(2.31) represent the mass flow rate and the mass heat capacity, respectively.

Table 2.6 Stream data for composite curves construction

Stream	Name	T_s (°C)	T_t (°C)	CP (kW/°C)	ΔH (kW)
1	hot 1	220	60	100	-16,000
2	hot 2	180	90	200	-18,000
3	cold 1	50	150	150	15,000
4	cold 2	150	180	400	20,000

The graphical construction of the hot composite curve is shown in Figure 2.9. The two streams hot 1 and hot 2 are represented by the segments ab and cd with CP1 and CP2 equal to 100 and 200 kW/°C, respectively. The total enthalpy variation is $\Delta H_h = \Delta H_1 + \Delta H_2 =$ 16,000 + 18,000 = 34,000 kW. The interval between the target and supply temperatures is divided into three subintervals: 60-90, 90-180 and 180-220 °C. In each interval, the overall CP can be obtained simply by adding the CP of the active streams. For instance, in the first and third interval, there is only hot 1, so that CP = 100. In the second interval, both hot 1 and hot 2 are active, therefore CP = CP1+CP2 = 300. Thus, each change in the slope of the composite curve corresponds to the entry or to the exit of a stream. Slope close to zero (horizontal position) means very high CP, as in the case of phase transitions.

The graphical construction of the cold composite curve can be done using the same method (Figure 2.10). There are three temperature intervals: 50-130, 130-150 and 150-180 °C, where CP3 = 150, CP3 + CP4 = 550 and CP4 = 400. The total enthalpy variation is $\Delta H_c = \Delta H_3 + \Delta H_4 =$ 15,000+20,000 = 35,000 kW.

The hot and cold composite curves can be plotted on the same diagram as shown in Figure 2.11. The position of hot composite curve is fixed and that of the cold composite curve shifts to the right by adding an amount of heat to achieve the

$\Delta T_{\min}$. The graph shows that for $\Delta T_{\min} = 10\ ^{\circ}\text{C}$, $Q_{c} = 6{,}000$ kW and $Q_{h} = 7{,}000$ kW. The pinch is situated between 130 and 140 $^{\circ}\text{C}$.
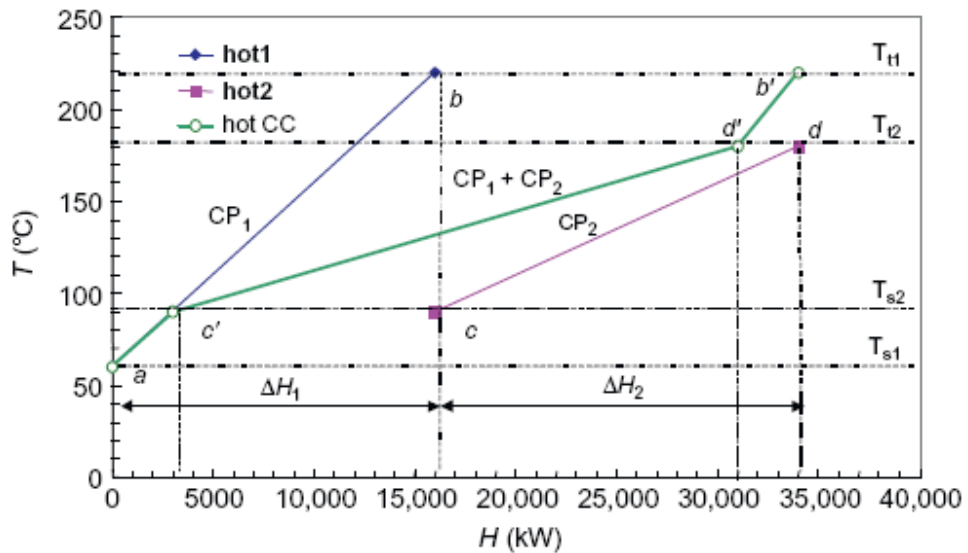
Figure 2.9 Construction of hot composite curve (Dimian et al., 2014)
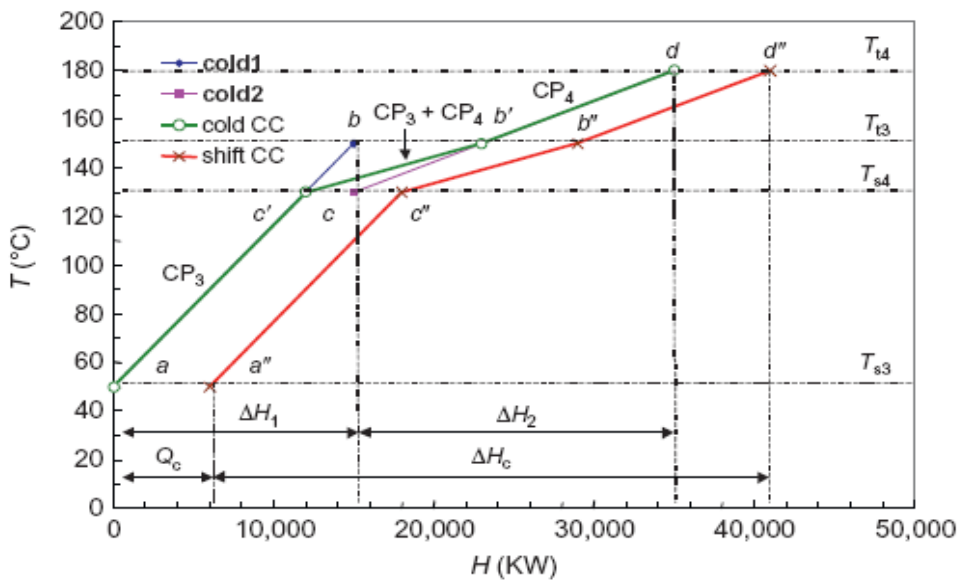
Figure 2.10 Construction of cold composite curve (Dimian et al., 2014)
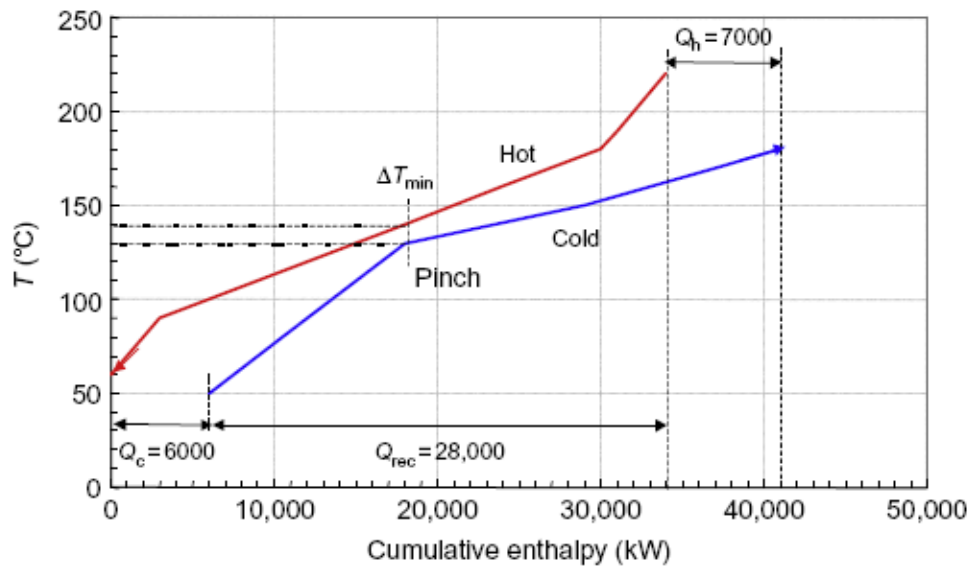
Figure 2.11 Hot and cold composite curves (Dimian et al., 2014)

2.6.2.2 Heat exchanger network design in the grid diagram

The optimum structure of heat exchanger is designed based on the pinch design method. The design of HEN in the balanced grid consists of the following steps:

1. Specify the process streams on the grid diagram showing the pinch division, the hot streams run from left to right at the top and the cold streams runs counter-currently at the bottom.

2. Divide the diagram at the pinch into two regions e.g., above (at the left) and below (at the right), then design for the stream systems above and below the pinch separately (Figure 2.12).
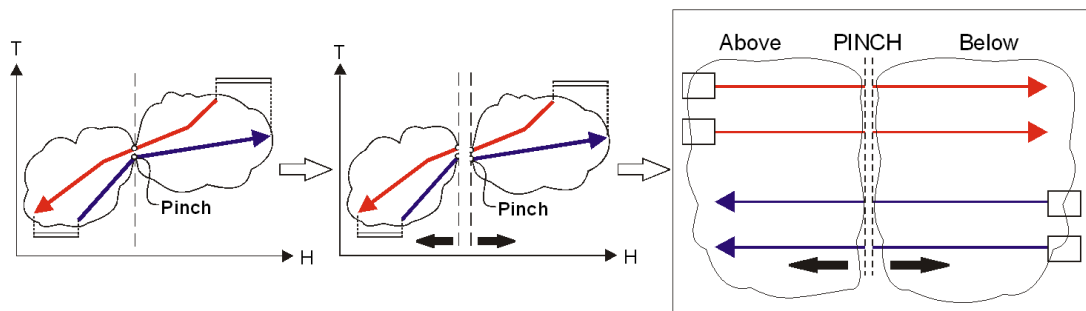
Figure 2.12 Diagram showing the pinch division (Kamp, 2007)

3. The design starts at the pinch where the heat transfer is the most constrained. The match procedure has to respect some feasibility rules. To maintain feasible temperature driving forces above the pinch, the following heuristic has to be respected;

$$CP_{hot} \leq CP_{cold} \qquad (2.32)$$

Similarly, below the pinch, the heuristic is shown below;

$$CP_{hot} \geq CP_{cold} \qquad (2.33)$$

where CP_{hot} and CP_{cold} are CP of hot and cold streams, respectively. The general CP rule can be formulated as;

$$CP_{in} \leq CP_{out} \qquad (2.34)$$

where CP_{in} and CP_{out} referring to CP of streams in and out of the pinch, respectively (regardless of being above or below the pinch).

For the case that the matches at pinch are not feasible (obeying the CP rule for all pinch matches is not possible), the count rule (number of streams rule) should be considered. Some common situations are depicted in Figure 2.13. The following explanations address the subsystem above the pinch. Two situations will be examined:
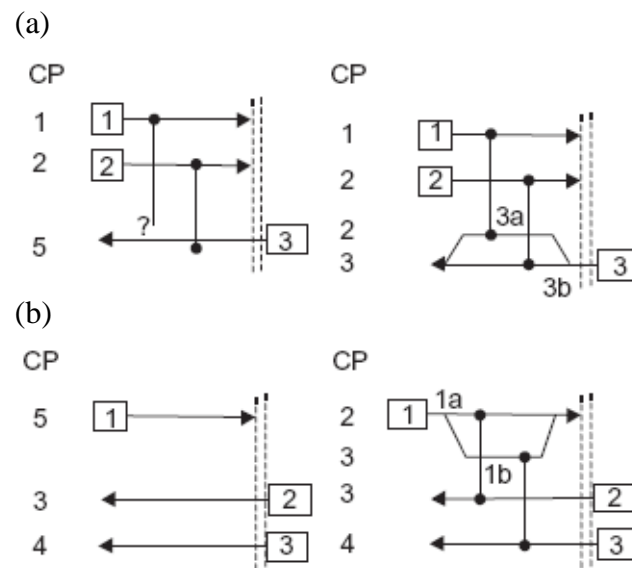
Figure 2.13 Principle of stream splitting at pinch; (a) the number of hot streams smaller than that of cold streams, (b) count rule is satisfied, but not the CP rule (Dimian et al., 2014)

1. The number of hot streams smaller than the number of cold streams

Figure 2.13a (left) shows that there are two hot streams against one cold streams. Above the pinch all hot streams have to be cooled down to pinch temperature without using cold utility. Therefore, there should be a partner cold stream for every hot stream at the pinch:

$$N_{hot} \leq N_{cold} \tag{2.35}$$

By splitting the cold stream into two segments, two matches become possible. Moreover, the split must be done such to respect the CP rule, as shown in Figure 2.13a (right).

2. Count rule is satisfied, but not the CP rule

Figure 2.13b (left) illustrates this situation by one hot stream and two cold streams. The hot stream must be split into two parts such as the CP of hot streams becomes smaller than that of the corresponding cold streams as shown in Figure 2.13b

(right). It may appear also that the count rule is satisfied, but the CP rule fulfilled only partially. In this case, the largest cold stream should be splitted. The analysis can be extended below the pinch, where the count rule becomes:

$$N_{\text{cold}} \leq N_{\text{hot}} \tag{2.36}$$

Considering that the hot and cold streams are in and out, respectively, the general count rule can be formulated as:

$$N_{\text{out}} \leq N_{\text{in}} \tag{2.36}$$

The CP and count rules can be put together into a general design procedure at pinch, as illustrated by Figure 2.14. First, the stream count rule is checked. If not fulfilled, a first stream split is performed to balance streams, cold stream above the pinch, or hot stream below the pinch. Then the CP rule is checked for matches close to the pinch. If not fulfilled, again stream splitting is executed, this time opposite to the first. Note that the above rules might be not respected away from the pinch.
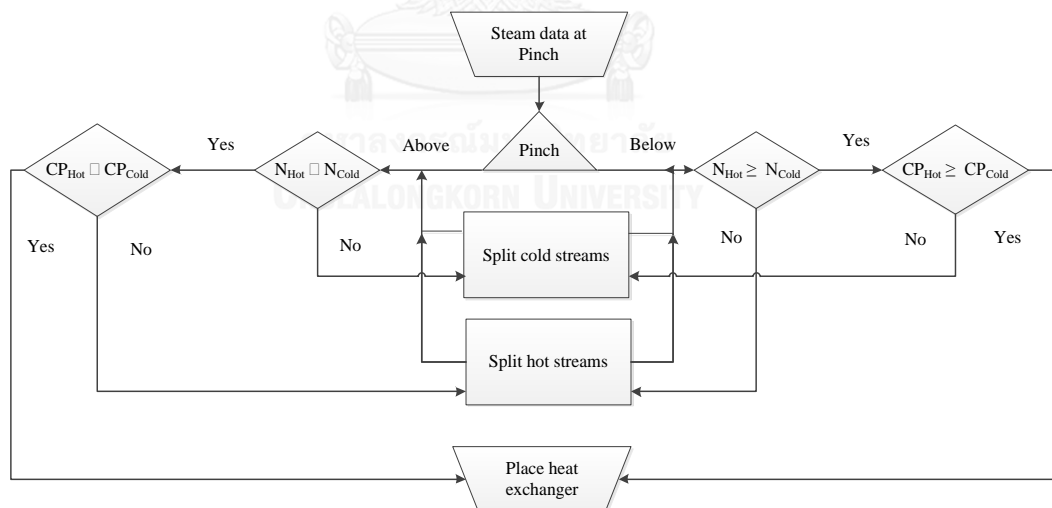
Figure 2.14 General HEN design procedure at pinch (Dimian et al., 2014)

2.7 Economic analysis

In this study, the NPV is used as an economic indicator to justify whether the considered process is feasible. The incremental NPV is also used when two processes are compared. The expressions and parameters used in the economic evaluation are discussed as follow:

2.7.1 Capital cost

The total capital cost consists of the direct costs (e.g., equipment, installation and construction) and the indirect costs (e.g., design, power distribution, utilities and control building). It is determined using the factored estimation method (Eq.(2.37)) by scaling from a base capacity and base cost reported in the previous works as summarized in Table 2.7 (Hamelinck et al., 2004; Ng and Sadhukhan, 2011).

$$\frac{COST_{size2}}{COST_{size1}} = \left(\frac{SIZE_2}{SIZE_1} \right)^{sf} \tag{2.37}$$

where $COST_{size1}$ is the cost of the base scale and $COST_{size2}$ is the cost of the desired scale. $SIZE_1$ and $SIZE_2$ are the capacity of the base scale and that of the desired scale, respectively. sf is the power scaling factor or scale exponent.

The cost index method is applied to update the capital cost of a chemical plant from a past time to the present time. The Chemical Engineering Plant Cost Index (CEPCI) for the years 1999, 2002 and 2014 are 390.6, 395.6 and 579.7, respectively (Jenkins, 2015). The present cost can be calculated from Eq.(2.38).

$$\text{Present cost} = \text{Original cost} \times \left(\frac{\text{Index at present}}{\text{Index when original cost was obtained}} \right) \tag{2.38}$$

Table 2.7 Data for capital cost evaluation (Hamelinck et al., 2004; Ng and Sadhukhan, 2011)

Direct capital cost (M€, 2002)

ISBL

Item No.	Process unit	Base Cost	Scale factor, R	Base scale
1	Air separation unit	27.9	0.75	576 ton/day
2	Gasifier	25.5[(M€, 1999)]	0.7	400 MW HHV
3	Particle filter	1.9	0.65	12.2 m3/s gas
4	Heat exchanger	8.1	0.6	138.1 MW
5	Reformer	31.1	0.6	100 m3 NTP/s
6	Water gas shift reactor	12.2	0.65	8819kmol of H_2+CO/s
7	Compressor	12.9	0.85	13.2 MW
8	FT slurry reactor	11.93	0.72	2.5 Mft^3/h gas
9	Expander	5	0.7	10.3 MW

OSBL

Item No.	Specification	Cost estimation (% of ISBL)
10	Instrumentation and control	5
11	Building	1.5
12	Grid connections	5.0
13	Site preparation	0.5
14	Civil works	10.0
15	Electronics	7.0
16	Piping	4.0
	Total Direct Capital (TDC)	**ISBL+OSBL**

Indirect Capital Cost (M€, 2002)

Item No.	Specification	Cost estimation (% of TDC)
17	Engineering	15
18	Contingency	10
19	Fees/overheads/profits	10
20	Start-up	5
	Total Indirect capital (TIC)	
	Total Capital Costs	**TDC+TIC**

2.7.2 Operating cost

The operating cost considered in this study consists of maintenance, personnel, laboratory, supervision, plant overhead, etc. The operating cost is calculated based on percentages of the total indirect capital or personnel costs, as shown in Table 2.8.

Table 2.8 Data for operating cost calculation (Ng and Sadhukhan, 2011)

Item No.	Specification	Cost estimation
1	Maintenance	10% of TIC
2	Personnel	0.595 Million Euro/100MW LHV
3	Laboratory costs	20% of personnel
4	Supervision	20% of personnel
5	Plant overheads	50% of personnel
6	Capital charge	10% of TIC
7	Insurance	1% of TIC
8	Local taxes	2% of TIC
9	Royalties	1% of TIC
	Total operating cost (TOC)	

2.7.3 Product cost

The valuable products from the BG-FT process are the diesel fuel and the electricity. The price of diesel and electricity are assumed to be 0.85 Euro/liter and 0.0794 Euro/kWh (base on the average data of Thailand in year 2014), respectively.

2.7.4 Net Present Value (NPV)

The NPV is the sum of the present values (PVs) of incoming and outgoing cash flows over a period of time. Incoming and outgoing cash flows can be described as income and expenditure, respectively. The net cash flow, which derived from the

incoming cash flow minus the outgoing cash flow, is discounted back to its PV. The PV is calculated by Eq.(2.39).

$$PV = \frac{R_{netcash,t}}{(1+i)^t} \qquad (2.39)$$

where $R_{netcash,t}$ is the net cashflow at time t and i is the discount rate which is the rate of return that can be earned on an investment. Therefore, at a period of time N, the NPV can be calculated from Eq.(2.40).

$$NPV(i,N) = \sum_{t=0}^{N} \frac{R_{netcash,t}}{(1+i)^t} \qquad (2.40)$$

2.7.5 Incremental Net Present Value

Incremental NPV is one of the economic indicators used to evaluate the investment for a new project (e.g., installation of new equipment or plant expansion). Positive value of incremental NPV indicates that the project is attractive to invest due to its high return, while the opposite result is found when the value of incremental NPV is negative. The incremental NPV is calculated using the same method as NPV; however, when calculating incremental NPV, the larger initial project investment cost is subtracted from that of the project with the smaller one. This procedure ensures that the incremental initial investment cost will be negative.

2.8 Environmental evaluation using wasted reduction (WAR) algorithm

The WAR algorithm is used to evaluate the environmental impact of the chemical and biochemical processes or used to compare the environment impact of difference processes by determining the overall potential environmental impact (PEI), which is a quantity representing the average indirect effect that mass and energy emissions would have on the environment. The considered impact is separated into two major categories; (1) the global atmospheric impact which consists of the global warming potential (GWP), ozone depletion potential (ODP), acidification or acid rain potential (AP) and photochemical oxidation or smog formation potential (PCOP), (2) the local toxicological impact which consists of human toxicity potential by ingestion

(HTPI), human toxicity potential by either inhalation or dermal exposure (HTPE), aquatic toxicity potential (ATP) and terrestrial toxicity potential (TTP).

The PEI is represented by the total rate of the environmental impact output ($\dot{I}_{out}^{(t)}$) which calculated from the summation of the rate of impact output from chemical process ($\dot{I}_{out}^{(cp)}$), energy process ($\dot{I}_{out}^{(ep)}$) and waste energy ($\dot{I}_{we}^{(cp)}, \dot{I}_{we}^{(ep)}$) as shown in Eq.(2.41). As the impact of energy emission is low, therefore the impact of mass emission from chemical process is only considered. The PEI of gas stream is higher than that of the solid stream and the impact of valuable product is not taken into account (Young and Cabezas, 1999). The calculation of PEI is performed based on the procedure reported in the previous work (Cabezas et al., 1999). The total rate of environmental impact output and the total environmental impact output per mass of desired product ($\hat{I}_{out}^{(t)}$) are calculated from Eqs.(2.41)-(2.42).

$$\dot{I}_{out}^{(t)} = \dot{I}_{out}^{(cp)} + \dot{I}_{out}^{(ep)} + \dot{I}_{we}^{(cp)} + \dot{I}_{we}^{(ep)} \tag{2.41}$$

$$= \sum_{j}^{cp} \dot{M}_{j}^{(out)} \sum_{k} x_{kl} \psi_{k} + \sum_{j}^{ep-g} M_{j}^{(out)} \sum_{k} x_{kl} \psi_{k}$$

$$\hat{I}_{out}^{(t)} = \frac{\dot{I}_{out}^{(cp)} + \dot{I}_{out}^{(ep)} + \dot{I}_{we}^{(cp)} + \dot{I}_{we}^{(ep)}}{\sum_{p} \dot{P}_{p}} \tag{2.42}$$

$$= \frac{\sum_{j}^{cp} \dot{M}_{j}^{(out)} \sum_{k} x_{kl} \psi_{k} + \sum_{j}^{ep-g} M_{j}^{(out)} \sum_{k} x_{kl} \psi_{k}}{\sum_{p} \dot{P}_{p}}$$

where $\dot{M}_{j}^{(out)}$ is the mass flow rate of stream j which may be an input or an output stream, x_{kl} is the mass fraction of component k for the impact category l, $\dot{P}_{p}$ is the mass flow rate of product p and ψ_{k} is the potential environmental impact for chemical k which can be calculated from Eq.(2.43).

$$\psi_{k} = \sum_{l} \alpha_{l} \psi_{kl}^{s} \tag{2.43}$$

where α_l is the relative weighting factor of impact category l which is assumed to be a value of 1 ($\alpha_l = 1$) for all impact categories and ψ_{kl}^s is the specific potential environmental impact of chemical k for the impact category l which can be calculated from Eq.(2.44).

$$\psi_{kl}^s = \frac{(Score)_{kl}}{\langle (Score)_k \rangle_l} \tag{2.44}$$

where $(Score)_{kl}$ is the relative score of chemical k on some arbitrary scale within impact category l which derived from literature (Guinee et al., 2002) and $\langle (Score)_k \rangle_l$ is the arithmetic average of the scores of all chemicals k within impact category l. Table 2.9 shows the score of chemicals within each environmental impact category.

2.9 Multi-criteria decision analysis method (MCDA) using the analytic hierarchy process (AHP)

AHP is widely used for practical MCDA method in various domains, such as social, economic, agricultural, industrial, ecological and biological systems, in addition to energy systems. It is a decision analysis methodology that calculates ratio-scaled importance of alternatives through pair-wise comparison of evaluation criteria and alternative. It involves decomposing a complex decision into a hierarchy with goal (objective) at the top of the hierarchy, criteria and sub criteria at levels and sub-levels of the hierarchy, and decision alternatives at the bottom of the hierarchy. AHP is a type of weighted sum method. After obtaining the weights, each performance at the given level is then multiplied with its weight and then the weighted performances are summed to get the score at a higher level (Eq.(2.45)). The procedure is repeated upward for each hierarchy, until the top of the hierarchy is reached. The overall weights with respect to goal for each decision alternative are then obtained. The alternative with the highest score is the best alternative (J. Wang et al., 2009).

Table 2.9 Score of each environmental impact category (PEI/kg) (Guinee et al., 2002)

Components	Score of each environmental impact category (PEI/kg)							
	GWP	**ODP**	**PCOP**	**AP**	**HTPE**	**HTPI**	**ATP**	**TTP**
C_1H_4	21.0000	0.0000	0.0060	0.0000	0.0000	0.0000	0.0000	0.0000
C_2H_6	0.0000	0.0000	0.1230	0.0000	0.0000	0.0000	0.0000	0.0000
C_3H_8	0.0000	0.0000	0.1760	0.0000	0.2557	0.0000	0.0000	0.0000
C_4H_{10}	0.0000	0.0000	0.3520	0.0000	0.3196	0.0000	0.0000	0.0000
C_5H_{12}	0.0000	0.0000	0.3950	0.0000	0.4262	0.0000	0.0000	0.0000
C_6H_{14}	0.0000	0.0000	0.4820	0.0000	12.7849	0.0000	0.0001	0.0000
C_7H_{16}	0.0000	0.0000	0.4940	0.0000	0.6392	0.0000	0.0004	0.0000
C_8H_{18}	0.0000	0.0000	0.4530	0.0000	0.0000	0.0000	0.0005	0.0000
C_9H_{20}	0.0000	0.0000	0.4140	0.0000	0.0000	0.0000	0.0011	0.0000
$C_{10}H_{22}$	0.0000	0.0000	0.3840	0.0000	0.0000	0.0000	0.0038	0.0000
$C_{11}H_{24}$	0.0000	0.0000	0.3840	0.0000	0.0000	0.0000	0.0113	0.0000
$C_{12}H_{26}$	0.0000	0.0000	0.3570	0.0000	0.0000	0.0000	0.0000	0.0000
$C_{13}H_{28}$	0.0000	0.0000	0.0000	0.0000	0.0000	0.0000	0.0000	0.0000
$C_{14}H_{30}$	0.0000	0.0000	0.0000	0.0000	0.0000	0.0000	0.0182	0.0000
$C_{15}H_{32}$	0.0000	0.0000	0.0000	0.0000	0.0000	0.0000	0.3223	0.0000
$C_{16}H_{34}$	0.0000	0.0000	0.0000	0.0000	0.0000	0.0000	0.1410	0.0000
$C_{17}H_{36}$	0.0000	0.0000	0.0000	0.0000	0.0000	0.0000	2.2559	0.0000
$C_{18}H_{38}$	0.0000	0.0000	0.0000	0.0000	0.0000	0.0000	1.1279	0.0000
$C_{19}H_{40}$	0.0000	0.0000	0.0000	0.0000	0.0000	0.0000	19.1176	0.0000
CO	1.9000	0.0000	0.0270	0.0000	8.5233	0.0000	0.0000	0.0000
CO_2	1.0000	0.0000	0.0000	0.0000	0.0511	0.0000	0.0000	0.0000
H_2	0.0000	0.0000	0.0000	0.0000	0.0000	0.0000	0.0000	0.0000
N_2	0.0000	0.0000	0.0000	0.0000	0.0000	0.0000	0.0000	0.0000

$$AHP = P_1 \times w_1 + P_2 \times w_2 + ... + P_i \times w_i \qquad (2.45)$$

where P_i is the normalization performance value of domain i calculated from the ratio between the considered performance and the sum of all performances derived from alternative condition of considered domain. And w_i is the weight of domain i.

CHAPTER III
LITERATURE REVIEW

In this chapter, the literatures related to this work are summarized. The topic of the interested literatures are divided in four major parts i.e., potential of biomass in Thailand, biomass gasification, FT synthesis and BG-FT process.

3.1 Potential of biomass in Thailand

Biomass is nowadays given attention due to its CO_2 neutral and environmental friendliness. Moreover, the utilization of biomass as a feedstock for fuel production is supported by current energy policy. Thailand is one of the agricultural countries which produce a wide variety of agricultural products as illustrated in Table 3.1. In the year 2010, rice was the second favorite agricultural product next to sugarcane, but it provided the highest amount of biomass residue, which was called rice straw. Based on the rice production of 31.5 million tons, the 25.6 million tons of rice straw was approximately produced (DEDE, 2012).

Table 3.1 Quantities of biomass from agricultural activities in Thailand (DEDE, 2012)

Agricultural product	Production (tones per day)	Type of biomass	Quantities of biomass (ton/y)
Sugarcane	66,816,446	Bagasse	4,190,794
Rice	31,508,364	Rice straw	25,646,548
Soybean	190,480	Trunk/ Shell/ Leaf	170,383
Corn	4,616,119	Trunk/ Corn cob	3,343,317
Palm oil	8,162,379	Shell/ Fiber	1,024,868
Cassava	30,088,025	Cassava residual	4,273,703
Coconut	1,380,980	Shell/ Fiber	1,222,178
Rubber tree	3,090,280	Branch	312,118

Rice straw is the stalk of the rice plant that is left over as waste products on the field upon harvesting of the rice grain. In Thailand, around 90% of rice straw collected during the peak harvesting season between November and December are burned in the open fields. This practice leads to air pollution and public health issues. Rice straw is grouped into a lignocellulosic biomass. Unlike carbohydrate or starch, it is not easily digestible by humans; therefore, its use for biogas or bio-oil productions does not threaten the world food supply (Lim et al., 2012). Table 3.2 shows the property analysis of rice straw; it mainly contains carbon, hydrogen and oxygen which have a potential to be converted to energy. The conversion of rice straw to energy has many advantages, including the reduction of agricultural waste generated from rice industry, the reduction of environmental impact and the acquisition of new alternative energy resource for in-house energy production which reduces the import of fossil energy.

Table 3.2 Characteristic of rice straw (Garivait et al., 2006)

Proximate analysis			Ultimate analysis		
Moisture	wt. %	6.71	Carbon	wt. %	44.4
Fixed carbon	wt. %	11.09	Hydrogen	wt. %	5.0
Volatile matter	wt. %	58.64	Nitrogen	wt. %	0.6
Ash	wt. %	23.55	Oxygen	wt. %	30.8
			Sulfur	wt. %	0.1
			Ash	wt. %	23.55

3.2 Biomass gasification

There were several works studied the gasification process both setting up the experiment and developing mathematical model (thermodynamic and kinetic models) in order to investigate the influence of feedstock characteristics (i.e., particle size and moisture content) and operating parameters (i.e., gasifying agent, gasifying temperature and pressure) on the gasification process performance.

3.2.1 Influence of feedstock characteristic

Different biomass with different physical and chemical characteristics, such as particle size and moisture content, may affect the gasification behavior. Zainal et al. (2001) studied the influence of initial moisture content in the wood and temperature of gasifying zone on the calorific value of produced gas using equilibrium model of biomass gasification in down draft gasifier. Atnaw et al. (2013) studied the gasification of palm oil fronds and found that the heating value of produced syngas and the values of obtained cold gas and carbon conversion efficiencies were comparable with woody biomass. The results showed that the calorific value of produced gas decreased when the moisture content in wood or the gasifying temperature increased. The influence of using different types of biomass feedstock was also investigated. Mavukwana et al. (2013) studied the sugarcane bagasse gasification by developing the thermodynamic model. Their model prediction showed that the concentration of CH_4 was under predicted, whereas that of H_2 was slightly over predicted. However, the overall predictions were fairly agreed with experimental data reported in literature. Ramzan et al. (2011) studied the effect of moisture content on the performance of the gasification of solid wastes generated from both household and industrial sectors (i.e., food waste, municipal solid waste and poultry waste feedstock). The effect of biomass particle size on the gasification process in downdraft fixed bed gasifier was investigated by Tinaut et al. (2008). They found that the maximum efficiency was obtained with the smaller particle size.

3.2.2 Parametric study of gasification

3.2.2.1 Gasifying agents

The use of different types of gasifying agents (i.e., air, oxygen, steam or a mixture thereof) results in different heating values of the produced gases due to the different composition. The energy consumption of the system using different gasifying agents was also found. There were several works studied the influence of using different types and amount of gasifying agent on the composition and heating value of produced gas and the overall energy consumption of the system. Previous works reported that the use of steam could increase the heating value of the synthesis

gas to 10-18 MJ/Nm^3 compared to 4-7 MJ/Nm^3 that of air (Basu, 2010b; Higman and van der Burgt, 2008). Bhattacharya et al. (2014) studied the influence of oxygen percentage in the gasifying agent and equivalence ratio on the system exergetic efficiency. They found that the concentration of hydrogen in the produced syngas increased as the equivalence ratio increased; as a result, the cold gas efficiency as well as the exergetic efficiency also increased. On the other hand, both the efficiencies were not much affected by the purity of oxygen in the gasifying agent. The influence of gasifying agent on the inorganic substances contained in produced gas was also investigated. Gai et al. (2014) reported that the equivalent ratio (ER) and the steam to biomass ratio (SB) had a major effect on the distribution of gaseous chlorides. Beside air, oxygen and steam, carbon dioxide was selected to be a gasifying agent due to several advantages, such as no energy required for vaporization, a wide range of H$_2$/CO ratios in synthesis gas could be achieved, and more volatiles were derived in the devolatilization step because the Boudouard reaction played a crucial role, resulting efficient gasification. Moreover, the environmental benefit of CO$_2$ recycling was also achieved (Irfan et al., 2011). Chaiwatanodom et al. (2014) performed the thermodynamic analysis of biomass gasification with CO$_2$ recycled. They proved that the CO$_2$ recycle could improve the syngas production. However, there were only some ranges of operating conditions (high pressure and low temperature) offering the benefit of the CO$_2$ recycling in term of the additional energy demand. Hanaoka et al. (2013) studied the gasification of aquatic biomass using CO$_2$ and O$_2$ as a gasifying agent. The result found that the used of CO$_2$/O$_2$ could increase the conversion to syngas. As the CO$_2$ feed rate increased, the concentration of CO in produced gas increased while that of H$_2$ decreased. However, the concentration of both CO and H$_2$ were found to increase with O$_2$ feed rate. Sadhwani et al. (2013) reported that the steam and CO$_2$ enhanced gasification process offered advantages in terms of economic, environmental and social performance over the traditional biomass gasification process.

3.2.2.2 Gasifying condition

To date, the gasification process has been gained extensively attentions. The parametric analysis of the biomass gasification process using air, oxygen, steam, carbon dioxide or a mixture thereof as a gasifying agent, was performed to investigate the process performance. The influence of change on the operating parameters, such as gasifying temperature, gasifying pressure and feed condition, on the product gas composition, heating value and overall energy consumption of the system was mostly investigated in previous studied. With the purpose to preliminarily study the influences of these parameters for different gasifier configurations, the thermodynamic model is preferable because it is independent of gasifier design and requires less data; only the feed elemental composition data and the chemical reactions data are needed. Li et al. (2004) presented the results of the biomass gasification from the pilot test using sawdust as a feed. They found that temperature, air ratio, suspension density, fly ash re-injection and steam injection influenced on the composition and heating value of the product gas. The experimental results were compared with the prediction results derived from equilibrium model developed based on Gibbs free energy minimization method and the deviation was found due to the slow rate of char gasification reaction. Therefore, the model was modified by accounting the unconverted carbon and methane derived from experiment as non-equilibrium factors, to improve the model accuracy. Renganathan et al. (2012) studied the effects of varying the gasifying temperature and pressure and gasifying agents (CO_2, oxygen, steam and a mixture thereof) on the product gas composition, cold gas efficiency and CO_2 emissions. Loha et al. (2011) did the experiment and developed the equilibrium model of steam gasification of rice husk in fluidized bed gasifier. The influence of gasifying temperature and steam to biomass ratio on the product gas composition was investigated. And the correlation of H_2 yield from rice husk at difference temperature and difference steam to biomass ratio was proposed. Ardila et al. (2012) investigated the influence of operating parameters of sugarcane bagasse gasification in a circulating fluidized bed gasifier on synthesis gas composition, heating value and conversion efficiency. Ramzan et al. (2011) developed the biomass gasification model of food waste, municipal solid waste and poultry waste feedstock

in Aspen plus. The developed model was used to study the effect of operating parameters i.e. temperature, equivalence ratio, moisture content and steam injection on synthesis gas composition, high heating value, cold gas efficiency and hydrogen production. The possibility of waste tyre gasification was investigated by Mitta et al. (2006) using their gasification model developed in Aspen plus. The model results were compared with the data from pilot plant test. And the effect of gasifying temperature on the composition of produced gas was investigated.

Even though the kinetics models require a lot of experimental data in order to derive the reaction kinetics of main reactions, it can envision the clear picture of the complex phenomena occurring in each section of gasifier and offers the high accuracy performance. There were several works focused on the kinetic model development. Kojima et al. (1993) reported the kinetics data of sawdust char gasification which was conducted using experimental fluidized bed with inert particle under the differential and stable condition. Nikoo and Mahinpey (2008) developed the biomass gasification in fluidized bed reactor model including hydrodynamic parameters and reaction kinetic data of char gasification using Aspen plus and external FORTRAN subroutines. Their model results were compared with the experimental data from gasification of pine in a lab-scale fluidized bed gasifier. The influence of gasifying temperature, equivalence ratio, steam to biomass ratio and average particle size of biomass on the composition of produced gas and carbon conversion efficiency were investigated. Gao and Li (2008) simulated the behavior of a global fixed bed biomass gasifier by developing the mathematical model of combined pyrolysis and reduction zone including kinetic rates of reactions in the latter zone. The volatiles left from the pyrolysis zone entered the reduction zone as initial concentrations. The concentration of each component in produced gas and the temperature along the length of reduction zone at various time were investigated. Xu et al. (2011) developed mathematical model of char gasification using steam as a gasifying agent based on reaction kinetics and gas transportation of the producer gas. The chars were considered to be biomass char, coal char and chars of blended biomass and coal. The influence of char structures on the gasification characteristic was investigated. Kaushal et al. (2010) develop the one-dimensional mathematical model based on reaction kinetic of

biomass gasification in bubbling fluidized bed gasifier by considering two-phase (bubble and emulsion) and two-zone (bottom dense bed and upper freeboard). The developed model could predict the bed temperature, tar yield, produced gas composition, heating value and production rate and show good agreement with other bubbling bed gasification models. Miao et al. (2013) developed the mathematical model of biomass gasification in a circulating fluidized bed including the hydrodynamics and reaction kinetics. The model was divided in two sections i.e., dense and dilute regions. The distribution of bed temperature and concentration of each gas contained in produced gas along the gasifier length, the heating value of produced gas, the gasification efficiency, the carbon conversion and the gas production rate were investigated and found consistent with published data. Sharma (2011) proposed the one-dimensional mathematical model of a downdraft biomass gasifier. The model was developed in three stages, the first stage was the fluid flow module, the second stage was the heat transfer module and the final stage was the thermochemical process which the chemical equilibrium was considered in oxidation zone, the experimentally results was used to predict the pyrolysis products and the kinetic modeling was considered in reduction zone. The model results were in good agreement with experimental data. The comparison between equilibrium and kinetics model of char reduction reactions in downdraft biomass gasifier was also investigated by Sharma (2008). The effect of reaction temperature on dry gas composition, unreacted char, and endothermic heat absorption rate in reduction zone were investigated. Moreover, the critical char bed length and the critical reaction temperature in reduction zone derived from equilibrium and kinetics model were reported.

3.2.3 Design of plant configuration

To achieve the efficient synthesis gas production in term of product gas specification and productivity as well as the energy consumption, the improvement of gasification process is required. There were several attempts to increase the performance of gasifier such as running at the optimum condition, process modification i.e., process stream preheating, installation of synthesis gas cleaning and tar reforming. Shen et al. (2008) reported that both a high hydrogen yield and relative

great hydrogen content could be obtained from biomass gasification in interconnected fluidized beds which the combustion and gasification sections were separated. The influences of operating conditions were also investigated using their developed Aspen plus model and the favorable condition was proposed. Arpornwichanop et al. (2014) proposed the suitable operating condition of the autothermal biomass gasification in supercritical water for hydrogen production. Doherty et al. (2009) studied the effect of air preheating in a biomass atmospheric circulating fluidized bed (CFB) technology using Aspen plus model which developed based on Gibbs free energy minimization method. They found that as the air preheating rate increased the production rate of H_2 and CO increased resulting in the increase of the heating value of produced gas and cold gas efficiency of gasifier. Chaiwatanodom et al. (2014) developed and compared three biomass gasification models including CO_2 recycling i.e., direct-heated, indirect-heated using synthesis gas and indirect-heated using biomass as a fuel. The results implied that the recycle of CO_2 gave the benefit on the synthesis gas production and the indirect-gasification using biomass as a fuel gave the highest gasifying efficiency at the lowest CO_2 emission. The biomass gasification was integrated with other processes such as fuel cell, power plant or Fischer-Tropsch synthesis, to increase the overall process performance. Francois et al. (2008) investigated the energy efficiency of combined heat and power (CHP) production via wood gasification using the model developed in Aspen plus with external FORTRAN user-subroutines. They found that 67% of the overall energy performance of CHP plant was achieved. Chutichai et al. (2013) performed the performance analysis of an integrated biomass gasification and PEMFC (proton exchange membrane fuel cell) systems using the model developed in Aspen plus. Their results showed that based on an electrical load of 5 kW, the electrical efficiency of the PEMFC integrated system was 22%, and, when waste heat recovery was considered, the total efficiency 51% of the PEMFC system was achieved. Hamelinck et al. (2004) performed the performance analysis of the integrated process of biomass gasification and Fischer-Tropsch synthesis.

3.2.4 Tar formation and removal

The tar contained in the raw syngas may cause fouling of downstream equipment and deactivation of the FT-catalyst, resulting in a decrease in process performance. Therefore, the understanding of tar formation and the attempts at minimizing tar formation as well as the removal of generated tar become the interesting topics. Basu (2010a) reported that the tar concentration around 2% wt. was normally found in the produced gas leaving downdraft gasifier. The influence of different chemical compositions in biomass on the tar formation was investigated by Qin et al. (2015). The forest residue sawdust, rich in lignin, and agriculture waste cornstalks, rich in cellulose, were gasified in a spout-fluidized bed reactor from 700-900 $^{\circ}$C. The result showed that sawdust tar and cornstalks tar both showed aromatic character, while cornstalks tar contained more aliphatic compounds than sawdust tar. Li et al. (2004) investigated the tar formation in their biomass gasification pilot test using sawdust as a feed, and found that the tar yield decreased exponentially when temperature increased. Attempts at minimizing the tar formation, such as selecting suitable operating conditions, using a catalyst and the installation of secondary equipment to remove the generated tar from the produced gas, were widely studied (Pereira et al., 2012). Nakamura et al. (2016) proposed biomass gasification process with the tar removal technologies utilizing bio-oil scrubber and char bed. They found that 98% of tar could be eliminated without using any primary methods. The conversion of tar to syngas via chemical reactions (i.e., steam reforming and autothermal reforming (ATR)) was also studied because it could increase the amounts of syngas and also downstream products which used syngas as a feedstock. Vivanpatarakij and Assabumrungrat (2013) proposed the combined unit of biomass gasifier and tar steam reformer in order to remove tar and increased hydrogen production simultaneously. The model was developed and used to analyze the proposed unit and the result revealed that the integrated unit could completely remove tar and increase H_2 production around 1.6 times under thermally self-sufficient condition. Josuinkas et al. (2014) reported that benzene (the tar model compound) and methane were completely converted to H_2 and CO via the steam reforming reaction over a Ni-based catalyst at the operating condition of 780 $^{\circ}$C and 1 atm.

3.3 Fischer-Tropsch synthesis

The FT synthesis is the exothermic polymerization reactions using Cobalt- or Iron-based catalyst. Previous studies on FT reaction mostly focused on the catalyst performance and improvement, and reactor design, due to their strong effect on the overall reaction performance.

3.3.1 Catalyst performance improvement

The improvement of catalyst performance to meet the maximum yield of desired product was one of the key successes of FT synthesis process. Lohitharn et al. (2008) reported that addition of Chromium, Manganese, Molybdenum, Tantalum, Vanadium and Zirconium on the Iron based catalyst could increase its activity for CO hydrogenation and water gas shift reactions due to a higher degree of Iron dispersion. The effect of noble metal promoters on the activity and selectivity of Cobalt based catalyst was also investigated by Ma et al. (2012). The results showed that the promoted catalyst could increase the rate of CO hydrogenation. Moreover, the addition of Ruthenium (Ru) and Nickel (Ni) promoters could increase the catalytic activity for gasoline range hydrocarbons production (S. Wang et al., 2013). As the FT synthesis process consists of complex reactions and requires the suitable fraction of H_2 and CO in the synthesis gas, therefore the influence of this fraction on the hydrocarbon products over various type of catalyst were investigated. Lu and Lee (2007) reported that to maximize the high quality diesel production, the H_2/CO ratio in feed gas should be controlled close to 2.0 and in the range of 1.1 to 1.7 when the FT reaction carried on over Cobalt and Iron based catalysts, respectively. The influences of feed gas composition over the CO/γ-Al$_2$O$_3$ and CO-Re/γ-Al$_2$O$_3$ catalysts were investigated by Tristantini et al. (2007). They found that the CO conversion and CH_4 selectivity decreased while the selectivity of C_{5+} hydrocarbon and olefin-to-paraffin ratio for C_2-C_4 slightly increased.

3.3.2 Parametric study of Fischer-Tropsch synthesis

The parametric study of the influence of operating parameters i.e., FT operating temperature, pressure and feed gas composition on process performance, was performed in several works via experimental and modeling works. In modeling

approach, there were many attempts to develop the mathematical model in order to explain the behavior of catalyst and hydro- and aero-dynamics of fluid inside the different FT reactors, as well as to predict the FT product distributions. Rafiq et al. (2011) developed a two-dimensional model of fixed bed reactor including the transport and the reaction rate equations. The model results were good agreement with the experimental data. This developed model was use to investigate the conversion of CO and H_2, the productivity of hydrocarbons and the fluid temperature along the reactor axis. YiNing Wang et al. (2003) proposed the one-dimensional heterogeneous model of fixed bed reactor which developed based on the kinetic data and the fact that catalyst pores were filled with liquid wax under realistic condition. The equilibrium between the gases in the bulk and the wax in the catalyst pores was correlated by using Soave Redlich Kwong (SRK) equation of state. The developed model was used to investigate the effect of process parameters on the reaction behavior of the system with recycle operation. Furthermore, the modeling of bubble column slurry reactor was widely studied. de Swart and Krishna (2002) developed the model of this reactor type and used it to investigate the mixing behavior of liquid and catalyst particle phase inside the commercial scale reactor. The mathematical model of slurry CSTR with Co/P-Al_2O_3 catalyst for Fischer-Tropsch synthesis was developed based on detailed reaction mechanisms. The model result was good agreement with experimental data reported by Kwack et al. (2011).

3.3.3 Empirical correlation of chain growth probability

Since the chain growth probability (α) is the important parameter used to predict the FT product distribution, however it is difficult to measure. The work focused on developing empirical correlations for α by combining the dependency on the operating temperature, pressure and H_2/CO ratio were extensively studied. The correlations derived from experimental research for cobalt based catalyst were proposed. (Yermakova and Anikeev, 2000) developed correlation based on several experiments at 533 K and 20 atm over an alumina supported cobalt catalyst promoted with zirconium as expressed in Eq.(3.1).

$$\alpha = A \frac{a_{CO}}{a_{CO} + a_{H_2}} + B \tag{3.1}$$

where the value of constants A and B were 0.2332 ± 0.0740 and 0.6330 ± 0.042, respectively. H. S. Song et al. (2004) developed the correlation between α and the operating temperature in Kelvin as shown in the following equation.

$$\alpha = \left(A \frac{\gamma_{CO}}{\gamma_{CO} + \gamma_{H_2}} + B \right) [1 - 0.0039(T - 533)] \tag{3.2}$$

Moreover, the dependency of α on the operating temperature in Kelvin, the operating pressure in bar and the H_2/CO ratio was proposed by Hamelinck et al. (2004). The selectivity of the hydrocarbons with chain length longer than 5 (S_{C5+}) was also proposed as shown in the following equations.

$$\alpha = 0.75 - 0.373\sqrt{-\log(S_{C5+})} + 0.25S_{C5+} \tag{3.3}$$

$$S_{C5+} = 1.7 - 0.0024T - 0.088\frac{[H_2]}{[CO]} + 0.18([H_2] + [CO]) + 0.0079P_{Total} \tag{3.4}$$

The kinetic expression of FT synthesis process using iron-based catalyst Eq.(3.5) and that of cobalt-based catalyst Eq.(3.6) were reported in previous work (Pondini and Ebert, 2013).

$$-R_{CO} = \frac{k_{FT}P_{CO}P_{H_2}}{P_{CO} + aP_{H_2O}} \tag{3.5}$$

$$-R_{CO} = \frac{k_{FT}P_{CO}P_{H_2}}{(1 + bP_{CO})^2} \tag{3.6}$$

where R_{CO} is the CO consumption rate (mol/s kg$_{cat}$), P_{CO} and P_{H_2} are the partial pressures of CO and H_2 (bar), respectively. Eq.(3.6) could be rewritten in term of kinetic parameters (a and b) as shown in Eq.(3.7).

$$-R_{CO} = \frac{aP_{CO}P_{H_2}}{(1 + bP_{CO})^2} \tag{3.7}$$

The expressions of kinetic parameters a and b were also reported in previous works. Hamelinck et al. (2004) defined these parameters in the Eqs.(3.8)-(3.9), the value of related constant the for solid bed and slurry reactors were summarized in Table 3.3.

$$a = k_0 \times \exp\left(\frac{E_{A,reaction}}{RT}\right)\frac{mol}{s.kg_{cat}bar^2} \tag{3.8}$$

$$b = k_1 \times \exp\left(\frac{-\Delta H_{ads}}{RT}\right)\frac{1}{bar} \tag{3.9}$$

Table 3.3 Kinetic parameters for solid bed and slurry reactor (Hamelinck et al., 2004)

	E_A [kJ/mol]	k_0 [mol/s.kg$_{cat.}$bar^2]	ΔH_{ads} [kJ/mol]	k_1 [1/bar]	ρ [kg$_{cat.}$/m$^3_{reactor}$]
Solid bed	68	1.5×10^5	192	3.5×10^{-23}	1200
Slurry bed	115	1.0×10^{10}	192	3.5×10^{-23}	600

Krishna and Sie (2000) proposed the expression of a and b as shown in the Eqs.(3.10)-(3.11).

$$a = 8.8533 \times 10^{-3} \times \exp\left[4494.41\left(\frac{1}{493.15} - \frac{1}{T}\right)\right]\frac{mol}{s.kg_{cat}bar^2} \tag{3.10}$$

$$b = 2.226 \times \exp\left[-8236\left(\frac{1}{493.15} - \frac{1}{T}\right)\right]\frac{1}{bar} \tag{3.11}$$

Another expression reported by Panahi et al. (2010) was expressed as follows;

$$a = 8.01368 \times \exp\left(\frac{-37326}{RT}\right)\frac{kmol}{s.kg_{cat}MPa^2} \tag{3.12}$$

$$b = 1.248 \times 10^{-6} \exp\left(\frac{68402}{RT}\right)\frac{1}{MPa} \tag{3.13}$$

3.4 Integration of gasification and Fischer-Tropsch synthesis process

An integrated process of biomass gasification and Fischer-Tropsch (BG-FT) synthesis, is a promising technology used to produce green liquid fuel that can be applied to existing infrastructure and automotive technologies (Hu et al., 2012; Omer, 2008). The study of the BG-FT process has gained extensive attention regarding to both technical and economic feasibilities because of increasing concerns regarding the decrease of globally reserved fossil fuel and the increase of greenhouse gas emissions; however, it is still in the research and development phase. Even though the technology and economic of BG-FT process are not currently proven, the benefit in term of environmental friendliness is obviously revealed. As a result, the continuous improvement of this technology in order to compete with liquid fossil fuel is the topic of interest.

The technical feasibility of a bench-scale BG-FT process was proven by long-term operation for 500 h over several runs with stable conditions (Kim et al., 2013). The high overall thermal process efficiency of 51%, which corresponded to 40% gasification and 75% Fischer-Tropsch, was reported by Leibbrandt et al. (2013), while that of the BG-FT pilot scale located at National Science and Technology Development Agency (NSTDA), Thailand was reached 36.92% thermal process efficiency (Hunpinyo et al., 2013). Exergy analysis was also performed and the highest exergetic efficiency of 36.4% was achieved (Prins et al., 2005). Furthermore, the techno-economic performance of the BG-FT process, including the influence of changes in the type of gasifying agent (i.e., air, enriched air and oxygen), gasifying pressure, plant configuration and plant scale on investment cost and electricity efficiency that resulted in the FT diesel price, was investigated by Hamelinck et al. (2004). Avella et al. (2016) performed an economic analysis by investigating the influence of various costs associated with plant configurations (i.e., cost of investment, operating cost, maintenance, depreciation and financing charge) on the price of electricity and synthesized liquid fuel. They found that the cost of both products strongly depended on the plant configurations. Moreover, a decrease of investment cost per plant capacity was also found when the size of the production plant increased (Hunpinyo et al., 2013). The improvement of the BG-FT process

efficiency by designing a suitable heat integration and combined heat and power (CHP) network, as well as the enhancement of economic feasibility by employment of a full conversion configuration using bio-oil as a feedstock was also studied (Ng and Sadhukhan, 2011). The two various pathways (i.e., the BG-FT process and the integrated gasification combined cycle (IGCC) in which biomass was co-fired with coal) used to produce liquid transportation fuel and electricity were analyzed in term of total product yield (electricity and liquid fuels), carbon dioxide emissions, and total production cost. The result showed that the total energy yield (electricity and liquid fuels) and carbon dioxide emissions of the two processes were almost identical (Reichling and Kulacki, 2011). Tijmensen et al. (2002) reported that overall lower heating value (LHV) efficiencies of the BG-FT process in the range of 33-40% and 42-50% could be achieved in atmospheric and pressurized gasification systems, respectively. They also found that the production costs of both concepts could not compete with current diesel costs. B. Wang et al. (2013) developed a multi-objective mixed-integer nonlinear programming (MINPL) model in which the net present value (NPV) and global warming potential (GWP) derived from a life cycle assessment procedure were used as economic and environmental indicators, respectively. The optimal solution revealed that the use of high-temperature gasification, direct cooling, internal hydrogen production and cobalt catalysis had the best environmental and economic performances.

CHAPTER IV
MODELLING

This chapter presents the development of stand-alone biomass gasification and the BG-FT models of rice straw feedstock, which its proximate and ultimate analyses are given in Table 3.2. Two gasification models are developed i.e., the gasification model based on thermodynamic approach and the other including the tar formation and the reaction kinetic of char gasification reactions. The latter is further integrated with the model of several downstream-units (e.g., tar reforming, H_2/CO ratio adjusting, FT synthesis and power generation) to form the BG-FT model. The correlations, parameters and the model assumptions used in this study are presented in this chapter.

4.1 Gasification modelling

Two gasification models i.e. the equilibrium model and the other including the tar formation and the reaction kinetic of char gasification reactions are developed. The former model is the zero-dimensional analysis which the gasifier dimension is not considered in the mass and energy balance calculation and the tar formation is also neglected. For the latter, the tar formation and the one-dimensional analysis in the reduction zone are taken into account. The model accuracy is also investigated by comparing the model prediction results with the experimental results.

Because the gasifier is the highest temperature unit in the BG-FT process, the heat generated at downstream units cannot effectively cover all of the heat required in the gasifier. However, the gasifier consists of both exothermic oxidation reactions and endothermic reduction reactions that can be balanced by adjusting the amount of oxidative gasifying agent to achieve the thermal self-sufficiency condition, in which external heat sources are not required during steady state operation. In this study, the gasifier is therefore considered to be operated in this condition.

4.1.1 Equilibrium model

4.1.1.1 Model development

The equilibrium model of biomass gasification is developed using Aspen plus. The following assumptions are made in the model development: (1) the process is under steady state conditions, (2) the pyrolysis is considered to be instantaneous, and char and volatiles are formed, (3) char is assumed to be 100% carbon (graphite) (4) tar and heavy hydrocarbons are negligible and (5) ash, the mixture of inorganic elements, is considered to be a non-reactive inert. The gasification model is divided into three sections, i.e., the biomass decomposition section, the reaction section, in which the pyrolysis, gasification and combustion reactions are considered, and the synthesis gas separation section. The simulation flowsheet is shown in Figure 4.1.
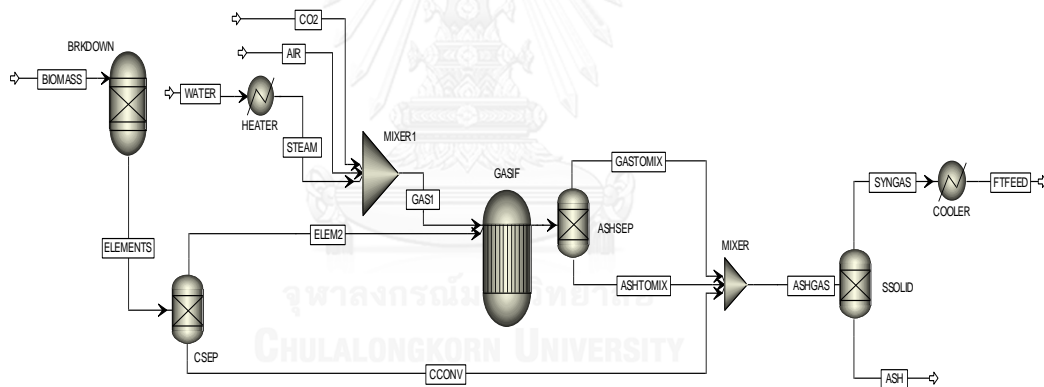
Figure 4.1 Simulation flowsheet of the biomass gasification.

The descriptions of the Aspen plus unit operation blocks used in the simulation of the gasification are given in Table 4.1. Type of BIOMASS feed stream is specified as a non-conventional component and the HCOALGEN and DCOALIGT models in Aspen Plus are used to calculate the enthalpy and density of a solid biomass from biomass ultimate and proximate analyses. The RYIELD reactor, denominated as BRKDOWN, is used to simulate the decomposition of biomass into its constituting components, e.g., carbon, hydrogen, oxygen, sulfur, nitrogen and ash, by specifying

the yield distribution in the calculator block according to the biomass ultimate analysis and the mass flow of each component in the ELEMENTS stream is calculated afterwards. The generated tar is not considered in this work because it can be cracked or reformed to form H_2, CO, CO_2 and other light hydrocarbons at temperatures higher than 800 $^{\circ}$C (Basu, 2010a). However, at lower gasifying temperatures (~ 500 $^{\circ}$C), the tar content in the product gas was found around 0.6 % and can be negligible (Vivanpatarakij and Assabumrungrat, 2013). As the carbon conversion in the biomass gasifier are mostly in a range of 90 to 99% (Hughes, 1998), in this study, the CSEP separator is therefore used to simulate this carbon conversion by separating out the specified portion of unreacted carbon of 1%. The biomass pyrolysis, gasification and combustion reactions are simulated using RGIBB reactors, denominated as GASIF. Gasifying agents (i.e., steam, air and carbon dioxide) are mixed before they are sent to the gasifier (MIXER 1). In the RGIBB, the composition of the product gas is estimated using the Gibbs free energy minimization method. Ash contained in the product gas is separated at the ASHSEP separator and mixed with the unreacted carbon separated from the upstream unit in the MIXER. Finally, the separation of the synthesis gas, mixed ash and unreacted carbon is performed in the SSOLID separator block.

Table 4.1 Description of the unit operation blocks

Block name	Block ID	Descriptions
RYIELD	BRKDOWN	Yield reactor - Converted the non-conventional biomass into the conventional component.
SEP2	CSEP	Separator - Simulate carbon conversion by separating specified portion of unreacted carbon
	ASHSEP	Separator - Separate the ash from synthesis gas.
	SSOLID	Separator - Separate the ash and unreacted carbon from the synthesis gas for removal from the system
RGIBBS	GASIF	Gibbs free energy reactor - Simulate pyrolysis, gasification and combustion reaction.

Table 4.1 Description of the unit operation blocks (Cont.)

Block name	Block ID	Descriptions
MIXER	MIXER	Mixer - Mixes the unreacted carbon, ash and synthesis gas together.
	MIXER1	Mixer – Mixes the gasifying agents i.e. mixture of steam with air or CO_2 together
HEAT EXCHANGER	HEATER	Heater - Simulate water vaporization to produce steam at 150 °C 1 atm
	COOLER	Cooler - Cool the product gas from gasifying temperature to 200 °C

4.1.1.2 Model validation

The developed gasification model is first validated with the experimental data reported by Jayah et al. (2003), which was conducted on a pilot scale downdraft gasifier. The fuel used for model validation is rubber wood. The ultimate and proximate analyses of this biomass are shown in Table 4.2. The input data are a biomass flow rate of 1 kmol/h, oxygen to biomass ratio of 0.33, gasifying temperature of 1000 K and gasifying pressure of 1.01 bar. It is noted that due to the lack of complete information on the gasification of rice straw which is the feedstock type used in this study, the experimental data of rubber wood gasification were used in the model validation. The properties of rubber wood from the proximate and ultimate analyses are not significantly different from that of rice straw. In addition, the ranges of steam and air to biomass ratios in the experimental data are quite close to those used in this study.

The comparison of the model predictions and the experimental results is summarized in Table 4.3. The model predictions are in good agreement with the experimental data. The water gas shift and steam methane reforming reactions are assumed at the equilibrium condition. The result shows that CH_4 completely react

with steam to form CO and H_2 whereas CO further reacts with steam to form CO_2 and H_2. Thus, compared with the experimental data, the concentrations of CH_4 are under-predicted, whereas those of H_2 and CO are over-predicted.

Table 4.2 The ultimate and proximate analyses of the rubber wood (Jayah et al., 2003)

Proximate analysis			Ultimate analysis		
Moisture	wt.%	16	Carbon	wt.%	50.6
Fixed carbon	wt.%	19.2	Hydrogen	wt.%	6.5
Volatile matter	wt.%	80.1	Nitrogen	wt.%	0.2
Ash	wt.%	0.7	Oxygen	wt.%	42
			Sulfur	wt.%	0
			Ash	wt.%	0.7

Table 4.3 Comparison between the equilibrium model predictions and the experimental results

	Experimental (Jayah et al., 2003)	Model
Gas composition [a]		
H_2	17.00	20.41
CO	18.40	20.42
CO_2	10.60	10.58
CH_4	1.30	0.00

[a] volume %, dry basis

4.1.2 Kinetic model

4.1.2.1 Model development

To improve the model accuracy, the reaction kinetic of char gasification reactions and the formation of tar are taken into account. In this section, the dry biomass is represented by molecular formula of $C_x H_y O_z$ where x, y, z can be determined from Eq.(4.1).

$$x = \frac{CM_C}{CM_C}, \, y = \frac{HM_C}{CM_H}, \, z = \frac{OM_C}{CM_O} \tag{4.1}$$

M_C, M_H and M_O are the molecular weight of carbon, hydrogen and oxygen, respectively, and C, H and O are the mass fraction of those elements derived from ultimate analysis. For simplification, the biomass gasification model is separated in two sections i.e., zone 1 represents combined pyrolysis and oxidation of pyrolysis product and zone 2 represents the char reduction reactions, as discussed in the following sections.

a) Zone 1: Combined pyrolysis and oxidation (Zero-dimensional analysis)

The combined pyrolysis and oxidation section is assumed to take place at the isothermal condition at 1128 K (Sharma, 2008), the thermal decomposition of biomass into volatiles and char is occurred; the derived volatiles are further continuously oxidized with the restricted amount of oxygen and steam to formed CO, CO_2 and H_2O. Because the pyrolysis and oxidation reactions are relatively fast, thermodynamic equilibrium can be assumed. The overall reaction of combined pyrolysis and oxidation of pyrolysis products can be represented by Eq.(4.2).

$$\begin{aligned} C_x H_y O_z + wH_2O + mO_2 + 3.76mN_2 \rightarrow n_{CO}CO + n_{CO_2}CO_2 + n_{H_2}H_2 \\ + n_{H_2O}H_2O + n_{CH4}CH_4 + n_{C_6H_6}C_6H_6 + n_{Char}Char + 3.76mN_2 \end{aligned} \tag{4.2}$$
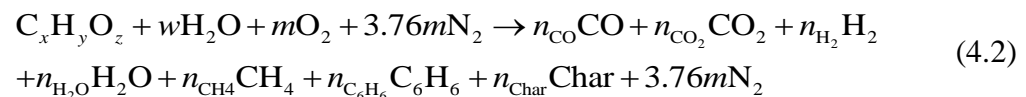
where $n_{CO}, n_{CO_2}, n_{H_2}, n_{H_2O}, n_{CH4}, n_{C_6H_6}$ and n_{Char} are the number of moles of CO, CO_2, H_2, H_2O, CH_4, C_6H_6 and Char. w and m are the amount of water and oxygen per mole of biomass, respectively.

Due to tar is the complex mixture of various condensable hydrocarbons such as benzene toluene naphthalene etc., which can cause the problems (plugging and poor heat transfer) to the downstream units, tar yield depends on the operating parameters i.e. reaction temperature, type of gasifier and type of gasifying medium, therefore consideration of all tar reactions is very difficult. The previous studies reported that benzene was the highest component found in tar. In downdraft gasifier around 2 % wt of tar yield was typically found when one unit mass of biomass was gasified (Basu, 2010a). The present study therefore considered tar as benzene which has the same amount of typically founded tar yield and assigned its corresponding mole fraction as one of the model input. The char generated from this section is obtained from the value of fixed carbon derived from proximate analysis. Shafizadeh (1982) reported that hydrogen and oxygen content in char decreases sharply as temperature increases, char is therefore assumed to be pure carbon.

The elemental balance for the pyrolysis and oxidation section is formulated as shown in Eqs.(4.3) - (4.6).

Carbon balance:
$$x = n_{CO} + n_{CO_2} + n_{CH_4} + 6n_{C_6H_6} + n_{Char} \tag{4.3}$$

Hydrogen balance:
$$y + 2w = 2n_{H_2} + 2n_{H_2O} + 4n_{CH_4} + 6n_{C_6H_6} \tag{4.4}$$

Oxygen balance:
$$z + w + 2m = n_{CO} + 2n_{CO_2} + n_{H_2O} \tag{4.5}$$

Nitrogen balance:
$$3.76m = n_{N_2} \tag{4.6}$$

As the water gas shift and methane reactions are relatively fast at high temperature (Blom et al., 1994; Bradford and Vannice, 1996), therefore the chemical equilibrium of this reaction is assumed. The equilibrium constant of these two reactions can be calculated from Eqs.(4.7)-(4.8).

Water-gas shift reaction: $CO + H_2O \leftrightarrow CO_2 + H_2$

$$K_{WGS} = \frac{x_{CO_2} x_{H_2}}{x_{CO} x_{H_2O}} \tag{4.7}$$

Methane reaction: $C + 2H_2 \leftrightarrow CH_4$

$$K_{MT} = \frac{x_{CH_4}}{(x_{H_2})^2} \tag{4.8}$$

where x_i is the mole fraction of individual species. The relation between standard Gibbs-energy change of reaction j (ΔG_j°) and equilibrium constant for reaction j (K_j) at gasifying temperature (T_{Gs}) in Kelvin (K) is presented by Eq.(4.9). And the standard Gibbs-energy change of water gas shift and methanation reactions are shown in Eqs.(4.10)-(4.11).

$$\ln K_{eq,j} = \frac{-\Delta G_j^{\circ}}{RT_{Gs}} \tag{4.9}$$

$$\Delta G_{WGS}^{\circ} = g_{CO_2}^{\circ} + g_{H_2}^{\circ} - g_{CO}^{\circ} - g_{H_2O}^{\circ} \tag{4.10}$$

$$\Delta G_{MT}^{\circ} = g_{CH_4}^{\circ} - 2g_{H_2}^{\circ} - g_{Char}^{\circ} \tag{4.11}$$

where g_i° is the Gibbs function of species i and R is the universal gas constant (8.314 J/mol.K). Eqs.(4.3) - (4.11) can be solved simultaneously to determine the amount of each species leaving from this section.

   b) Zone 2: Reduction (One-dimensional analysis)

   The produced gas leaving combine pyrolysis and oxidation zone is used as a feed gas of reduction zone. In this zone, the reaction of char and pyrolysis product gases, i.e., CO_2, H_2O and H_2, to produce CO, H_2 and CH_4 is assumed to take place at isothermal condition of 1000 K (Jayah et al., 2003) The reactions occurred in this section can be described by the following equations.

R1: Boudouard reaction: $C + CO_2 \leftrightarrow 2CO$ (4.12)

R2: Water gas reaction: $C + H_2O \leftrightarrow CO + H_2$ (4.13)

R3: Methane reaction: $C + 2H_2 \leftrightarrow CH_4$ (4.14)

R4: Methane Steam reforming reaction: $CH_4 + H_2O \leftrightarrow CO + 3H_2$ (4.15)

Because the rate of the char reduction reactions is relatively low, the chemical kinetics is considered. The rate expressions of these reactions are shown in Eqs.(4.16)-(4.19).

$$r_1 = C_{RF}k_1(x_{CO_2} - \frac{x_{CO}^2}{K_{eq,1}})$$ (4.16)

$$r_2 = C_{RF}k_2(x_{H_2O} - \frac{x_{CO}x_{H_2}}{K_{eq,2}})$$ (4.17)

$$r_3 = C_{RF}k_3(x_{H_2}^2 - \frac{x_{CH_4}}{K_{eq,3}})$$ (4.18)

$$r_4 = C_{RF}k_4(x_{H_2}^2 x_{CO} - \frac{x_{H_2O}x_{CH_4}}{K_{eq,4}})$$ (4.19)

where x_i is the mole fraction of component i, k_j is rate constant of reaction j which can be calculated from Eq. (4.20).

$$k_j = A_j \exp(\frac{-E_j}{RT})$$ (4.20)

The kinetic data for such reactions are taken from the previous study as shown in Table 4.4 (Y. Wang and Kinoshita, 1993). As the char combustion proceeds, the char size decreases while the porosity increases; as a result, the gas can encounter more active sites causing the increase of char gasification reaction rate. To account this phenomena, the char reactivity factor (C_{RF}) which represents the reactivity of char (or the number of active sites on the char surface) is therefore considered. The constant value of char reactivity factor of 1000 which was recommended in the previous study (Giltrap et al., 2003) is also used in this study.

Table 4.4 Rate constant parameters of reduction reactions (Y. Wang and Kinoshita, 1993)

Reactions	A_j (1/s)	E_j (kJ/mol)
Boudouard reaction	3.616×10^1	77.39
Water gas reaction	1.517×10^4	121.62
Methane reaction	4.189×10^{-3}	19.21
Steam reforming reaction	7.301×10^{-2}	36.15

The net rate of production of species i (Rt_i) can be calculated from Eqs.(4.21)-(4.25).

$$Rt_{CO} = 2r_1 + r_2 + r_4 \tag{4.21}$$

$$Rt_{H_2} = r_2 - 2r_3 + 3r_4 \tag{4.22}$$

$$Rt_{CO_2} = -r_1 \tag{4.23}$$

$$Rt_{H_2O} = -r_2 - r_4 \tag{4.24}$$

$$Rt_{Char} = -r_1 - r_2 - r_3 \tag{4.25}$$

To calculate the composition of the product gas leaving this zone, the reduction section is divided into small control volumes (CV) and the mass balance of each CV is performed as depicted in Figure 4.2. The molar flow rate of species i leaving each CV is computed from Eq.(4.26).

$$\dot{n}_{i,out} = \dot{n}_{i,in} + V_{CV} . Rt_i \tag{4.26}$$
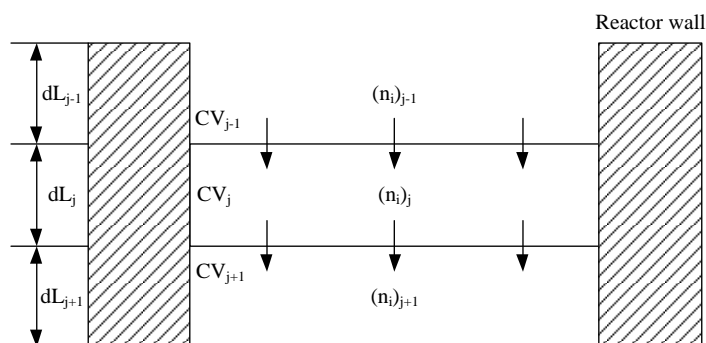
Figure 4.2 Single CV used in the calculation of gas molar flow rate leaving the reduction zone.

4.1.2.2 Model validation

The developed gasification model is first validated with the experimental data reported by Jayah et al. (2003), as discussed in section 4.1.2.1. The comparison of the model predictions and the experimental results is summarized in Table 4.5. The model predictions are in good agreement with the experimental data. Compared with the experimental data, the concentrations of CO and CH_4 are under-predicted, whereas those of H_2 and CO_2 are over-predicted.

Table 4.5 Comparison of kinetic model predictions and experimental results

	Experimental (Jayah et al., 2003)	**Model**
Gas composition [a]		
H_2	17	19.38
CO	18.4	15.89
CO_2	10.6	12.63
CH_4	1.3	0.03
C_6H_6	N/A	0.28

[a] volume %, dry basis

The comparison between two gasification models of rice straw feedstock i.e. equilibrium model and the one including the tar formation and the reaction kinetic of char gasification reactions is illustrated in Figure 4.3. It shows that the concentrations of CO and H_2 calculated from equilibrium model overestimate that obtained from the experiment due to complete conversion of CH_4 and C_6H_6, whereas calculated CO_2 concentration slightly under-predicts the experimental result. For the other model, the concentration of CO is under-predicted, while those of H_2 and CO_2 are over-predicted. The concentration of CH_4 can be predicted using the model including tar formation and reaction kinetic of char gasification; however, the model prediction result is under-predicted compare to the experimental result. The concentration of C_6H_6 is also predicted in this model based on the normally found value of tar content. In actual operation, the produced syngas normally contained tar and CH_4, therefore, the gasification model including tar formation and reaction kinetic of char gasification is selected to integrate with the model of downstream units to form the BG-FT model.
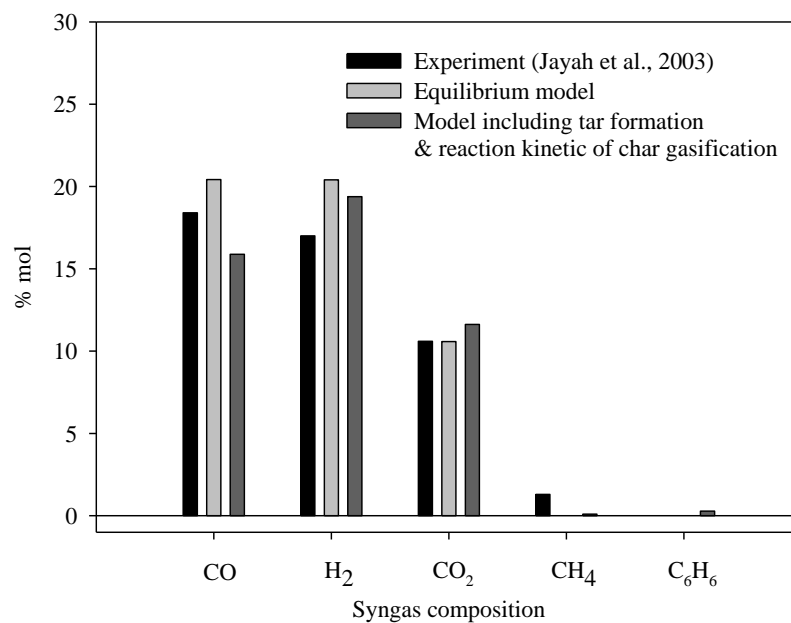
Figure 4.3 Comparison between the prediction of equilibrium and kinetic model with experimental result (Jayah et al., 2003)

As the developed model is also used to investigate the performance of gasification with rice straw feedstock; the composition of rubber wood is therefore replaced by that of rice straw as given in Table 3.2.

4.2 Gas cleaning and conditioning modeling

The composition of synthesis gas derived from gasification depends on type of biomass, type of oxidizing agent, operating condition, etc. The derived synthesis gas contains impurities such as tar, inorganic impurities (NH_3, HCN, COS and HCl), dust and soot. In this work assumes that the impurities, contained in the raw synthesis gas, consist of tar (benzene), ash and unreacted carbon. The high temperature resisted metal screen filter is used to physically remove ash and unreacted carbon. Moreover, the raw syngas is further purified via the tar removal and H_2/CO adjusting units in order to achieve the FT-feed gas specification.

4.2.1 Tar removal unit

The generated tar contained in raw syngas possibly causes fouling of downstream equipment and deactivating of FT-catalyst resulting in the decrease of process performance. The present study focuses on the conversion of tar to syngas via steam reforming and ATR reactions because it could increase the amount of syngas and also liquid fuel. The composition of reformed gas leaving each tar removal unit is determined in the following sections.

4.2.1.1 Steam reforming process

In tar steam reforming process, benzene (a tar model compound) and methane react with stream to form synthesis gas. The main reactions occur in this unit are represented in Eqs.(4.13), (4.15) and (4.27).

Water gas reaction: $$C + H_2O \leftrightarrow CO + H_2 \tag{4.13}$$

Methane steam reforming reaction: $CH_4 + H_2O \leftrightarrow CO + 3H_2$ (4.15)

Benzene steam reforming reaction: $C_6H_6 + 6H_2O \leftrightarrow 6CO + 9H_2$ (4.27)

In this process, benzene and methane are completely converted to H_2 and CO via steam reforming reaction over Ni-based catalyst at 1053 K and 1.01 bar (Basu, 2010a; Josuinkas et al., 2014). As the rate of water gas shift reaction is fast at high temperature, the chemical equilibrium of this reaction can be assumed. The equilibrium constant and the standard Gibbs-energy change of water gas shift reaction are shown in Eq.(4.7) and (4.10), respectively. The relation between standard Gibbs-energy change ($\Delta G_{j,RM}^{\circ}$) and equilibrium constant of steam reforming reaction ($K_{eq,RM}$) at reforming temperature (T_{RM}) is computed from Eq.(4.28). These equations can be solved simultaneously to determine the amount of each species leaving the steam reforming process.

$$\ln K_{eq,RM} = \frac{-\Delta G_{RM}^{\circ}}{RT_{RM}} \tag{4.28}$$

4.2.1.2 Autothermal reforming (ATR) process

In ATR process, oxygen is supplied in order to produce the heat of combustion for the steam reforming reaction. The operating condition is set at 1053 K, 1.01 bar. The ATR process consists of both exothermic oxidation reactions and endothermic steam reforming reactions, therefore the thermal self-sufficient condition can be achieved by adjusting the amount of oxygen. As the benzene and methane are completely reacted in this condition, therefore the overall reaction of ATR process can be constructed by specifying the possible products as represented in Eq.(4.29).

$$\begin{aligned}
&n_{ATR,C_6H_6}C_6H_6 + n_{ATR,CH_4}CH_4 + w_{ATR}H_2O + m_{ATR}O_2 = n_{ATR,CO}CO \\
&+n_{ATR,CO_2}CO_2 + n_{ATR,H_2}H_2 + n_{ATR,H_2O}H_2O
\end{aligned} \tag{4.29}$$
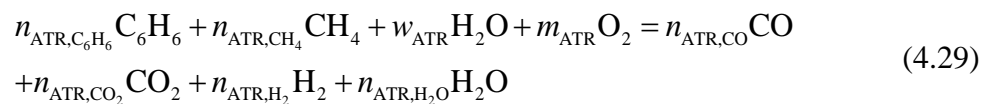
where $n_{ATR,CO}, n_{ATR,CO_2}, n_{ATR,H_2}, n_{ATR,H_2O}, n_{ATR,CH4}, n_{ATR,C_6H_6}$ are the number of moles of CO, CO_2, H_2, H_2O, CH_4 and C_6H_6. w_{ATR} and m_{ATR} are the amount of supplied water and oxygen, respectively.

To calculate the composition of product gas leaving this unit, the chemical equilibrium of water gas shift reaction is assumed, the equilibrium constant and the standard Gibbs-energy change of this reaction at reforming temperature are

determined using the same equations as that found in the above section (Eqs.(4.7), (4.10) and (4.28)), and the C-, H-, O-element balances are performed as shown in Eqs.(4.30)-(4.32).

Carbon balance: $\quad 6 \times n_{\text{ATR},C_6H_6} + n_{\text{ATR},CH_4} = n_{\text{ATR},CO} + n_{\text{ATR},CO_2}$ (4.30)

Hydrogen balance: $6 \times n_{\text{ATR},C_6H_6} + 4 \times n_{\text{ATR},CH_4} + 2 \times w_{\text{ATR}} = 2 \times n_{\text{ATR},H_2} + 2 \times n_{\text{ATR},H_2O}$ (4.31)

Oxygen balance: $\quad w_{\text{ATR}} + 2 \times m_{\text{ATR}} = n_{\text{ATR},CO} + 2 \times n_{\text{ATR},CO_2} + n_{\text{ATR},H_2O}$ (4.32)

4.2.2 H$_2$/CO ratio adjustment

Because the H$_2$/CO ratio of syngas of approximately 2 is suitable for FT synthesis using Cobalt-based catalyst, while that of the syngas from the gas processing process is normally lower, this ratio needs to be adjusted via the water gas shift reaction which steam is supplied as a reactant (Eq.(4.13)). The operating condition is set at 423 K, 1.01 bar, and a chemical equilibrium of this reaction is assumed. The composition of syngas leaving this unit can be calculated using the same equations as discussed in the above section (Eqs.(4.7) and (4.10)). The relation between standard Gibbs-energy change (ΔG°_{WGS}) and equilibrium constant of water gas shift reaction ($K_{eq,WGS}$) at water gas shift temperature (T_{WGS}) is shown in Eq.(4.33).

$$\ln K_{\text{eq,WGS}} = \frac{-\Delta G^{\circ}_{WGS}}{RT_{\text{WGS}}}$$ (4.33)

4.2.3 Compressor

The clean syngas with a desired fraction of H$_2$ and CO at water gas shift condition (T_{in}, P_{in}) is compressed to the FT operating pressure (P_{out}) of 20 bar. The temperature of compressor effluent gas (T_{out}) and the power consumption ($\dot{W}_{comp}$) can be estimated from Eqs.(4.34) and (4.35), respectively. The efficiency of compressor (η_{comp}) is assumed to be 75% (Kaneko et al., 2006).

$$T_{out} = T_{in}[1 + \frac{1}{\eta_{comp}}(\frac{P_{out}}{P_{in}})^{\frac{\gamma-1}{\gamma}} - 1] \tag{4.34}$$

$$\dot{W}_{comp} = n_{Total}\int_{T_{in}}^{T_{out}} C_p dT \tag{4.35}$$

where, $\quad \gamma = \dfrac{C_p}{C_p - R}$ $\hspace{4cm}$ (4.36)

4.3 Fischer-Tropsch synthesis modelling

4.3.1 Model development

The slurry phase FT reactor using cobalt-based catalyst is selected in this study because of its advantages in terms of good temperature control and simple configuration. Moreover, the experimental data of the FT reaction over the cobalt-based catalyst are widely available. Normally, the operating temperature and pressure are in the range of 200-250 ^{o}C and 20-60 bar, respectively. As the FT hydrocarbon products mainly contain the linear paraffin, therefore only this form of generated FT products having carbon number from C_1-C_{20} is assumed in this study. The considered FT-reaction is shown in Eq.(4.37).

$$nCO + (2n+1)H_2 \rightarrow C_nH_{2n+2} + nH_2O \tag{4.37}$$

The distribution of hydrocarbon products can be estimated from the ASF (Anderson-Schulz-Flory) distribution as shown in Eq.(2.28).

$$M_n = \alpha^{n-1}(1-\alpha) \tag{2.28}$$

where, M_n is the mole fraction of hydrocarbon with chain length n and α is the chain growth probability factor which can be calculated from the correlations reported in the previous work as shown in Eqs.(3.3)-(3.4).

$$\alpha = 0.75 - 0.373\sqrt{-\log(S_{C5+})} + 0.25S_{C5+} \tag{3.3}$$

$$S_{C5+} = 1.7 - 0.0024T_{FT} - 0.088\frac{[H_2]}{[CO]} + 0.18([H_2]+[CO]) + 0.0079P_{Total} \tag{3.4}$$

where S_{C5+} is the selectivity of hydrocarbon with a chain length longer than 5, $[H_2]$ and $[CO]$ are the molar concentration of H_2 and CO in the FT-feed gas, and T_{FT} and P_{Total} are the FT operating temperature (K) and pressure (bar), respectively. Eq.(3.7) shows the reaction rate used to determine the conversion of carbon monoxide during the FT synthesis which derived from the kinetic study of Yate and Satterfield (1991).

$$-R_{CO} = \frac{aP_{CO}P_{H_2}}{(1+bP_{CO})^2} \tag{3.7}$$

where R_{CO} is the CO consumption rate (mol/s kg_{cat}), P_{CO} and P_{H_2} are the partial pressures of CO and H_2 (bar), respectively, a and b are kinetic parameters which calculated from correlation developed by Krishna and Sie (2000) (Eqs.(3.10)-(3.11)).

$$a = 8.8533 \times 10^{-3} \exp\left[4494.41(\frac{1}{493.15} - \frac{1}{T})\right]\frac{mol}{s.kg_{cat}bar^2} \tag{3.10}$$

$$b = 2.226 \exp\left[-8236(\frac{1}{493.15} - \frac{1}{T})\right]\frac{1}{bar} \tag{3.11}$$

The CO consumption rate is used to calculate the reactor size from the kinetic theory for a continuous stirred tank reactor (CSTR) as shown in Eq.(4.44). This equation can be rearranged to be expressed in terms of CO conversion (X_{CO}) (Eq.(4.45)), therefore the CO conversion achieved in a specific reactor volume can be determined (Fogler, 1999).

$$V_{FT} = \frac{CO_{in} - CO_{out}}{r_{CO}} \tag{4.44}$$

$$V_{FT} = \frac{CO_{in}X_{CO}}{r_{CO,exit}} \tag{4.45}$$

According to the correlation shown in Eqs.(4.44)-(4.45), R_{CO} can be converted to r_{CO} (mol/s dm^3) by multiplying with the catalyst density, ρ_{cat} ($kg_{cat}/m^3_{reactor}$).

The molar flow rate of each linear hydrocarbons and the total molar flow rate of hydrocarbon product, which is assumed to consist of C_1-C_{20} hydrocarbons, can be calculated from Eqs. (4.46)-(4.47).

$$Z_n = M_n \times Z \tag{4.46}$$

$$Z = \sum_{n=1}^{n=20} Z_n \tag{4.47}$$

where Z_n is the molar flow rate of hydrocarbon with chain length n (kmol/h) and Z is the total molar flow rate of hydrocarbon product (kmol/h). The amount of H_2 and CO consumed and the amount of water generated during FT reactions are calculated from the stoichiometric balance of FT-reaction (Eq.(4.37)).

To calculate the exact composition of both vapor and liquid products leaving FT reactor, the vapor liquid equilibrium (VLE) needs to be considered. The previous work reported that Raoult's law is sufficient to be used to model the VLE in FT reactor (Masuku et al., 2012), therefore this theoretical correlation is applied in this study. There are two major assumptions using Raoult's law e.g. the vapor phase is an ideal gas and the liquid phase is an ideal solution. The mathematical expression showed in Eq.(4.48) (Smith et al., 2008).

$$y_n P_{Total} = x_n \times P_n^{sat} \tag{4.48}$$

where x_n is a mole fraction of hydrocarbon with chain length n in liquid, y_n is a mole fraction of hydrocarbon with chain length n in vapor, P_{Total} is the total pressure (or FT operating pressure) and P_n^{sat} is the vapor pressure of hydrocarbon with chain length n, which can be calculated from Antoine equation (Eq.(4.49)) (Smith et al., 2008).

$$\ln P_n^{sat} = A - \frac{B}{T + C} \tag{4.49}$$

where A, B and C are Antione constants for selected substances which given in Table A.6 of Appendix A.

Figure 4.4 represents the FT-feed flow rate of F kmol/h, total vapor product flow rate of V kmol/h and total liquid product flow rate of L kmol/h, respectively.
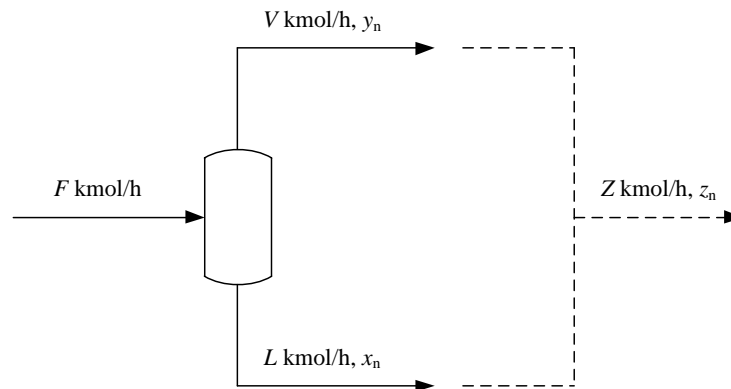
Figure 4.4 The schematic diagram of the FT reactor

The overall balance of FT hydrocarbon products and the component balance of hydrocarbon product with chain length n, leaving a FT reactor, are represented by Eqs.(4.50) and (4.51).

$$V + L = Z \tag{4.50}$$

$$Vy_n = Lx_n \times Zz_n \tag{4.51}$$

4.3.2 Model validation

The FT model results in terms of hydrocarbon product distribution predicted using the ASF distribution is validated with the experimental result reported by Patzlaff et al. (1999), in which the FT reaction takes place over a cobalt-based catalyst in a slurry reactor under the reaction temperature of 493 K and the molar H_2/CO ratio of 1. As shown in Figure 4.5, the model predictions are in good agreement with the experimental data; however, the slight deviation observed is due to the double alpha effect caused by the re-adsorption of primary alkenes (A.P. Steynberg and Dry, 2004). The trend of product distribution in both weight and on a molar basis predicted using the developed model corresponds to the information reported in the previous work (Ng and Sadhukhan, 2011; Pondini and Ebert, 2013). The total product yield decreases exponentially with increasing chain length as illustrated in Figure 4.6(a) and 4.6(b), respectively.
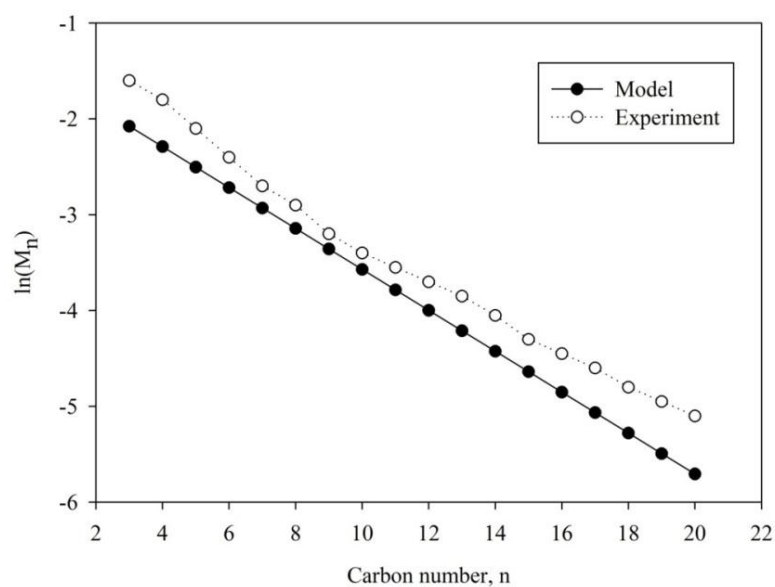
Figure 4.5 Comparison of ASF model predictions and experimental results of the cobalt catalyst system under FT temperature = 493 K, H_2/CO ratio = 1

(a)

(b)
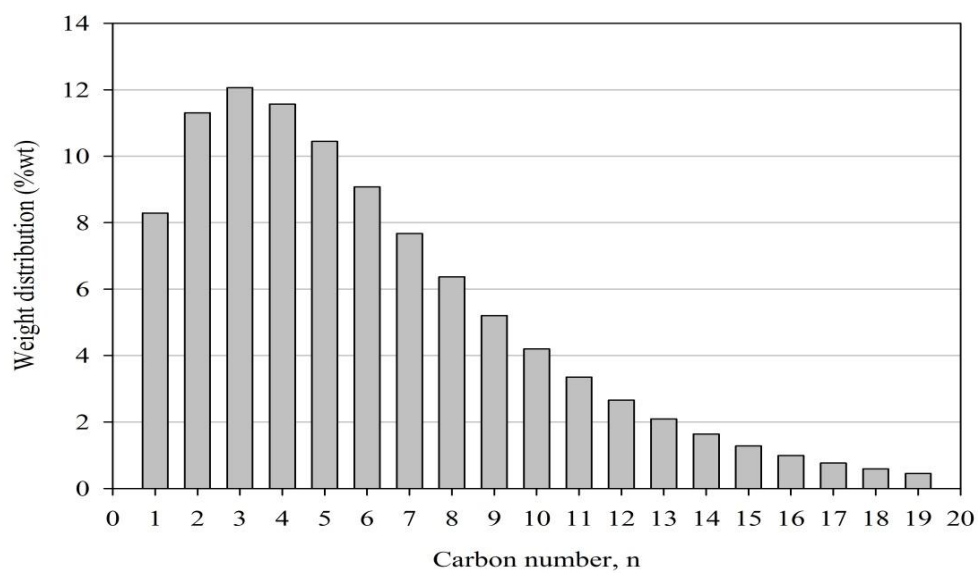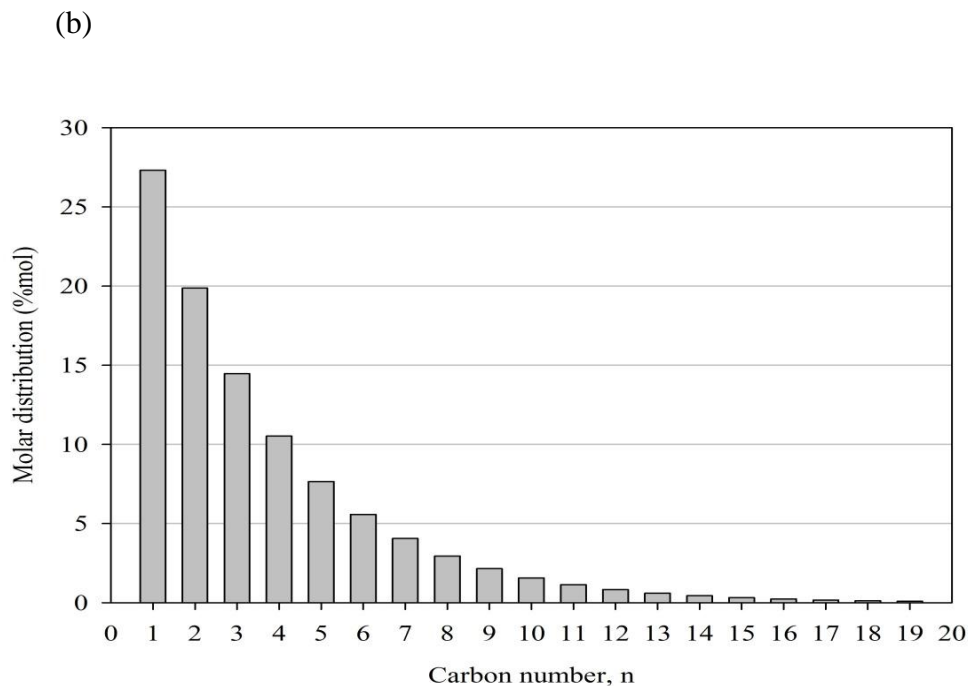
Figure 4.6 (a) Weight distribution of FT products, (b) Molar distribution of FT products predicted using ASF model. Operating condition of FT reactor: T = 493 K, P = 20 bar which corresponds to $\alpha = 0.73$

4.4 Power generation modelling

The pressure of the FT-offgas is reduced to the operating pressure of the gasifier (1.01 bar) through the expansion turbine, which is connected to the generator; as a result, some electricity is generated. The temperature of expansion turbine effluent gas and the power consumption can be estimated from the same equation as compressor (Eqs.(4.34)-(4.36)). The efficiency of the expansion turbine (η_{exp}) is also assumed to be 75%.

4.5 Energy balance

The energy equation is modeled to estimate the energy consumption of each unit and that of the whole BG-FT process. It accounted for the heat inflows and outflows in the considered unit due to fluid and fuel flows (Eqs.(4.52)-(4.54)). The overall energy consumption of the BG-FT process derived from the summation of the energy consumption of each unit.

$$H_{\text{reactant}} + Q_{\text{in}} = H_{\text{product}} + Q_{\text{out}} \tag{4.52}$$

$$H_{\text{reactant}} = \sum_{\text{reactants}} n_i h_{fi}^0 \tag{4.53}$$

$$H_{\text{product}} = \sum_{\text{products}} n_i [h_{fi}^0 + \Delta h_{Ti}] \tag{4.54}$$

where, h_{fi}^0 is the enthalpy of formation in kJ/kmol at the reference state (298 K, 1 atm) and Δh_{Ti} is the enthalpy difference between a given state and the reference state which can be estimated from the equation below:

$$\Delta h_{Ti} = \int_{298}^{T} C_p(T) dT \tag{4.59}$$

where, $C_p(T)$ (kJ/kmol.K) is a specific heat at constant pressure which changes with temperature in Kelvin as shown in Eq.(4.60).

$$C_p(T) = a + bT + cT^2 + dT^3 \tag{4.60}$$

$$\int_{298}^{T} C_p(T) dT = \left| aT + b\frac{T^2}{2} + c\frac{T^3}{3} + d\frac{T^4}{4} \right|_{298}^{T} \tag{4.61}$$

where a, b, c, d are the specific gas (or liquid) species coefficients which given in Table A1-A4 of Appendix A (Smith et al., 2008). However, the specific heat capacity of solid biomass ($C_{p_{DB}}$) and that of char ($C_{p_{Char}}$) are estimated from the correlations reported in the previous study as shown in Eqs.(4.62)-(4.63) (Sharma, 2011).

$$C_{p_{DB}}(T) = 0.1031 + 0.003867T \tag{4.62}$$

$$C_{p_{Char}}(T) = 1.39 + 0.00036T \tag{4.63}$$

The developed models (e.g., biomass gasification including tar formation and reaction kinetic of char gasification, Gas cleaning and conditioning, Fischer-Tropsch synthesis, power generation and energy balance) are integrated to be one BG-FT model as shown in Figure 4.7.
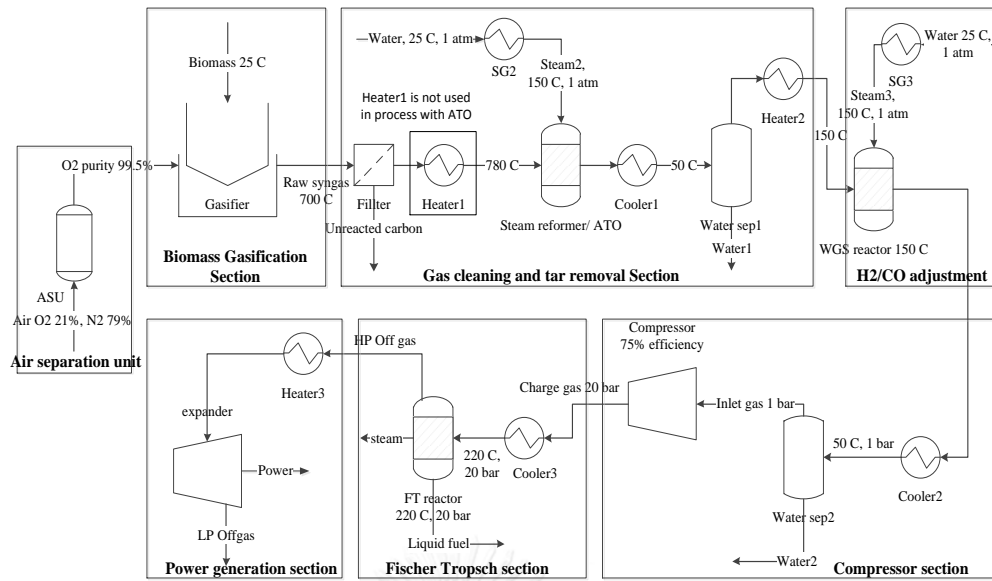
Figure 4.7 Biomass gasification and Fischer-Tropsch integrated model

CHAPTER V
STUDY OF APPROPRIATE GASIFYING AGENT FOR FISCHER-TROPSCH FEED GAS PRODUCTION

This chapter studies the production of syngas with desired H_2/CO ratio in gasification process utilizing different types of gasifying agent (i.e., steam-air and steam-CO_2). The effects of changes in the ratio of gasifying agent on the syngas yield, H_2/CO ratio, total energy consumption and cold gas efficiency (CGE) of the system at different gasifying temperatures are discussed. The feasibility of FT feed gas production at thermal self-sufficient condition is also investigated.

5.1 Introduction

In the gasification process, solid biomass reacts with controlled gasifying agents, such as steam, carbon dioxide, oxygen or air to form synthesis gas, char, tar and heavy hydrocarbons. Generally, the use of air, oxygen, steam or a mixture thereof as the gasifying agent results in different heating values of the produced gases. Due to the low cost, air is widely used as a gasifying agent. However, the high percentage of nitrogen present in air causes low synthesis gas heating value. Higher heating values are derived when pure oxygen is used, but the operating cost of this practice is high due to the oxygen production unit. The use of steam can increase the heating value and hydrogen content of the synthesis gas to 10-18 MJ/Nm^3 compared to 4-7 MJ/Nm^3 when air is used (Basu, 2010a; Higman and van der Burgt, 2008). The use of carbon dioxide as a gasifying agent offers several advantages, such as no energy required for vaporization, a wide range of H_2/CO ratios in synthesis gas can be achieved, and more volatiles are derived in the devolatilization step because the Boudouard reaction plays a crucial role, resulting efficient gasification. Moreover, the environmental benefit of CO_2 recycling is also achieved (Chaiwatanodom et al., 2014; Hanaoka et al., 2013).

The product gas derived from gasification process can be directly used as a fuel gas for a combustion unit or converted to hydrogen and used as a fuel for fuel cells.

Moreover, it is also converted to synthesis gas mainly containing hydrogen and carbon monoxide, which can be used as a raw material for many chemical plants. Different properties of the synthesis gas are required for different chemical productions. For example, synthesis gas with an H_2/CO molar ratio of approximately 1.0 is required for the oxo-synthesis process in aldehyde and alcohol production, whereas an H_2/CO ratio close to 2.0 is required for the Fischer–Tropsch synthesis process using Cobalt-based catalyst and the methanol production process (Fatih Demirbas, 2009; X. Song and Guo, 2006; Swain et al., 2011). As this study aims at the green fuel production via biomass gasification and Fischer-Tropsch integrated (BG-FT) process using Cobalt-based catalyst, therefore the FT feed gas with H_2/CO ratio around 2 is considered in this study.

Previous studies mostly performed a parametric analysis with regard to changes in operating parameters, e.g., equivalent ratio, steam to biomass ratio, operating temperature and pressure, affecting the gasification process performance. However, a detailed analysis of the biomass gasification process using a mixture of steam with air or carbon dioxide as gasifying agents to produce synthesis gas having the desired fractions of H_2 and CO at thermal self-sufficient operation of gasifier has been less extensively studied. Therefore, the objective of this study is to analyze the gasification process utilizing different types of gasifying agent (i.e., steam-air and steam-CO_2) using an equilibrium gasification model developed in Aspen plus as discussed in section 4.1.1 in chapter IV. The rice straw is considered feedstock.

5.2 Process configuration and scope of work

The gasification process configuration considered in this chapter consists of the biomass decomposition section, the reaction section, in which the pyrolysis, gasification and combustion reactions are considered, and the synthesis gas separation section as shown in Figure 4.1. The effect of changes in the ratio of the gasifying agents (i.e. air-steam and CO_2-steam) on the product gas composition, syngas yield (H_2+CO), H_2/CO ratio, total energy consumption as well as the CGE of the system is investigated. Suitable conditions offering the highest amount of synthesis gas with the desired fraction of H_2 and CO at thermal self-sufficient operation of the gasifier are also determined. The scope of work in this chapter is illustrated in Figure 5.1.
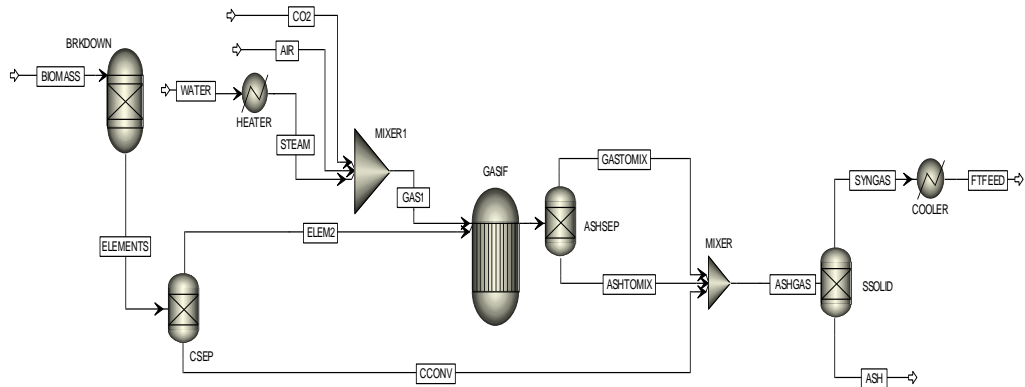
Figure 4.1 Simulation flowsheet of the biomass gasification
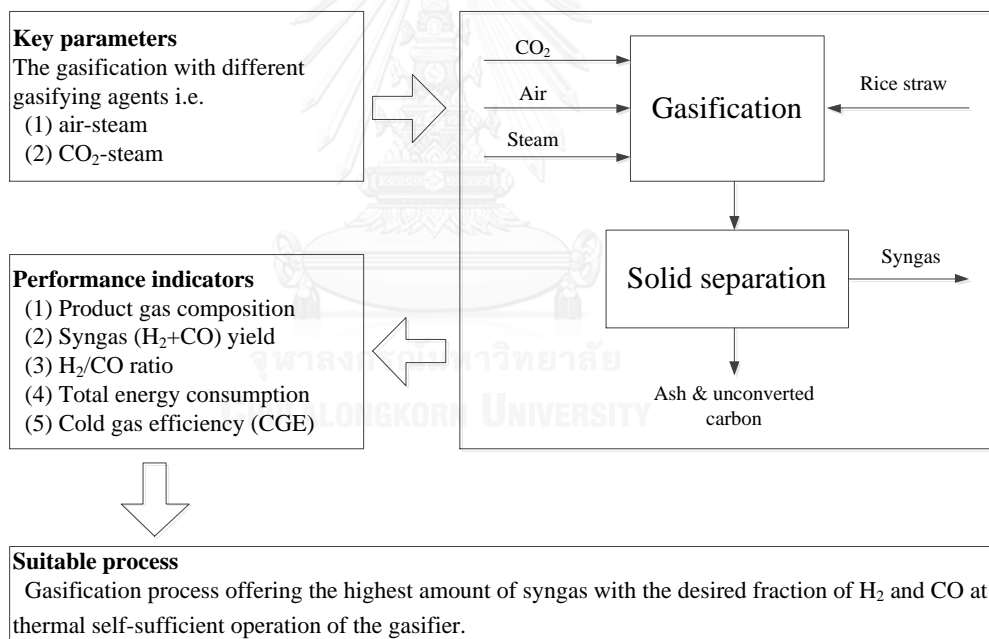
Figure 5.1 Scope of work in chapter V

5.3 Results and discussion

5.3.1 Steam-air system

5.3.1.1 Effect of temperature on the product gas composition

The effects of the gasifying temperature on the product gas composition are investigated by setting the steam and air to biomass ratios at 0.57 and 0.89, respectively, and varying the gasifying temperatures in the range of 500 to 1000 °C. The variation of the product gas composition, syngas yield and H_2/CO ratios are shown in Figure 5.2. The concentration of CO in the product gas significantly increases when the temperature is raised from 500 to 700 °C due to the domination of the reverse water gas shift reaction, in which CO is primarily produced. Steam reforming of the methane also occurs, hence the concentrations of CH_4 and H_2O decrease, whereas that of H_2 increases, causing the H_2/CO ratio sharply decreases. At temperature higher than 700 °C, the concentration of H_2O slightly increases, whereas that of H_2 and CO_2 decreases due to the absence of steam reforming reaction of methane and the domination of Boudouard and reverse water gas shift reactions. As a result, a decreasing rate of the H_2/CO ratio is observed. Moreover, a stabilized syngas yield is found.
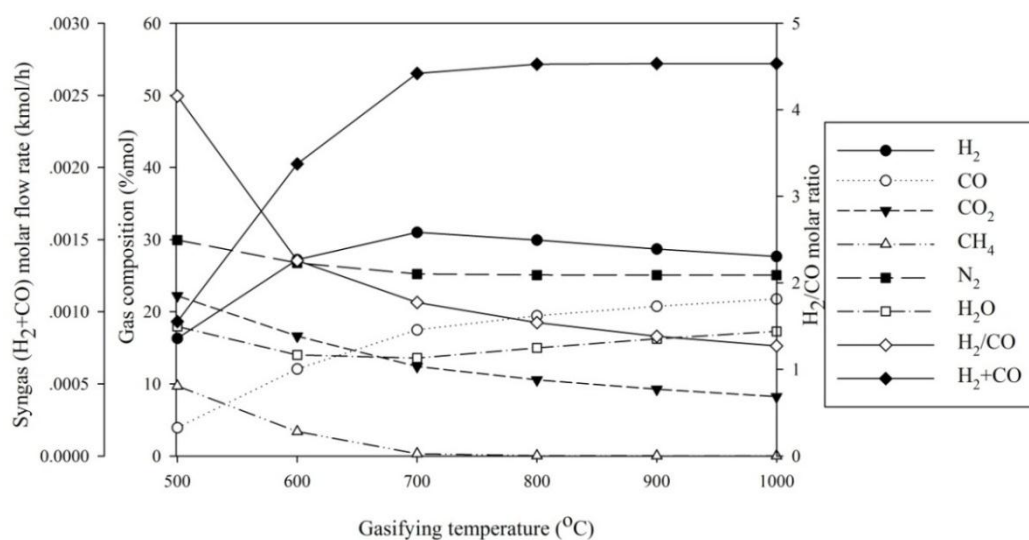
Figure 5.2 Effect of temperature on the product gas composition, syngas yield and H_2/CO ratio (S/B 0.57 and A/B 0.89).

5.3.1.2 Effect of the air to biomass ratio on the product gas composition

The effects of the air to biomass ratio on the product gas composition are investigated by setting the steam to biomass ratio at 0.57 and varying the air to biomass ratio in the range of 0.89 to 2.67 for each constant temperature in the range of 500 to 1000 °C. The variations of the product gas composition, syngas yield and H_2/CO ratio at 500-800 °C are shown in Figures 5.3(a)-(d). At lower temperatures in the range of 500-600 °C, the concentrations of CO and H_2 continuously decrease with an increase in air to biomass ratio, whereas that of H_2O increases due to the domination of the combustion reaction of hydrocarbon. At temperatures higher than 700 °C, the results show the same trend. However, the concentrations of CO and H_2O at this condition are higher; whereas that of H_2 is lower due to the absence of methane steam reforming reaction and the domination of reverse water gas shift reaction. Therefore, the increasing rate of the H_2/CO ratio in this condition is lower than the one found at 500-600 °C. The syngas yield also continuously decreases with the air to biomass ratio due to the increase of N_2 dilution in the system for all gasifying temperatures.

(a)
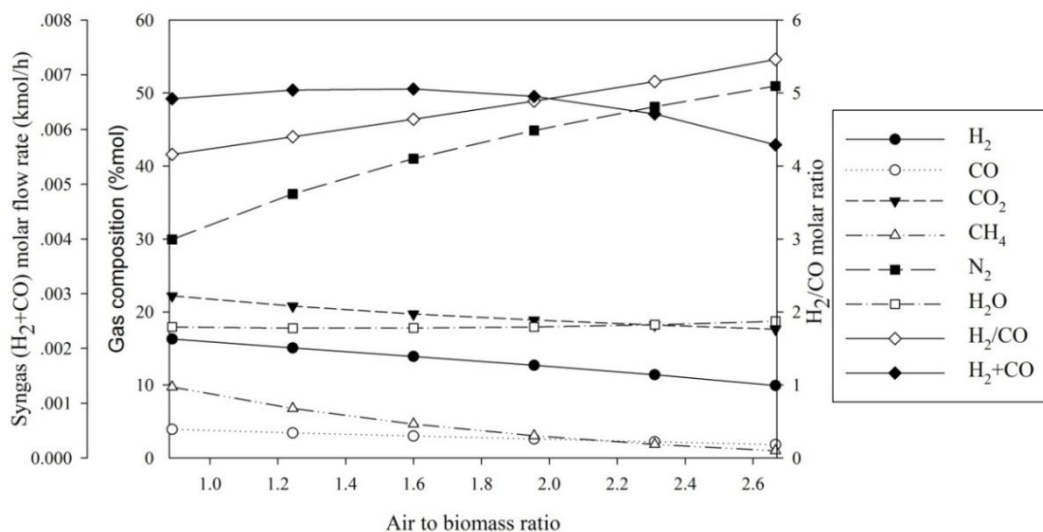
(b)
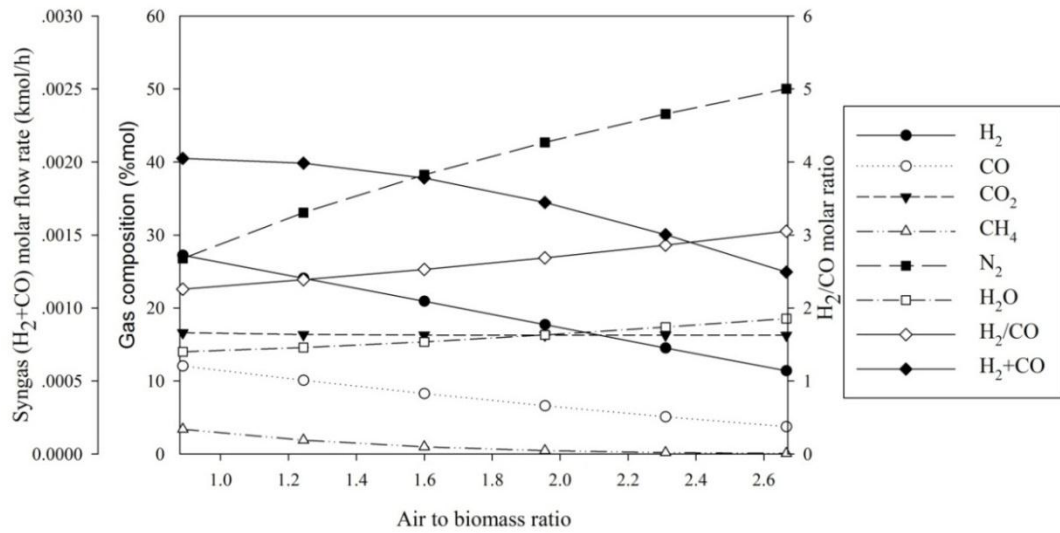
(c)
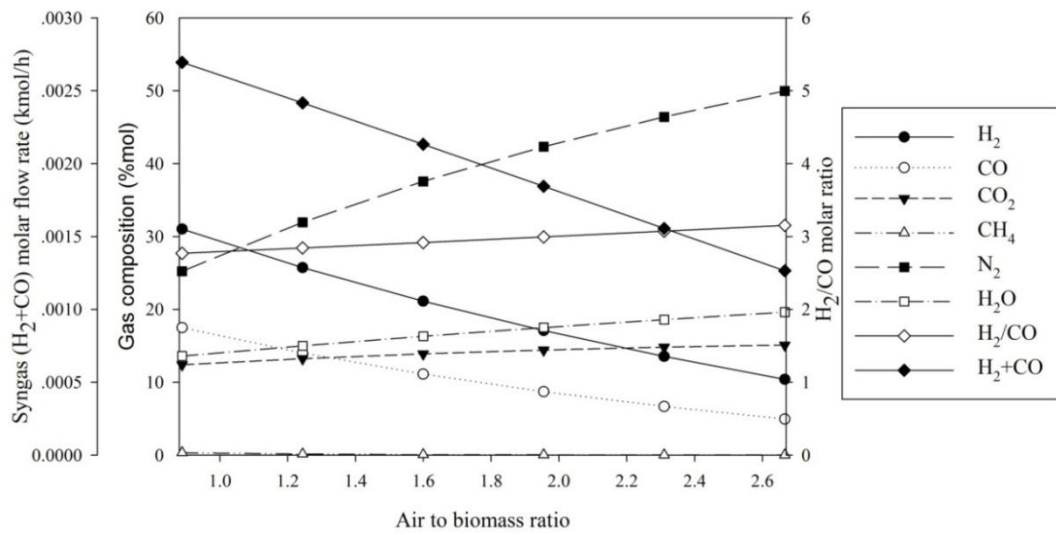
(d)
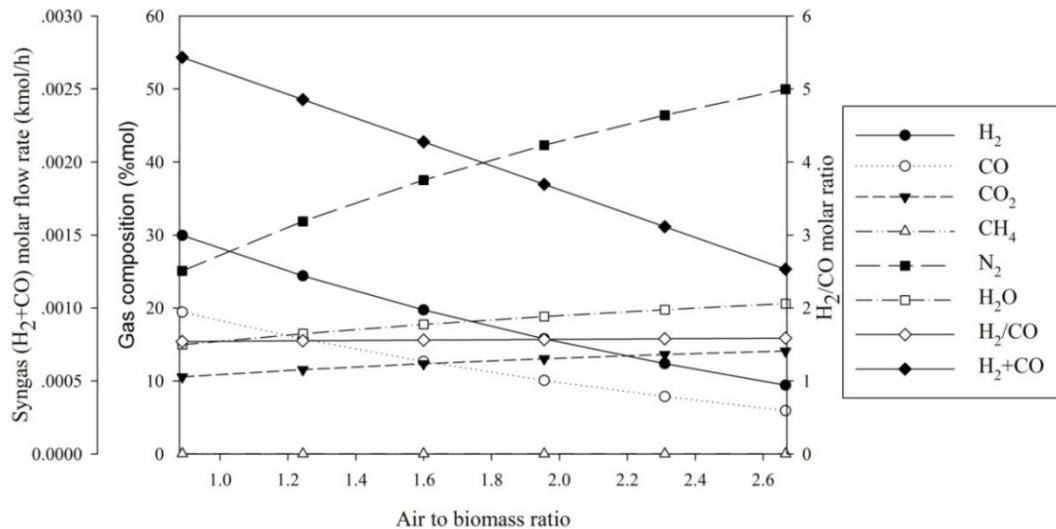
Figure 5.3 Effect of the air to biomass ratio on the product gas composition, syngas yield and H_2/CO ratio: (a) S/B 0.57 and T_{Gs} 500 °C, (b) S/B 0.57 and T_{Gs} 600 °C, (c) S/B 0.57 and T_{Gs} 700 °C and (d) S/B 0.57 and T_{Gs} 800 °C.

5.3.1.3 Effect of the air to biomass ratio on the total energy consumption of the system

The effect of the air to biomass ratio on the total energy consumption is investigated for each constant steam to biomass ratio and gasifying temperature in the range of 0.57 to 2.86 and 500 to 1000 °C, respectively. The air to biomass ratio is varied in the range of 0.89 to 2.67. The total energy consumption of the system is calculated by a summation of the energy consumption at the steam generator, gasifier and product gas cooler. The variation of the total energy consumption at 800 °C is shown in Figure 5.4. The total energy consumption continuously decreases as the air to biomass ratio increases at a constant steam to biomass ratio due to the domination of the highly exothermic of combustion reaction, through which a large amount of heat is released from the system. At a constant air to biomass ratio, the total energy consumption is inversely affected by the steam to biomass ratio due to the effect of the endothermic reaction, i.e., water gas, steam reforming and dry reforming of

methane. An external heat source is required when the total energy consumption is higher than zero. This condition occurs at elevated gasifying temperatures, high steam to biomass ratios and low air to biomass ratios, as shown in Figures 5.4-5.5.
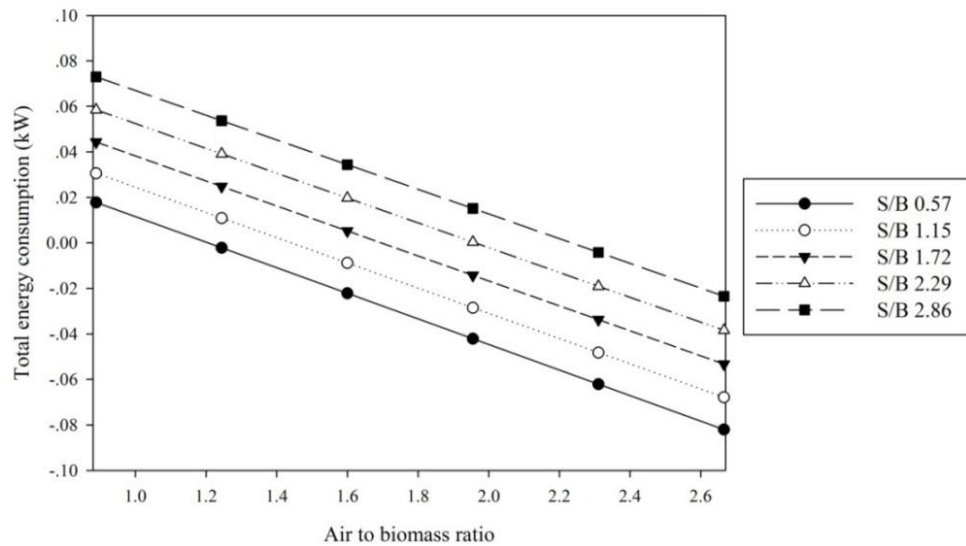
Figure 5.4 Effect of the air to biomass ratio on the total energy consumption (S/B 0.57 - 2.86, T_{Gs} 800 °C)
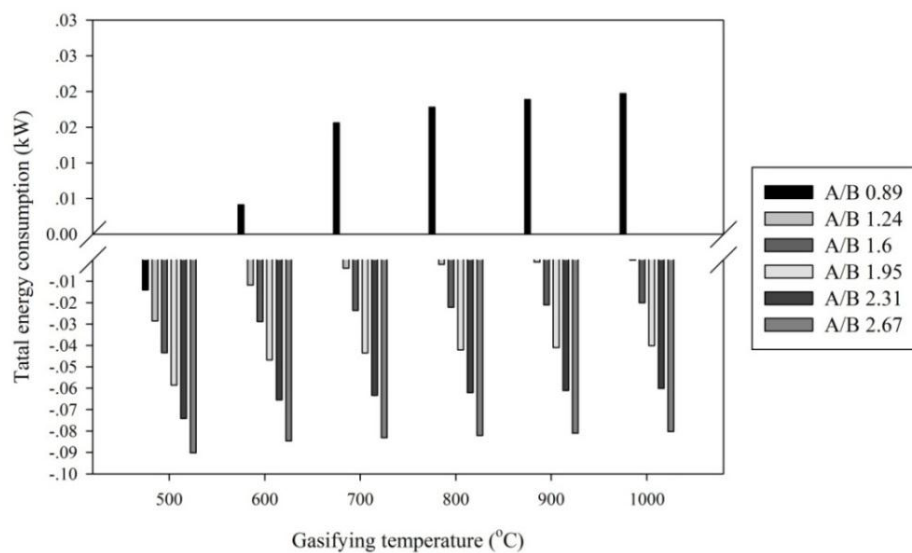
Figure 5.5 Effect of the air to biomass ratio on the total energy consumption (S/B 0.57, T_{Gs} 500-1000 °C)

5.3.1.4 Effect of the air to biomass ratio on the cold gas efficiency

The effect of the air to biomass ratio on the cold gas efficiency (CGE), defined based on the concept explained in chapter II, that explains in Eq. (5.1) is investigated for the steam to biomass ratio and gasifying temperatures in the range of 0.57 to 2.86 and 500 to 1000 $^{\circ}$C, respectively. The air to biomass ratio is varied in the range of 0.89 to 2.67.

$$CGE = \frac{(n_{H_2} \text{ x } LHV_{H_2}) + (n_{CO} \text{ x } LHV_{CO})}{(n_{Biomass} \text{ x } LHV_{Biomass})} \tag{5.1}$$

The changes in CGE and syngas concentration, which is the molar ratio of H_2 and CO to all product components contained in syngas, at temperatures of 500 and 600 $^{\circ}$C are shown in Figures 5.6 (a)-(b). It is found that the CGE and the concentration of syngas continuously decrease with an increase in air to biomass ratio due to the domination of the combustion reaction which CO_2 and H_2O are primarily produced, resulting in the decrease of syngas yield. At a constant air to biomass ratio, the CGE increases with the steam to biomass ratio due to the domination of the water gas and methane steam reforming reactions. However, the syngas concentration decreases because of an excess amount of supplied steam. At gasifying temperature of 700 $^{\circ}$C or higher, the CGE and the syngas concentration shows the same trend as found at lower temperatures (Figures 5.6 (c)-(d)). As methane is completely consumed at this condition, the methane steam reforming reaction does not occur; it is therefore observed that the steam to biomass ratio has less effect on the CGE.

The thermal self-sufficient conditions are also observed at various conditions as summarized in Table 5.1. Based on the thermal self-sufficient conditions for syngas production, the ideal operating conditions offer the highest syngas yield of 42 % with FT specification, at which an H_2/CO ratio of approximately 2 can be obtained at a gasifying temperature of 700 °C and steam and air to biomass ratios of 0.57 and 1.17, respectively. At these conditions, the CGE of 38% is achieved.

(a)
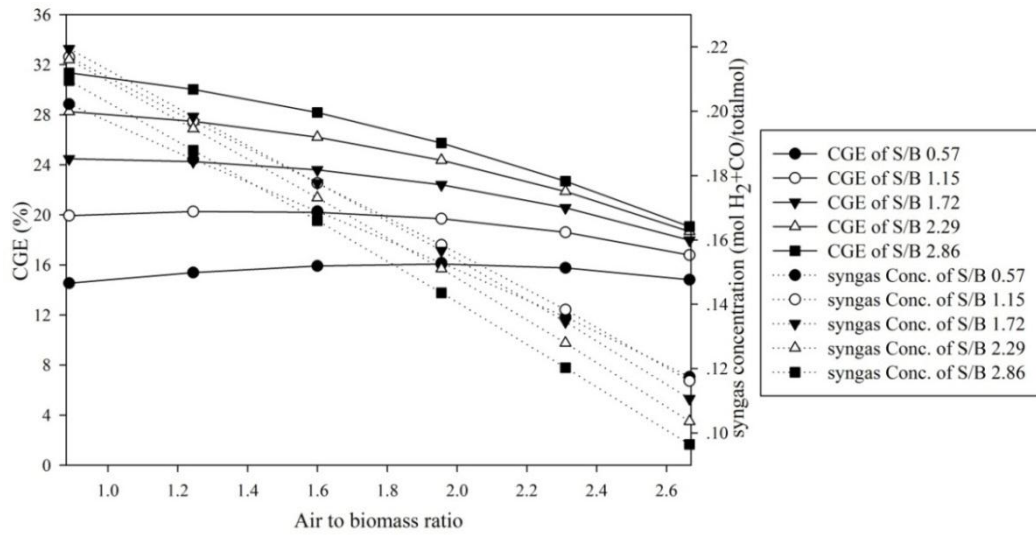
(b)
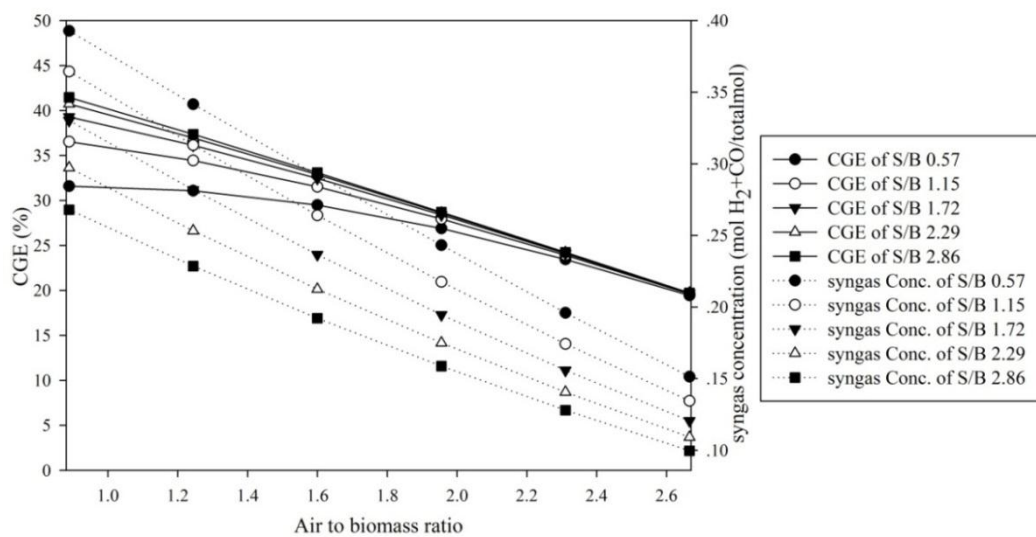
(c)
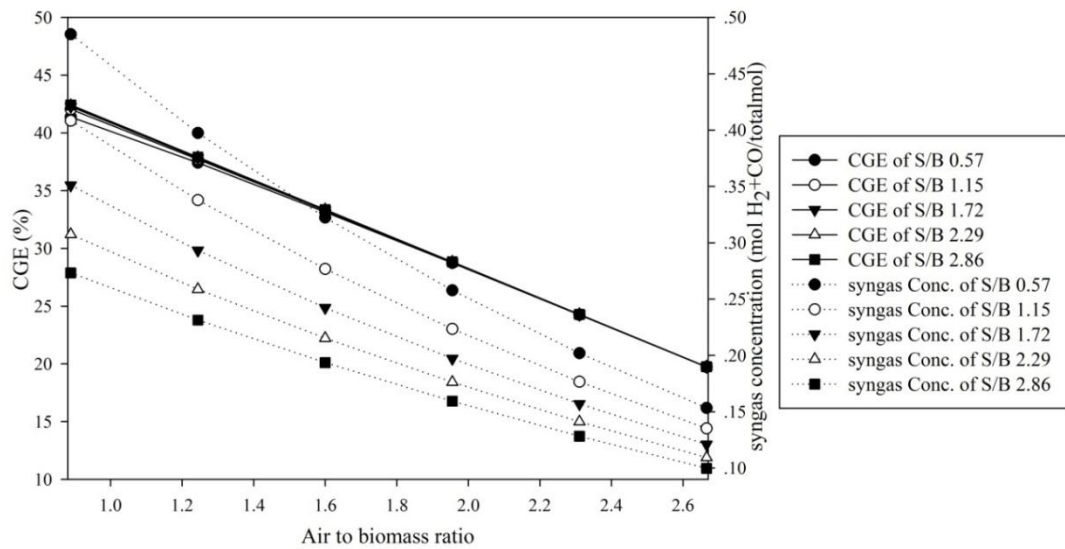
(d)
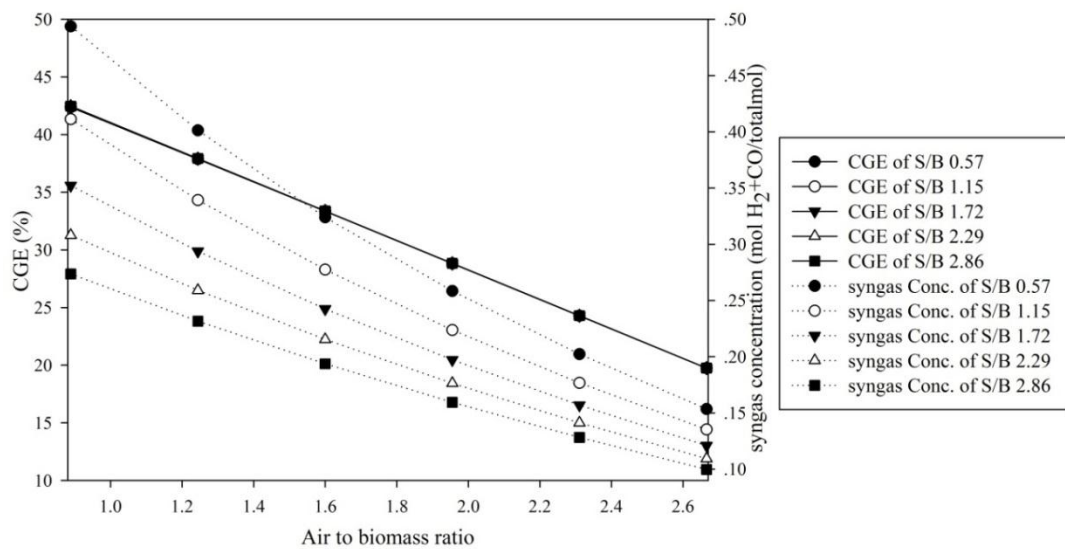
Figure 5.6 Effect of the air to biomass ratio on the CGE at S/B 0.57-2.86: (a) T_{Gs} 500 °C, (b) T_{Gs} 600 °C, (c) T_{Gs} 700 °C and (d) T_{Gs} 800 °C.

Table 5.1 Thermal self-sufficient conditions (S/B = 0.57-2.86, A/B = 0.89-2.67, T_{Gs} = 500-1000 °C and biomass feed rate = 0.48 kg/h).

T_{Gs} (°C)	S/B	A/B	H_2 %mol	CO %mol	CO_2 %mol	CH_4 %mol	N_2 %mol	H_2O %mol	H_2+CO Kmol/h	H_2/CO	CGE (%)
500	0.57	0.57	17.48	4.23	23.61	12.67	23.78	18.19	21.71	4.13	13.24
	1.15	1.03	18.61	2.39	19.11	5.45	25.49	28.95	20.99	7.80	20.09
	1.72	1.44	17.23	1.53	16.38	2.28	26.96	35.60	18.77	11.24	24.00
	2.29	1.78	14.97	1.03	14.48	0.87	27.79	40.85	16.00	14.60	25.19
	2.86	2.12	12.43	0.69	12.99	0.28	28.15	45.47	13.12	18.03	24.21
600	0.57	1.00	26.23	11.52	16.52	2.92	28.55	14.12	37.75	2.28	31.58
	1.15	1.31	24.23	6.00	16.27	0.67	28.50	24.41	30.23	4.04	33.63
	1.72	1.64	20.28	3.41	15.12	0.15	28.50	32.93	23.69	5.95	31.72
	2.29	1.89	16.26	2.05	13.78	0.04	28.46	39.81	18.30	7.94	28.93
	2.86	2.17	12.65	1.28	12.52	0.01	28.42	45.32	13.94	9.87	25.65
700	0.57	1.17	26.80	14.72	13.05	0.16	30.55	14.70	41.52	1.82	38.15
	1.15	1.43	22.90	7.97	14.29	0.03	29.40	25.41	30.87	2.87	35.57
	1.72	1.66	18.61	4.68	13.81	0.01	28.93	33.95	23.29	3.98	32.39
	2.29	1.91	14.86	2.91	12.88	0.00	28.72	40.64	17.76	5.11	29.03
	2.86	2.24	11.73	1.87	11.89	0.00	28.59	45.92	13.60	6.26	25.51
800	0.57	1.21	25.05	16.18	11.43	0.01	31.04	16.29	41.24	1.55	38.40
	1.15	1.44	21.18	9.31	12.84	0.00	29.80	26.88	30.49	2.27	35.43
	1.72	1.70	17.25	5.74	12.68	0.00	29.24	35.10	22.99	3.01	32.13
	2.29	1.96	13.84	3.70	12.04	0.00	28.94	41.48	17.54	3.74	28.77
	2.86	2.21	10.99	2.45	11.28	0.00	28.76	46.51	13.44	4.48	25.30
900	0.57	1.23	23.53	17.27	10.20	0.00	31.51	17.62	40.81	1.36	37.57
	1.15	1.46	19.74	10.38	11.66	0.00	30.20	28.11	30.12	1.90	34.96
	1.72	1.72	16.08	6.63	11.72	0.00	29.51	36.08	22.71	2.43	31.80
	2.29	1.98	12.94	4.40	11.30	0.00	29.12	42.22	17.34	2.94	28.50
	2.86	2.26	10.31	2.98	10.72	0.00	28.88	47.06	13.29	3.46	25.04
1000	0.57	1.25	22.30	18.14	9.23	0.00	31.79	18.69	40.43	1.23	37.38
	1.15	1.48	18.55	11.25	10.71	0.00	30.46	29.11	29.80	1.65	34.71
	1.72	1.71	15.09	7.37	10.92	0.00	29.74	36.89	22.46	2.05	31.57
	2.29	2.00	12.16	4.99	10.66	0.00	29.30	42.86	17.15	2.43	28.30
	2.86	2.28	9.71	3.45	10.23	0.00	29.03	47.55	13.16	2.81	24.86

5.3.2 Steam-CO2 system

5.3.2.1 Effect of the temperature on the product gas composition

The effects of the gasifying temperature on the product gas composition are investigated by setting the steam and CO_2 to biomass ratios at 0.57 and 0.82, respectively, and varying the gasifying temperatures in the range of 500 to 1000 °C. The variation of the product gas composition, syngas yield and H_2/CO ratio are shown in Figure 5.7. The results show the same effect as that found in the steam-air system, but a higher yield of syngas is achieved because the effect of N_2 dilution does not exist and the Boudouard and methane dry reforming reactions play a crucial role. The char from the devolatization step further reacts with CO_2 to result in more CO formation. This factor causes the H_2/CO ratio of the product gas derived from this system to be lower than the ratio derived from the steam-air system.
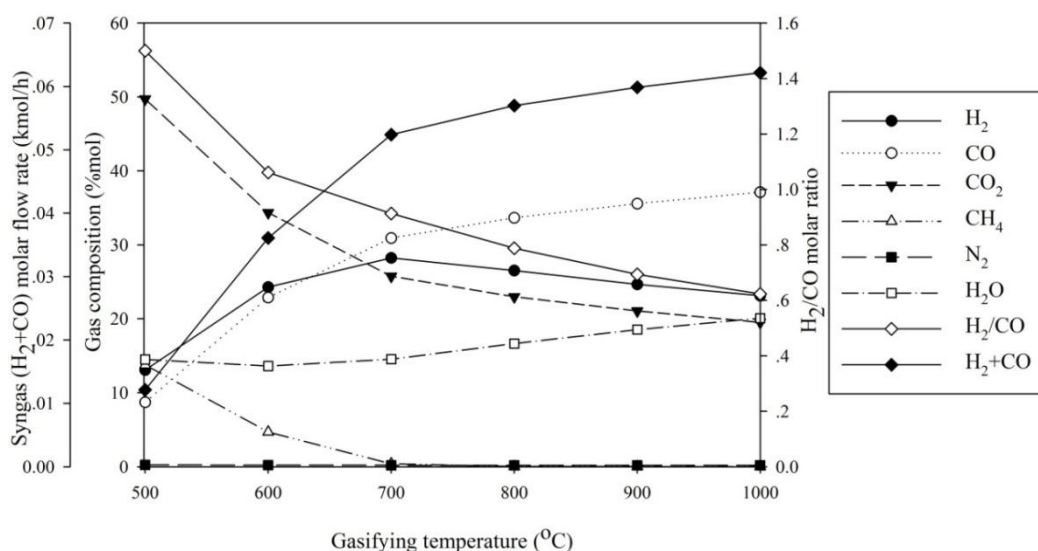
Figure 5.7 Effect of the temperature on the product gas composition, syngas yield and H_2/CO ratio (S/B 0.57 and CO_2/B 0.82)

5.2.2.2 Effect of the CO_2 to biomass ratio on the product gas composition

The effects of the CO_2 to biomass ratio on the product gas composition are investigated by setting the steam to biomass ratio at 0.57 and varying the CO_2 to

biomass ratio in the range of 0.58 to 1.75 for each temperature in the range of 500 to 1000 °C. The variation of the product gas composition, syngas yield and H_2/CO ratio at 500 and 600 °C are shown in Figures 5.8(a)-(b). At these conditions, as the CO_2 to biomass ratio increases, the Boudouard and dry reforming of methane reactions play a crucial role, and the methane steam reforming and the water gas reactions also occur. Therefore, the concentration of CO slightly increases, whereas the concentrations of H_2O and CH_4 decrease. Moreover, it is found that the concentration of CO_2 at the lower temperature system is significantly increased and higher than that at higher temperature system due to the domination of water gas shift reaction and the increase of CO_2 dilution effect. The variation of the product gas composition, syngas yield and H_2/CO ratio at 700 °C and 800 °C are shown in Figures 5.8(c)-(d). At these conditions, the concentration of H_2O in the system slightly increases; whereas that of H_2 significantly decreases due to the absence of methane steam reforming reaction and the domination of the reverse water gas shift. Moreover, the CO_2 dilution effect is also observed for all gasifying temperatures. These factors cause the syngas yield and the H_2/CO ratio to decrease with an increase in CO_2 to biomass ratio. Compared with the steam-air system, the concentration of CO in this system is always higher than that of H_2; therefore, a lower H_2/CO ratio is achieved.

(a)
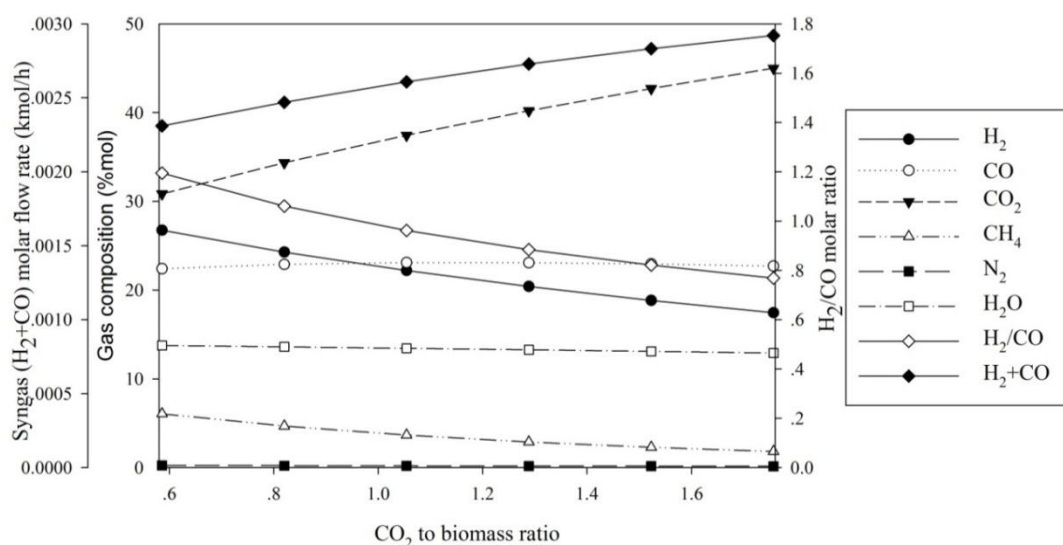
(b)
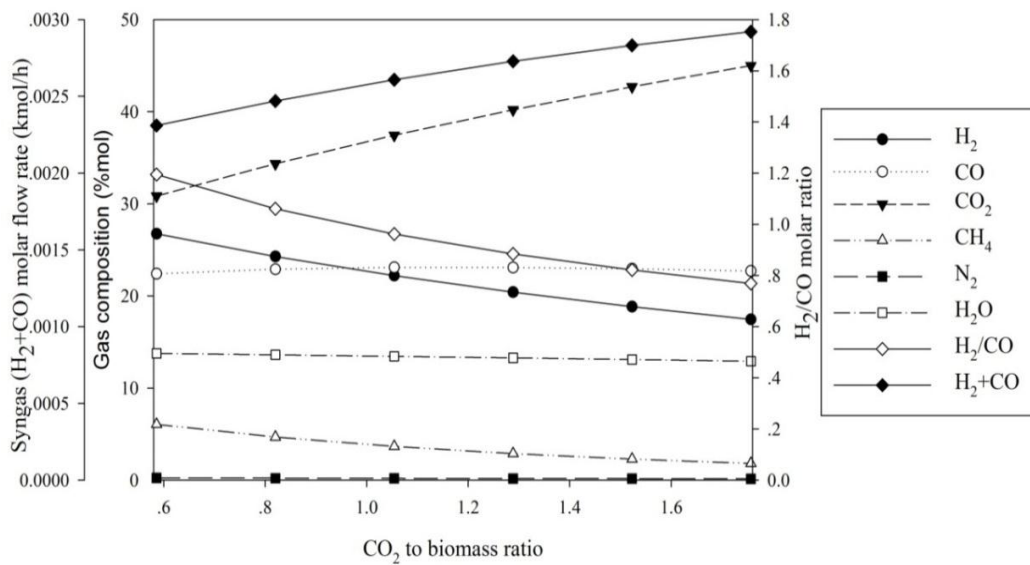
(c)
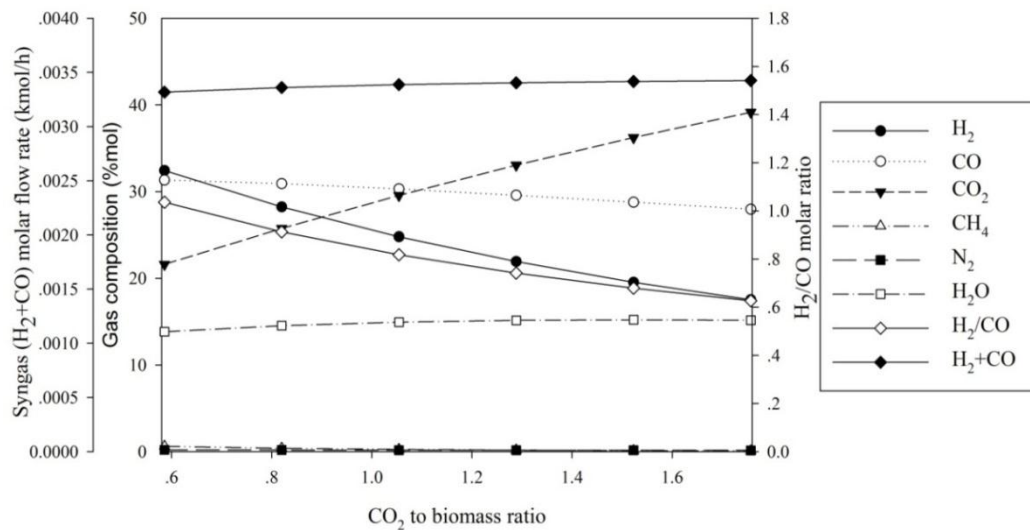
(d)
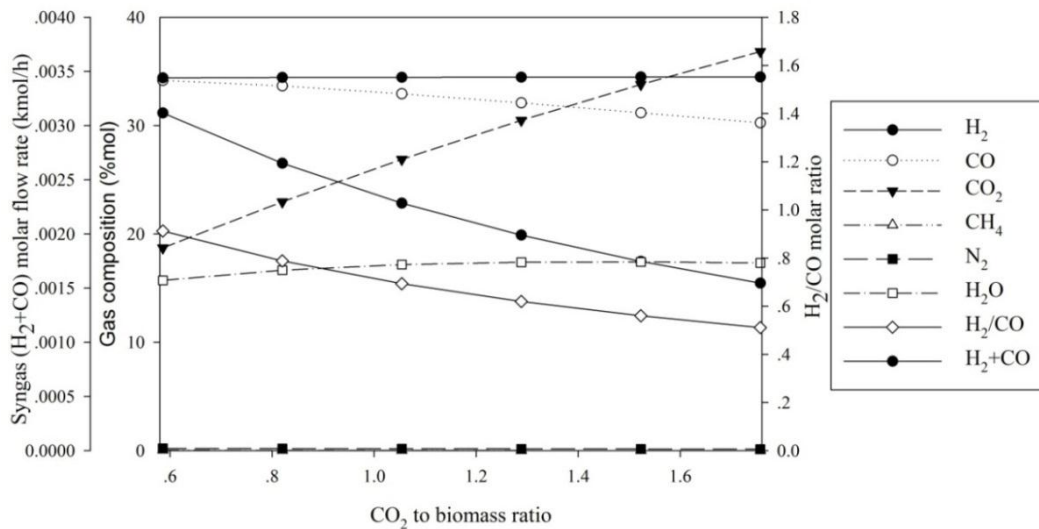
Figure 5.8 Effect of the CO_2 to biomass ratio on the product gas composition, syngas yield and H_2/CO ratio: (a) S/B 0.57 and T_{Gs} 500 °C, (b) S/B 0.57 and T_{Gs} 600 °C, (c) S/B 0.57 and T_{Gs} 700 °C and (d) S/B 0.57 and T_{Gs} 800 °C

5.3.2.3 Effect of CO_2 to biomass ratio on the total energy consumption of the system

The effects of CO_2 to biomass ratio on the total energy consumption are investigated for various steam to biomass ratios and gasifying temperatures in the range of 0.57 to 2.86 and 500 to 1000 °C, respectively. The CO_2 to biomass ratio is varied in the range of 0.59 to 1.76. The variation of the total energy consumption at 800 °C is shown in Figure 5.9. At constant steam to biomass ratio, the total energy consumption continuously increases with the CO_2 to biomass ratio due to the domination of the highly endothermic Boudouard and methane dry reforming reactions. The total energy consumption also increases with the steam to biomass ratio at a constant CO_2 to biomass ratio due to the effect of other endothermic reactions, i.e., water gas and steam reforming of methane. Moreover, the required external heat source increases as the gasifying temperature, and the steam and CO_2 to biomass ratios increase, as shown in Figures 5.9-5.10. Compared with the steam-air system,

the required external heat source in this system is much higher, and the thermal self-sufficient condition is not achieved.
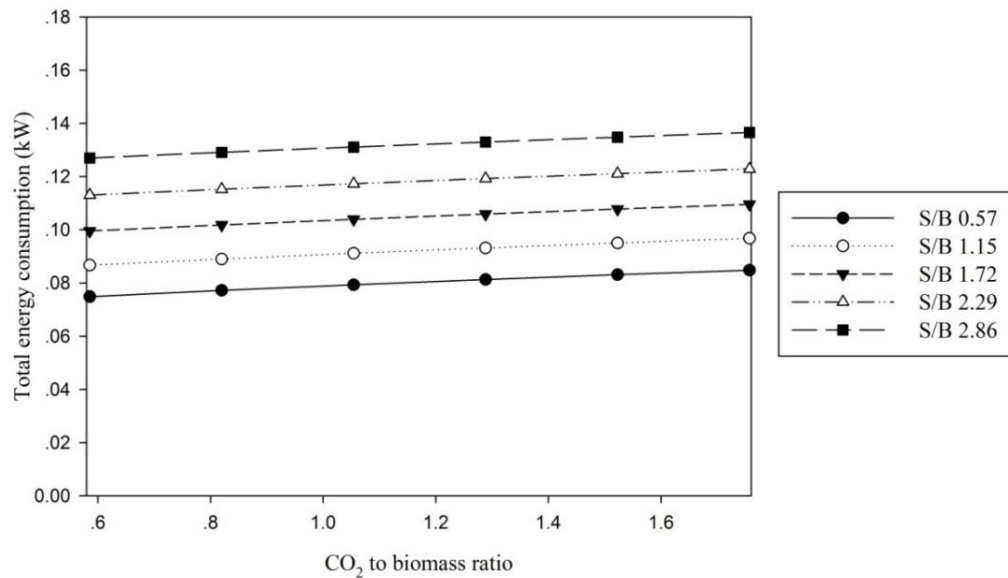
Figure 5.9 Effect of the CO_2 to biomass ratio on the total energy consumption (S/B 0.57 - 2.86, T_{Gs} 800 °C).
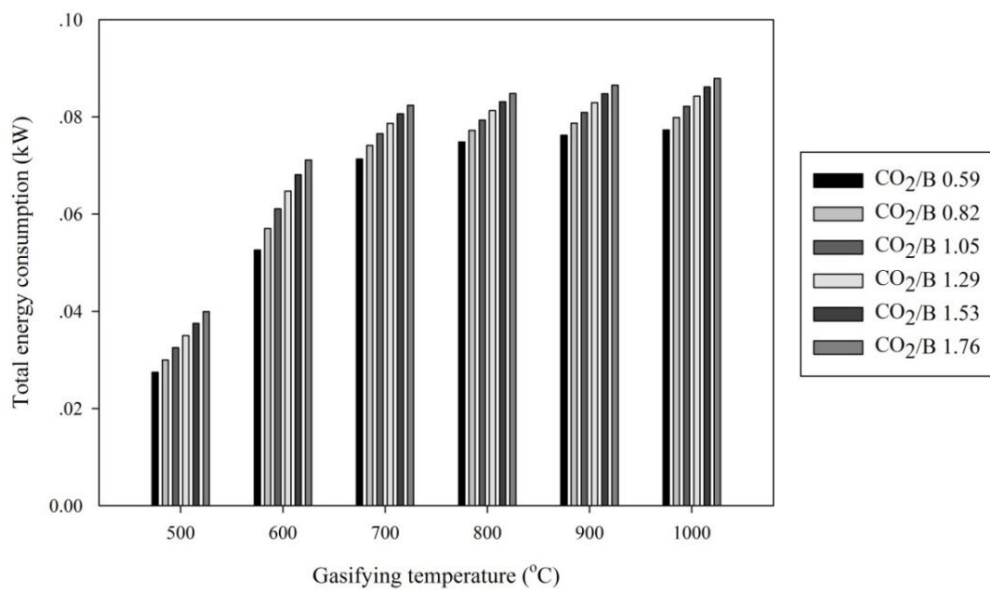
Figure 5.10 Effect of the CO_2 to biomass ratio on the total energy consumption (S/B 0.57, T_{Gs} 500 - 1000 °C).

5.3.2.4 Effect of the CO_2 to biomass ratio on the cold gas efficiency

The effect of CO_2 to biomass ratio on the CGE is investigated for the steam to biomass ratio and gasifying temperature in the range of 0.57 to 2.86 and 500 to 1000 ^{o}C, respectively. The CO_2 to biomass ratio is varied from 0.59 to 1.76. The variation of CGE and syngas concentration at temperatures of 500 and 600 ^{o}C is shown in Figures 5.11(a)-(b). It is found that the CGE increases with the CO_2 to biomass ratio due to the domination of Boudouard and methane dry reforming reactions, resulting in the increase of syngas yield. However, the decrease of syngas concentration due to CO_2 dilution is found. At a constant CO_2 to biomass ratio, the CGE also increases with the steam to biomass ratio, caused by the domination of the water gas and methane steam reforming reactions. At gasifying temperature of 700 ^{o}C or higher, the CGE shows the same trend as found at lower temperature operation (Figures 5.11(c)-(d)).

(a)
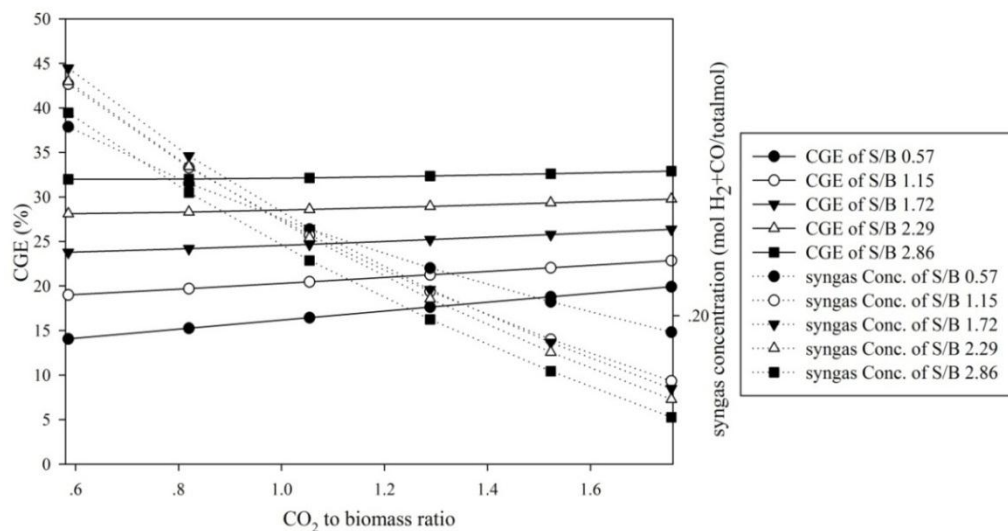
(b)
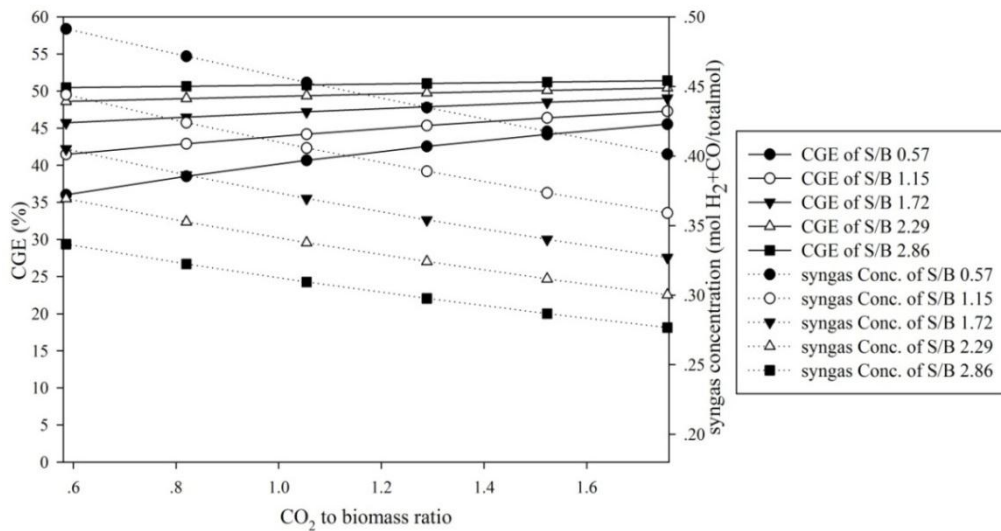
(c)
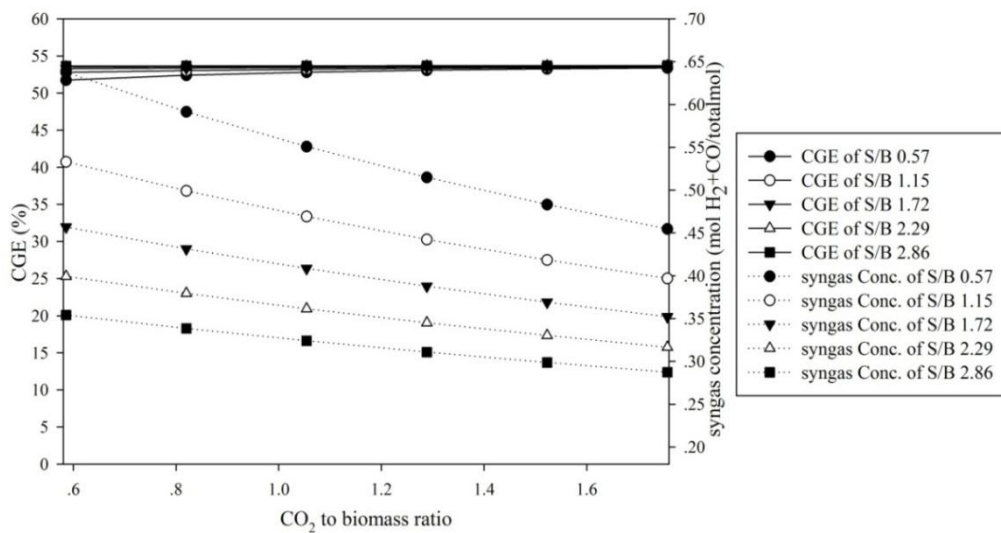
(d)
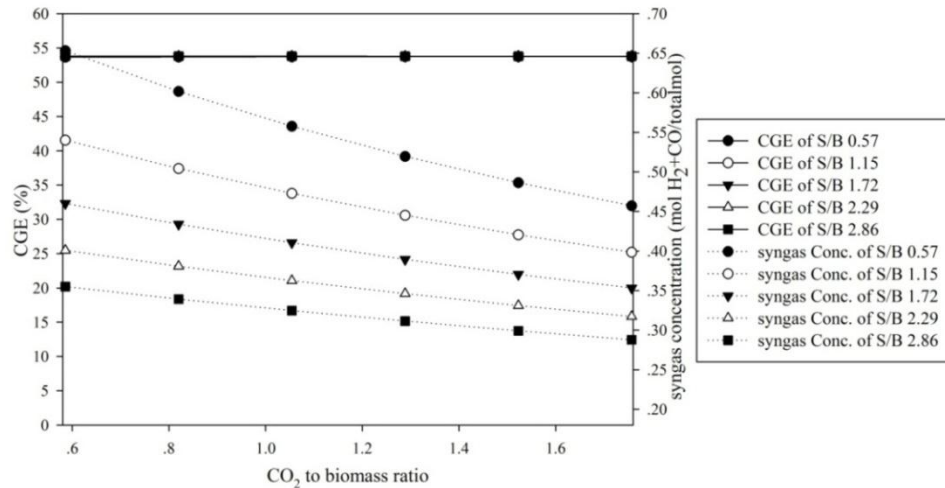
Figure 5.11 Effect of the CO_2 to biomass ratio on the CGE at S/B 0.57-2.86: (a) T_{Gs} 500 °C, (b) T_{Gs} 600 °C, (c) T_{Gs} 700 °C and (d) T_{Gs} 800 °C

5.4 Conclusions

The performance of two rice straw gasification systems i.e., steam-air and steam-CO_2, is investigated in this study. Effects of changes in the ratio of gasifying agent on the product gas composition, syngas yield, H_2/CO ratio, total energy consumption as well as CGE are analyzed at different gasifying temperatures. The syngas production rate of both systems significantly increases as temperature increases from 500 to 700 °C, and becomes stable at temperature higher than 700 °C. However, the steam-CO_2 system offers higher syngas productivity and a lower H_2/CO ratio. For the steam-air system, the syngas yield decreases as the air-to-biomass ratio increases, resulting in the decrease of CGE; however, the H_2/CO ratio is found to increase with air-to-biomass ratio. In the steam-CO_2 system, the syngas yield increases with the CO_2-to-biomass ratio, causing the increase in CGE, whereas the H_2/CO decreases. At high temperature, the CGE does not depend on the steam-to-biomass ratio. For the aspect of total energy consumption, the steam-air system consumes less energy, and thermal self-sufficient conditions can be achieved. The production of FT feed gas at the thermal self-sufficient operation of gasifier is possible when a mixture of steam and air is selected as a gasifying agent.

CHAPTER VI
TECHNCAL AND ECONOMIC STUDIES OF THE BG-FT
PROCESS WITH OFF-GAS RECIRCULATION

In this chapter, techno-economic analysis of a BG-FT process with different configurations (i.e., once-through and with recirculation concepts) for green fuel production is presented. The influence of changing an FT off-gas recycle fraction at different values of the FT reactor volume on the performance of the syngas processor, the FT synthesis and the overall energy efficiency of BG-FT process is discussed. The economic analysis is also performed to investigate the feasibility of the BG-FT process with the FT off-gas recycle, compared with the once-through concept.

6.1 Introduction

Regarding to chapter V, the production of syngas with FT specification process using air and steam as a gasifying agent is possible. However, the nitrogen gas, which derived from air, contained in FT-feed gas is limited; the pure oxygen derived from air separation unit (ASU) is selected. As a result, the volume of produced gas decreases and the smaller size of process equipment are required (Hamelinck et al., 2004; Im-orb et al., 2015). However, the H2/CO ratio of the produced syngas is lower than 2. Normally, the adjustment of the H_2/CO ratio can be performed in several practices, such as partially CO_2 or H_2 separation and conversion of CO to H_2 via water gas shift reaction which can be done in gasifier or external water gas shift reactor. For example, the biomass gasification and the FT pilot scale located at National Science and Technology Development Agency (NSTDA), Thailand, included the water gas shift reactor contained Ni-based catalyst to adjust the H_2/CO ratio to a value close to 2 (Hunpinyo et al., 2014). The favorable H_2/CO ratio in the methanol production could be achieved via the combined water gas shift reactor and a CO_2 removal unit (Hamelinck and Faaij, 2006). Although the H_2/CO ratio adjustment can be simultaneously done in gasifier by varying the ratio of gasifying

agents (i.e., air or oxygen and steam), the temperature of the steam supplied to the gasifier is lower than the gasification temperature, a significant amount of heat is needed to raise the steam temperature results in the decrease of gasifier bed temperature. Hence a steam to biomass ratio above a threshold, steam offers negative effects on the product (Kumar et al., 2009). The installation of water gas shift reactor to adjust the H_2/CO ratio is therefore selected in this study. According to the above reasons, the BG-FT process consists of oxygen gasification, tar steam reforming, water gas shift, FT synthesis and power generation.

Previous studies usually performed the performance analysis of the BG-FT process from the aspect of technical and economic feasibilities for developing a new technology offering liquid transportation fuel that could be competitive with the existing one from crude distillation. Nevertheless, the analyses were mostly restricted to the once-through process. In general, the derived FT off-gas consisting of unreacted syngas (CO and H_2) can be recycled to upstream processes, e.g., gasifier or FT reactor, in order to improve the product yield. Moreover, CO_2 by-product can be used as a gasifying agent to increase the production rate of syngas and also FT products as discussed in chapter V. The objective of this study is therefore to perform the techno-economic analysis comparing two configurations of the BG-FT process with rice straw feedstock (i.e., the once-through and the included long recycle loop concept in which the various fractions of the FT off-gas is recycled to the gasifier) using the BG-FT model developed in Aspen Custom Modeler (ACM) program as discussed in chapter IV. The gasifier is considered to be operated in the thermal self-sufficiency condition

6.2 Process configuration and scope of work

The BG-FT process considered in this study consists of oxygen gasification, tar steam reforming, water gas shift, FT synthesis and power generation as shown in Figure 6.1. The technical and economic studies of two configurations of the BG-FT process with rice straw feedstock (i.e., the once-through and the included long recycle loop concept in which the various fractions of the FT off-gas is recycled to the gasifier) are investigated and compared. Regarding the technical aspect, the influence of changes in the FT off-gas recycle fraction in the ranges of 0.1-0.9 for constant FT

reactor volume on the performance of the syngas processor, the FT synthesis process as well as the overall BG-FT process are investigated. As the FT reactor volume influences on the CO conversion, the change of this parameter is also considered in this study by varying the FT reactor volume 30% above (150-190 m^3) and below (90-130 m^3) the base volume of 140 m^3. The economic analysis using the incremental NPV as an indicator is performed to investigate the feasibility of the BG-FT process with the FT off-gas recycle, compared with the once-through concept. Analysis of uncertain parameters, such as product cost, plant life and interest rate, on the economic indicator is also performed. The scope of work considered in this chapter is summarized in Figure 6.2.
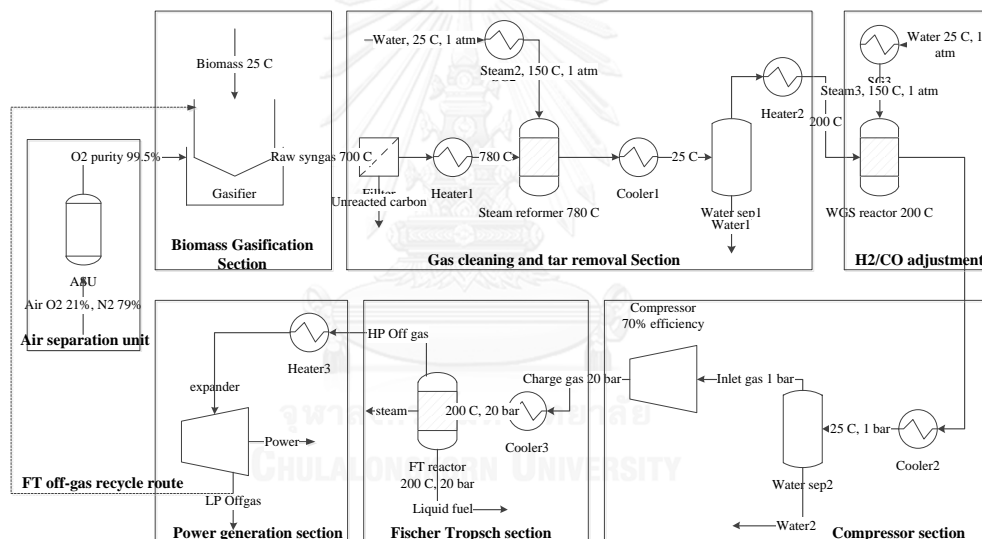
Figure 6.1 The BG-FT process configuration
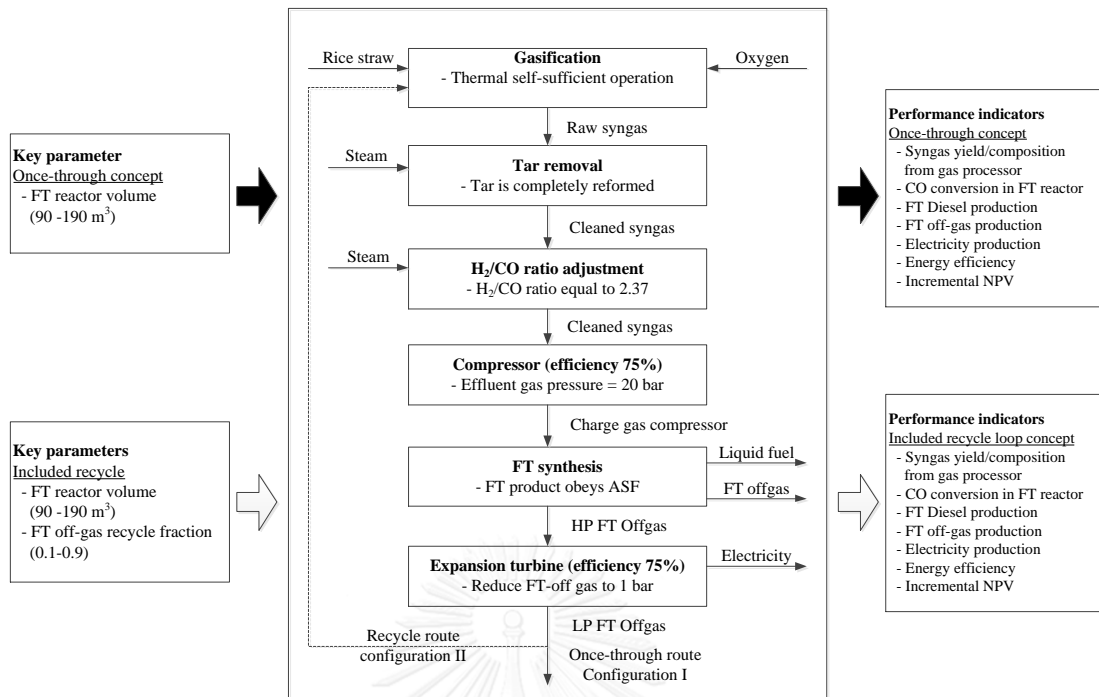
Figure 6.2 The scope of work considered in chapter VI

6.3 Results and discussion

6.3.1 Process analysis

The performance analysis of the BG-FT process where the gasifier is operated under the thermal self-sufficient condition is performed to investigate the effect of the long loop recycle of the FT off-gas back to the gasifier on the performance of the syngas processor and FT synthesis process. Firstly, the preliminary study is performed to determine the suitable ratio of H_2 and CO of syngas offering maximum diesel production rate, using the BG-FT model. The mixture of oxygen and steam is considered gasifying agent. Figures 6.3(a) and (b) show that the maximum diesel production rate is achieved when the H_2/CO ratio of the syngas (outlet of gas processing unit) is adjusted to be a value of 2.37. The H_2/CO ratio considered in this study is therefore fixed at this value and the FT off-gas recycle fraction is varied from 0 to 0.9 for each constant FT reactor volume in the range of 90 to 190 m^3.

(a)
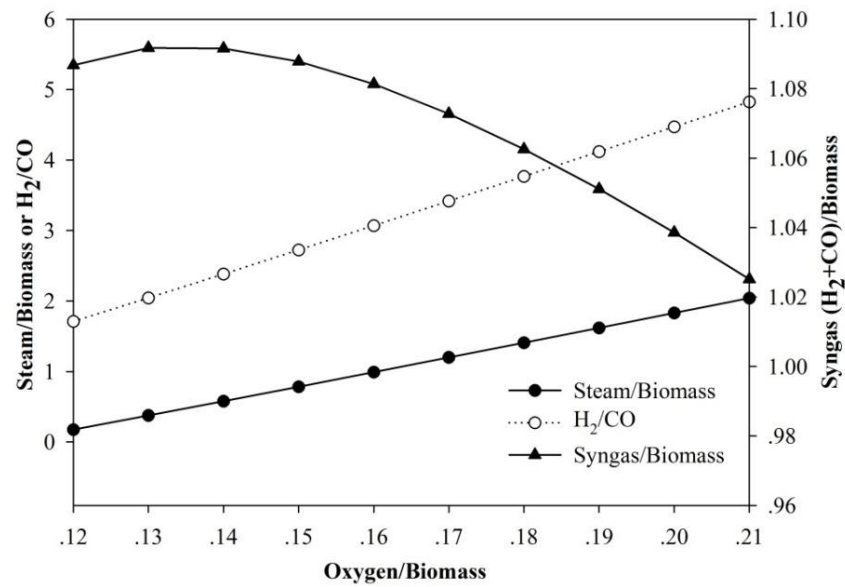
(b)
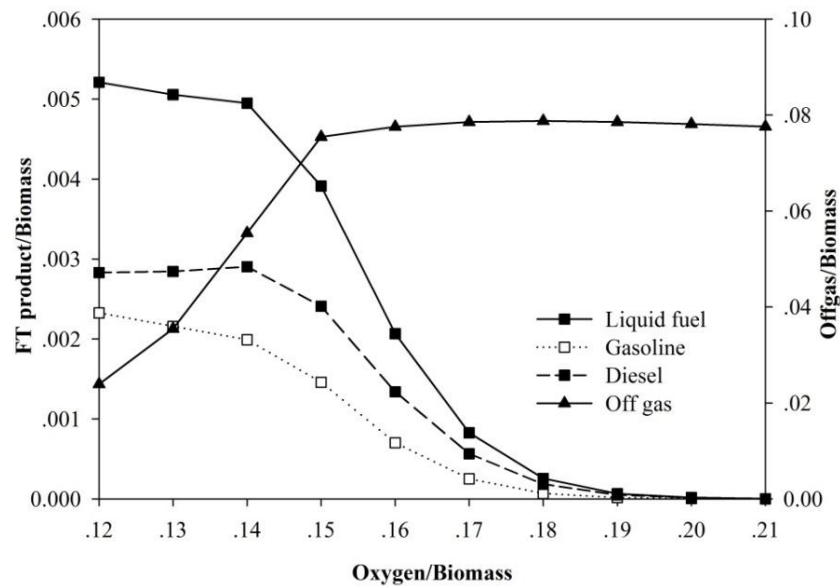
Figure 6.3 Effect of gasifying agents (oxygen and steam) on: (a) syngas (H_2+CO) yield and H_2/CO ratio and (b) FT product distribution.

6.3.1.1 Effect of FT off-gas recycle fraction on the performance of syngas processor

The compositions of FT off-gas derived from the FT synthesis unit at various FT off-gas recycle fractions (0 to 0.9) for the constant FT reactor volume of 90 m^3 is summarized in Table 6.1. The concentrations of CO_2, CO and H_2 increase when the recycle fraction increases from 0 to 0.8. It is shown in Figure 6.4 that, as the FT off-gas recycle fraction increases at each FT reactor volume, a greater amount of oxygen is required to maintain the thermal self-sufficiency condition in the gasifier. A similar trend is found when the FT reactor volume increases at each recycle fraction; however, a smaller amount of oxygen is required. The amount of syngas with an H_2/CO ratio of 2.37 leaving the gas processor of the BG-FT process with FT off-gas recirculation is also considered. It is shown in Figure 6.5 that at a constant FT off-gas recycle fraction, the amount of syngas decreases when the FT reactor volume increases. The inverse effect is observed when the FT off-gas recycle fraction increases from 0 to 0.8 at a constant reactor volume. However, a decrease in the amount of syngas is seen when the fraction exceeds this range because of significant increases in the accumulation of the inert gases (CO_2 + N_2), as shown in Figure 6.6. At a constant FT reactor volume, the concentration of H_2 and CO gradually increase when the recycle fraction increases from 0 to 0.8 due to the domination of the Boudouard reaction and the steam reforming of hydrocarbon gases. Nevertheless, it decreases due to the domination of oxidation reactions when the recycle fraction becomes higher than the above range. As a result, a significant increase in CO_2 and H_2O concentrations are observed.

Table 6.1 The FT off-gas composition (kmol/h) at different recycle fractions (the constant FT reactor volume = 90 m^3)

FT Offgas	Off gas recycle fraction									
	0	**0.1**	**0.2**	**0.3**	**0.4**	**0.5**	**0.6**	**0.7**	**0.8**	**0.9**
H_2	0.19489	0.26513	0.34591	0.44208	0.56066	0.71182	0.91021	1.17212	1.46578	1.07133
CO	0.07222	0.10215	0.13649	0.17729	0.22753	0.29151	0.37546	0.48630	0.61090	0.44696
H_2O	0.24360	0.23769	0.23291	0.22903	0.22579	0.22303	0.22066	0.21866	0.21720	0.21927
CO_2	0.28300	0.32233	0.37265	0.43933	0.53174	0.66776	0.88613	1.28714	2.21738	5.71408
N_2	0.00056	0.00069	0.00086	0.00110	0.00144	0.00197	0.00287	0.00467	0.00928	0.02857
CH_4	0.01836	0.01803	0.01780	0.01765	0.01757	0.01759	0.01773	0.01809	0.01906	0.02279
C_2H_6	0.01335	0.01309	0.01290	0.01277	0.01270	0.01267	0.01272	0.01291	0.01343	0.01546
C_3H_8	0.00969	0.00949	0.00934	0.00923	0.00916	0.00912	0.00912	0.00920	0.00946	0.01048
C_4H_{10}	0.00702	0.00687	0.00675	0.00666	0.00660	0.00655	0.00653	0.00655	0.00666	0.00711
C_5H_{12}	0.00507	0.00496	0.00487	0.00480	0.00474	0.00470	0.00467	0.00466	0.00468	0.00482
C_6H_{14}	0.00363	0.00355	0.00348	0.00343	0.00338	0.00335	0.00332	0.00329	0.00328	0.00326
C_7H_{16}	0.00259	0.00252	0.00247	0.00243	0.00240	0.00237	0.00234	0.00232	0.00229	0.00221
C_8H_{18}	0.00182	0.00177	0.00174	0.00171	0.00168	0.00166	0.00164	0.00162	0.00159	0.00149
C_9H_{20}	0.00125	0.00122	0.00120	0.00118	0.00116	0.00114	0.00113	0.00111	0.00109	0.00100
$C_{10}H_{22}$	0.00084	0.00082	0.00081	0.00079	0.00078	0.00077	0.00076	0.00075	0.00074	0.00067
$C_{11}H_{24}$	0.00054	0.00053	0.00052	0.00051	0.00051	0.00050	0.00050	0.00049	0.00049	0.00045
$C_{12}H_{26}$	0.00034	0.00033	0.00032	0.00032	0.00032	0.00032	0.00031	0.00031	0.00032	0.00030
$C_{13}H_{28}$	0.00020	0.00020	0.00019	0.00019	0.00019	0.00019	0.00019	0.00019	0.00020	0.00019
$C_{14}H_{30}$	0.00011	0.00011	0.00011	0.00011	0.00011	0.00011	0.00011	0.00011	0.00012	0.00012
$C_{15}H_{32}$	0.00006	0.00006	0.00006	0.00006	0.00006	0.00006	0.00006	0.00006	0.00007	0.00008
$C_{16}H_{34}$	0.00003	0.00003	0.00003	0.00003	0.00003	0.00003	0.00003	0.00003	0.00004	0.00005
$C_{17}H_{36}$	0.00002	0.00002	0.00002	0.00002	0.00002	0.00002	0.00002	0.00002	0.00002	0.00003
$C_{18}H_{38}$	0.00000	0.00000	0.00000	0.00000	0.00000	0.00000	0.00000	0.00000	0.00000	0.00000
$C_{19}H_{40}$	0.00000	0.00000	0.00000	0.00000	0.00000	0.00000	0.00000	0.00000	0.00001	0.00001
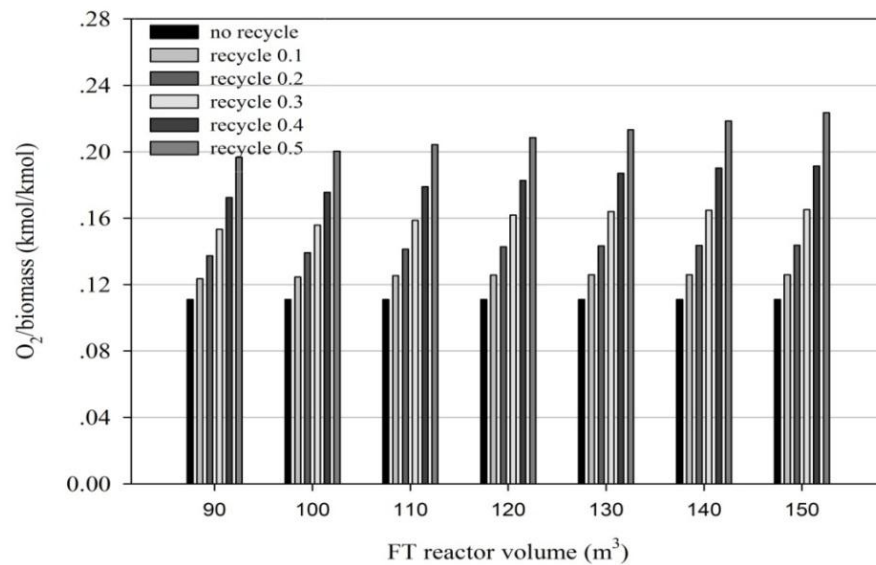
Figure 6.4 The amount of oxygen required to maintain the thermal self-sufficient condition in the gasifier at various FT off-gas recycle fractions in the range of 0 to 0.5 for each constant FT reactor volume in the range of 90 to 150 m^3.
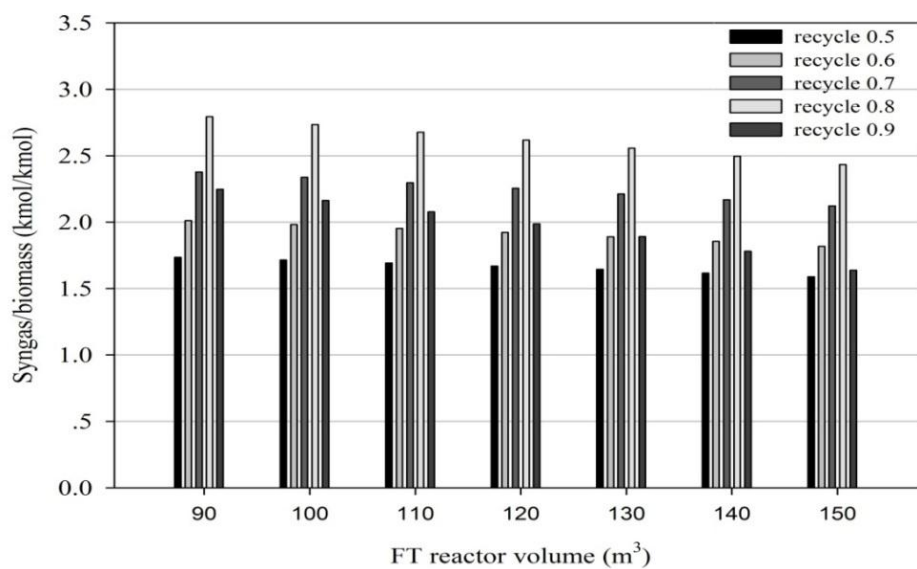
Figure 6.5 The amount of syngas (H_2+CO) derived from gas processor at various FT off-gas recycle fractions in the range of 0 to 0.5 for each constant FT reactor volume in the range of 90 to 150 m^3
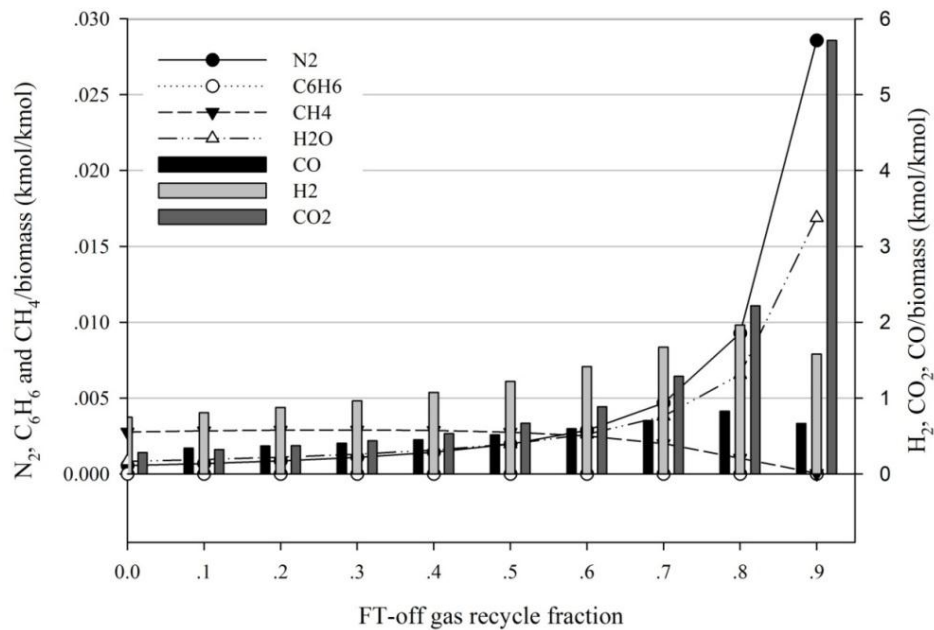
Figure 6.6 The composition of syngas derived from gas processor at various FT off-gas recycle fractions in the range of 0 to 0.9 for constant FT reactor volume at 90 m^3

6.3.1.2 Effect of FT off-gas recycle fraction on the performance of FT synthesis

The effect of the FT off-gas recycle fraction on the CO conversion at various FT reactor volumes is shown in Figure 6.7. It is found that at a constant recycle fraction, the CO conversion increases when the reactor volume increases and seems to be stable at a value of approximately 0.98. At a constant reactor volume, the CO conversion decreases when the recycle fraction increases. However, the CO conversion for the recycle fraction of 0.9 is higher than that of 0.7-0.8, which is caused by the significant decreases in CO concentration of the FT feed gas.
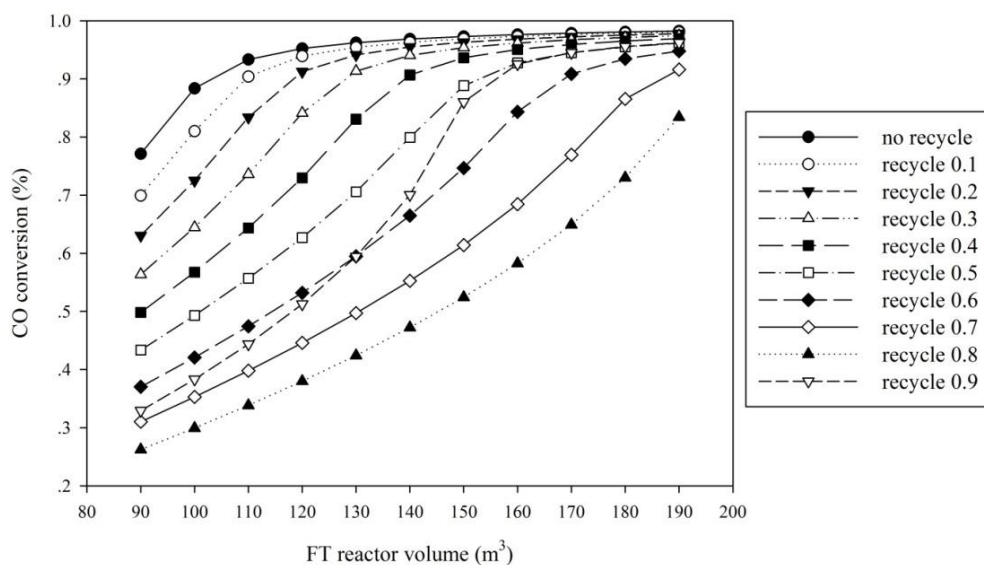
Figure 6.7 The CO conversion at various FT off-gas recycle fractions in the range of 0 to 0.9 for each constant FT reactor volume in the range of 90 to 190 m^3.

The production rate of diesel and off-gas from the BG-FT process at various FT off-gas recycle fractions and FT reactor volumes are illustrated in Figures 6.8 and 6.9, respectively. At a constant recycle fraction, the diesel production rate increases when the reactor volume increases and seem to be stable at the optimum reactor volume, which is the smallest volume for which the diesel production rate does not depend on reactor size. For example, the optimum reactor volume of the system with a recycle fraction of 0.1 is 130 m^3. It is found that the optimum reactor volume increases when the FT off-gas recycle fraction increases. Moreover, it is seen from Figure 6.8 that at the optimum reactor volume, the amount of diesel product increases when the recycle fraction rises in the range of 0 to 0.4; however, the inverse effect is found when the recycle fraction is higher than the above range. The maximum diesel production rate is found in the system with the conditions of 190 m^3 FT reactor volume and 0.4 FT off-gas recycle fraction.

At a constant recycle fraction, the amount of FT off-gas decreases when the reactor volume increases and seems to be stable at an optimum reactor volume (Figure 6.9). The inverse effect is found when the reactor volume is fixed and the

recycle fraction is raised from 0 to 0.9. A significant increase in the amount of FT off-gas is found at the recycle fraction of 0.9 for every reactor size. Moreover, the electricity generated from the reduction of FT off-gas pressure through the expansion turbine which is connected to the generator is also investigated. The result shows the same trend as the FT off-gas (Figure 6.10).
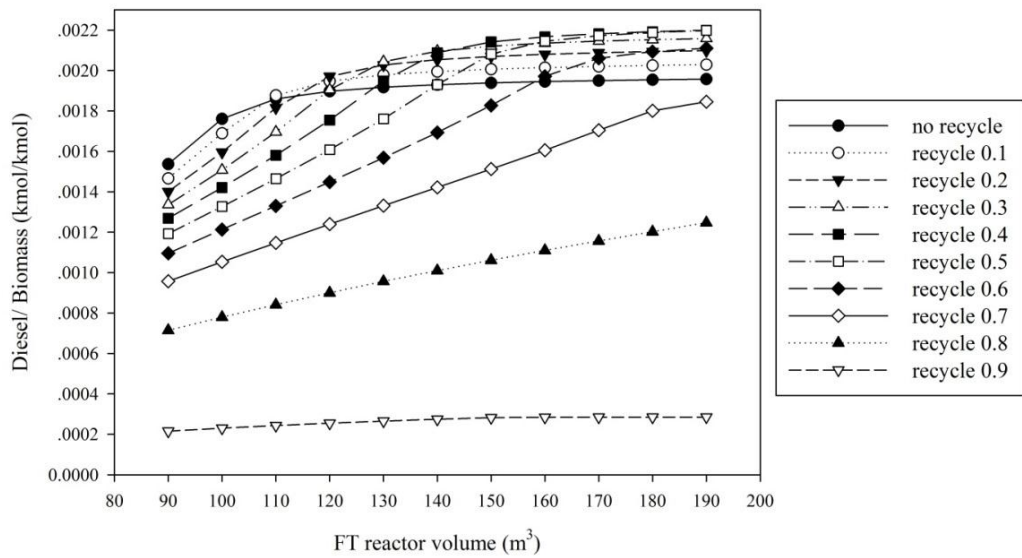
Figure 6.8 The amount of diesel product at various FT off-gas recycle fractions in the range of 0 to 0.9 for each constant FT reactor volume in the range of 90 to 190 m^3.
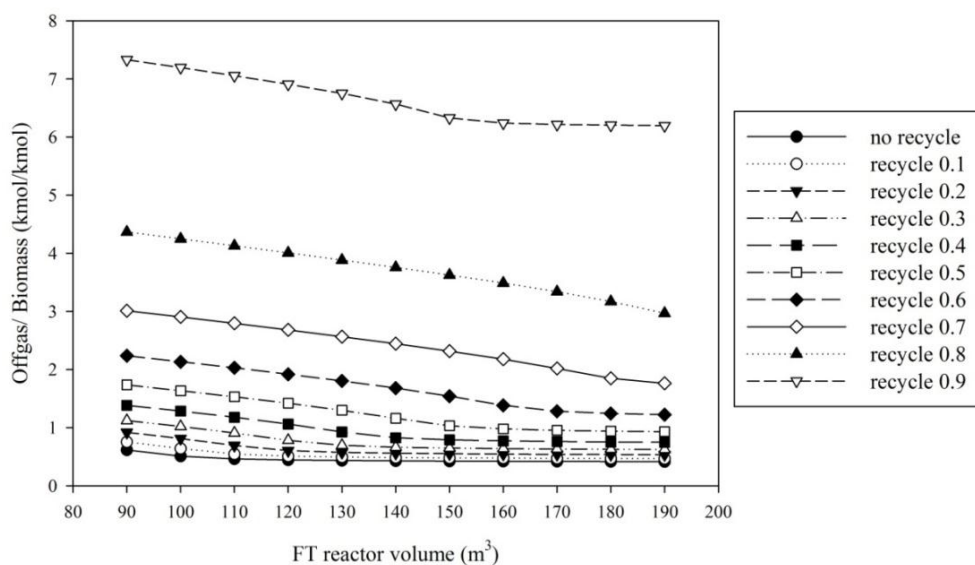
Figure 6.9 The amount of off-gas product at various FT off-gas recycle fractions in the range of 0 to 0.9 for each constant FT reactor volume in the range of 90 to 190 m^3.
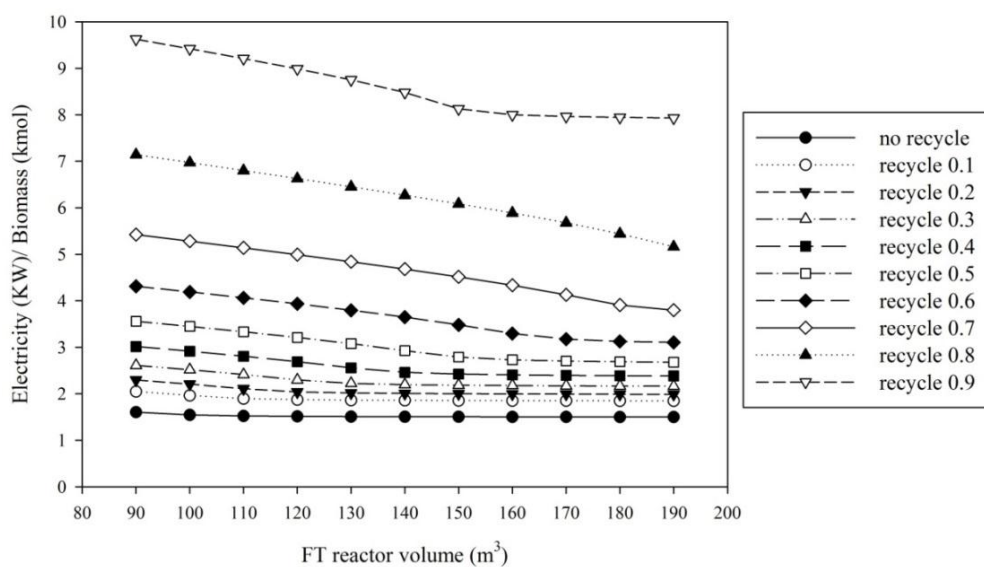
Figure 6.10 The electricity generated at various FT off-gas recycle fractions in the range of 0 to 0.9 for each constant FT reactor volume in the range of 90 to 190 m^3.

6.3.2 Energy analysis

As discussed in chapter II, the energy efficiency of the BG-FT process operated at various FT off-gas recycle fractions and FT reactor volumes is calculated from Eq.(6.1).

$$\text{valuable product energy efficiency} = \frac{\text{energy of diesel (HHV)} + \text{electricity}}{\text{energy of biomass (HHV)}} \qquad (6.1)$$

It is found from Figure 6.11 that at a constant recycle fraction in the range of 0-0.6, the energy efficiency based on the valuable products slightly increases when the reactor volume increases. An opposite trend is observed at higher recycle fraction because the generated electricity continuously decreases. At a constant reactor volume, the energy efficiency increases with the increased recycle fraction. The energy consumption at each unit is also investigated. It is found that the required heat for endothermic units (e.g. ASU, heater1, reformer, heater 2, steam generator, compressor and heater 3) increases when FT off-gas recycle fraction increases and the released heat from exothermic units (e.g. cooler 1, WGS, cooler 2, cooler 3 and expansion turbine) shows the same trend as illustrated in Figure 6.12. However, the inverse effect is found for FT synthesis unit due to the lower extent of reaction.
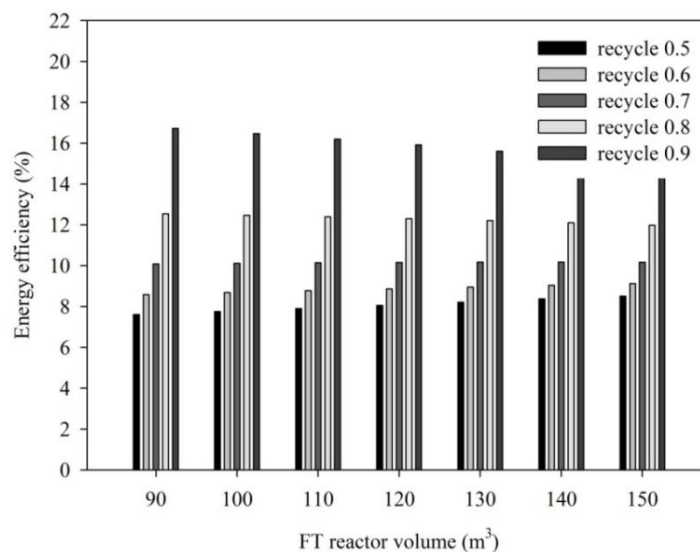
Figure 6.11 The energy efficiency at various FT off-gas recycle fractions for each constant FT reactor volume (90 to 150 m^3).
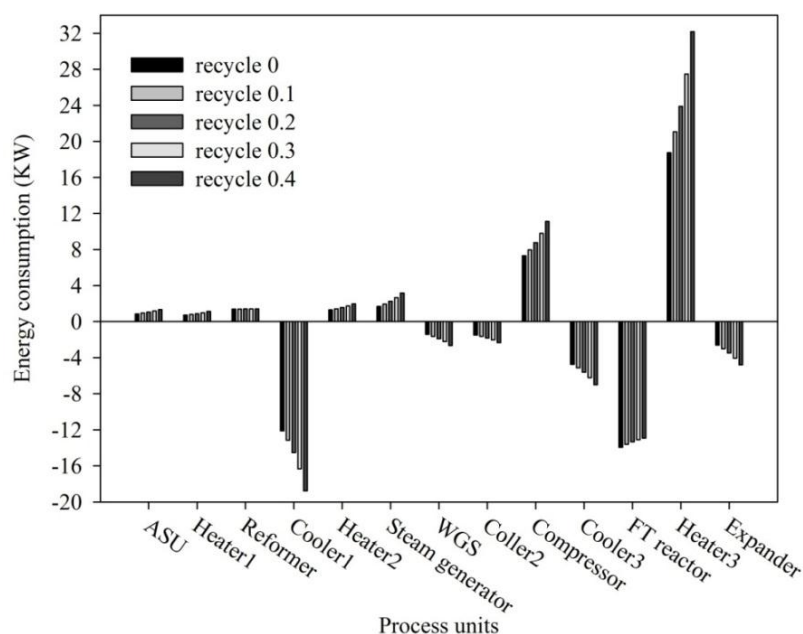
Figure 6.12 The energy consumption of each unit in the BG-FT process with different FT off-gas recycle fractions at the constant FT reactor volume of 90 m³.

6.3.3 Economic analysis

According to the previous section, as the FT off-gas recycle fraction increases, the volume of the process gas also increases; therefore, larger equipment is required, which results in higher investment and operating costs. To justify which process configuration of the BG-FT process (i.e., once-through or one of the included recycle concepts) offers both technical and economic advantages, an economic analysis should be performed. In this study, the incremental NPV is used as an economic indicator to compare two process configurations for 393 MW HHV of rice straw (80 t/h). The calculation procedure of the incremental NPV is explained in chapter II, a discount rate of 10% and the operating period (project lifetime) of 15 years and the period of plant operation time of 8000 hours per year are assumed in this study (Hamelinck et al., 2004; Tijmensen et al., 2002). The considered products from the BG-FT process are the diesel fuel and the electricity. The price of diesel and electricity are assumed to be 0.7895 Euro/liter and 0.0732 Euro/kWh (base on the

average data of Thailand in year 2014), respectively. The comparison of the incremental NPV of the BG-FT process at various FT off-gas recycle fractions and FT reactor volumes is summarized in Table 6.2. All of the calculated values are negative, which implies that the once-through operation mode is more attractive than the inclusion of the FT off-gas recycle concept without any installation of secondary equipment. Because the FT off-gas contains high amounts of inert gases, higher volumes of process gas are found when the off-gas recycle fraction increases. As a result, process equipment of a larger size with a higher price is required. The comparison of the equipment size at various FT off-gas recycle fractions (the FT reactor volume of 90 m^3) is summarized in Table 6.3. It is found that an increase in the FT off-gas recycle fraction increases the size of equipment, especially compressor, expander and heat exchanger. To evaluate the project feasibility, the sensitivity analysis of uncertain parameters, such as valuable product cost, plant life or interest rate, is investigated in the next section.

Table 6.2 Incremental NPV of various FT off-gas recycle fractions and FT reactor, compared with the once-through operation.

FT reactor volume (m^3)	FT off-gas recycle fraction								
	0.1	0.2	0.3	0.4	0.5	0.6	0.7	0.8	0.9
90	-59.0	-111.8	-170.0	-247.8	-321.1	-446.2	-592.0	-857.5	-1357.9
100	-58.9	-122.8	-190.1	-274.7	-354.8	-485.9	-639.6	-916.0	-1433.3
110	-24.3	-75.6	-155.0	-249.9	-338.8	-477.1	-639.3	-927.1	-1460.7
120	-11.7	-29.6	-87.7	-195.4	-296.7	-443.9	-615.7	-915.2	-1464.3
130	-7.7	-15.3	-40.9	-126.1	-243.7	-402.8	-585.6	-897.6	-1461.0
140	-5.8	-9.8	-25.7	-75.4	-181.2	-356.9	-552.9	-878.1	-1454.1
150	-4.8	-7.1	-19.3	-57.8	-124.6	-305.6	-518.4	-858.0	-1443.7
160	-4.2	-5.5	-16.0	-50.3	-101.9	-249.4	-482.0	-837.8	-1441.5
170	-3.8	-4.4	-13.9	-46.3	-92.9	-215.0	-442.4	-817.5	-1442.2
180	-3.5	-3.7	-12.5	-43.8	-88.2	-202.9	-403.2	-796.6	-1443.0
190	-3.2	-3.1	-11.6	-42.1	-85.4	-197.2	-385.5	-775.0	-1443.9

Table 6.3 The equipment size of the BG-FT process with different FT off-gas recycle fractions (the FT reactor volume = 90 m^3)

Process units	scale units	FT off-gas recycle fractions									
		0	0.1	0.2	0.3	0.4	0.5	0.6	0.7	0.8	0.9
Air separation unit	Ton/h	278.3	309.7	344.4	384.3	432.2	493.0	576.2	703.1	930.4	1432.6
Gasifier	MW HHV	393.4	393.4	393.4	393.4	393.4	393.4	393.4	393.4	393.4	393.4
Particle Filter	m^3/s gas	114.1	123.9	136.4	152.6	174.1	203.8	247.1	315.4	436.4	704.7
Reformer	m^{3}NTP/s	27.6	30.0	33.0	36.9	42.1	49.3	59.8	76.3	105.6	170.5
WGS reactor	kmol of H$_2$+CO/s	3476.6	3741.0	4066.4	4472.8	4990.3	5664.5	6562.6	7761.1	9117.0	7334.9
Compressor	MW	22.0	26.0	28.6	31.9	36.3	42.2	50.8	64.0	87.0	137.6
Expansion turbine	MW	5.2	6.7	7.5	8.5	15.7	11.6	23.6	17.7	23.3	31.4
Steam generator	MW	5.5	6.4	7.4	8.7	10.4	12.7	16.2	21.9	32.5	43.6
Cooler1	MW	39.6	43.0	47.4	53.3	61.3	72.6	89.7	117.7	170.9	298.0
Cooler2	MW	4.9	5.3	5.9	6.6	7.6	8.9	10.9	14.0	19.8	34.7
Cooler3	MW	13.6	16.7	18.3	20.3	22.9	26.3	31.1	38.2	49.2	65.7
Heater1	MW	2.4	2.6	2.9	3.2	3.7	4.3	5.3	6.9	10.0	18.5
Heater2	MW	4.3	4.6	5.1	5.7	6.4	7.5	9.1	11.5	16.1	29.5
Heater3	MW	52.7	59.9	67.5	77.2	105.1	107.9	158.2	178.2	257.0	326.0

6.3.4 Sensitivity analysis

There are several parameters (i.e., project life, interest rate, electricity and diesel cost) that influence on the incremental NPV, indicating the project feasibility from an economic point of view. A sensitivity analysis is performed on these parameters in order to investigate the effect of changes in their values from 10 to 100 % on the incremental NPV of the BG-FT process at the FT reactor volume of 190 m^3 and FT off-gas recycle fraction of 0.2. Figure 6.13 shows that at the project year of 15, the incremental NPV increases when the diesel and electricity costs increase whereas the inverse effect is found when the interest rate increases. The increase in the incremental NPV with the project life is also found. The BG-FT process with FT off-gas recirculation will become more feasible than the once-through concept when the diesel cost and plant life increase higher than 1% and 35%, respectively. Moreover, the reduction in a process gas volume by installing a CO_2 removal unit should be one of the possible practices.
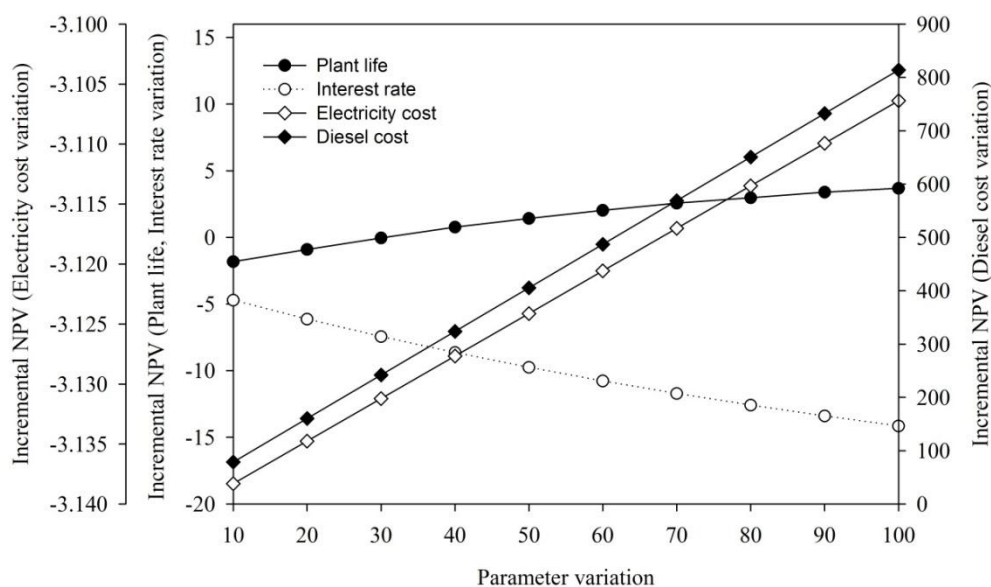
Figure 6.13 Effect of the uncertain parameters on the incremental NPV of the BG-FT process (the FT reactor volume = 190 m^3 and the FT off-gas recycle fraction = 0.2)

6.4 Conclusions

The techno-economic analysis of green diesel production from rice straw via two configurations of the BG-FT process (i.e., once-through and with recirculation concepts) which gasifier is operated under the thermal self-sufficient condition is performed. Regarding the technical aspect, it is found that a greater amount of oxygen is required to maintain the thermal self-sufficient condition in the gasifier when a FT off-gas recycle fraction increases at the constant FT reactor volume. The increase in syngas production rate is also found when the value of recycle fraction is less than 0.9. The CO conversion and the production rate of diesel from a FT synthesis unit increase whereas the generated electricity decreases when the FT reactor volume increases at a constant recycle fraction. The valuable products, i.e., diesel and electricity, from the BG-FT process can be maximized by suitable adjustment of the FT off-gas recycle fraction and the selection of the FT reactor volume. The result of energy analysis shows that the energy efficiency based on the valuable products of the BG-FT process with FT off-gas recycle fraction less than 0.7 increases with the reactor volume. Regarding the economic aspect, the BG-FT process with an off gas recirculation is less feasible than the once-through concept. Nevertheless, it will become more feasible when the diesel cost and plant life increase.

CHAPTER VII
TECHNICAL AND ENVIRONMETAL STUDIES OF
THE BG-FT PROCESS EQUIPPED WITH DIFFERENT
TAR REMOVAL UNITS

In this chapter, the performance of BG-FT process with and without tar removal unit based on steam reforming and ATR are analyzed and compared in term of technical and environmental aspects. The demand of hot and cold utilities for each process is determined from the pinch analysis. The multi-criteria decision analysis method (MCDA) taking into account the technical (diesel production rate) and environmental (PEI) performances is also investigated using the analytical hierarchy process (AHP). The most practical BG-FT process is selected to design the heat exchanger network. Then, the effect of major operating parameters on the NPV is investigated. Finally, the optimization respected to the economic objective is performed to determine the optimum conditions offering the maximum NPV.

7.1 Introduction

As the FT synthesis process requires high purity syngas feedstock to prevent catalyst deactivation and undesired product formation, the syngas derived from the syngas processor needs to be cleaned and conditioned to achieve the FT-specification. The tar contained in raw syngas consists of heavy hydrocarbon which can condense when the process temperature decreases causes fouling of downstream equipment and piping system. Moreover, tar can deposit on the FT-catalyst surface causing deactivation, resulting in a decrease of product yield. Therefore, attempts at minimizing tar formation, such as selecting suitable operating conditions, thermal cracking, reforming via catalytic reactions and the installation of secondary equipment to physically remove tar from the produced gas, are still topics of interest (Pereira et al., 2012). The thermal cracking at high temperature seems to be an interesting approach, however; the low heating value syngas is achieved due to the

combustion of some syngas (Han and Kim, 2008). The necessary degree of tar reduction in the physical removal unit such as scrubber or filter cannot be achieved in one unit. The conversion of tar to syngas via steam reforming and autothermal reforming reactions using catalyst has been widely used because it could increase the amounts of syngas in mild condition. Due to the low price, abundant available and good catalytic activity, the dolomites, alkali metals, and nickel are mostly used as a reforming catalyst. Di Carlo et al. (2015) found that 90% conversion of tar steam reforming reaction using their synthesized Ni/Mayenite catalyst was achieved at the reforming temperature of 800 ^{o}C. Benzene (the tar model compound) and methane were completely converted to H_2 and CO via the steam reforming reaction over a Ni-based catalyst at the operating condition of 780 $^{\circ}$C and 1 atm (Josuinkas et al., 2014). Vivanpatarakij and Assabumrungrat (2013) reported that the integrated unit of biomass gasification and tar steam reforming could completely remove tar and increase H_2 production around 1.6 times under thermally self-sufficient condition. The thermodynamic performance of two gasification processes including steam reforming and shift reactions (i.e., the heat required for steam methane reforming was supplied by fractioned syngas and the steam methane reformer combustion (SMR-COMB) was provided with externally supplied methane) for hydrogen production was investigated by Cohce et al. (2010). They found that the second case had higher energy and exergy efficiencies than the first case.

Previously, the reforming unit in the BG-FT process was mostly considered as a passageway, although some reactions and heat transfer occurred. The present study therefore focuses on the performance analysis of the BG-FT process of rice straw feedstock with and without a tar removal unit based on two reforming processes i.e., steam reforming and ATR. Although the process without tar reforming is not presently applied in the BTL process due to the constraint of the FT-feed gas specification which the tar content must be lower than 1 ppmv (Hamelinck et al., 2004), it may be possible if the contaminant resistance of the FT-catalysts is improved. The performance analysis of each process configuration is performed using the BG-FT model developed in Aspen custom modeler as explained in chapter IV, and the results are compared in the aspect of technical, environmental and

combination thereof. Moreover, the design of a high energy efficiency process is achieved by performing pinch analysis, which is a promising methodology used to maximize the energy efficiency of production processes by minimizing their energy consumption (Domenichini et al., 2010). In this study, the most practical BG-FT process configuration including the heat exchanger network offering the optimal heat integration and the optimal operating condition offering the maximum NPV are finally proposed.

7.2 Process configuration and scope of work

The BG-FT process configuration with and without tar removal unit based on the steam reforming and ATR reactions, are investigated in this chapter. It should be noted that steam is supplied as a reactant for steam reforming unit and a mixture of oxygen and steam is supplied for ATR. The three BG-FT process configurations are shown in Figures 7.1(a)-(c).

(a)

(b)

(c)
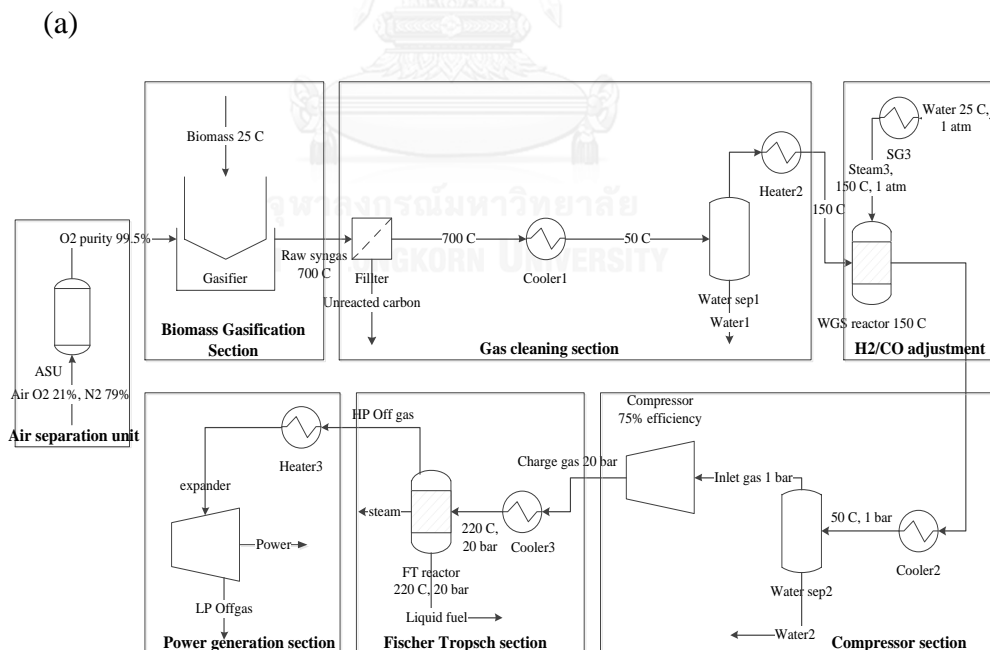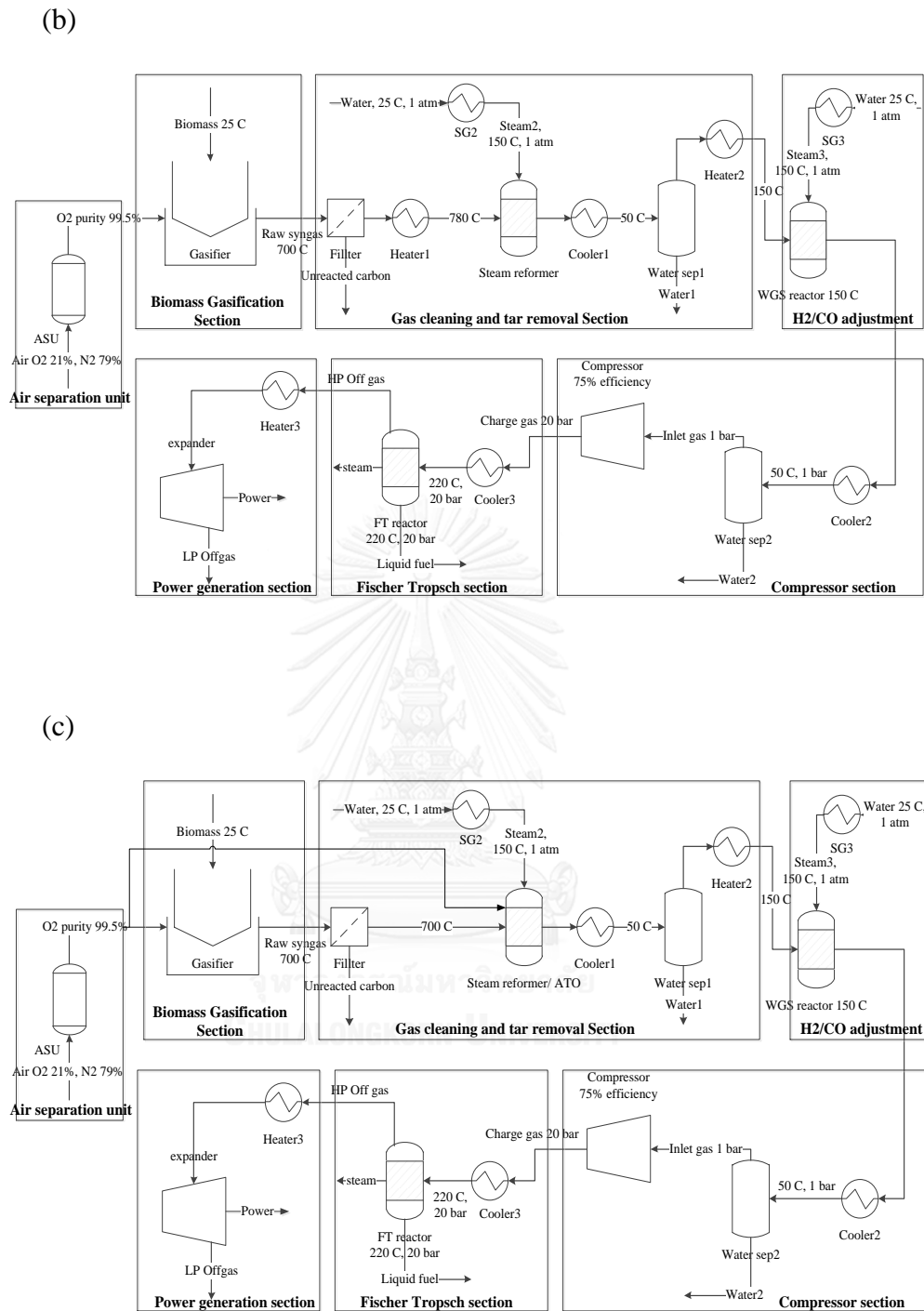
Figure 7.1 The BG-FT process configurations: (a) without a tar removal unit, (b) with steam reforming and (c) ATR units

The scope of work in this chapter is illustrated in Figure 7.2. In this study the performance of each BG-FT process configuration is investigated and the results are compared in term of the amounts of produced electricity and green diesel as well as the demand of hot and cold utilities. The environmental impact is also investigated using the PEI, which calculated based on the waste reduction (WAR) algorithm, as an indicator. The MCDA using the AHP analysis taking into account the technical and the environmental performances into one AHP index is performed to justify whether the process offers the best performance in both technical and environmental point of view. The most practical BG-FT process is proposed and the optimum structure of heat exchangers is further designed based on the pinch design method to meet the energy efficient condition. The optimization of the newly design BG-FT process including heat integration system is finally performed to determine the optimum operating condition offering the maximum NPV.
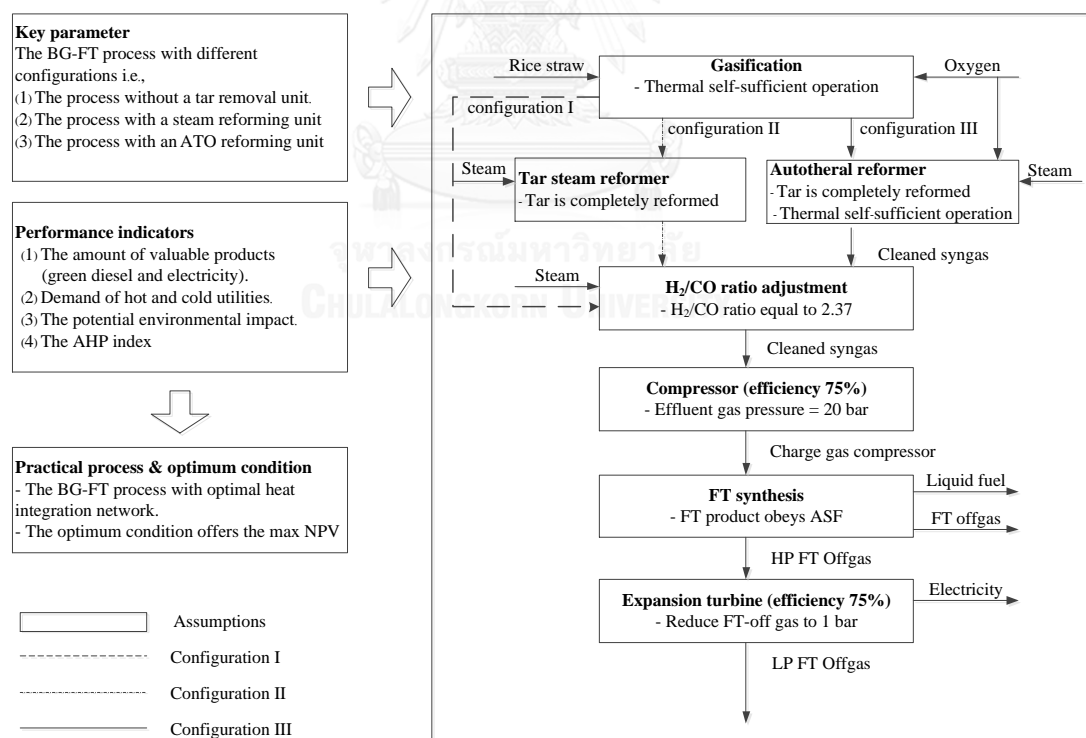
Figure 7.2 The scope of work in chapter VII

7.3 Result and discussion

7.3.1 Performance analysis of BG-FT process with different tar removal units

The performance of the BG-FT process with different configurations, i.e., the processes without reforming, with steam reforming and with ATR, is summarized in Table 7.1. It is found that the process with steam reforming offers the highest amount of syngas (H_2+CO) due to the complete conversion of tar and methane into syngas, and thereby the highest amounts of electricity and green diesel are achieved. In the process with ATR, the combustion reaction occurs, so the amount of syngas is found to decrease, whereas that of CO_2 increases, resulting in decreased electricity and green diesel products. However, the derived FT-products are not significantly different from those derived from the process with steam reforming. As the additional syngas derived from the reforming reaction does not appear in the process without reforming, the lowest amount of FT-products are found in this process. Moreover, the lifetime of the FT-catalyst may decrease due to the tar deposition. The overall energy consumption calculated from the summation of the energy consumptions of each sub-unit in the BG-FT process is also investigated. As the steam reforming unit involves the highly endothermic tar steam reforming reactions which large amount of energy from external heat source is required. Therefore, the process with steam reforming consumes the highest amount of energy. The process with ATR is the second mostly energy consumed process, in which the heat of combustion is produced and supplied to the steam reforming reactions. The ATR process involves both exothermic combustion reactions and endothermic steam reforming reactions that can be balanced by adjusting the amount of supplied oxygen to achieve the thermal self-sufficient condition, in which external heat sources are not required during a steady state operation. The process without reforming consumes the lowest energy because the energy consumption at the reforming unit does not exist and the temperature of syngas entering the cooler no.1 is lower than that of the other processes, resulting in the lower energy consumption at this unit and the overall process.

Table 7.1 Performance BG-FT processes (biomass feed rate = 1 kmol/h)

	Steam reforming	ATO reforming	Process without reforming
Syngas processor			
Syngas (kmol/h)	1.065	1.054	0.965
Syngas composition (mol%)			
C_6H_6	0.000	0.000	0.465
CH_4	0.204	0.000	0.313
CO	23.355	23.102	21.158
CO_2	20.928	21.385	20.226
H_2	55.410	54.810	50.198
H_2O	0.062	0.063	0.060
N_2	0.041	0.045	0.041
Fischer-Tropsch synthesis			
Diesel (kmol/h)	0.001537	0.001529	0.001526
Gasoline (kmol/h)	0.000659	0.000655	0.000649
Liquid fuel (kmol/h)	0.002288	0.002275	0.002265
FT-offgas (kmol/h)	0.615590	0.607196	0.483003
Water (kmol/h)	0.243597	0.244634	0.251240
Electricity (kW)	0.956728	0.938008	0.721023
Overall energy consumption			
BG-FT process (kW)	-23.00	-24.54	-25.19

7.3.2 Environmental evaluation

The potential environmental impact (PEI) represented by two output indices, i.e., the total output rate of environmental impact and the total environmental impact output per mass of diesel product of each process configuration, which is calculated from the composition and flow rate of the FT-offgas, are investigated. The effect of CO_2 emission is neglected in this study due to the CO_2-neutral characteristic of biomass feedstock. It is found from Figure 7.3 that the process with steam reforming has the highest environmental impact due to the large amount of emitted CO, which has a strong impact on human toxicity potential by either inhalation or dermal exposure (HTPE) and global warming potential (GWP), followed by the process with ATR and that without reforming. Although the process with steam reforming offers the highest amount of diesel product, the total impact output per mass of diesel product has the same trend as that of the total output rate of environmental impact (Figure 7.4). This implies that the amount of diesel product derived from this configuration is not significantly greater than that from the others. The raw data used to determine the PEI as shown in Figures 7.3 and 7.4 are given in Appendix B.
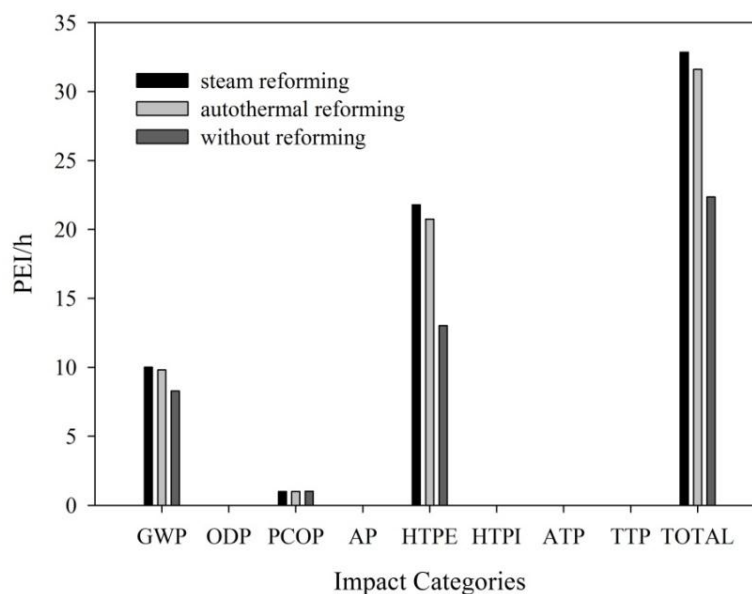
Figure 7.3 Total rates of environmental impact output for the BG-FT processes with steam reforming, ATR and without a reforming process
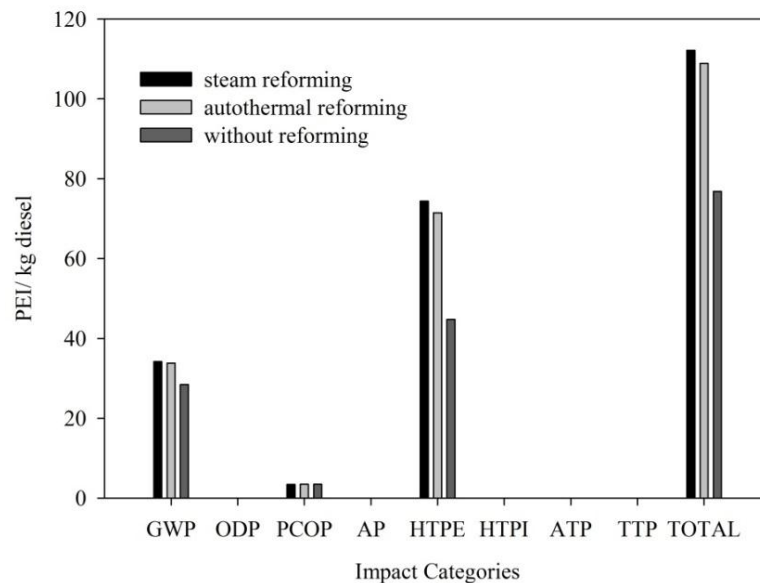
Figure 7.4 Total environmental impact output per mass of diesel product for the BG-FT processes with steam reforming, ATR and without reforming process.

7.3.3 Combined technical and environmental impact evaluation

As discussed in chapter II, the multi-criteria decision analysis method (MCDA) using the analytical hierarchy process (AHP) is performed to evaluate different processes whether process offers the best performance by taking into account the performance of several criteria in the decision. In this study, the different BG-FT processes i.e., with and without a tar removal unit based on steam reforming and ATR are compared, the technical and environmental performances in term of diesel production rate and potential environmental impact (PEI) are summed to get one AHP index (Eq.(7.1)). The hierarchy structure used in this study is illustrated in Figure 7.5.

$$AHP = P_{DP} \times weight_{DP} + P_{Env} \times weight_{Env} \tag{7.1}$$

where P_{DP} is the normalized diesel production rate calculated from the ratio between the diesel production rate of the process and that of the sum of all considered three processes. However, for ease of analysis, the environmental impact is represented in terms of environmental friendliness, which is calculated by subtracting the PEI from one (1-PEI); therefore, the normalized environmental friendliness (P_{Env}) is the ratio between (1-PEI) for the process and that of the sum of all considered three processes. $weight_{DP}$ and $weight_{Env}$ are the weighting factors of the diesel production rate and environmental friendliness, respectively. The process with a higher AHP index offers a higher process performance at a specified weighting factor of diesel production rate.
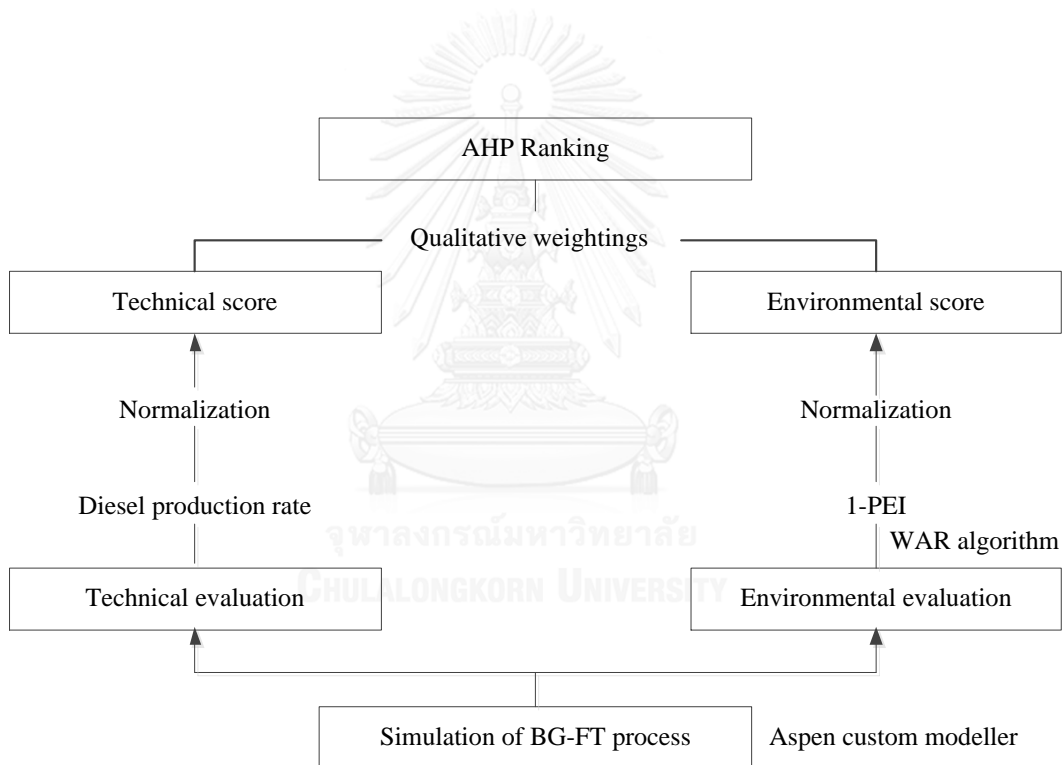
Figure 7.5 Analytical hierarchy structure used for the analysis of the three BG-FT processes

The effect of changes in the weighting factor of the diesel production rate from 0 to 1 on the AHP index is investigated. Figure 7.6 shows that the AHP index continuously decreases when the weighting factor of the diesel production rate increases for all process configurations. However, the process without reforming

offers the best performance when the weighting factor is less than 0.79, followed by the process with ATR and that with steam reforming. The opposite effect is found when the weighting factor increases above this value. Moreover, it is found that all process configurations offer identical performance at the weighting factor of 0.79. At this condition, the AHP index of 0.40 is achieved.
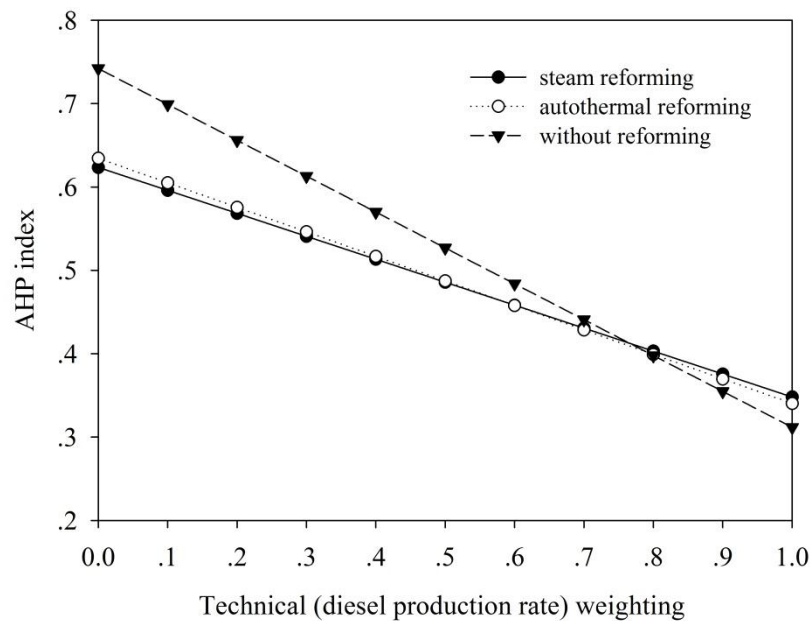
Figure 7.6 Effect of weighting factor of diesel production rate on the AHP index of the BG-FT processes with steam reforming, ATR and without a reforming process

7.3.4 Interpretation of composite curve

Table 7.2 shows the steam data used to construct the hot and cold composite curves for each BG-FT process configuration. The composite curves of the three BG-FT processes i.e., without reforming, with steam reforming and with ATR, are shown in Figure 7.7 (a)-(c). At the specified minimum temperature difference $\Delta T_{\min}$ of 20 °C, the overshoot of the hot composite curve over the cold composite curve and that of the cold composite curve over the hot composite curve are found for the process with steam reforming Figure 7.7 (b). This indicates that thermal energies of approximately 1.59 and 30.05 kW are required for the hot and cold utilities, respectively.

Nevertheless, this process is not practical because a working temperature of hot utility higher than 780 °C is required. In the ATR process, the heat of combustion is produced and supplied to the steam reforming reaction. Only the overshoot of the hot composite curve over the cold composite curve is found at both the low and high-temperature ends of the composite curve, which indicates that only two cold utilities are required, i.e., with working temperatures lower than 25 and 150 °C, with thermal energies of 3.89 and 27.13 kW, respectively. The process without reforming shows the same trend as that with ATR, and the demands of cold utilities with working temperatures of 25 and 150 °C are quite similar (approximately 4.03 and 26.42 kW).

Table 7.2 Stream data for composite curves construction

Stream	Name	Descriptions	T_s (°C)	T_t (°C)	CP (kJ/K)	ΔH (kJ/h)
Without reforming						
1	Hot 1	Reformer effluent gas	700	50	47.18	31845.73
3	Hot 2	Water gas shift effluent gas	150	50	40.29	4029.08
4	Hot 3	Charge gas compressor	597	220	43.71	16493.60
2	Hot 4	Water gas shift reactor	150	150	Infinity	4765.57
5	Hot 5	FT reactor	220	220	Infinity	52354.20
6	Cold 1	Steam generator	25	150	8.99	5712.90
7	Cold 2	Gasifier effluent gas (not used)	-	-	-	-
9	Cold 3	Water gas shift feed gas	50	150	35.43	3543.43
8	Cold 4	Reformer (not used)	-	-	-	-

Table 7.2 Stream data for composite curves construction (Cont.)

Stream	Name	Descriptions	T_s (°C)	T_t (°C)	CP (kJ/K)	ΔH (kJ/h)
Steam reforming						
1	Hot 1	Reformer effluent gas	780	50	47.53	34741.79
3	Hot 2	Water gas shift effluent gas	150	50	42.89	4288.60
4	Hot 3	Charge gas compressor	612	220	46.11	18101.10
2	Hot 4	Water gas shift reactor	150	150	Infinity	5053.33
5	Hot 5	FT reactor	220	220	Infinity	50201.90
6	Cold 1	Steam generator	25	150	9.50	6056.86
7	Cold 2	Gasifier effluent gas	700	780	33.03	2642.49
9	Cold 3	Water gas shift feed gas	50	150	37.74	3773.74
8	Cold 4	Reformer	780	780	Infinity	5002.63
Autothermal reforming						
1	Hot 1	Reformer effluent gas	780	50	48.10	35113.29
3	Hot 2	Water gas shift effluent gas	150	50	42.53	4252.58
4	Hot 3	Charge gas compressor	610	220	45.74	17812.30
2	Hot 4	Water gas shift reactor	150	150	Infinity	4888.90
5	Hot 5	FT reactor	220	220	Infinity	50810.80
6	Cold 1	Steam generator	25	150	9.23	5862.41
7	Cold 2	Gasifier effluent gas (not used)	-	-	-	-
9	Cold 3	Water gas shift feed gas	50	150	37.54	3754.16
8	Cold 7	Reformer	780	780	Infinity	0.00

(a)
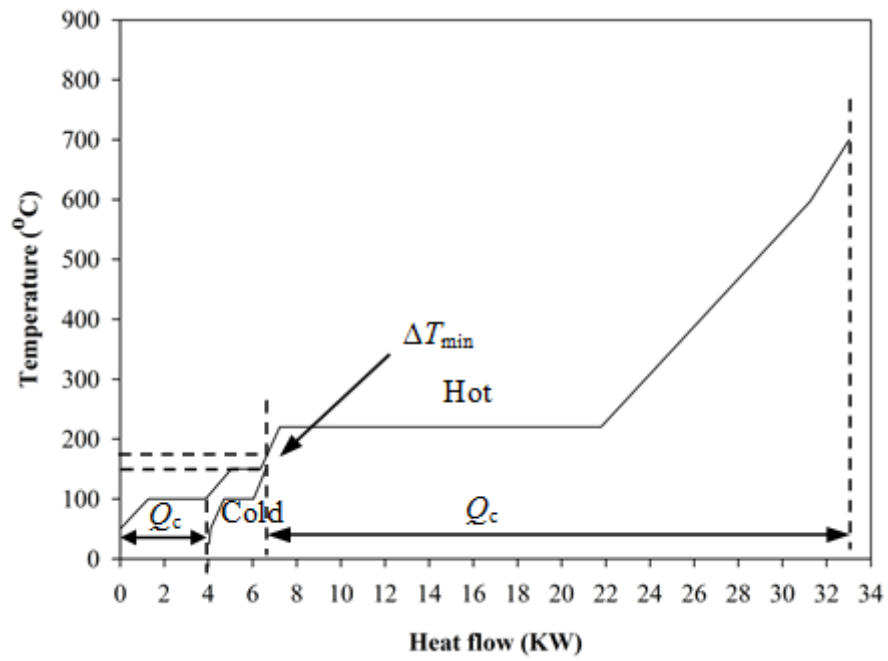
(b)
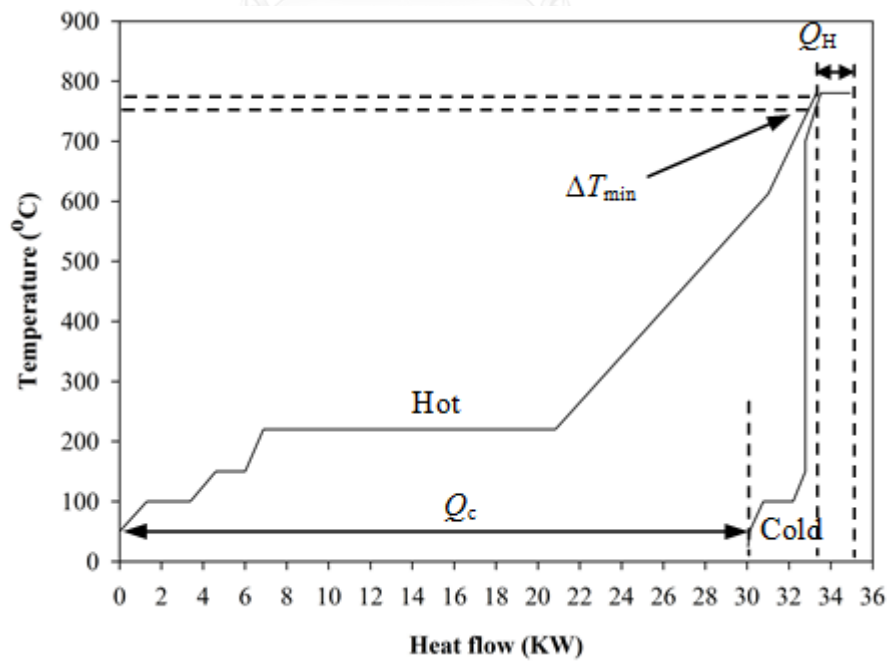
(c)
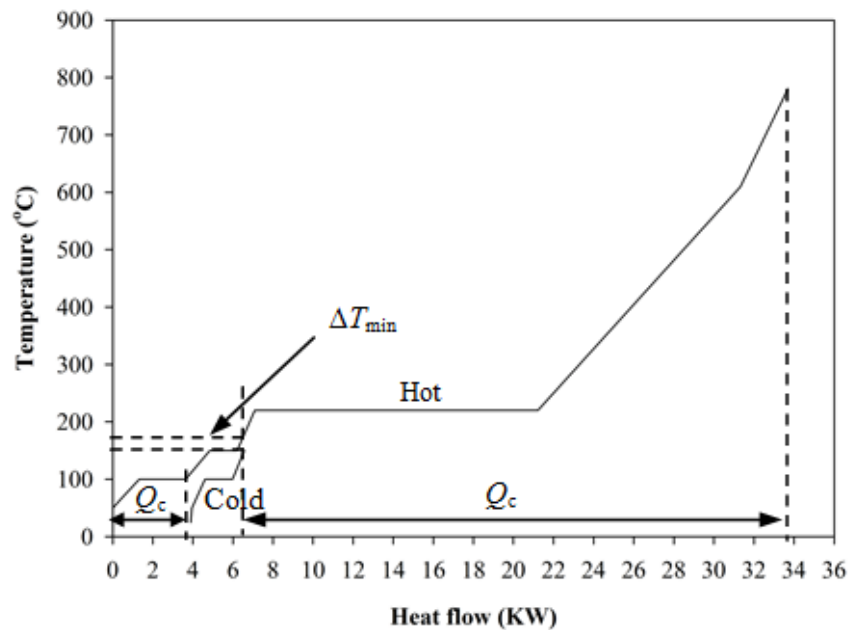
Figure 7.7 Composite curves, pinch points and minimum energy requirements of the processes: (a) without reforming, (b) with steam reforming and (c) with ATR

7.3.5 Heat exchanger network (HEN) design

As the syngas leaving the syngas processor of the BG-FT process without reforming contains tar (C_6H_6) with 0.465 mol%, which does not meet the FT feed gas specification (< 1 ppmv), and the high-temperature hot utility is required in the process with steam reforming, the BG-FT process with ATR is therefore the most suitable from a technical point of view. This process is selected to design the optimal heat integration network. The design of HEN is performed on the balance grid diagram; the pinch is located at 150 and 170 ^{o}C as illustrated in Figure 7.8. It is found that the heat of the hot reformer effluent gas (Hot 1) is recovered and used to produce steam at the steam generator (Cold 1) and also used to heat the syngas to the operating temperature of the water gas shift reactor (Cold 3). An additional cooler has to be installed in this newly designed process, as it is a highly exothermic process that

requires a large amount of cooling media. The process flow diagram of the newly design BG-FT process is illustrated in Figure 7.9.
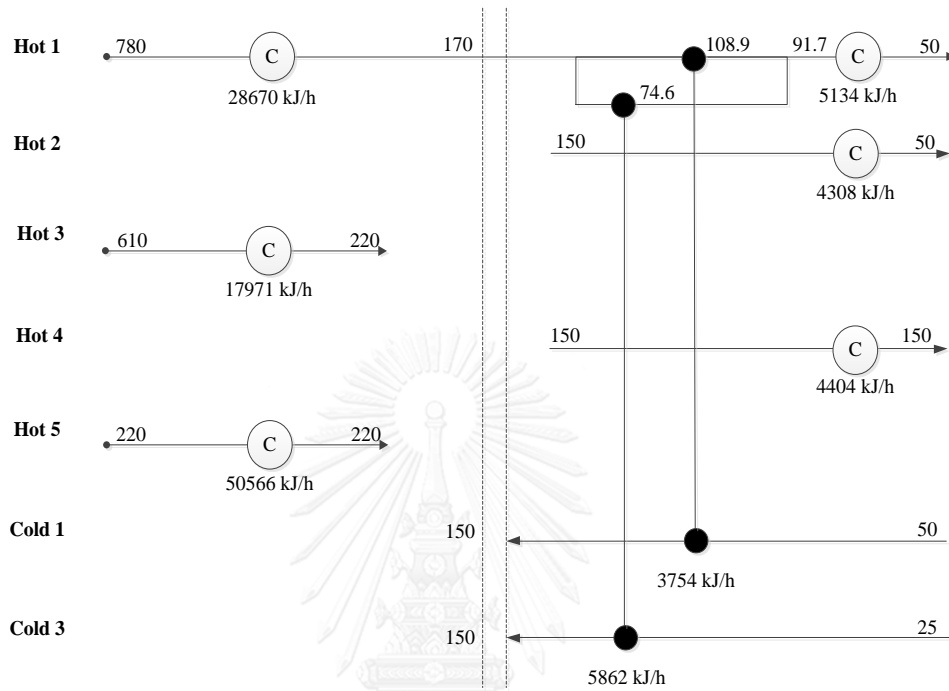
Figure 7.8 The heat exchanger network
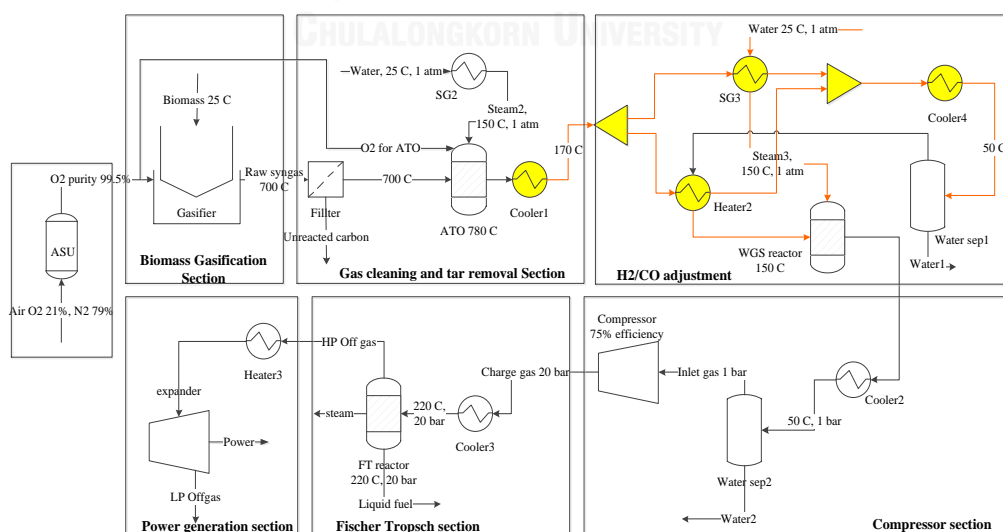
Figure 7.9 The BG-FT process with heat integration system

7.3.6 Effect of operating parameter on NPV

The effect of key operating parameters, i.e., gasifying temperature, FT temperature and FT pressure, on the net present value (NPV) is shown in Figure 7.10 (a)-(d). It is found that the NPV increases as the gasifying temperature and FT pressure increase, whereas the inverse effect is found when the FT temperature increases.

(a)
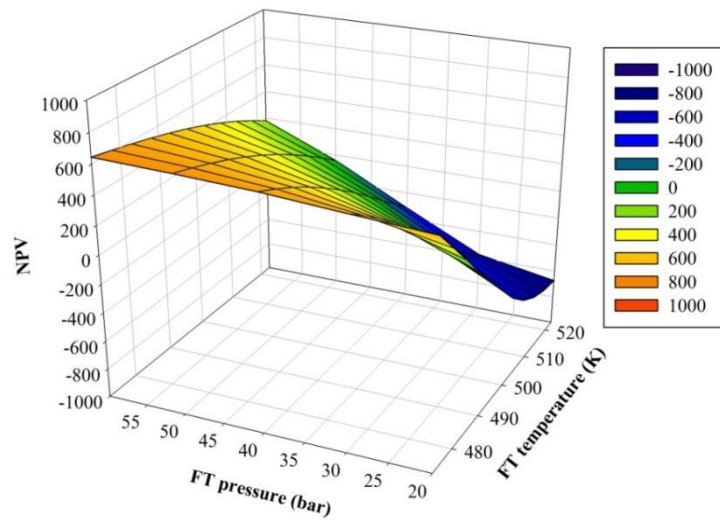
(b)
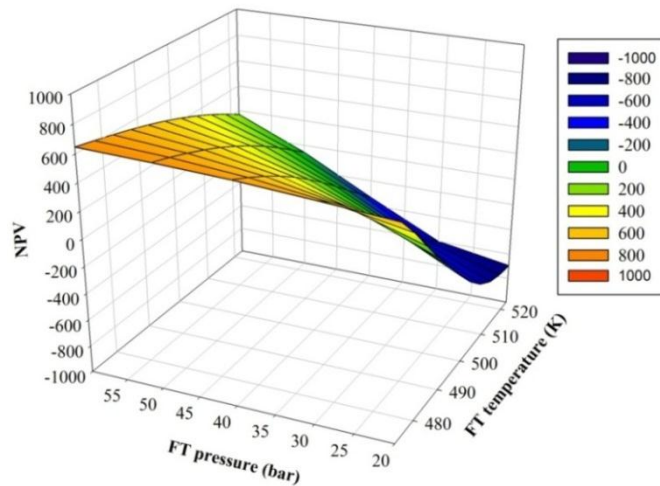
(c)
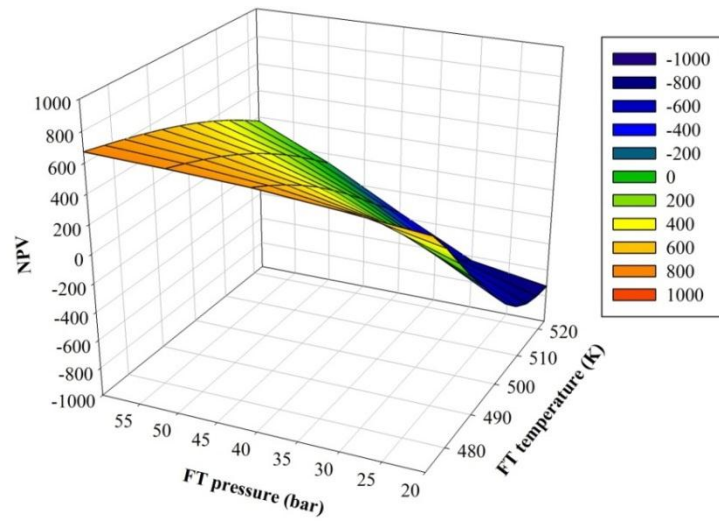
(d)
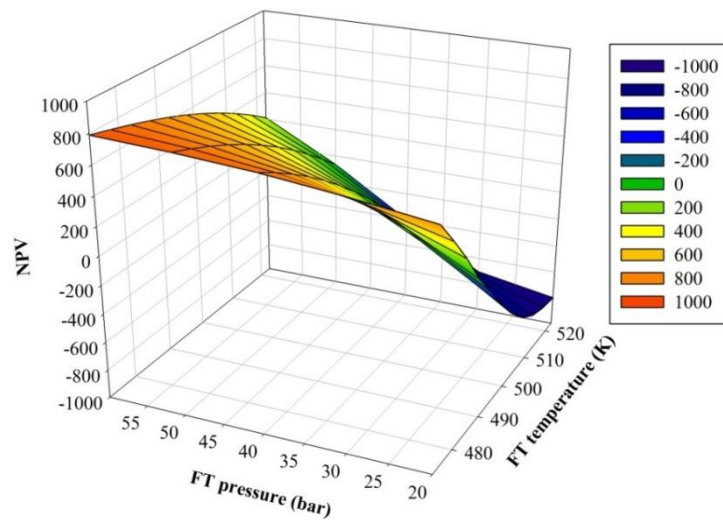
Figure 7.10 Effect of gasifying temperature, FT temperature and FT pressure on the NPV: (a) T_{Gs} 973 K, (b) T_{Gs} 1073 K, (c) T_{Gs} 1173 K and (d) T_{Gs} 1273 K.

7.3.7 Optimization of BG-FT process

In this section, the optimization of the newly designed BG-FT process including a heat integration system is performed with respect to the economic objective, aiming at the maximization of the NPV as shown in Eq.(7.2).

$$\max_{x} \ NPV \qquad\qquad (7.2)$$

where x is the design variables (i.e., gasifying temperature, supplied steam flow rate, FT temperature and FT pressure). The optimization is done based on the following constraints:

$$u_1 = 2.37 \qquad\qquad (7.3)$$

$$0 \leq u_2 \leq 1 \qquad\qquad (7.4)$$

where u_1 and u_2 are the H_2/CO ratio of the WGS reactor outlet gas and the chain growth probability, respectively.

A FEASOPT optimizer embedded in Aspen Custom Modeller (ACM) is applied using a reduced space method to determine the optimum operating condition giving the maximum NPV. FEASOPT evaluates the objective variable at the current point and moves the design variables, initial and control variables to take the objective variable towards its optimum value. After solving with the new values of the design, initial, and control variables, FEASOPT re-evaluates the objective variable. In this way, FEASOPT steps towards the optimum solution.

The NPV, the objective function of this optimization formulation, is calculated from Eq.(2.40), however; the investment cost is adjusted by adding the cost of additional heat exchangers and the utility costs, which a hot utility cost at the coal equivalent of 4.45 USD/GJ and a cold utility cost of 8.24 USD/GJ (Petersen et al., 2015) are included in the operating costs. The temperature level of gasification and FT synthesis units and the pressure level of the latter are the considered design variables and related bounds are summarized in Table 7.3. The problem is solved by the mixed newton nonlinear method and the optimum gasifying temperature is found to be 1273 K, given the supplied steam feeding rate to WGS reactor of 0.217 kmol/h

and the optimum FT temperature and pressure of 493 K and 60 bar. Under these optimum operating conditions, the maximum NPV of 789.475 can be achieved.

Table 7.3 The design variables and related bounds.

Unit	Parameters	Ranges	Units
Gasification	Gasifying temperature	973-1273	K
WGS reactor	Supplied steam flow rate	0.1-0.3	kmol/h
FT reactor	Temperature	473-523	K
	Pressure	20-60	Bar

In this study, the breakeven diesel price (the diesel price offering zero NPV) of the proposed BG-FT process is calculated as 0.2757 Euro/liter. The result from this study indicates that the diesel production using BG-FT process is more attractive than that using crude distillation in economical point of view because the breakeven diesel price is lower than the 2014 average diesel price of 0.7895 Euro/liter. However, it is noted that the economic analysis of the proposed BG-FT process is based on only the reaction section, including gasification, WGS and FT reactors. The cost of pre-processing (e.g., drying and size reduction) and post-processing (e.g., separation) sections is not taken into account.

7.4 Conclusions

The performances of the BG-FT processes with and without a tar removal unit based on steam reforming or ATR are compared. The highest amounts of electricity and green diesel are achieved in the process with steam reforming followed by that with ATR and that without any reforming. On the other hand, the last process consumes the least energy and causes the lowest environment impact. The combined criteria of the diesel production rate and environmental friendliness are also investigated. The process without reforming shows the best performance when the weighting factor of the diesel production rate is less than 0.79, followed by the

processes with ATR and that with steam reforming. The opposite effect is found when this factor increases higher than this value. The pinch analysis showed that the process with steam reforming requires both hot and cold utilities, while the others require only the cold utility. As the process without reforming offers lowest amount of FT-products and the produced syngas cannot meet FT-feed gas specification, and the process with steam reforming is not practical because high temperature hot utility is required, therefore it can be concluded from this study that the process with ATR is the most practical process and can be designed the optimum structure of heat exchanger to achieve the maximum internal heat recovery and the minimum external utility requirements. The optimum operating condition offering the maximum NPV is achieved at the gasifying temperature of 1273 K, the supplied steam feeding rate to WGS reactor of 0.217 kmol/h and the FT temperature and pressure of 493 K and 60 bar, respectively.
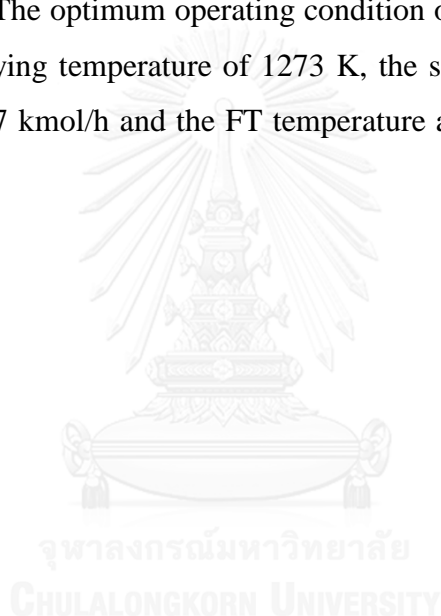
CHAPTER VIII
ECONOMIC AND ENVIRONMENTAL EVALUATION OF
THE NEW-DESIGNED BG-FT PROCESS

In this chapter, the parametric analysis of the new designed BG-FT process is performed. The effect of changes in gasifying temperature, FT operating temperature and FT pressure on the diesel production rate, the potential environmental impact (PEI) and the combination thereof is investigated. The suitable condition offers the best performance in economic and environmental point of view is determined.

8.1 Introduction

As discussed in chapter VII, the BG-FT process equipped with ATR is the most practical process. The optimum structure of heat exchanger network is designed to meet the energy efficient condition and the optimum operating condition offering maximum NPV is proposed. However, to justify whether process offers the best performance, not only the economic objective is a major concern topic, but also the environmental impact must be taken into account. B. Wang et al. (2013) proposed the optimum solution for the synthesis of hydrocarbon biorefinery via gasification calculated from a multi-objective mixed-integer nonlinear programming (MINPL) model in which the NPV and global warming potential (GWP) derived from a life cycle assessment procedure were considered as economic and environmental objectives, respectively. Buddadee et al. (2008) performed a multi-objective optimization of two scenarios of excess bagasse utilization i.e., used for the onsite electricity production and processed for the offsite ethanol production, respected to two objectives that aiming at minimizing the GWP and the associated cost. As the multi-criteria decision analysis (MCDA) method using the analytical hierarchy process (AHP) is used to investigate whether the process offers the best performance when several criteria are taken into account. Nixon et al. (2013) used the hierarchical analytical network process (HANP) model for evaluating alternative technologies for

generating electricity from municipal solid waste (MSW) in India. And they identified that the anaerobic digestion is the preferred technology for generating electricity from MSW in India.

In this study, the combined economic and environmental evaluation is performed to investigate the process performance at various operating conditions. As the NPV significantly increases when the diesel production rate increases while decreases when the amount of generated electricity increases as shown in Figures 8.1. Hence, the diesel production rate can reasonably use as an economic indicator. The environmental impact is considered in term of the PEI. There are several operating parameters (i.e., gasifying temperature, FT operating temperature and FT pressure) influence on the economic and the environmental performances, therefore this study is firstly performed the sensitivity of these operating parameters on the diesel production rate and the PEI using the BG-FT model developed in ACM as discussed in chapter IV. The combined evaluation of economic and environmental is further performed using the AHP index as an indicator. The suitable condition offering the best performance in economic and environmental point of view is finally determined.
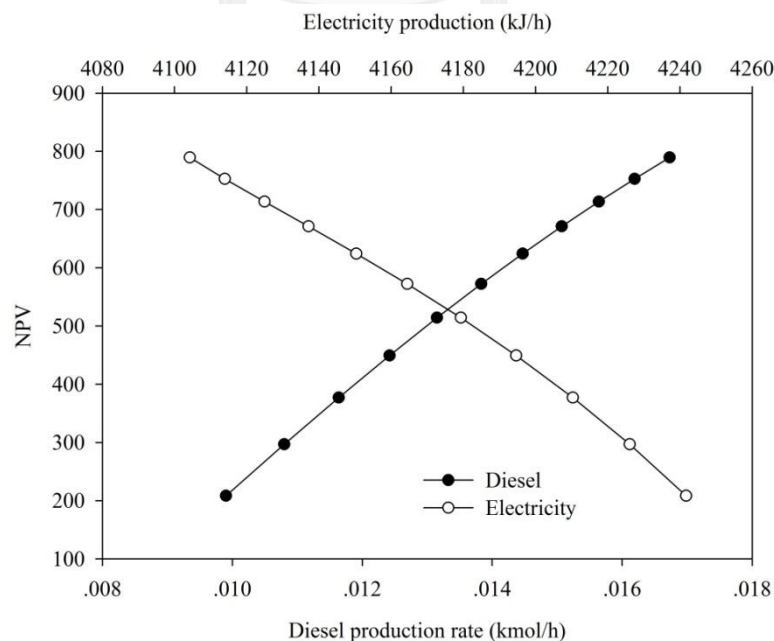
Figure 8.1 The effect of diesel and electricity production rate on the NPV

8.2 Process description and scope of work

The new designed BG-FT process considered in this chapter is shown in Figure 8.2. The parametric analysis is performed to investigate the effect of changing of gasifying temperature; FT operating temperature and FT pressure on the performance of new designed BG-FT process. The diesel production rate, the PEI calculated based on the waste reduction (WAR) algorithm discussed in chapter II are used as economic and environmental performance indicators. The combination of economic and environmental performance is indicated by the AHP index derived from the multi-criteria decision analysis method (MCDA) using the analytical hierarchy process (AHP) discussed in chapter II and VII. In this study, the gasifying temperature is considered in the range of 973-1273 K. The FT operating temperature and pressure are varied in the ranges of 473-523 K and 20-60 bar, respectively. The scope of the present study is summarized in Figure 8.3.
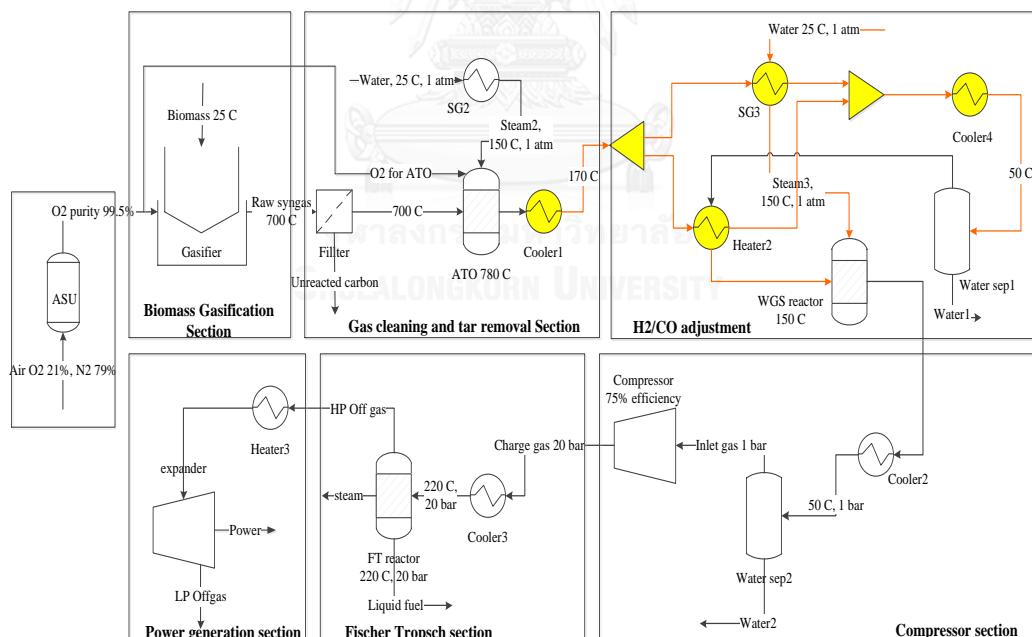
Figure 8.2 The new designed BG-FT process including heat exchanger network
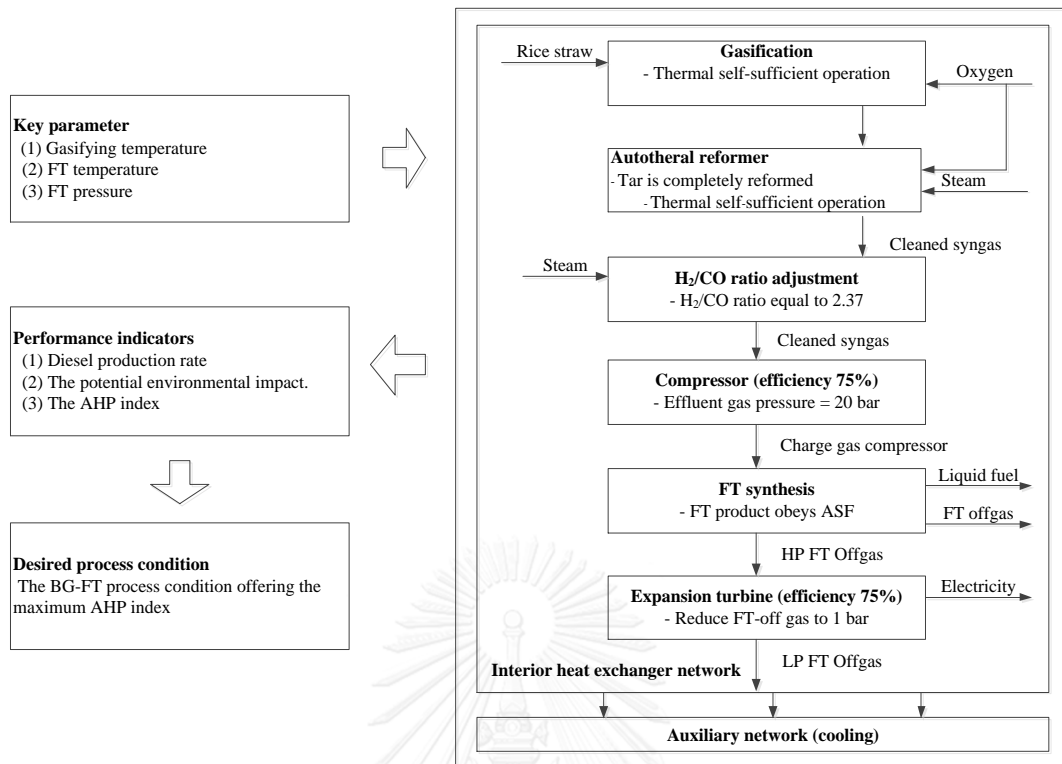
Figure 8.3 The scope of work in chapter VIII

8.3 Result and discussions

8.3.1 Effect of operating parameters on the diesel production rate

The changes in the diesel production rate for each gasifying temperature are shown in Figures 8.4 (a)-(d). It is found that at constant FT operating conditions, the diesel production rate increases with the gasifying temperature due to the increase in the syngas feed rate. However, a slight increase is observed because the syngas feed rate does not significantly change at the gasifying temperature higher than 973 K as discussed in chapter V. The same effect is found when the FT operating pressure increases at constant gasifying and FT operating temperatures. As the FT operating temperature has less effect on the CO conversion than the pressure, the CO conversion is therefore found to be stable when the FT operating temperature increases at constant gasifying temperature and FT operating pressure. However, the

production rate of diesel is found to continuously decrease while that of FT-offgas increases at this condition (Figure 8.5) due to the decrease in chain growth probability and consequently decrease in selectivity towards long chain hydrocarbon.

(a)
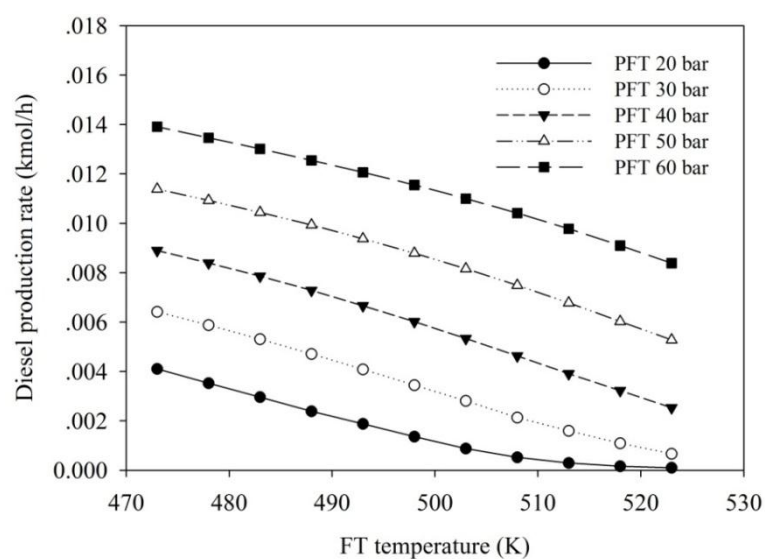
(b)
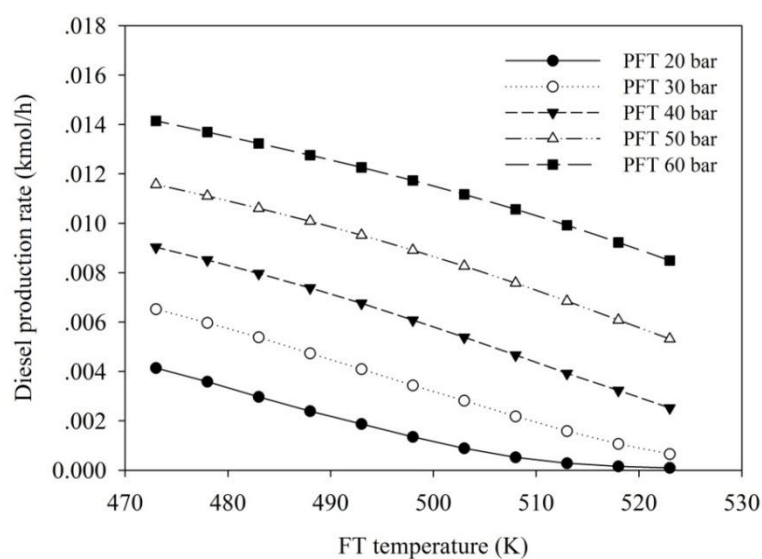
(c)
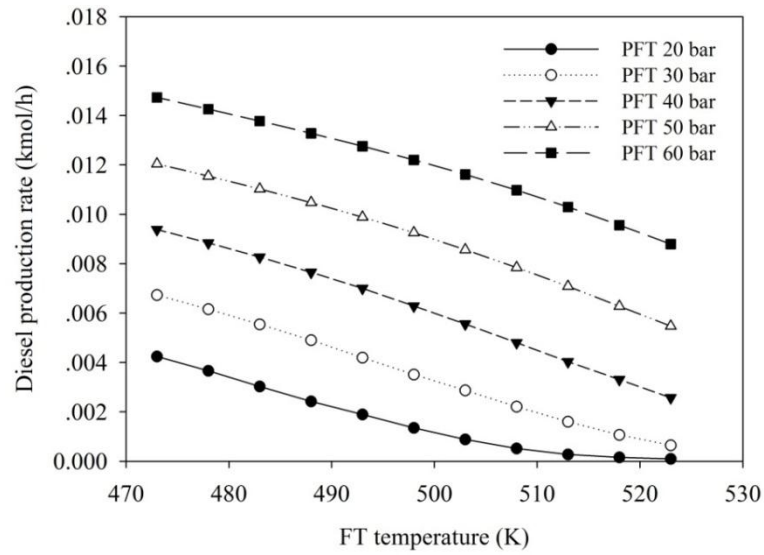
(d)
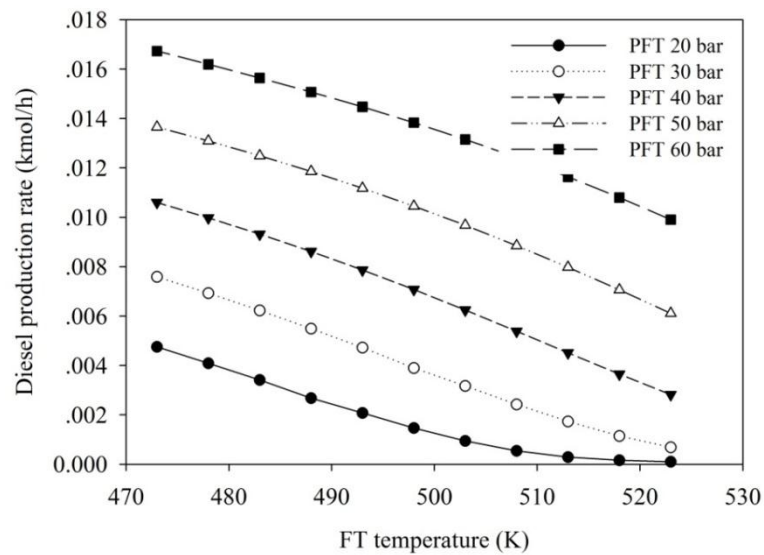
Figure 8.4 Effect of operating parameters on diesel production rate: (a) T_{Gs} 973 K, (b) T_{Gs} 1073 K, (c) T_{Gs} 1173 K and (d) T_{Gs} 1273 K
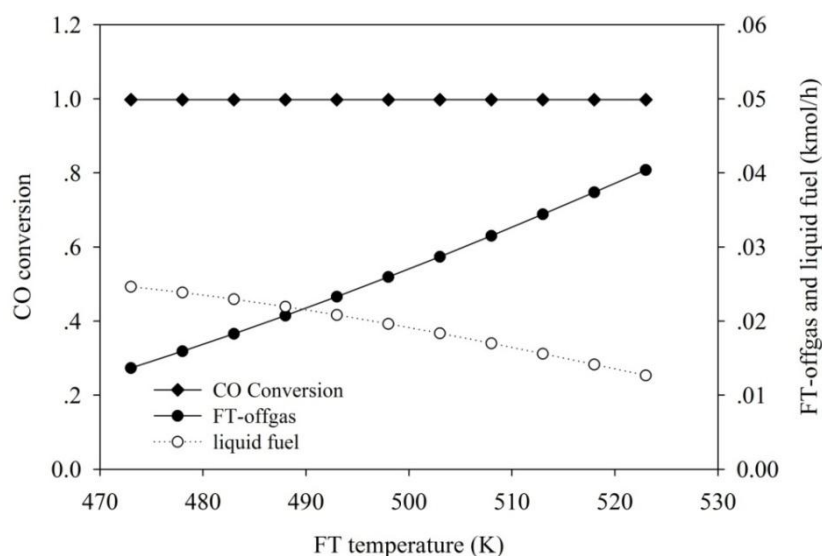
Figure 8.5 CO conversion, liquid fuel and FT-offgas production rate of FT reactor (T_{Gs} 1173 K, FT operating pressure 60 bar)

8.3.2 Effect of operating parameters on the PEI

It is found in Figures 8.6 (a)-(d) that the PEI, which depends on the generated FT-offgas, slightly increases with the gasifying temperature due to the slight increase in the production rate of syngas and also FT-offgas which their composition does not significantly change at gasifying temperature higher than 973 K as shown in chapter V. The opposite effect is found when the FT operating pressure increases. Regarding the high selectivity of the FT-offgas at high temperature, therefore the PEI is also found to increase with the FT operating temperature at a constant gasifying temperature and FT operating pressure.

(a)
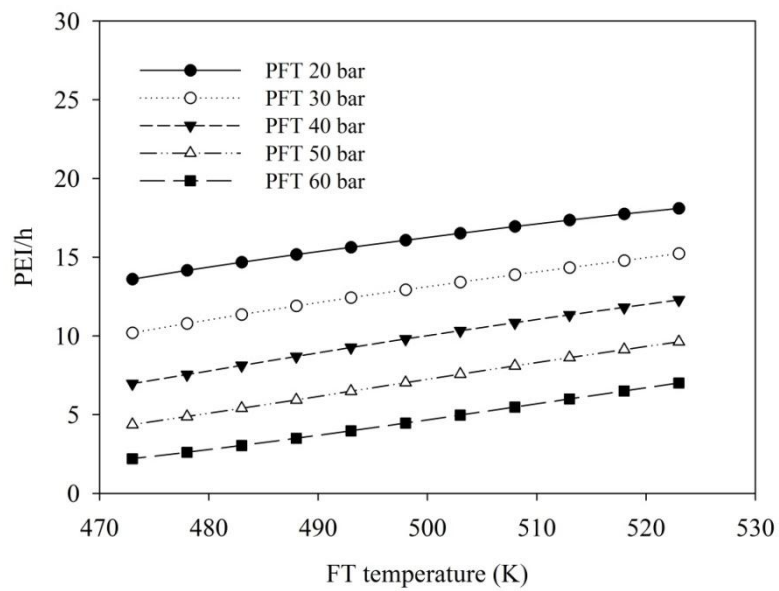
(b)
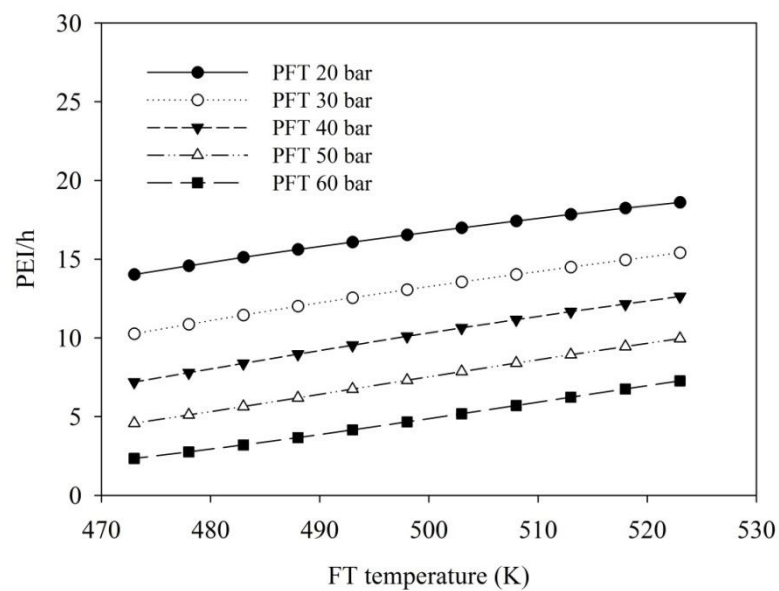
(c)
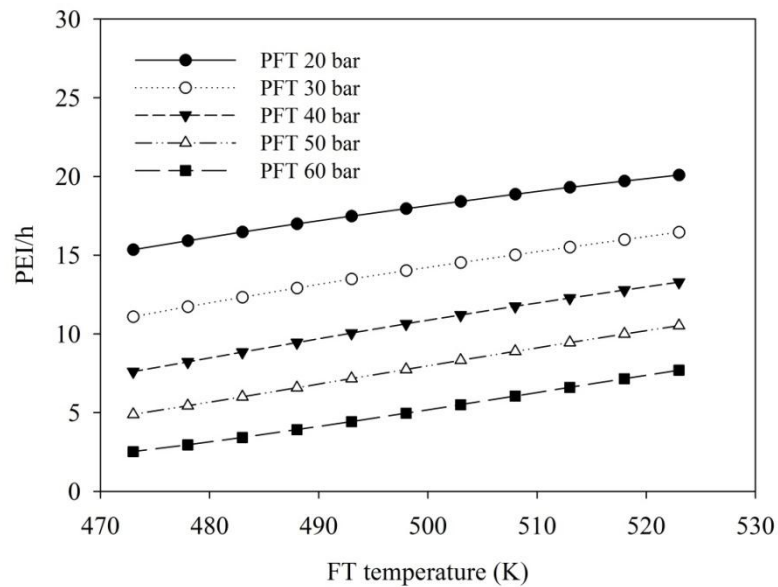
(d)
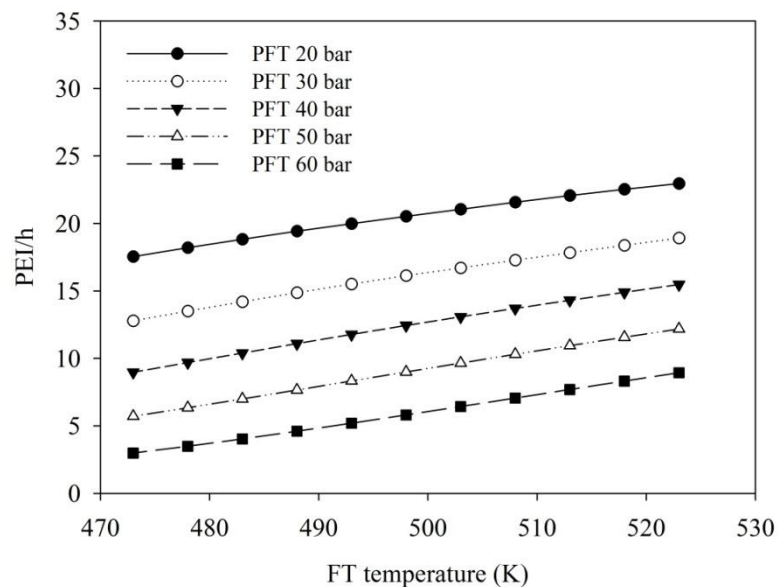
Figure 8.6 Effect of operating parameters on overall potential environmental impact: (a) T_{Gs} 973 K, (b) T_{Gs} 1073 K, (c) T_{Gs} 1173 K and (d) T_{Gs} 1273 K.

8.3.3 Effect of operating parameters on the AHP index

Figures 8.7 (a)-(d) shows the effect of changes in the values of the gasifying temperature, FT operating temperature and pressure on the AHP index, which is the integration of the diesel production rate and environmental friendliness. Weighting factors of 0.82 and 0.18, which are commonly applied for chemical processes (Chen et al., 2002) are applied for the diesel production rate and environmental objectives, respectively. As the diesel production rate is considered the major contributor, the variation of the AHP index offers similar trend to it. It is noted that the variation of gasifying temperature does not significantly affect the AHP index because the diesel production rate increases as the gasifying temperature increases whereas the environmental friendliness shows inverse effect, resulting in stable AHP index. Therefore the Figures 8.7 (a)-(d) are found to be almost identical. The maximum AHP index of 0.2133 is achieved at the gasifying temperature of 1273 K and the FT operating temperature and pressure of 473 K and 60 bar, respectively.

(a)
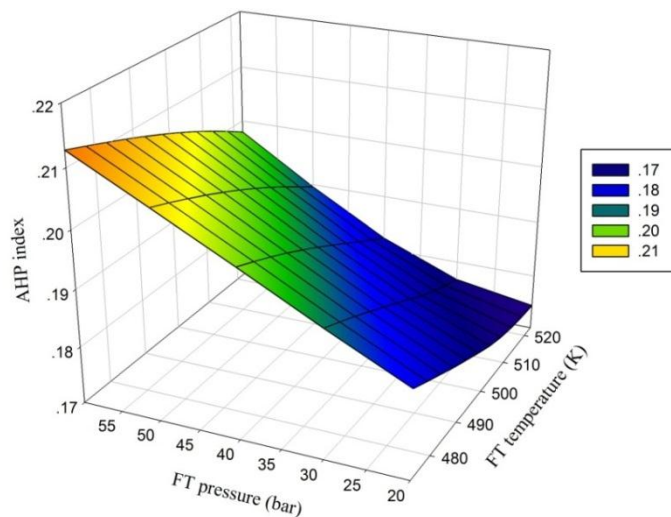
(b)
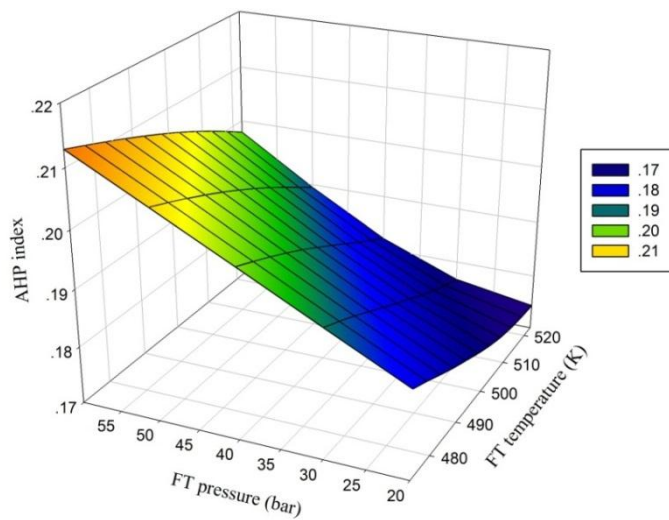
(c)
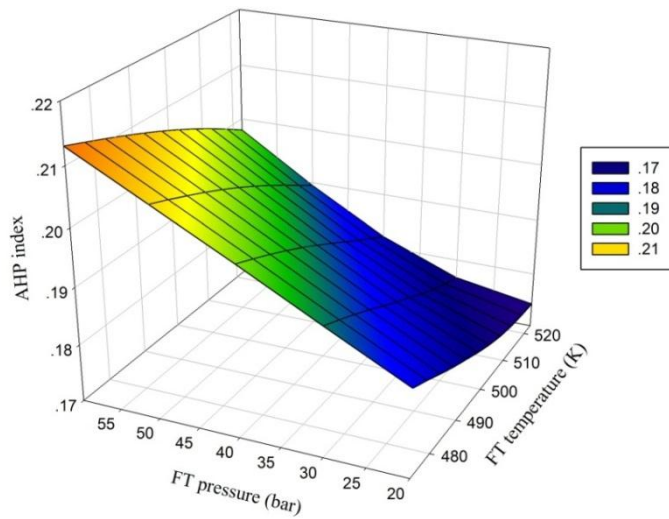
(d)
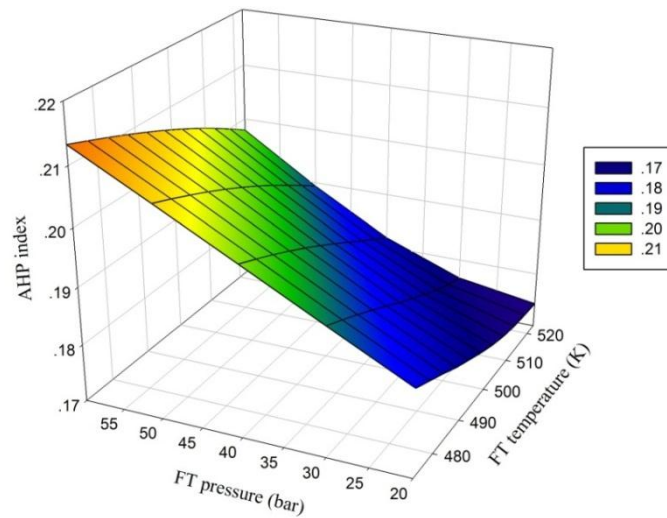
Figure 8.7 Effect of operating parameters on AHP index: (a) T_{Gs} 973 K, (b) T_{Gs} 1073 K, (c) T_{Gs} 1173 K and (d) T_{Gs} 1273 K

8.4 Conclusions

The parametric analysis of the new-designed BG-FT process is performed. The gasifying temperature, FT operating temperature and FT pressure strongly influence the diesel production rate, the overall potential environmental impact, and the combination thereof. The highest AHP index of 0.2133 for a newly designed BG-FT process is achieved at the gasifying temperature of 1273 K, the FT operating temperature of 473 K and the FT operating pressure of 60 bar when the weighting factors of the diesel production rate and environmental friendliness are specified at 0.82 and 0.18, respectively.

CHAPTER IX
CONCLUSIONS AND FUTURE WORK RECOMMENDATIONS

9.1 Conclusions

The energy production from rice straw via the BG-FT process is studied in this research. The performance of sub-units such as gasification, tar removal, FT synthesis as well as the overall BG-FT process is investigated using the developed model. The effect of changes in the ratio of gasifying agent for two gasification systems utilizing different types of gasifying agent (i.e., steam-air and steam-CO_2) at various gasifying temperatures is firstly investigated using the model developed in Aspen plus. The type and amount of gasifying agents and the gasifying temperature have strong effect on the gasification performance. The steam-CO_2 offers higher syngas yield and lower H_2/CO ratio; however, the thermal self-sufficient condition is not achieved.

The technical, economic and environmental studies of the overall BG-FT process are performed using the BG-FT model developed in Aspen custom modeler (ACM), which tar formation and reaction kinetic of char gasification are taken into account at oxygen gasification process operated at thermal self-sufficient condition and the H_2/CO ratio of FT feed gas derived from syngas processor is fixed at 2.37. The feasibility of FT off-gas recycle to gasifier is investigated and the greater amount of required oxygen is found to maintain the thermal self-sufficient condition at gasifier when the FT off-gas recycle fraction increases. The valuable products, i.e., diesel and electricity, from the BG-FT process can be maximized by suitable adjustment of the FT off-gas recycle fraction and the selection of the FT reactor volume, however, the process including FT off-gas recycle is still less feasible than the once-through concept from economic point of view. The different performance is revealed when the BG-FT process is equipped with different types of tar removal units. The process without reforming offers lowest amount of FT-products and the produced syngas cannot meet FT-feed gas specification, and the process with steam reforming is not practical because high temperature hot utility is required, the process with ATR is the most practical process and its optimum structure of heat exchanger is

designed to achieve the maximum internal heat recovery and the minimum external utility requirements. The optimization of the new designed BG-FT process based on the economic objective, aiming at the NPV maximization is performed using a FEASOPT optimizer embedded in ACM. The optimum operating condition offering the maximum NPV is achieved at the gasifying temperature of 1273 K, the supplied steam feeding rate to WGS reactor of 0.217 kmol/h and the FT temperature and pressure of 493 K and 60 bar, respectively. The gasifying temperature, FT operating temperature and FT pressure strongly influence the diesel production rate, the PEI and the combination thereof. The combined evaluation of economic and environmental point of view is performed using the AHP index, calculated based on the multi-criteria decision analysis (MCDA) method using the analytical hierarchy process (AHP), as an indicator. The highest AHP index of 0.2133 is achieved at the gasifying temperature of 1273 K, the FT operating temperature of 473 K and the FT operating pressure of 60 bar when the weighting factors of the diesel production rate and environmental friendliness are specified at 0.82 and 0.18, respectively.

9.2 Future work recommendations

The more detail studies about the BG-FT process should be further investigated. The interesting topics are shown as follow;

9.2.1 In this study, rice straw was selected to be the biomass feedstock as it is abundantly available compared with other types of biomass. The physical and chemical characteristics, i.e., size distribution of biomass, the contained organic and inorganic substances, were not considered. Hence, the detail analysis in term of the biomass characteristics should be further investigated in order to justify which is the most suitable agricultural biomass for Thailand energy production.

9.2.2 To calculate the exact value of diesel price, the cost of pre-processing (drying and size reduction) and post-processing (separation) should be considered.

9.2.3 To improve the accuracy of the FT model, other FT products, i.e., unsaturated hydrocarbon and oxygenate compounds should be taken into account.

NOMENCLATURES

M_n	Mole fraction of hydrocarbon with chain length n
W_n	Mass fraction of hydrocarbon with chain length n
ΔT_{min}	Minimum temperature difference (°C)
Q_h	Minimum hot utility requirement (KW)
Q_c	Minimum cold utility requirement (KW)
T_s	Supply temperature (°C)
T_t	Target temperature (°C)
ΔH	Enthalpy variation over the temperature interval
CP_{hot}	Heat capacity of hot stream
CP_{cold}	Heat capacity of cold stream
CP_{in}	Heat capacity of stream in the pinch
CP_{out}	Heat capacity of stream out of the pinch
N_{hot}	Number of hot stream
N_{cold}	Number of cold stream
N_{in}	Number of stream in the pinch
N_{out}	Number of stream out of the pinch
$COST_{size1}$	Cost of base scale (million Euros)
$COST_{size2}$	Cost of desired scale (million Euros)
sf	Power scaling factor or scale exponent
$SIZE_1$	Capacity of base scale
$SIZE_2$	Capacity of desired scale

PV	Present Value
NPV	Net Present Value
$R_{netcash,t}$	Net cash flow at time t
i	Discount rate
N	Period of plant life time
$\dot{I}_{out}^{(t)}$	Total rate of environmental impact output
$\hat{I}_{out}^{(t)}$	Total environmental impact output per mass of desired product
$\dot{I}_{out}^{(cp)}$	Rate of environmental impact output from chemical process
$\dot{I}_{out}^{(ep)}$	Rate of environmental impact output from energy process
$\dot{I}_{we}^{(cp)}$	Rate of environmental impact output of waste energy from chemical process
$\dot{I}_{we}^{(ep)}$	Rate of environmental impact output of waste energy from energy process
$\dot{M}_{j}^{(out)}$	Mass flow rate of stream j (kg/h)
x_{kl}	Mass fraction of component k for impact category l
$\dot{P}_{p}$	Mass flow rate of product p (kg/h)
$(Score)_{kl}$	Characteristic quantity of chemical k for impact category l
$\left\langle (Score)_{k} \right\rangle_{l}$	Average value of all k chemicals in category l
P_{i}	Normalization performance value of domain i
w_{i}	Weight of domain i
x	Number of carbon atom

y	Number of hydrogen atom
z	Number of oxygen atom
M_C	Molecular weight of carbon
M_H	Molecular weight of hydrogen
M_O	Molecular weight of oxygen
C	Mass fraction of carbon element
H	Mass fraction of hydrogen element
O	Mass fraction of oxygen element
n_i	Number of moles of component i per mole of biomass
m	Amount of oxygen per mole of biomass
w	Amount of water per mole of biomass
$K_{eq,j}$	Equilibrium constant of reaction j
ΔG_j°	Standard Gibbs-energy change of reaction j
g_i°	Gibbs function of species i
R	Universal gas constant (8.314 J/mol.K)
x_i	Mole fraction of component i
k_j	Rate constant of reaction j
x_n	Mole fraction of component n in liquid phase
r_j	Reaction rate of reaction j (mol/dm^3.s)
C_{RF}	Char reactivity factor
E_j	Activation energy of reaction j (kJ/mol)
Rt_i	Net rate of production of species i (mol/dm^3.s)

$\overset{.}{n}_{i,\text{in}}$	Molar flow rate of species i entering the control volume (kmol/h)
$\overset{.}{n}_{i,\text{out}}$	Molar flow rate of species i leaving the control volume (kmol/h)
T_{Gs}	Gasifying temperature (K)
T_{RM}	Reforming temperature (K)
T_{WGS}	Water gas shift temperature (K)
$n_{\text{ATR},i}$	Number of moles of component i in ATR process (kmol/h)
w_{ATR}	Amount of supplied water to ATR process (kmol/h)
m_{ATR}	Amount of supplied oxygen to ATR process (kmol/h)
P_{in}	Compressor inlet pressure (bar)
P_{out}	Compressor outlet pressure (bar)
$\overset{.}{W}_{comp}$	Power consumption at compressor (KW)
V_{CV}	Volume of the control volume (m^3)
X_{CO}	CO conversion (%)
P_{CO}	Partial pressure of CO (bar)
P_{H2}	Partial pressure of H$_2$ (bar)
R_{CO}	CO consumption rate (mol/s kg$_{\text{cat}}$)
r_{CO}	CO consumption rate (mol/s dm^3)
a	kinetic parameters (mol/s.kg$_{\text{cat}}$.bar^2)
b	kinetic parameters (1/bar)
$S_{\text{C5}}+$	Selectivity for hydrocarbons with a chain length longer than 5
$[H_2]$	Molar concentration of H$_2$ in the FT-feed gas
$[CO]$	Molar concentration of CO in the FT-feed gas

T_{FT}	FT operating temperature (K)
P_{FT}	FT operating pressure (bar)
Z_n	The molar flow rate of hydrocarbon with chain length n (kmol/h)
Z	Total molar flow rate of hydrocarbon product (kmol/h)
F	FT feed flow rate (kmol/h)
V	Total vapor product flow rate (kmol/h)
L	Total liquid product flow rate (kmol/h)
A, B, C	Antione constants
P_n^{sat}	Vapor pressure of hydrocarbon with chain length n (kPa)
CO_{in}	Molar flow rate of CO entering FT reactor (kmol/h)
CO_{out}	Molar flow rate of CO leaving FT reactor (kmol/h)
V_{FT}	FT reactor volume (m^3)
h_{fi}^{0}	Enthalpy of formation at the reference state (298 K, 1 atm) (kJ/kmol)
Δh_{Ti}	Enthalpy difference between a given state and the reference state (kJ/kmol)
H_{reactant}	Enthalpy of reactant (kJ)
H_{product}	Enthalpy of product (kJ)
a, b, c, d	Specific gas (or liquid) species coefficients
$C_{p,i}$	Specific heat at constant pressure of component I (kJ/kmol.K)
PEI	Potential environmental impact
P_{DP}	Normalized value of diesel production rate
P_{Env}	Normalized value of environmental friendliness

AHP	Analytical hierarchy process
weight$_{DP}$	Weighting factor of diesel production rate
weight$_{Env}$	Weighting factor of environmental friendliness
S/B	Steam to biomass mole ratio
A/B	Air to biomass mole ratio
CO_2/B	CO_2 to biomass mole ratio
H_2/CO	Molar ratio of H_2 to CO in syngas
CGE	Cold gas efficiency (%)
LHV$_{H_2}$	Lower heating value of H_2 (MJ/mol)
LHV$_{CO}$	Lower heating value of CO (MJ/mol)
LHV$_{Biomass}$	Lower heating value of biomass (MJ/mol)

Greek letters

α	Chain growth probability
ψ_k	Potential environmental impact for chemical k
ψ_{kl}^{s}	Specific potential environmental impact of chemical k for impact category l
α_l	Relative weighting factor of impact category l
η_{comp}	The efficiency of compressor
η_{exp}	The efficiency of expansion turbine
γ	Ratio of heat capacity
ρ_{cat}	Catalyst density (kg$_{cat}$/m$^3_{reactor}$)

REFERENCES

Anfray, J., Bremaud, M., Fongarland, P., Khodakov, A., Jallais, S., & Schweich, D. (2007). Kinetic study and modeling of Fischer–Tropsch reaction over a catalyst in a slurry reactor. *Chemical Engineering Science, 62*(18–20), 5353-5356.

Ardila, Y. C., Figueroa, J. E. J., Lunelli, B. H., Filho, R. M., & Wolf Maciel, M. R. (2012). Syngas production from sugar cane bagasse in a circulating fluidized bed gasifier using Aspen Plus™: Modelling and Simulation. In B. Ian David Lockhart & F. Michael (Eds.), *Computer Aided Chemical Engineering* (Vol. Volume 30, pp. 1093-1097): Elsevier.

Arpornwichanop, A., Boonpithak, N., Kheawhom, S., Ponpesh, P., & Authayanun, S. (2014). Performance Analysis of a Biomass Supercritical Water Gasification Process under Energy Self-sufficient Condition. In P. S. V. Jiří Jaromír Klemeš & L. Peng Yen (Eds.), *Computer Aided Chemical Engineering* (Vol. Volume 33, pp. 1699-1704): Elsevier.

Atnaw, S. M., Sulaiman, S. A., & Yusup, S. (2013). Syngas production from downdraft gasification of oil palm fronds. *Energy, 61*, 491-501.

Avella, R., Cornacchia, G., & Matera, D. A. (2016). *Liquid fuels from biomass and urban waste by integrated gasification – Fischer Tropsch process: economic evaluations.* Paper presented at the International conference on Bio fuels vision 2015, Bikaner, India.

Basu, P. (2010a). Biomass gasification and pyrolysis: practical design and theory (pp. 365). United States: Elsevier Inc.

Basu, P. (2010b). Chapter 9 - Production of Synthetic Fuels and Chemicals from Biomass *Biomass Gasification and Pyrolysis* (pp. 301-323). Boston: Academic Press.

Bengtsson, S. (2011). The CHRISGAS project. *Biomass and Bioenergy, 35, Supplement 1*, S2-S7.

Bhattacharya, A., Das, A., & Datta, A. (2014). Exergy based performance analysis of hydrogen production from rice straw using oxygen blown gasification. *Energy, 69*, 525-533.

Blom, R., Dahl, I. M., Slagtem, Å., Sortland, B., Spjelkavik, A., & Tangstad, E. (1994). Carbon dioxide reforming of methane over lanthanum-modified catalysts in a fluidized-bed reactor. *Catalysis Today, 21*(2–3), 535-543.

Boerrigter, H., Slort, D. J., Calis, H. P., Bodenstaff, H., Kaandorp, A. J., Den Uil, H., & Rabou, L. P. L. (2004). Gas cleaning for integrated Biomass Gasification (BG) and Fischer-Tropsch (FT) systems; experimental demonstration of two BG-FT systems. Petten, The Netherlands: Energy research Centre of the Netherlands (ECN).

BP. (2015). BP Statistical Review of World Energy June 2015 (64 ed.). UK.

Bradford, M. C. J., & Vannice, M. A. (1996). Catalytic reforming of methane with carbon dioxide over nickel catalysts II. Reaction kinetics. *Applied Catalysis A: General, 142*(1), 97-122.

Buddadee, B., Wirojanagud, W., Watts, D. J., & Pitakaso, R. (2008). The development of multi-objective optimization model for excess bagasse utilization: A case study for Thailand. *Environmental Impact Assessment Review, 28*(6), 380-391.

Cabezas, H., Bare, J. C., & Mallick, S. K. (1999). Pollution prevention with chemical process simulators: the generalized waste reduction (WAR) algorithm—full version. *Computers & Chemical Engineering, 23*(4–5), 623-634.

Chaiwatanodom, P., Vivanpatarakij, S., & Assabumrungrat, S. (2014). Thermodynamic analysis of biomass gasification with CO2 recycle for synthesis gas production. *Applied Energy, 114*, 10-17.

Chen, H., Wen, Y., Water, M. D., & Shonnard, D. R. (2002). Design guidance for chemical processes using environmental and economic assessments. *Industrial & Engineering Chemistry Research, 41*, 4503-4513.

Choosri, N., Swadchaipong, N., Utistham, T., & Hartley, U. W. (2012). Gasoline and Diesel Production via FischerTropsch Synthesis over Cobalt based Catalyst. *International Journal of Chemical, Molecular, Nuclear, Materials and Metallurgical Engineering, 6*, 12-23.

Chutichai, B., Authayanun, S., Assabumrungrat, S., & Arpornwichanop, A. (2013). Performance analysis of an integrated biomass gasification and PEMFC (proton exchange membrane fuel cell) system: Hydrogen and power generation. *Energy, 55*, 98-106.

Cohce, M. K., Dincer, I., & Rosen, M. A. (2010). Thermodynamic analysis of hydrogen production from biomass gasification. *International Journal of Hydrogen Energy, 35*(10), 4970-4980.

De Filippis, P., Borgianni, C., Paolucci, M., & Pochetti, F. (2004). Gasification process of Cuban bagasse in a two-stage reactor. *Biomass and Bioenergy, 27*(3), 247-252.

de Swart, J. W. A., & Krishna, R. (2002). Simulation of the transient and steady state behaviour of a bubble column slurry reactor for Fischer–Tropsch synthesis. *Chemical Engineering and Processing: Process Intensification, 41*(1), 35-47.

DEDE, D. o. a. e. d. a. e. M. o. e., Thailand. (2012). Thailand energy consumption. Retrieved 1 October 2014, 2014, from www.dede.go.th.

Di Carlo, A., Borello, D., Sisinni, M., Savuto, E., Venturini, P., Bocci, E., & Kuramoto, K. (2015). Reforming of tar contained in a raw fuel gas from biomass gasification using nickel-mayenite catalyst. *International Journal of Hydrogen Energy, 40*(30), 9088-9095.

Dimian, A. C., Bildea, C. S., & Kiss, A. A. (2014). Chapter 13 - Pinch Point Analysis. In C. S. B. Alexandre C. Dimian & A. K. Anton (Eds.), *Computer Aided Chemical Engineering* (Vol. Volume 35, pp. 525-564): Elsevier.

Doherty, W., Reynolds, A., & Kennedy, D. (2009). The effect of air preheating in a biomass CFB gasifier using ASPEN Plus simulation. *Biomass and Bioenergy, 33*(9), 1158-1167.

Domenichini, R., Gallio, M., & Lazzaretto, A. (2010). Combined production of hydrogen and power from heavy oil gasification: Pinch analysis, thermodynamic and economic evaluations. *Energy, 35*(5), 2184-2193.

Dry, M. E. (2002). The Fischer–Tropsch process: 1950–2000. *Catalysis Today, 71*(3–4), 227-241.

Fatih Demirbas, M. (2009). Biorefineries for biofuel upgrading: A critical review. *Applied Energy, 86, Supplement 1*, 151-161.

Fogler, H. S. (1999). *Elements of chemical reaction engineering*. NJ: Prentice Hall International.

Francois, J., Abdelouahed, L., Mauviel, G., Patisson, F., Mirgaux, O., Rogaume, C., Gao, N., & Li, A. (2008). Modeling and simulation of combined pyrolysis and reduction zone for a drowndraft biomass gasifier. *Energy Conversion and Management, 40* 3483-3490.

Gai, C., Dong, Y., & Zhang, T. (2014). Downdraft gasification of corn straw as a non-woody biomass: Effects of operating conditions on chlorides distribution. *Energy, 71*, 638-644.

Gao, N., & Li, A. (2008). Modeling and simulation of combined pyrolysis and reduction zone for a downdraft biomass gasifier. *Energy Conversion and Management, 49*(12), 3483-3490.

Garivait, S., Chaiyo, U., Patumsawad, S., & Deakhuntod, J. (2006, 1-23 November 2006). *Physical and Chemical Properties of Thai Biomass Fuels from Agricultural Residues.* Paper presented at the The 2nd Joint International Conference on "Sustainable Energy and Environment (SEE 2006), Bangkok, Thailand.

Giltrap, D. L., McKibbin, R., & Barnes, G. R. G. (2003). A steady state model of gas-char reactions in a downdraft biomass gasifier. *Solar Energy, 74*(1), 85-91.

Guinee, J. B., Gorree, M., Heijungs, R., Huppes, G., Kleijn, R., de Koning, A., L., v. O., Sleeswijk, A. W., Suh, S., Udo de Haes, H. A., de Bruijn, H., van Duin, R.,

& Huijbregts, M. A. J. (2002). *Handbook on Life Cycle Assessment*. New York: Kluwer academic   publishers.

Hamelinck, C. N., & Faaij, A. P. C. (2006). Outlook for advanced biofuels. *Energy Policy, 34*(17), 3268-3283.

Hamelinck, C. N., Faaij, A. P. C., den Uil, H., & Boerrigter, H. (2004). Production of FT transportation fuels from biomass; technical options, process analysis and optimisation, and development potential. *Energy, 29*(11), 1743-1771.

Han, J., & Kim, H. (2008). The reduction and control technology of tar during biomass gasification/pyrolysis: An overview. *Renewable and Sustainable Energy Reviews, 12*(2), 397-416.

Hanaoka, T., Hiasa, S., & Edashige, Y. (2013). Syngas production by CO2/O2 gasification of aquatic biomass. *Fuel Processing Technology, 116*, 9-15.

Higman, C., & van der Burgt, M. (2008). Chapter 5 - Gasification Processes *Gasification (Second Edition)* (pp. 91-191). Burlington: Gulf Professional Publishing.

Hu, J., Yu, F., & Lu, Y. (2012). Application of fischer-tropsch synthesis in biomass to liquid conversion. *Catalysts, 2*(2), 303-326.

Hughes, W. E. (1998). *Biomass Integrated-Gasification/ Gas Turbine Power Generation in Zimbabwe.* (PhD), Princeton University.

Hunpinyo, P., Cheali, P., Narataruksa, P., Tungkamani, S., & Chollacoop, N. (2014). Alternative route of process modification for biofuel production by embedding the Fischer–Tropsch plant in existing stand-alone power plant (10 MW) based on biomass gasification – Part I: A conceptual modeling and simulation approach (a case study in Thailand). *Energy Conversion and Management, 88*, 1179-1192.

Hunpinyo, P., Narataruksa, P., Tungkamani, S., Pana-Suppamassadu, K., & Chollacoop, N. (2013). Evaluation of Techno-economic feasibility Biomass-

to-energy by Using ASPEN Plus®: A Case Study of Thailand. *Energy Procedia, 42*, 640-649.

Im-orb, K., Simasatitkul, L., & Arpornwichanop, A. (2015). Performance Analysis and Optimization of the Biomass Gasification and Fischer-Tropsch Integrated Process for Green Fuel Productions. In J. K. H. Krist V. Gernaey & G. Rafiqul (Eds.), *Computer Aided Chemical Engineering* (Vol. Volume 37, pp. 275-280): Elsevier.

Irfan, M. F., Usman, M. R., & Kusakabe, K. (2011). Coal gasification in CO2 atmosphere and its kinetics since 1948: A brief review. *Energy, 36*(1), 12-40.

Jayah, T. H., Aye, L., Fuller, R. J., & Stewart, D. F. (2003). Computer simulation of a downdraft wood gasifier for tea drying. *Biomass and Bioenergy, 25*(4), 459-469.

Jenkins, S. (2015). Chemical Engineering Features Report Guidebook 2014. Retrieved 30 March 2015, from www.chemengonline.com

Josuinkas, F. M., Quitete, C. P. B., Ribeiro, N. F. P., & Souza, M. M. V. M. (2014). Steam reforming of model gasification tar compounds over nickel catalysts prepared from hydrotalcite precursors. *Fuel Processing Technology, 121*, 76-82.

Kamp, I. P. (2007). *Pinch Analysis and Process Integration*. Butterworth-Heinemann: Elsevier.

Kaneko, T., Brouwer, J., & Samuelsen, G. S. (2006). Power and temperature control of fluctuating biomass gas fueled solid oxide fuel cell and micro gas turbine hybrid system. *Journal of Power Sources, 160*(1), 316-325.

Kaushal, P., Abedi, J., & Mahinpey, N. (2010). A comprehensive mathematical model for biomass gasification in a bubbling fluidized bed reactor. *Fuel, 89*(12), 3650-3661.

Kim, K., Kim, Y., Yang, C., Moon, J., Kim, B., Lee, J., Lee, U., Lee, S., Kim, J., Eom, W., Lee, S., Kang, M., & Lee, Y. (2013). Long-term operation of

biomass-to-liquid systems coupled to gasification and Fischer–Tropsch processes for biofuel production. *Bioresource Technology, 127*, 391-399.

Kojima, T., Assavadakorn, P., & Furusawa, T. (1993). Third International Rolduc Symposium on Coal Science and Technology and Related Processes Measurement and evaluation of gasification kinetics of sawdust char with steam in an experimental fluidized bed. *Fuel Processing Technology, 36*(1), 201-207.

Krishna, R., & Sie, S. T. (2000). Design and scale-up of the Fischer-Tropsh bubble column slurry reactor. *Fuel Processing Technology, 64*, 73-105.

Kumar, A., Jones, D. D., & Hanna, M. A. (2009). Thermochemical Biomass Gasification: A Review of the Current Status of the Technology. *Energies, 2*, 556-581.

Kwack, S.-H., Park, M.-J., Bae, J. W., Park, S.-J., Ha, K.-S., & Jun, K.-W. (2011). Modeling a slurry CSTR with Co/P–Al2O3 catalyst for Fischer–Tropsch synthesis. *Fuel Processing Technology, 92*(12), 2264-2271.

Leibbrandt, N. H., Aboyade, A. O., Knoetze, J. H., & Görgens, J. F. (2013). Process efficiency of biofuel production via gasification and Fischer–Tropsch synthesis. *Fuel, 109*, 484-492.

Li, X. T., Grace, J. R., Lim, C. J., Watkinson, A. P., Chen, H. P., & Kim, J. R. (2004). Biomass gasification in a circulating fluidized bed. *Biomass and Bioenergy, 26*(2), 171-193.

Lim, J. S., Abdul Manan, Z., Wan Alwi, S. R., & Hashim, H. (2012). A review on utilisation of biomass from rice industry as a source of renewable energy. *Renewable and Sustainable Energy Reviews, 16*(5), 3084-3094.

Loha, C., Chatterjee, P. K., & Chattopadhyay, H. (2011). Performance of fluidized bed steam gasification of biomass – Modeling and experiment. *Energy Conversion and Management, 52*(3), 1583-1588.

Lohitharn, N., Goodwin Jr, J. G., & Lotero, E. (2008). Fe-based Fischer–Tropsch synthesis catalysts containing carbide-forming transition metal promoters. *Journal of Catalysis, 255*(1), 104-113.

Lu, Y., & Lee, T. (2007). Influence of the feed gas composition on the Fischer-Tropsch synthesis in comercial operation. *Journal of Natural Gas Chemistry, 16*, 329-341.

Ma, L., Wang, T., Liu, Q., Zhang, X., Ma, W., & Zhang, Q. (2012). A review of thermal–chemical conversion of lignocellulosic biomass in China. *Biotechnology Advances, 30*(4), 859-873.

Masuku, C. M., Ma, W., Hildebrandt, D., Glasser, D., & Davis, B. H. (2012). A vapor–liquid equilibrium thermodynamic model for a Fischer–Tropsch reactor. *Fluid Phase Equilibria, 314*, 38-45.

Mavukwana, A., Jalama, K., Ntuli, F., & Harding, K. (2013, April 15-13, 2013). *Simulation of sugarcane bagasse gasification using Aspen plus.* Paper presented at the International conference on chemical and environmental engineering (ICCEE 2013), Johannesburg, South Africa.

Miao, Q., Zhu, J., Barghi, S., Wu, C., Yin, X., & Zhou, Z. (2013). Modeling biomass gasification in circulating fluidized beds. *Renewable Energy, 50*, 655-661.

Mitta, N. R., Ferrer-Nadal, S., Lazovic, A. M., Parales, J. F., Velo, E., & Puigjaner, L. (2006). Modelling and simulation of a tyre gasification plant for synthesis gas production. In W. Marquardt & C. Pantelides (Eds.), *Computer Aided Chemical Engineering* (Vol. Volume 21, pp. 1771-1776): Elsevier.

Nakamura, S., Kitano, S., & Yoshikawa, K. (2016). Biomass gasification process with the tar removal technologies utilizing bio-oil scrubber and char bed. *Applied Energy, 170*, 186-192.

Ng, K. S., & Sadhukhan, J. (2011). Techno-economic performance analysis of bio-oil based Fischer-Tropsch and CHP synthesis platform. *Biomass and Bioenergy, 35*(7), 3218-3234.

Nikoo, M. B., & Mahinpey, N. (2008). Simulation of biomass gasification in fluidized bed reactor using ASPEN PLUS. *Biomass and Bioenergy, 32*(12), 1245-1254.

Nixon, J. D., Dey, P. K., Ghosh, S. K., & Davies, P. A. (2013). Evaluation of options for energy recovery from municipal solid waste in India using the hierarchical analytical network process. *Energy, 59*, 215-223.

Omer, A. M. (2008). Green energies and the environment. *Renewable and Sustainable Energy Reviews, 12*(7), 1789-1821.

Panahi, M., Skogestad, S., & Yelchuru, R. (2010, 10-14 January 2010). *Steady State Simulation for Optimal*

Design and Operation of a GTL Process. Paper presented at the 2nd Annual Gas Processing Symposium, Qatar.

Patzlaff, J., Liu, Y., Graffmann, C., & Gaube, J. (1999). Studies on product distributions of iron and cobalt catalyzed Fischer–Tropsch synthesis. *Applied Catalysis A: General, 186*(1–2), 109-119.

Pereira, E. G., da Silva, J. N., de Oliveira, J. L., & Machado, C. S. (2012). Sustainable energy: A review of gasification technologies. *Renewable and Sustainable Energy Reviews, 16*(7), 4753-4762.

Petersen, A. M., Melamu, R., Knoetze, J. H., & Görgens, J. F. (2015). Comparison of second-generation processes for the conversion of sugarcane bagasse to liquid biofuels in terms of energy efficiency, pinch point analysis and Life Cycle Analysis. *Energy Conversion and Management, 91*, 292-301.

Pondini, M., & Ebert, M. (2013). *Process synthesis and design of low temperature Fischer-Tropsch crude production from biomass derived syngas.* (Master), CHALMERS UNIVERSITY OF TECHNOLOGY, Göteborg, Sweden.

Prins, M. J., Ptasinski, K. J., & Janssen, F. J. J. G. (2005). Exergetic optimisation of a production process of Fischer–Tropsch fuels from biomass. *Fuel Processing Technology, 86*(4), 375-389.

Qin, Y., Campen, A., Wiltowski, T., Feng, J., & Li, W. (2015). The influence of different chemical compositions in biomass on gasification tar formation. *Biomass and Bioenergy, 83*, 77-84.

Rafiq, M. H., Jakobsen, H. A., Schmid, R., & Hustad, J. E. (2011). Experimental studies and modeling of a fixed bed reactor for Fischer–Tropsch synthesis using biosyngas. *Fuel Processing Technology, 92*(5), 893-907.

Rajvanshi, A. K. (1986). Biomass gasification. In D. Yogi Goswami (Ed.), *Alternative Energy in Agriculture* (Vol. 2). Maharashtra, India.

Ramzan, N., Ashraf, A., Naveed, S., & Malik, A. (2011). Simulation of hybrid biomass gasification using Aspen plus: A comparative performance analysis for food, municipal solid and poultry waste. *Biomass and Bioenergy, 35*(9), 3962-3969.

Reichling, J. P., & Kulacki, F. A. (2011). Comparative analysis of Fischer–Tropsch and integrated gasification combined cycle biomass utilization. *Energy, 36*(11), 6529-6535.

Renganathan, T., Yadav, M. V., Pushpavanam, S., Voolapalli, R. K., & Cho, Y. S. (2012). CO2 utilization for gasification of carbonaceous feedstocks: A thermodynamic analysis. *Chemical Engineering Science, 83*, 159-170.

Sadhwani, N., Liu, Z., Eden, M. R., & Adhikari, S. (2013). Simulation, Analysis, and Assessment of CO2 Enhanced Biomass Gasification. In K. Andrzej & T. Ilkka (Eds.), *Computer Aided Chemical Engineering* (Vol. Volume 32, pp. 421-426): Elsevier.

Shafizadeh, F. (1982). Pyrolytic reactions and products of biomass. *Journal of Analytical and Applied Pyrolysis, 3*, 283–305.

Sharma, A. K. (2008). Equilibrium and kinetic modeling of char reduction reactions in a downdraft biomass gasifier: A comparison. *Solar Energy, 82*(10), 918-928.

Sharma, A. K. (2011). Modeling and simulation of a downdraft biomass gasifier 1. Model development and validation. *Energy Conversion and Management, 52*(2), 1386-1396.

Shen, L., Gao, Y., & Xiao, J. (2008). Simulation of hydrogen production from biomass gasification in interconnected fluidized beds. *Biomass and Bioenergy, 32*(2), 120-127.

Smith, J. M., Van Ness, H. C., & M.M., A. (2008). *Introduction to chemical engineering thermodynamics* (6 ed.). Singapore: McGraw-Hill.

Song, H. S., Ramkrishna, D., Trinh, S., & Wright, H. (2004). Operating Strategies for Fischer-Tropsch Reactors: A Model-Directed Study. *Korean Journal of Chemical Engineering, 21*(2), 308-317.

Song, X., & Guo, Z. (2006). Technologies for direct production of flexible H2/CO synthesis gas. *Energy Conversion and Management, 47*(5), 560-569.

Stemmler, M., & Müller, M. (2011). Chemical hot gas cleaning concept for the "CHRISGAS" process. *Biomass and Bioenergy, 35, Supplement 1*, S105-S115.

Steynberg, A. P., & Dry, M. E. (2004). *Fischer-Tropsch Technology* (A. P. Steynberg & M. E. Dry Eds. 1 ed. Vol. 152). The Netherland: Elsevier E.V.

Steynberg, A. P., Dry, M. E., Davis, B. H., & Breman, B. B. (2004). Chapter 2 - Fischer-Tropsch Reactors. In S. André & D. Mark (Eds.), *Studies in Surface Science and Catalysis* (Vol. Volume 152, pp. 64-195): Elsevier.

Swain, P. K., Das, L. M., & Naik, S. N. (2011). Biomass to liquid: A prospective challenge to research and development in 21st century. *Renewable and Sustainable Energy Reviews, 15*(9), 4917-4933.

Tijmensen, M. J. A., Faaij, A. P. C., Hamelinck, C. N., & van Hardeveld, M. R. M. (2002). Exploration of the possibilities for production of Fischer Tropsch liquids and power via biomass gasification. *Biomass and Bioenergy, 23*(2), 129-152.

Tinaut, F. V., Melgar, A., Pérez, J. F., & Horrillo, A. (2008). Effect of biomass particle size and air superficial velocity on the gasification process in a downdraft fixed bed gasifier. An experimental and modelling study. *Fuel Processing Technology, 89*(11), 1076-1089.

Tristantini, D., Lögdberg, S., Gevert, B., Borg, Ø., & Holmen, A. (2007). The effect of synthesis gas composition on the Fischer–Tropsch synthesis over Co/γ-Al2O3 and Co–Re/γ-Al2O3 catalysts. *Fuel Processing Technology, 88*(7), 643-649.

UNFCCC, U. N. F. C. o. C. C. (2015). United Nations Framework Convention on Climate Change (UNFCCC) Historic Paris Agreement on Climate Change. Retrieved 15 January, 2016, from http://newsroom.unfccc.int/unfccc-newsroom/finale-cop21/

Vaezi, M., Passandideh-Fard, M., Moghiman, M., & Charmchi, M. (2008). *Modeling biomass gasification: a new approach to utilize renewable sources of energy.* Paper presented at the 2008 ASME International Mechanical Engineering Congress and Exposition (IMECE2008), Boston, Massachusetts, USA.

Vivanpatarakij, S., & Assabumrungrat, S. (2013). Thermodynamic analysis of combined unit of biomass gasifier and tar steam reformer for hydrogen production and tar removal. *International Journal of Hydrogen Energy, 38*(10), 3930-3936.

Wang, B., Gebreslassie, B. H., & You, F. (2013). Sustainable design and synthesis of hydrocarbon biorefinery via gasification pathway: Integrated life cycle assessment and technoeconomic analysis with multiobjective superstructure optimization. *Computers & Chemical Engineering, 52*, 55-76.

Wang, J., Jing, Y., Zhang, C., & Zhao, J. (2009). Review on multi-criteria decision analysis aid in sustainable energy decision-making. *Renewable and Sustainable Energy Reviews, 13*(9), 2263-2278.

Wang, S., Yin, Q., Guo, J., Ru, B., & Zhu, L. (2013). Improved Fischer–Tropsch synthesis for gasoline over Ru, Ni promoted Co/HZSM-5 catalysts. *Fuel, 108*, 597-603.

Wang, Y., & Kinoshita, C. M. (1993). Kinetic model of biomass gasification. *Solar Energy, 51*, 19-25.

Wang, Y., Xu, Y. Y., Li, Y. W., Zhao, Y. L., & Zhang, B. J. (2003). Heterogeneous modeling for fixed-bed Fischer–Tropsch synthesis: Reactor model and its applications. *Chemical Engineering Science, 58*(3–6), 867-875.

Wood, D. A., Nwaoha, C., & Towler, B. F. (2012). Gas-to-liquids (GTL): A review of an industry offering several routes for monetizing natural gas. *Journal of Natural Gas Science and Engineering, 9*, 196-208.

Xu, Q., Pang, S., & Levi, T. (2011). Reaction kinetics and producer gas compositions of steam gasification of coal and biomass blend chars, part 2: Mathematical modelling and model validation. *Chemical Engineering Science, 66*(10), 2232-2240.

Yang, H., & Chen, H. (2015). 11 - Biomass gasification for synthetic liquid fuel production A2 - Speight, Rafael LuqueJames G *Gasification for Synthetic Fuel Production* (pp. 241-275): Woodhead Publishing.

Yate, I. C., & Satterfield, C. N. (1991). Intrinsic Kinetics of the Fischer-Tropsch Synthesis on a Cobalt Catalyst. *Energy, 5*, 168-173.

Yermakova, A., & Anikeev, V. (2000). Thermodynamic calculations in the modeling of multiphase processes and reactors, Industrial and Engineering. *Chemistry Research, 39*(5), 1453–1472.

Young, D. M., & Cabezas, H. (1999). Designing sustainable processes with simulation: the waste reduction (WAR) algorithm. *Computers & Chemical Engineering, 23*(10), 1477-1491.

Zainal, Z. A., Ali, R., Lean, C. H., & Seetharamu, K. N. (2001). Prediction of performance of a downdraft gasifier using equilibrium modeling for different biomass materials. *Energy Conversion and Management, 42*(12), 1499-1515.

APPENDIX

APPENDIX A
THERMODYNAMIC DATA OF SELECTED COMPONENT

Table A.1 Heat capacity coefficient for gases

Table A.2 Heat of formation (H_f^0) and entropy of formation (S_f^0) of selected

   component at standard state (273 K, 1 atm)

Table A.3 Heat capacity coefficient for gas phase hydrocarbon products

Table A.4 Heat capacity coefficient for liquid phase hydrocarbon products

Table A.5 Heat of formation (H_f^0) of gas and liquid hydrocarbon products

Table A.6 Antione constant for hydrocarbon products
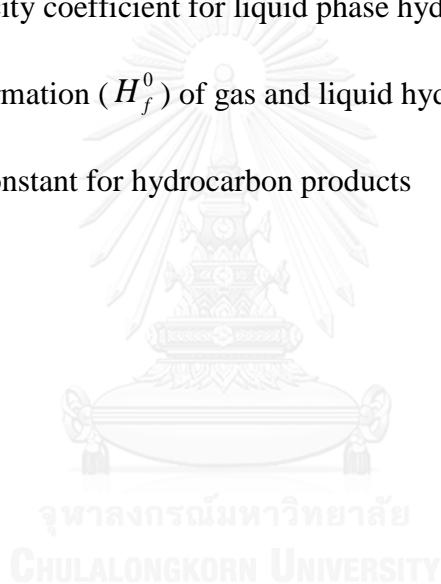
Table A.1 Heat capacity coefficient for gases

Components	$\dfrac{C_p}{R} = A + BT + CT^2 + \dfrac{D}{T^2}$ (J/mol)			
	A	**B**	**C**	**D**
CO	3.38E+00	5.57E-04	0.00E+00	-3.10E+03
CO_2	5.46E+00	1.05E-03	0.00E+00	-1.16E+05
H_2	3.25E+00	4.22E-04	0.00E+00	8.30E+03
H_2O (gas)	3.47E+00	1.45E-03	0.00E+00	1.21E+04
H_2O (liquid)	8.71E+00	1.25E-03	-1.80E-07	0.00E+00
O_2	3.64E+00	5.06E-04	0.00E+00	-2.27E+04
N_2	3.28E+00	5.93E-04	0.00E+00	4.00E+03

Table A.2 Heat of formation (H_f^0) and entropy of formation (S_f^0) of selected component at standard state (273 K, 1 atm)

Components	H_f^0 **(J/mol)**	S_f^0 **(J/mol.K)**
CO	-110.525E+3	197.7
CO_2	-393.509E+3	213.8
H_2	0	130.7
H_2O (g)	-241.818E+3	188.8
H_2O (l)	-285.83E+3	-
O_2	0	205
N_2	0	191.5

Table A.3 Heat capacity coefficient for gas phase hydrocarbon products

Gas phase hydrocarbons	$C_p = A + BT + CT^2 + DT^3 + ET^4$ (J/mol.K)				
	A	**B**	**C**	**D**	**E**
CH_4	34.942	0.039957	0.0001918	-1.5303E-07	3.932E-11
C_2H_6	28.146	0.043447	0.0001895	-1.9082E-07	5.335E-11
C_3H_8	28.277	0.116	0.000196	-2.3271E-07	6.867E-11
C_4H_{10}	20.056	0.28153	-1.31E-05	-9.4571E-08	3.415E-11
C_5H_{12}	26.671	0.22324	4.282E-05	1.6639E-07	5.604E-11
C_6H_{14}	25.924	0.41927	-1.25E-05	-1.5916E-07	5.878E-11
C_7H_{16}	26.984	0.5087	-4.47E-05	-1.6835E-07	6.518E-11
C_8H_{18}	29.053	0.5087	-5.71E-05	-1.9548E-07	7.661E-11
C_9H_{20}	29.687	0.66821	-9.65E-05	-2.0014E-07	8.22E-11
$C_{10}H_{22}$	31.78	0.74489	-0.000109	-2.2668E-07	9.346E-11
$C_{11}H_{24}$	125.212	0.31401	0.0007914	-9.141E-07	2.757E-10
$C_{12}H_{26}$	71.498	0.72559	0.0001155	-4.1196E-07	1.414E-10
$C_{13}H_{28}$	110.4	0.53321	0.0007398	-1.0212E-06	3.242E-10
$C_{14}H_{30}$	115.502	0.60882	0.0006804	-9.7091E-07	3.076E-10
$C_{15}H_{32}$	124.647	0.62706	0.0008316	-1.1689E-06	3.733E-10
$C_{16}H_{34}$	131.75	0.67397	0.0008777	-1.243E-06	3.979E-10
$C_{17}H_{36}$	111.903	0.95987	0.000279	-6.752E-07	2.255E-10
$C_{18}H_{38}$	124.715	0.98653	0.0003427	-7.4838E-07	2.48E-10
$C_{19}H_{40}$	132.53	1.0358	0.0003693	-7.9581E-07	2.636E-10

Table A.4 Heat capacity coefficient for liquid phase hydrocarbon products

Liquid phase hydrocarbons	$C_p = A + BT + CT^2 + DT^3 + ET^4$ (J/mol.K)				
	A	**B**	**C**	**D**	**E**
CH_4	-0.018	1.1982	-0.009872	0.00003167	0
C_2H_6	38.332	0.41006	-0.002302	5.9347E-06	0
C_3H_8	59.642	0.328131	-0.001538	3.6539E-06	0
C_4H_{10}	62.873	0.58913	-0.002359	4.2257E-06	0
C_5H_{12}	80.641	0.62195	-0.002268	3.7423E-06	0
C_6H_{14}	78.848	0.88729	-0.002948	4.1999E-06	0
C_7H_{16}	101.121	0.97739	-0.003071	4.1844E-06	0
C_8H_{18}	82.736	1.3043	-0.003825	4.6459E-06	0
C_9H_{20}	98.04	1.3538	-0.003806	4.4991E-06	0
$C_{10}H_{22}$	79.741	1.6926	-0.004529	4.9769E-06	0
$C_{11}H_{24}$	94.169	1.7806	-0.00463	4.9675E-06	0
$C_{12}H_{26}$	84.485	2.0358	-0.005098	5.2186E-06	0
$C_{13}H_{28}$	85.027	2.2008	-0.005368	5.4016E-06	0
$C_{14}H_{30}$	111.814	2.2092	-0.005256	5.0865E-06	0
$C_{15}H_{32}$	94.014	2.4973	-0.005803	5.5554E-06	0
$C_{16}H_{34}$	89.101	2.7062	-0.006148	0.000005752	0
$C_{17}H_{36}$	113.571	2.8548	-0.006396	5.8757E-06	0
$C_{18}H_{38}$	151.154	2.7878	-0.006154	5.5249E-06	0
$C_{19}H_{40}$	118.433	3.2613	-0.007088	0.000006303	0

Table A.5 Heat of formation (H_f^0) of gas and liquid hydrocarbon products

Hydrocarbons	H_f^0 (J/mol)	
	Gas phase	**Liquid phase**
CH_4	-74.85	-
C_2H_6	-84.68	-
C_3H_8	-103.85	-120.90
C_4H_{10}	-126.15	-147.30
C_5H_{12}	-146.44	-173.50
C_6H_{14}	-167.19	-198.70
C_7H_{16}	-187.78	-224.20
C_8H_{18}	-208.45	-250.10
C_9H_{20}	-229.03	-274.70
$C_{10}H_{22}$	-249.66	-300.90
$C_{11}H_{24}$	-270.29	-327.20
$C_{12}H_{26}$	-290.87	-350.90
$C_{13}H_{28}$	-311.50	-377.70
$C_{14}H_{30}$	-332.13	-403.30
$C_{15}H_{32}$	-352.75	-428.80
$C_{16}H_{34}$	-373.34	-456.10
$C_{17}H_{36}$	-393.92	-479.50
$C_{18}H_{38}$	-414.55	-505.40
$C_{19}H_{40}$	-435.14	-530.90

Table A.6 Antione constant for hydrocarbon products

| Hydrocarbons | $\log P^{sat} = A + \dfrac{B}{T} + C\log T + DT + ET^2$ | | | | |
	A	B	C	D	E
CH_4	14.6667	-5.71E+02	-3.34E+00	2.20E-09	1.31E-05
C_2H_6	20.6973	-1.13E+03	-5.25E+00	-9.88E-11	6.73E-06
C_3H_8	21.4469	-1.46E+03	-5.26E+00	3.28E-11	3.73E-06
C_4H_{10}	27.0441	-1.90E+03	-7.18E+00	-6.68E-11	4.22E-06
C_5H_{12}	29.2963	-2.18E+03	-7.88E+00	-4.65E-11	3.90E-06
C_6H_{14}	69.7378	-3.63E+03	-2.39E+01	1.28E-02	-1.68E-13
C_7H_{16}	65.0257	-3.82E+03	-2.17E+01	1.04E-02	1.02E-14
C_8H_{18}	29.0948	-3.01E+03	-7.27E+00	-2.27E-11	1.47E-06
C_9H_{20}	8.8817	-2.80E+03	1.53E+00	-1.05E-02	5.80E-06
$C_{10}H_{22}$	26.5125	-3.36E+03	-6.12E+00	-3.32E-10	4.86E-07
$C_{11}H_{24}$	82.923	-5.61E+03	-2.73E+01	1.05E-02	7.09E-13
$C_{12}H_{26}$	-5.6532	-3.47E+03	9.03E+00	-2.32E-02	1.12E-05
$C_{13}H_{28}$	49.2391	-4.96E+03	-1.38E+01	-2.11E-09	2.59E-06
$C_{14}H_{30}$	106.1056	-7.35E+03	-3.52E+01	1.24E-02	-8.40E-13
$C_{15}H_{32}$	116.5157	-8.04E+03	-3.88E+01	1.34E-02	-4.44E-13
$C_{16}H_{34}$	99.1091	-7.53E+03	-3.23E+01	1.05E-02	1.23E-12
$C_{17}H_{36}$	173.4039	-1.09E+04	-5.92E+01	2.07E-02	-1.34E-12
$C_{18}H_{38}$	-15.0772	-4.87E+03	1.45E+01	-3.16E-02	7.16E-06
$C_{19}H_{40}$	76.7647	-7.72E+03	-2.24E+01	6.51E-11	3.11E-06

APPENDIX B
RAW DATA FOR EVALUATING A POTENTIAL ENVIRONMENTAL IMPACT

Table B.1 Raw data for determining the potential environmental impact of BG-FT process without tar removal unit

Table B.2 Raw data for determining the potential environmental impact of BG-FT process with steam reforming unit

Table B.3 Raw data for determining the potential environmental impact of BG-FT process with autothermal reforming (ATR) unit
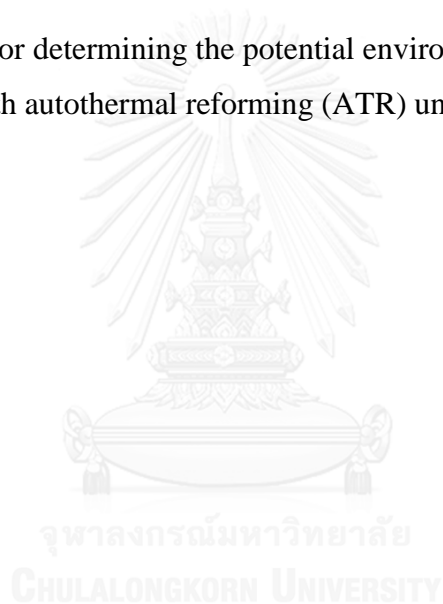
Table B.1 Raw data for determining the potential environmental impact of BG-FT process without tar removal unit

FT-Offgas compositions	mass flow rate (kg/h) $m_k = M_j^{(out)} x_{kj}$	Potential environmental impact of chemical k for impact category $l_k = M_j^{(out)} x_{kj} \psi_k$								Total PEI/h $\hat{I}_{out}^{(t)} = \sum_j M_j^{(out)} \sum_k x_{kl} \psi_k$
		GWP	ODP	PCOP	AP	HTPE	HTPI	ATP	TTP	
C_1H_4	0.3063	6.4325	0.0000	0.0018	0.0000	0.0000	0.0000	0.0000	0.0000	6.4343
C_2H_6	0.4166	0.0000	0.0000	0.0512	0.0000	0.0000	0.0000	0.0000	0.0000	0.0512
C_3H_8	0.4425	0.0000	0.0000	0.0779	0.0000	0.1131	0.0000	0.0000	0.0000	0.1910
C_4H_{10}	0.4218	0.0000	0.0000	0.1485	0.0000	0.1348	0.0000	0.0000	0.0000	0.2833
C_5H_{12}	0.3779	0.0000	0.0000	0.1493	0.0000	0.1610	0.0000	0.0000	0.0000	0.3103
C_6H_{14}	0.3228	0.0000	0.0000	0.1556	0.0000	4.1269	0.0000	0.0000	0.0000	4.2825
C_7H_{16}	0.2667	0.0000	0.0000	0.1318	0.0000	0.1705	0.0000	0.0001	0.0000	0.3024
C_8H_{18}	0.2136	0.0000	0.0000	0.0968	0.0000	0.0000	0.0000	0.0001	0.0000	0.0969
C_9H_{20}	0.1653	0.0000	0.0000	0.0684	0.0000	0.0000	0.0000	0.0002	0.0000	0.0686
$C_{10}H_{22}$	0.1236	0.0000	0.0000	0.0475	0.0000	0.0000	0.0000	0.0005	0.0000	0.0479
$C_{11}H_{24}$	0.0875	0.0000	0.0000	0.0336	0.0000	0.0000	0.0000	0.0010	0.0000	0.0346
$C_{12}H_{26}$	0.0594	0.0000	0.0000	0.0212	0.0000	0.0000	0.0000	0.0000	0.0000	0.0212
$C_{13}H_{28}$	0.0382	0.0000	0.0000	0.0000	0.0000	0.0000	0.0000	0.0000	0.0000	0.0000
$C_{14}H_{30}$	0.0232	0.0000	0.0000	0.0000	0.0000	0.0000	0.0000	0.0004	0.0000	0.0004
$C_{15}H_{32}$	0.0135	0.0000	0.0000	0.0000	0.0000	0.0000	0.0000	0.0044	0.0000	0.0044
$C_{16}H_{34}$	0.0075	0.0000	0.0000	0.0000	0.0000	0.0000	0.0000	0.0011	0.0000	0.0011
$C_{17}H_{36}$	0.0042	0.0000	0.0000	0.0000	0.0000	0.0000	0.0000	0.0094	0.0000	0.0094
$C_{18}H_{38}$	0.0001	0.0000	0.0000	0.0000	0.0000	0.0000	0.0000	0.0001	0.0000	0.0001
$C_{19}H_{40}$	0.0012	0.0000	0.0000	0.0000	0.0000	0.0000	0.0000	0.0225	0.0000	0.0225
CO	0.9763	1.8551	0.0000	0.0264	0.0000	8.3216	0.0000	0.0000	0.0000	10.2031
CO_2	12.0345	12.0345	0.0000	0.0000	0.0000	0.6154	0.0000	0.0000	0.0000	12.6499
H_2	0.2133	0.0000	0.0000	0.0000	0.0000	0.0000	0.0000	0.0000	0.0000	0.0000
N_2	0.0155	0.0000	0.0000	0.0000	0.0000	0.0000	0.0000	0.0000	0.0000	0.0000
Impact included CO_2	20.3221	20.3221	0.0000	1.0099	0.0000	13.6435	0.0000	0.0398	0.0000	35.0152
Impact excluded CO_2	8.2875	8.2875	0.0000	1.0099	0.0000	13.0280	0.0000	0.0398	0.0000	22.3652

Table B.2 Raw data for determining the potential environmental impact of BG-FT process with steam reforming unit

FT-Offgas compositions	mass flow rate (kg/h) $m_k = M_j^{(out)} x_{kj}$	Potential environmental impact of chemical k for impact category l, $= M_j^{(out)} x_{kj} \psi_k$								Total PEI/h $\hat{I}_{out}^{(t)} = \sum_j M_j^{(out)} \sum_k x_{kj} \psi_k$
		GWP	ODP	PCOP	AP	HTPE	HTPI	ATP	TTP	
C$_1$H$_4$	0.2938	6.1695	0.0000	0.0018	0.0000	0.0000	0.0000	0.0000	0.0000	6.1713
C$_2$H$_6$	0.4004	0.0000	0.0000	0.0493	0.0000	0.0000	0.0000	0.0000	0.0000	0.0493
C$_3$H$_8$	0.4262	0.0000	0.0000	0.0750	0.0000	0.1090	0.0000	0.0000	0.0000	0.1840
C$_4$H$_{10}$	0.4070	0.0000	0.0000	0.1433	0.0000	0.1301	0.0000	0.0000	0.0000	0.2734
C$_5$H$_{12}$	0.3654	0.0000	0.0000	0.1443	0.0000	0.1557	0.0000	0.0000	0.0000	0.3000
C$_6$H$_{14}$	0.3126	0.0000	0.0000	0.1507	0.0000	3.9963	0.0000	0.0000	0.0000	4.1470
C$_7$H$_{16}$	0.2586	0.0000	0.0000	0.1277	0.0000	0.1653	0.0000	0.0001	0.0000	0.2931
C$_8$H$_{18}$	0.2072	0.0000	0.0000	0.0939	0.0000	0.0000	0.0000	0.0001	0.0000	0.0940
C$_9$H$_{20}$	0.1603	0.0000	0.0000	0.0664	0.0000	0.0000	0.0000	0.0002	0.0000	0.0666
C$_{10}$H$_{22}$	0.1198	0.0000	0.0000	0.0460	0.0000	0.0000	0.0000	0.0005	0.0000	0.0465
C$_{11}$H$_{24}$	0.0846	0.0000	0.0000	0.0325	0.0000	0.0000	0.0000	0.0010	0.0000	0.0334
C$_{12}$H$_{26}$	0.0572	0.0000	0.0000	0.0204	0.0000	0.0000	0.0000	0.0000	0.0000	0.0204
C$_{13}$H$_{28}$	0.0367	0.0000	0.0000	0.0000	0.0000	0.0000	0.0000	0.0000	0.0000	0.0000
C$_{14}$H$_{30}$	0.0222	0.0000	0.0000	0.0000	0.0000	0.0000	0.0000	0.0004	0.0000	0.0004
C$_{15}$H$_{32}$	0.0129	0.0000	0.0000	0.0000	0.0000	0.0000	0.0000	0.0042	0.0000	0.0042
C$_{16}$H$_{34}$	0.0071	0.0000	0.0000	0.0000	0.0000	0.0000	0.0000	0.0010	0.0000	0.0010
C$_{17}$H$_{36}$	0.0040	0.0000	0.0000	0.0000	0.0000	0.0000	0.0000	0.0090	0.0000	0.0090
C$_{18}$H$_{38}$	0.0001	0.0000	0.0000	0.0000	0.0000	0.0000	0.0000	0.0001	0.0000	0.0001
C$_{19}$H$_{40}$	0.0011	0.0000	0.0000	0.0000	0.0000	0.0000	0.0000	0.0215	0.0000	0.0215
CO	2.0222	3.8422	0.0000	0.0546	0.0000	17.2358	0.0000	0.0000	0.0000	21.1326
CO$_2$	12.4519	12.4519	0.0000	0.0000	0.0000	0.6368	0.0000	0.0000	0.0000	13.0887
H$_2$	0.3898	0.0000	0.0000	0.0000	0.0000	0.0000	0.0000	0.0000	0.0000	0.0000
N$_2$	0.0155	0.0000	0.0000	0.0000	0.0000	0.0000	0.0000	0.0000	0.0000	0.0000
Impact included CO$_2$		22.4636	0.0000	1.0058	0.0000	22.4289	0.0000	0.0380	0.0000	45.9362
Impact excluded CO$_2$		10.0117	0.0000	1.0058	0.0000	21.7921	0.0000	0.0380	0.0000	32.8476

Table B.3 Raw data for determining the potential environmental impact of BG-FT process with autothermal reforming (ATR) unit

FT-Offgas compositions	mass flow rate (kg/h) $m_k = M_j^{(out)} x_{kj}$	Potential environmental impact of chemical k for impact category $I_s = M_j^{(out)} x_{kj} \psi_k$								Total PEI/h $\dot{I}_{out}^{(t)} = \sum_j M_j^{(out)} \sum_k x_{kj} \psi_k$
		GWP	ODP	PCOP	AP	HTPE	HTPI	ATP	TTP	
C_1H_4	0.2958	6.2118	0.0000	0.0018	0.0000	0.0000	0.0000	0.0000	0.0000	6.2136
C_2H_6	0.4030	0.0000	0.0000	0.0496	0.0000	0.0000	0.0000	0.0000	0.0000	0.0496
C_3H_8	0.4287	0.0000	0.0000	0.0754	0.0000	0.1096	0.0000	0.0000	0.0000	0.1851
C_4H_{10}	0.4093	0.0000	0.0000	0.1441	0.0000	0.1308	0.0000	0.0000	0.0000	0.2749
C_5H_{12}	0.3672	0.0000	0.0000	0.1450	0.0000	0.1565	0.0000	0.0000	0.0000	0.3015
C_6H_{14}	0.3140	0.0000	0.0000	0.1514	0.0000	4.0148	0.0000	0.0000	0.0000	4.1662
C_7H_{16}	0.2597	0.0000	0.0000	0.1283	0.0000	0.1660	0.0000	0.0001	0.0000	0.2944
C_8H_{18}	0.2081	0.0000	0.0000	0.0943	0.0000	0.0000	0.0000	0.0001	0.0000	0.0944
C_9H_{20}	0.1610	0.0000	0.0000	0.0667	0.0000	0.0000	0.0000	0.0002	0.0000	0.0668
$C_{10}H_{22}$	0.1203	0.0000	0.0000	0.0462	0.0000	0.0000	0.0000	0.0005	0.0000	0.0467
$C_{11}H_{24}$	0.0850	0.0000	0.0000	0.0326	0.0000	0.0000	0.0000	0.0010	0.0000	0.0336
$C_{12}H_{26}$	0.0576	0.0000	0.0000	0.0206	0.0000	0.0000	0.0000	0.0000	0.0000	0.0206
$C_{13}H_{28}$	0.0370	0.0000	0.0000	0.0000	0.0000	0.0000	0.0000	0.0000	0.0000	0.0000
$C_{14}H_{30}$	0.0224	0.0000	0.0000	0.0000	0.0000	0.0000	0.0000	0.0004	0.0000	0.0004
$C_{15}H_{32}$	0.0130	0.0000	0.0000	0.0000	0.0000	0.0000	0.0000	0.0042	0.0000	0.0042
$C_{16}H_{34}$	0.0072	0.0000	0.0000	0.0000	0.0000	0.0000	0.0000	0.0010	0.0000	0.0010
$C_{17}H_{36}$	0.0040	0.0000	0.0000	0.0000	0.0000	0.0000	0.0000	0.0091	0.0000	0.0091
$C_{18}H_{38}$	0.0001	0.0000	0.0000	0.0000	0.0000	0.0000	0.0000	0.0001	0.0000	0.0001
$C_{19}H_{40}$	0.0011	0.0000	0.0000	0.0000	0.0000	0.0000	0.0000	0.0217	0.0000	0.0217
CO	1.8974	3.6050	0.0000	0.0512	0.0000	16.1717	0.0000	0.0000	0.0000	19.8280
CO_2	12.7240	12.7240	0.0000	0.0000	0.0000	0.6507	0.0000	0.0000	0.0000	13.3747
H_2	0.3687	0.0000	0.0000	0.0000	0.0000	0.0000	0.0000	0.0000	0.0000	0.0000
N_2	0.0171	0.0000	0.0000	0.0000	0.0000	0.0000	0.0000	0.0000	0.0000	0.0000
Impact included CO_2	22.5408	22.5408	0.0000	1.0071	0.0000	21.4001	0.0000	0.0383	0.0000	44.9863
Impact excluded CO_2	9.8168	9.8168	0.0000	1.0071	0.0000	20.7494	0.0000	0.0383	0.0000	31.6116

APPENDIX C
LIST OF PUBLICATIONS

Internal publications

1) Im-orb K., Simasatitkul L., Arpornwichanop A. Performance analysis and optimization of the biomass gasification and Fischer-Tropsch integrated process for green fuel productions. Computer Aided Chemical Engineering 37 (2015) 275-280.

2) Im-orb K., Simasatitkul L., Arpornwichanop A. Analysis of synthesis gas production with a flexible H_2/CO ratio from rice straw gasification. Fuel 164 (2016) 361–373.

3) Im-orb K., Simasatitkul L., Arpornwichanop A. Techno-economic analysis of the biomass gasification and FischereTropsch integrated process with off-gas recirculation. Energy 94 (2016) 483-496.

4) Im-orb K., Arpornwichanop A. Techno-environmental analysis of the biomass gasification and Fischer-Tropsch integrated process for the co-production of bio-fuel and power. Energy 112 (2016) 121-132.

VITA

Miss Karittha Im-orb was born in December 16, 1982 in Loei, Thailand. She finished high school from Loeipitayakom School, Loei in 2001. She received her Bacherlor's Degree in Chemical Engineering, from Department of Chemical Engineering, Faculty of Engineering, King Mongkut's Institute of Technology Ladkrabang in 2005. Afterward, she continued studying Master degree of Chemical Engineering, Chulalongkorn University in 2004. She began her doctoral degree in Chemical Engineering, Chulalongkorn University since October 2012.